UNIVERSITY OF SOUTHAMPTON
FACULTY OF PHYSICAL SCIENCES AND ENGINEERING
SCHOOL OF ELECTRONICS AND COMPUTER SCIENCE

Resource Allocation for Heterogeneous Radio-Frequency and Visible-Light Networks

by

Fan Jin
B. Eng., M.Sc.

A doctoral thesis submitted in partial fulfilment of the
requirements for the award of Doctor of Philosophy
at the University of Southampton

June 2015

SUPERVISOR:
Professor Lajos Hanzo
FREng, FIEEE, FIEE, DSc, EIC of IEEE Press
Chair of Wireless Southampton Group
Dr. Rong Zhang
School of Electronics and Computer Science
University of Southampton
Southampton SO17 1BJ
United Kingdom

Dedicated to my family

UNIVERSITY OF SOUTHAMPTON

ABSTRACT

FACULTY OF PHYSICAL SCIENCES AND ENGINEERING
SCHOOL OF ELECTRONICS AND COMPUTER SCIENCE

Doctor of Philosophy

Resource Allocation for Heterogeneous Radio-Frequency and Visible-Light Networks

by Fan Jin

In recent years, mobile data traffic demands have been increased exponentially, and the conventional cellular systems can no longer support the capacity demands. A potential solution for meeting such demands may be Heterogeneous Network (HetNet) techniques. A HetNet may integrate diverse radio access technologies (RAT) such as UMTS Terrestrial Radio Access Networks (UTRAN), GSM/EDGE Radio Access and Network (GERAN), Wireless Local Area Network (WLAN) as well as possibly Visible Light Communication (VLC) networks. The improved channel gain of the HetNet techniques is achieved by employing the small cells and by reduced transmission distance. However, the deployment of HetNet techniques also impose several technical challenges, for example the interference management, handovers, resource management and modelling of HetNets.

A HetNet relies on multiple types of access nodes in a wireless network. These access nodes can use either the same technology or different technologies. When the access nodes employ the same technology and use the same frequency band, a major problem is the Co-Channel-Interference (CCI) between these access nodes. We firstly investigate a Radio-Frequency (RF) based HetNet in Chapter 3, which is constituted by the macrocells and the femtocells. More explicitly, the impacts of femtocells on traditional macrocells are studied, when the macrocells are relying on Fractional Frequency Reuse (FFR). The design, performance analysis and optimization problems of this FFR aided two-tier HetNet is investigated. We found the advantage of FFR eroded in dense femtocell scenarios and the optimized network tends to become a Unity Frequency Reuse (UFR) aided system. In order to mitigate the cross-tier interference, we proposed a statics spectrum allocation scheme, namely Swapping Spectrum Access (SSA). Both the Outage Probability (OP) of femtocell Mobile Terminals (MTs) in cell centre region and that of the macrocell MTs in the cell edge region is reduced by the proposed SSA. The optimized network using our SSA is more robust to the detrimental impact of femtocells.

Another constitution of a HetNet may rely on integrating different technologies of wireless communication networks. We focus on our attentions on a HetNet composing by a RF femtocell and a VLC network in Chapter 4 and 5. An important component of this architecture is its Resource Management (RM). We investigate the Resource Allocation (RA) problems, under the diverse quality of service (QoS) requirements in terms of data rate, fairness and the statistical de-

lay requirements. Two types of MTs, multi-homing MTs and multi-mode MTs are considered, where multi-homing MTs have the capability of aggregating resources from different networks, while the multi-mode MTs always select a single network for their connection. We proposed a sub-optimal decentralized method for solving the RA problems of both the multi-homing MTs and multi-mode MTs. The simulation results confirm the conceived method is capable of satisfying the QoS requirements. Furthermore, we employ more sophisticated transmission strategies for the VLC network and study their performance in Chapter 5. Again, the RA problems of the HetNet relying on different transmission strategies are investigated.

Declaration of Authorship

I, **Fan Jin**, declare that the thesis entitled **Resource Allocation for Heterogeneous Radio-Frequency and Visible-Light Networks** and the work presented in it are my own and has been generated by me as the result of my own original research. I confirm that:

- This work was done wholly or mainly while in candidature for a research degree at this University;
- Where any part of this thesis has previously been submitted for a degree or any other qualification at this University or any other institution, this has been clearly stated;
- Where I have consulted the published work of others, this is always clearly attributed;
- Where I have quoted from the work of others, the source is always given. With the exception of such quotations, this thesis is entirely my own work;
- I have acknowledged all main sources of help;
- Where the thesis is based on work done by myself jointly with others, I have made clear exactly what was done by others and what I have contributed myself;
- Parts of this work have been published.

Signed: ..... Date: .....

Acknowledgements

Firstly, I would like to thank my supervisors Professor Lajos Hanzo and Dr. Rong Zhang for their generous support and constance encouragement and for their wise advice that allowed this work to become reality. The discussions with them always inspire and enlighten me and I really appreciate their invaluable friendship.

I would also like to thank all my teachers and colleagues in the Southampton Wireless Group for their supports and helps. Special thanks to Dr. Cheng Dong, Dr. Shaoshi Yang Chao Xu, Dr. Peichang Zhang for their kindly and helpful advice on my work. It is so grateful to cooperative with Junyi Jiang, Dr. Jie Zhang and Xuan Li. Thank you both for sharing your precious knowledges with me.

Finally, My sincere thanks to my parents, my wife Ting Wen and my son Wenqi Jin for their endless love, support and understanding.

List of Publications

Journal Papers

1. **F. Jin, R. Zhang and L. Hanzo**, "Resource allocation under delay-guarantee constraint for heterogeneous visible-light and RF femtocell", *IEEE Transactions on Wireless Communications*, vol. 14, no. 2, pp. 1020-1034, February. 2015.

2. **F. Jin, R. Zhang, and L. Hanzo**, "Fractional frequency reuse aided twin-layer femtocell networks: analysis, design and optimization", *IEEE Transactions on Communications*, vol. 61, no. 5, pp. 2074-2085, May. 2013.

3. **F. Jin, X. Li, R. Zhang, C. Dong and L. Hanzo**, "Resource allocation under delay-guarantee constraints for visible-light communication", *Submitted to IEEE Transactions on Vehicular Technology*.

4. **J. Zhang, F. Jin, R. Zhang, G. Li and L. Hanzo**, "Analysis and design of distributed antenna-aided twin-layer femto- and macrocell networks relying on fractional frequency reuse ", *IEEE Transactions on Vehicular Technology*, vol. 63, no. 2, pp. 763-774, Feb. 2014.

5. **J. Zhang, F. Jin, Z. Tan, H. Wang, Q. Huang and L. Hanzo**, "Performance analysis of high-speed railway communication systems subjected to co-channel interference and channel estimation errors", *IET Communications*, vol. 8, no. 7, pp. 1151-1157, May. 2014.

6. **X. Li, F. Jin, R. Zhang, J. Wang, Z. Xu and L. Hanzo**, "Users first: user-centric cluster formation for interference-mitigation in visible-light networks.", *Submitted to IEEE Transactions on Wireless Communications*.

7. **J. Jiang, F. Jin, Y. Huo, R. Zhang and L. Hanzo**, "Content-Aware optimization for video streams in indoor visible light communication system.", *To be submitted*.

Conference Papers

1. **F. Jin, R. Zhang, and L. Hanzo**, "Frequency-swapping aided femtocells in twin-layer cellular networks relying on fractional frequency reuse", *in Proceedings of IEEE Wireless Communications and Networking Conference (WCNC)*, Paris, France, pp. 1-5, April. 2012.

2. **F. Jin, and L. Hanzo**, "Ergodic capacity of multi-user MIMO systems using pilot-based channel estimation, quantized feedback and outdated feedback as well as user selection", *in Proceedings of IEEE Vehicular Technology Conference (VTC)*, Quebec City, Canada, pp. 1-5, September. 2012.

3. **J. Zhang, F. Jin, R. Zhang, G. Li and L. Hanzo**, "Distributed antenna aided twin-layer femto-and macro-cell networks relying on fractional frequency-reuse", *in Proceedings of*

IEEE Wireless Communications and Networking Conference (WCNC), Shanghai, China, pp. 1-5, April. 2013.

Contents

List of Symbols

General Conventions

- The superscript * indicates complex conjugation. Hence, X^* represents the complex conjugate of the variable X.
- The superscript ^{T} indicates transpose operation. Hence, $\mathbf{X}^T$ represents the transpose of the matrix $\mathbf{X}$.
- The superscript ^{H} indicates complex conjugate transpose operation. Hence, $\mathbf{X}^H$ represents the hermitian of the matrix $\mathbf{X}$.
- The over line of $\overline{\mathbf{X}}$ or under line of $\underline{\mathbf{X}}$ are used to indicate that the vector or matrix $\mathbf{X}$ is constituted by amalgamating multi other vectors or matrices.
- Boldface characters are used to represent the vectors and matrices.

Mathematical Operators and Functions

$\sum$	The sum operation.
$\int$	The integral operation.
$\iint$	The double integral operation.
$\lvert \cdot \rvert$	The absolute value of a variable.
$\lVert \cdot \rVert$	The Euclidean $\mathtt{l}_2$ norm.
$\mathbb{P}(\cdot)$	The probability of a event.
$\prod$	The product operation.

$\mathcal{L}(\cdot)$	The Laplace transform of a variable.
$\mathbb{E}(\cdot)$	The expectation of argument.
$\exp(\cdot)$	The exponential operation.
$\ln(\cdot)$	Natural logarithm.
$\log_2(\cdot)$	Logarithm to base 2.
Ei	The exponential integral function.
$\Gamma(\cdot,\cdot)$	The incomplete gamma function.
$\mathcal{W}_{\cdot,\cdot}(\cdot)$	The Whittaker function.
∂	The partial derivative operation.
$\min(\cdot)$	The minimum value among a number of variables.
$\max(\cdot)$	The maximum value among a number of variables.

Specific Symbols

R_m	The radius of a macrocell.
ω	The ratio of the interior cell centre radius to the cell radius.
ρ	The ratio of the interior cell centre's available frequency band to the entire frequency band.
Y_{k_m}	The received signal of a MT k_m located in macrocell m.
L_{m,k_m}	The propagation path loss spanning from the MBS m to the MT k_m.
h_{m,k_m}	The uncorrelated Rayleigh fading channel spanning from the MBS m to the MT k_m.
σ^2	The variance of zero-mean AWGN.
N_0	Thermal noise density.
N_f	Number of femtocells per macrocell.
P_m	Downlink transmission power of the MBS.
P_f	Downlink transmission power of the FBS.
ξ_{m,k_m}	The SINR of the MT k_m served by MBS m.
R_{m,k_m}	The transmission bit rate of the MT k_m served by MBS m.

ϖ	The SINR discrepancy between the SINR experienced and the that required for meeting the target BER.
$\mathcal{B}_0$	Bandwidth of a subcarrier.
f_c	The carrier frequency.
A_O	Fixed outdoor pathloss.
A_I	Fixed indoor pathloss.
W	Wall penetration loss.
γ_1	Outdoor pathloss exponent.
γ_2	Indoor pathloss exponent.
F	The available frequency band.
T_m	The long-term spatially averaged macrocell throughput.
$\mathcal{S}_m$	ASE of macrocell.
ψ^{ir}	The angle of irradiation of the LED lights.
ψ^{in}	The angle of incidence.
q	The order of Lambertian emission.
$\phi_{1/2}$	The semi-angle at half illumination of an LED.
$\tilde{\pi}$	The physical area of the photo-detector.
O	The gain of the optical filter.
g^{oc}	The gain of an optical concentrator.
Ψ_c	The width of the FOV.
p	The blocking probability of LOS.
H^d	Channel gain on the LOS path.
H_r	Channel gain on the reflected path.
ψ_1^{ir}	The angle of irradiation to a reflective point.
ψ_2^{ir}	The angle of irradiation to a MT's receiver.
$\tilde{\rho}$	The reflectance factor.
$\sigma^2_{\textbf{short}}$	The variance of the shot noise.

$\sigma^2_{\textbf{thermal}}$	The variance of the thermal noise.
$\tilde{e}$	The electronic charge.
ς	The detector's responsivity.
I_{bg}	The background current.
$\tilde{n_1}$	The Boltzmann's constant.
$\tilde{n_2}$	The FET channel noise factor.
$\tilde{n_3}$	The FET transconductance.
$\tilde{T}$	The absolute temperature.
$\tilde{G}$	The open-loop voltage gain.
$\tilde{\eta}$	The fixed capacitance of the PD per unit area.
$\mathbf{M}_{QAM}$	The constellation size.
U	The number of LED lights.
N	The number of indoor MTs.
M	The number of networks/cells in the indoor HetNet.
$\mathcal{B}^{VLC}$	The achievable bandwidth of VLC.
$\mathcal{B}^{F}$	The achievable bandwidth of femtocell.
θ	The QoS exponent.
$\beta_{m,n}$	The transmission probability from network/cell m to MT n.
$\Delta_{m,n}$	The effective capacity of MT n transmitting from network/cell m.
α	The proportional fairness factor.
$\mathcal{R}_n$	The bit rate requirement of MT n.

Chapter 1

Introduction

1.1 Motivation

1.1.1 Motivations for Heterogeneous Networks

In recent years, mobile data traffic demands have been increased exponentially, especially in the Asia Pacific, region in North America and in Europe [1]. The key reason for this rapid growth of demand may be the explosive proliferation of intelligent mobile devices. Since the mobile devices continue to rely on larger device screen, the image resolution and mobile data traffic demands may continue to increase in the near future. Apart from the improved mobile devices and increased user population, another factor increasing the demand for enhanced data rates may be the emerging new applications of mobile devices. For example, social networking and other similar applications tend to produce small but frequent data transmission, which may contribute to the increased data capacity demands.

Conventional cellular systems, such as the 3rd Generation (3G) Universal Mobile Telecommunication System (UMTS) can no longer support the capacity demands. A straightforward way of meeting the growing data demands is to utilize more spectrum. Industry and academia are working together on investigating the new frequency bands, both licensed and unlicensed. However, utilizing more spectrum may be limited by the scarcity of available Radio Frequency (RF) bands. Recently, alternative wireless transmission technologies, such as Optical Wireless Communications (OWC) and Millimetre-Wave Mobile Broadband Systems, have also been explored [2]. Another approach of increasing the capacity may be to conceive sophisticated Modulation and Coding Schemes (MCS) [3]. At the time of writing, we are practically reaching the theoretical limit of radio channel capacity, which is known as the Shannon limit [4]. However, the capacity gain that may be achieved by improved modulation and coding is limited [5]. In addition to developing

sophisticated MCS, improving to spectrum reuse is another key technique of improving the capacity gains, which may be achieved by employing reduced-power nodes or small cells and by cell splitting.

On the other hand, the recent development of wireless technologies has totally revolutionized the communication systems. The International Telecommunications Union-Radio (ITU-R) communications sector specified a set of requirements for the 4th Generation (4G) systems under the International Mobile Telecommunications Advanced (IMT-Advanced) specifications. The 3rd Generation Partnership Project (3GPP) created the Long Term Evolution-Advanced (LTE-A) solution in order to meet the IMT-Advance specifications. Apart from the wireless wide area networks, a series of wireless local area networks (WLANs) standards, including IEEE 802.11a, IEEE 802.11b, IEEE 802.11G, IEEE 802.11nm etc., have been established for economic high-speed wireless access. Since all the above wireless communication networks may have a coverage area overlapping with one anther, the future capacity increases therefore have to come from a combination of diverse networking solutions, which results in forming a hybrid network for wireless access, termed as a heterogeneous network (HetNet).

To summarize, while the data capacity demands continue to increase the improvement in spectral efficiency in homogeneous networks remains limited owing to the Shannon limit. Hence, it becomes essential to improve the overall network efficiency with the aid of a HetNet architecture and sophisticated signal processing technologies.

Generally, a HetNet relies on multiple types of access nodes in a wireless network. These access nodes can use either the same technology or different technologies. In practice, HetNet deployments in LTE-A are defined as mixed deployments consisting of macrocells, picocells, femtocells and relay nodes [6]. However, a HetNet consisting of a macrocellular LTE network and a Wireless Fidelity (Wi-Fi) network is a multi-tier and multi-air-interface network. This architecture may also be invoked as a form of HetNet. As suggested in [2, 7], new wireless communication technologies using the higher frequency bands, such as Visible Light Communication (VLC) and Millimetre-Wave Radio Communication, are developed as a component of a HetNet. An example of a HetNet is illustrated in Fig. 1.1

1.1.2 Challenges in Heterogeneous Networks

Although, HetNets constitute an effective solution of increasing the network capacity, the small-cell deployment also imposes several technical challenges, for example the interference management [8], handovers [9], resource management [10] and modelling of HetNets [11]. In this thesis, we focus our attentions on the interference management and the resource management issues. Let us hence we briefly introduce these two challenges.

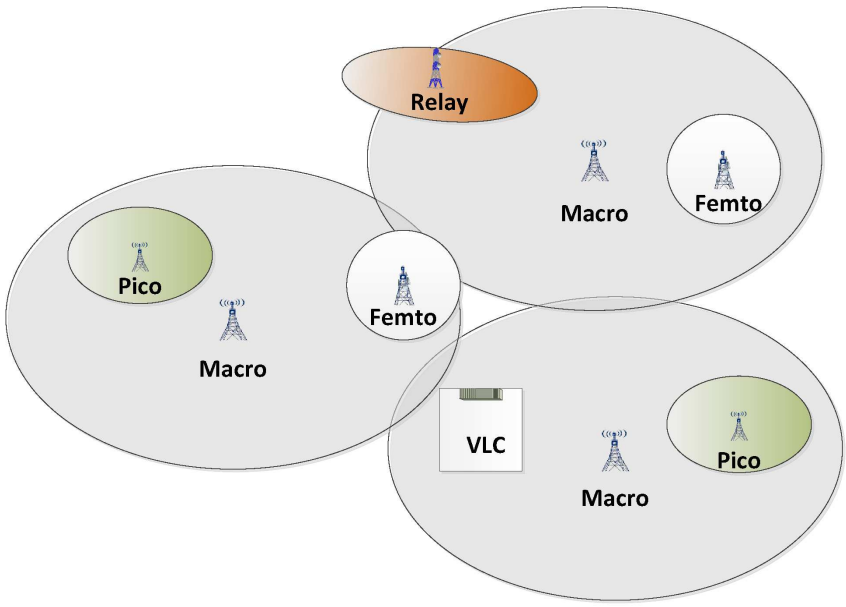

Figure 1.1: An example of a HetNet, which relies on macrocells, picocells, femtocells, relay nodes and VLC.

1.1.2.1 Interference Management

Sharing the same frequency band has the advantage of enhancing the Area Spectrum Efficiency (ASE) [12] and capacity, which is important in the face of a limited spectrum supply. However, the interference between these networks may become severe in the overlapping areas, if the spectrum access strategy is not properly designed. In Chapter 2, we will introduce the interference management issues encountered in a macro-femto two-tier network, and the state-of-the-art will be presented in Section 2.2.3. Furthermore, the interference management issues of two-tier femtocell HetNets will be investigated in Chapter 3 and a semi-static resource allocation scheme is proposed for mitigating the interference. Similarly, interference management is also a key challenge in macro-relay networks, also known as multi-hop networks. At the time of writing, most HetNet studies are focused on developing solutions for a specific combination of network layers. The long-term framework should be designed through an optimal distribution of functions among the associated access networks.

1.1.2.2 Resource Management

In HetNets, careful RA and sharing amongst the constituent networks has to be performed. The RA schemes have to maintain certain Quality-of-Service (QoS) requirements. Since one of the greatest challenges of future wireless communication networks is to achieve the target downlink and uplink data rates, the resource management scheme has to be designed in for maximizing either the

throughput or the spectral efficiency. Fairness is also an important issue of resource management in wireless networks. In HetNets, the fairness problem arises not only in scheduling but also in RA among the multiple tiers of the networks. In the context of this thesis, a generic fairness notion referred to as α-proportional fairness is used for designing the resource management scheme of a HetNet. Another important issue in designing the resource management scheme considered in this thesis is the delay requirements of mobile terminals (MTs). Future broadband wireless networks are expected to support a wide variety of communication services having diverse QoS requirements. Applications such as file transfer and email services are relatively delay-tolerant. As a result, it is important to consider the delay as a performance metrics in addition to the data rate requirements, which may require a careful cross-layer optimization [13]. Diverse approaches may be conceived for delay-aware resource control in wireless networks [13–19]. For example, the average delay-constraint may be converted into an equivalent average rate-constraint using the large deviation theory approach of [14–18]. In the thesis, we considered the resource management design issues associated with a variety of QoS requirements in Chapter 4 and Chapter 5.

1.2 Novel Contributions

The novel research aspects provided by this thesis are summarized as follows:

- We investigate the performance of a downlink multi-cell Fractional Frequency Reuse (FFR) aided two-tier femtocell network, where the interference management issues are considered. More specifically, we invoke the fluid model based method [20] for evaluating the cellular interference. Furthermore, we employ the stochastic geometry approach for modelling the random distribution of femtocells. Then the approximate per-tier Outage Probability (OP) and the long-term spatially averaged per-tier throughput of this FFR-aided scenario are derived. We study the impact of femtocells on the existing FFR aided macrocells. It is demonstrated that the femtocells erode the performance of both the outdoor macrocell MTs and of the indoor femtocell MTs. The derived OP and throughput is verified by simulations. In order to mitigate the cross-tier interference, we propose a Spectrum Swapping Access (SSA) scheme for this FFR-aided two-tier network for the sake of overcoming both the adverse near-far effects and the cross-layer interference. Our simulation results show that the proposed SSA scheme is capable of reducing the OP of both the macrocell MTs and of the femtocell MTs. - **These novel contributions were disseminated in papers “Journal No.2”and “Conference No.1” in the publication list.**

- We further extend the study of the downlink multi-cell FFR aided two-tier femtocell network to the optimization of FFR related parameters. More specifically, we formulate the optimization in terms of maximizing the ASE of the macrocells. Two design guidelines are considered, namely what we refer to as the area-proportional design and the QoS-constrained design

are considered. Then, we solve the optimization problems using a Genetic Algorithm (GA). The simulation results demonstrate that the GA based optimization process is capable of achieving an improved ASE. Furthermore, an increased macrocell ASE is achieved by the proposed SSA using a jointly optimized spectrum allocation and distance threshold policy. - **These novel contributions were published in "Journal No.2" in the publication list.**

- We investigated the Resource Allocation (RA) problems of an indoor HetNet scenario, where both an RF femtocell and LED light based VLC are used for providing indoor coverage. More specifically, a RA problem is formulated, where we apply the effective capacity approach of [14] for converting the statistical delay constraints into equivalent average rate constraints. Furthermore, the fairness of MTs is studied using the α-proportional fairness utility function defined in [21]. Two different types of MTs, namely multi-homing MTs and multi-mode MTs are considered. The RA problem is formulated as a non-linear programming (NLP) problem for the multi-homing MTs. We show mathematically that this NLP problem is concave with respect to the RA probability matrix, which hence can be solved by convex optimization techniques. We proposed the dual decomposition based approach of [22], in order to solve the QoS-constrained RA problem. We also demonstrate that the RA problem is formulated as a mixed-integer non-linear programming (MINLP) problem for the multi-mode MTs, which is mathematically intractable. In order to make the problem more tractable, a relaxation of the integer variables is introduced. Then, we formally prove that the relaxed problem is concave with respect to both the relaxed network selection matrix and to the RA probability matrix. Again, the proposed dual decomposition approach is used for solving the relaxed problem. Our simulation results demonstrate proposed decentralized approach is capable of achieving the same performance with the aid of the centralized algorithm. Furthermore, the effects of system parameters on the performance of this indoor HetNet are investigated. - **These novel contributions were published in "Journal No.1" in the publication list.**

- Rather than simply employing a Single Cell Multi-Point Transmission VLC scheme, we consider the RA problem of an indoor HetNet, relying on different transmission strategies for the VLC system. Four different transmission VLC strategies are introduced, namely the Single Cell Multi-point Transmission (SCMT), Unity Frequency Reuse (UFR) transmission, Combined Transmission (CT) and Frequency Reuse (FR) transmission. Furthermore, the performance of these strategies is compared. The simulation results illustrate that the FR-2 transmission relying on creating attocells illuminated LED lights is capable of achieving the highest bit rate. However, this FR-2 transmission exhibits the lowest bit rate, when the LOS rays are blocked. The RA problems are formulated, for the above-mentioned VLC transmission strategies, where the RA problems are formulated as NLP problems. Then a distributed algorithm is proposed for solving the RA problems. Our simulation results demonstrate that the FR-2 transmission is capable of achieving the highest effective capacity,

when the statistical delay requirements are loose. However, the CT transmission, which transmits the same information from two adjacent LED lights attains the best performance, when we tighten the delay requirements. Furthermore, the RF femtocell system becomes more reliable, when the VLC LOS blocking probability is high. **- These novel contributions were disseminated in "Journal No.3" in the publication list.**

1.3 Outline of the Thesis

Let us now highlight the outline of this thesis, which is organized, as shown in Figure 1.2.

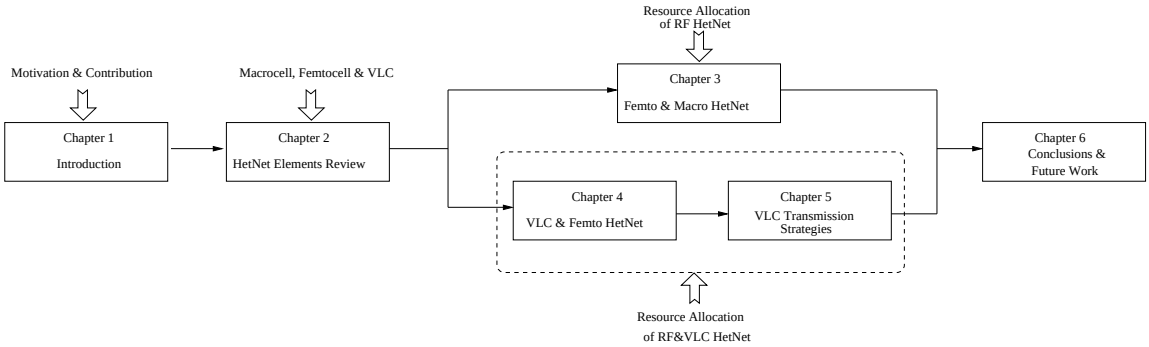

Figure 1.2: Organization of the thesis.

Chapter 2 : An Introduction to the Key Elements of Heterogeneous Networks

In Chapter 2, some key elements in HetNets are discussed, where the topology modelling of macrocells, femtocells and VLC systems are introduced. Firstly, the topology modelling of macrocells is presented in Section 2.1, where three types of cellular macrocell network modelling techniques are introduced, as depicted in Fig. 2.1. Specifically, the Wyner model is investigated in Section 2.1.1, where the cellular network is characterized as a 1-D linear model. A specific drawback of the Wyner model is its inaccuracy in capturing the randomness of MTs, especially for downlink transmission. In order to cope with this drawback, typically the grid-based model is used in practical systems [23]. In Section 2.1.2, the grid-based cellular networks illustrated in Fig. 2.4 are introduced and the history of analysing the Other Cell Interference (OCI) using a grid-based model was presented. The grid-based cellular network may accurately capture the randomness of MTs. However, the characterization of the OCI in a closed form remains an open problem. Instead of assuming the regular grid based macrocell, some researchers assumed that the cellular networks were conveniently modelled by a Poisson Point Process (PPP), which captures the network properties, as shown in Fig. 2.8. The PPP based cellular network is introduced in Section 2.1.4. Then, we turn our attention to femtocells in Section 2.2. In order to improve the coverage and enhance the

capacity of cellular wireless networks, a routinely used solution is to reduce the cell size and hence the transmission distance. One of most interesting trends emerging from the cellular evolution is constituted by femtocells, as depicted in Fig. 2.9. Both the concept and the brief history of femtocells was presented in Section 2.2.1. Then the modelling of femtocells was discussed in Section 2.2.2, where four modelling approaches were introduced. We then focus our attentions on the state-of-the-art in femtocells in Section 2.2.3, including their access control mode, mobility management, self organisation and interference management. One of the most significant challenges of the dense deployment of femtocells is the presence of strong interference, when the femtocells opt for co-channel deployment. We summarize the key contributions on interference management techniques in Table. 2.5, Table. 2.6 and Table. 2.7. Since the scarcity of RF bandwidth capable of providing a reasonable spatial coverage is a limiting factor, the increasing interest in VLC systems created a technology complementary to the traditional RF systems. We briefly introduced the history and the state-of-the-art of VLC in Section 2.3. Specifically, the state-of-the-art of VLC technologies was briefly presented in Section 2.3.1, including their modulation schemes, multiple-carrier techniques, as well as their networking issues, such as the transmission strategies, scheduling schemes and the RA schemes. The key contributions on VLC techniques were summarized in Table 2.10, Table 2.11 and Table 2.12.

Chapter 3: Fractional Frequency Reuse Aided Two-Tier Femtocell Networks: Analysis, Design and Optimization

In Chapter 2, several key elements of a HetNet are introduced. In Chapter 3, we consider an outdoor HetNet scenario, where the femtocells are overlaid onto the traditional macrocells. The inter-tier interference issues are investigated and addressed. Furthermore, we studied the optimal parameter design in this HetNet scenario. Before we investigate a two-tier HetNet, a review of the classical FFR scheme is presented in Section 3.2. In order to cope with Inter-Cell Interference (ICI), the FFR scheme, as depicted in Fig. 3.2, is designed for reducing the ICI and for improving the performance of macrocells. Then, the system model of the FFR aided two-tier femtocell networks is outlined in Section 3.3, and the topology of the FFR aided HetNet is depicted in Fig. 3.5. Two different spectrum allocation schemes were considered for the femtocells. In the Full Spectrum Allocation (FSA) scheme, femtocells reuse the entire available RF frequency bandwidth, whilst the femtocells reuse the frequency band that was not assigned in its over-sailing macrocell for SSA development, which was shown in Fig. 3.6. In Section 3.4, we investigate a HetNet scenario, where the femtocells operate the FSA regime and the system performance of FFR aided two-tier femtocell networks relying on FSA was studied. The per-tier OP is derived analytically in Section 3.4.1. Based on the OP equations derived, the long-term spatially averaged macrocell throughput is derived in Section 3.4.2. Furthermore, the optimal FFR parameter configurations are studied in Section 3.4.3. We consider two design guidelines, namely the area-proportional design and

the QoS-constrained design. The optimization problems under the area-proportional design and that under the QoS-constrained design were formulated as Problem 1 of Eq. (3.28) and Eq. (3.29), and as Problem 2 of Eq. (3.31) and Eq. (3.32). These two problems are then solved by GA. Later, we consider the scenario, where the femtocells develop SSA and the corresponding system performance of FFR aided two-tier femtocell networks relying on SSA is investigated in Section 3.5. Similarly, the OP of an outdoor macrocell MT and that of an indoor femtocell MT is derived in Lemma 3 and Lemma 4, respectively. Again, the optimal design problems of the FFR aided two-tier network using SSA are solved using a GA. The performance results of FFR aided two-tier femtocell networks are detailed in Section 3.6, where both the femtocell under FSA and that under SSA are discussed.

Chapter 4: Resource Allocation for Heterogeneous Visible-Light and RF Femtocell

As we stated in Chapter 2, optical wireless systems may become an important component of the integrated HetNet architecture. In this chapter, we shift our attention from an outdoor HetNet scenario to an indoor HetNet scenario in Chapter 4, where a combined femtocell and LED light based VLC are used for providing indoor coverage. The related RA scheme is investigated in this chapter, where diverse QoS requirements, such as the achievable data rate, the fairness and the statistic delay requirements are considered. We briefly introduce the system model of VLC using LED lights in Section 4.2, where the VLC model of the room using the LED light based VLC system is described. More specifically, the link characteristics of VLC are presented in Section 4.2.1, where the optical VLC channel is modelled as a 'two-rate' transmission channel according to zero LOS blocking and non-zero LOS blocking probability scenarios. The corresponding received SNR and the achievable bit rate of Asymmetrically Clipped Optical Orthogonal Frequency-Division Multiplexing (ACO-OFDM) aided VLC are simulated in Section 4.2.3. Then, the indoor HetNet model is described in Section 4.3, where a combined VLC and RF femtocell network is employed in a room, which is illustrated in Fig. 4.7. Again, the channel characteristics of the VLC and femtocell are presented. In order to take the delay requirement into account, the average delay-constraint may be converted into an equivalent average rate-constraint using the effective capacity approach. In this chapter, two different types of MTs: multi-homing MTs and multi-mode MTs are considered. The RA problem formulation was presented for both multi-homing MTs and multi-mode MTs in the indoor HetNet considered in Section 4.4. More specifically, the proportional fairness approach is used in Section 4.4.1 and the RA problems of multi-homing MTs and of multi-mode MTs are formulated in Section 4.4.2 and in Section 4.4.3, respectively. Then, in Section 4.5 we proposed a decentralized algorithms for solving the RA problems, where the optimization problems were de-composited into several parallel sub-problems and then the original problems were solved by an iteration approach. Our numerical performance results characterizing the proposed RA algorithms in the context of the indoor HetNet are presented in Section 4.6.

Chapter 5: Resource Allocation for an Indoor HetNet relying on Different VLC Transmission Strategies

In Chapter 4, the optimal RA problem is investigated. In Chapter 5, we extended this study, under the consideration of different VLC transmission strategies. The topology model and four different VLC transmission strategies are introduced in Section 5.2, where the SCMT, UFR transmission, CT-2 and FR-2 transmission are presented. More specifically, under the SCMT strategy all indoor LED lights operate by transmitting a single cell. In UFR transmission, each LED light operates by providing coverage for a single transmission cell. In CT-2, the neighbouring two LED lights are merged into a virtual transmission cell. Finally, in FR-2 transmission, the entire available optical frequency band of VLC is divided into two frequency band, forming a VLC system having a frequency reuse factor of 2. In Section 5.3, the performance of ACO-OFDM aided VLC is characterized by simulations. Furthermore, we investigate the QoS constrained RA problems, when different VLC transmission strategies are considered. In Section 5.4, we formulate the RA problems of an indoor HetNet, where both the femtocell and VLC are used. The proposed decentralized algorithm of Section 4.5 is used for solving the RA problems. The effective capacity of the HetNet is evaluated by simulations in Section 5.5.

Chapter 6: Conclusions and Future Work

In Chapter 6, we summarize the main findings of the entire thesis. Further potential research topics are also outlined for the future. For example, we may invoke cognitive radio in the RF femtocells, which allows femtocell users to exploit the unexploited spectrum opportunities of the licensed systems. Finding an optimal RA scheme is attractive for further research for the sake of improving the bandwidth or energy efficiency of the two-tier femtocell HetNet. For the indoor HetNet, we may invoke some more sophisticated transmission VLC strategies of VLC. Furthermore, we may design a holistic joint outdoor and indoor HetNet architecture and its optimal RA scheme.

Chapter 2

Introduction to the Key Elements in Heterogeneous Networks

As stated in the previous chapter, a heterogeneous network is typically composed of multiple radio access technologies, architectures, transmission solutions and base stations of varying transmission power. Some networks may opt for the same air interface for both over-sailing macrocells and the small-cell network relying on microcell, femtocells and relay base stations. However, the availability of the radio frequency (RF) bandwidth is a limiting factor. Hence it is beneficial to develop new complementary technologies may in support of a heterogeneous network, for the sake of providing an alternative connectivity solution for reducing the RF congestion. For example, optical wireless systems using visible light exhibit several advantages, including their license-free operation, immunity to electro-magnetic interference, network security and a high bandwidth potential [24]. In this chapter, we focus our attention on the introduction some of these technologies, which will be further exploited in the forthcoming chapters. The remainder of this chapter is organized as follows. In Section 2.1, the topology modelling methods conceived for traditional cellular networks are summarized. In Section 2.2, as one of the important elements of small-cell technologies, femtocell solutions are introduced, including their modelling and technical challenges. Then, we focus our attention operating VLC system in Section 2.3. We briefly introduce the history and principle of VLC systems. Finally, we conclude this chapter in Section 2.4.

2.1 The Topology Modelling of Cellular Networks

The operational wireless systems rely on homogeneous networks using a macro-centric planning process. A cellular macrocell network illuminates the cells with the aid of base stations positioned

in a planned layout for supporting the MTs, in which all the Base Stations (BSs) have similar transmit power levels, antenna patterns, receiver noise floors and similar back-haul connectivity to the data network. The locations of the Macrocell Base Stations (MBSs) are carefully chosen through network planning, and the BS are configurations are adjusted for maximizing the coverage, whilst mitigating the interference amongst BSs. The analytical performance modelling of cellular networks is still a debated issue [25], pursuing three main approaches in modelling macrocellular networks, as depicted in Fig. 2.1. The Wyner model of [26] has been widely used for analysing cellular networks as a benefit of its simplicity and analytical tractability. A more common and practical approach relies on assuming that the BSs of cellular networks follow a regular grid such as the traditional hexagonal grid model). Another recently proposed modelling approach [27], assumes that the network is abstracted to a convenient point process (PP). ICI is a key issue in studying cellular networks, hence we will brief;u introduce the modelling the ICI.

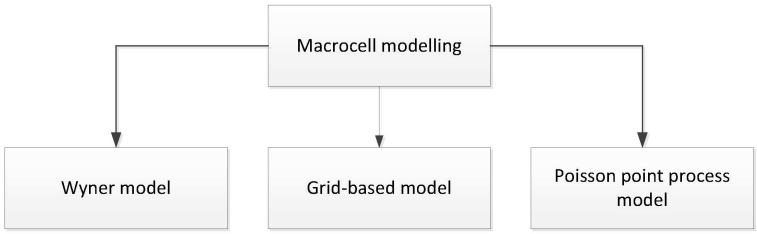

Figure 2.1: The most popular cellular macrocell network models.

2.1.1 The Wyner Model

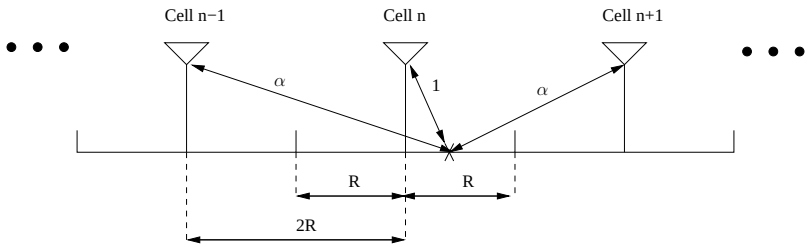

Figure 2.2: The 1-D linear Wyner model.

The Wyner model of [26] has been proposed for the analysis of cellular networks due to its simplicity and analytical tractability, which is typically invoked for a simple BS topography and assumes a unit-gain from each base station to the MTs considered and an equal gain that is less than one to the MTs from the two neighbouring cells [26]. Fig. 2.2 illustrates a typical One-

dimensional (1-D) linear Wyner model, where there are N 1-D cells, along a line, indexed by n, where each cell covers a segment of length $2R$. Each BS in Fig. 2.2 is located at the cell centre. As depicted in Fig. 2.2, the channel attenuation between each BS and its MT supported is normalized to 1, while the inter-cell interference intensity is characterized by a deterministic and homogeneous parameter α $(0 \leq \alpha \leq 1)$. As a result, the signal received by a given MBS is the sum of the signals transmitted from within that cell plus a factor α times the sum of the signals transmitted from the neighbouring cells plus the ambient Gaussian noise. Let us consider the classic 3G style Code-Division Multiple-Access (CDMA) systems communicating over an Additive White Gaussian Noise (AWGN) channel [26], assuming that the MT set in cell n and the kth MT in cell n are denoted by $\mathcal{K}_n$ and k_n, respectively. As a result, the signal Y_n received by the BS of cell n in an uplink scenario is given by:

$$\begin{aligned} Y_n = \sum_{k_n \in \mathcal{K}_n} \sqrt{P_{n,k_n}} X_{n,k_n} + \alpha \sum_{k_{n-1} \in \mathcal{K}_{n-1}} \sqrt{P_{n-1,k_{n-1}}} X_{n-1,k_{n-1}} \\ + \alpha \sum_{k_{n+1} \in \mathcal{K}_{n+1}} \sqrt{P_{n+1,k_{n+1}}} X_{n+1,k_{n+1}} + Z_n, \end{aligned} \tag{2.1}$$

where P_{n,k_n} and X_{n,k_n} are the transmitted power and the signal transmitted from the uplink transmitter (MT k_n) in cell n, respectively. Owing to the maximization total power constraint, we may have $\mathbb{E}\left[|X_{n,k_n}|^2\right] = 1$. Furthermore, Z_n is a mutually independent zero-mean additive white Gaussian process with a variance of σ^2. Similarly, for the downlink, the signal Y_{n,k_n} received at MT k_n in cell n is given by:

$$Y_{n,k_n} = \sqrt{P_{n,k_n}} X_{n,k_n} + \alpha \sqrt{P_{n-1,k_{n-1}}} X_{n-1,k_{n-1}} + \alpha \sqrt{P_{n+1,k_{n+1}}} X_{n+1,k_{n+1}} + Z_{n,k}, \tag{2.2}$$

where P_{n,k_n} and $X_{n,k}$ now denote the transmitted power and the signal transmitted from the downlink transmitter of BS n to MT k, respectively. Similarly, we also have $\mathbb{E}\left[|X_{n,k_n}|^2\right] = 1$.

In [26], the Wyner model was proposed and used for deriving the capacity of the uplink cellular relying on Multicell Processing (MCP), which uses a hig-speed optical backbone for sharing all signals amongst the cooperating BSs, while considering a non-fading channel and a wideband transmission scheme. These results were then extended by the authors of [28, 29] to flat-fading. Assuming that the flat-fading processes experienced between a MT k_n and a cell n may be modelled by h_{n,k_n}, Eq. (2.1) and (2.2) may be rewritten as:

$$\begin{aligned} Y_n = \sum_{k_n \in \mathcal{K}_n} \sqrt{P_{n,k_n} h_{n,k_n}} X_{n,k_n} + \alpha \sum_{k_{n-1} \in \mathcal{K}_{n-1}} \sqrt{P_{n-1,k_{n-1}} h_{n,k_{n-1}}} X_{n-1,k_{n-1}} \\ + \alpha \sum_{k_{n+1} \in \mathcal{K}_{n+1}} \sqrt{P_{n+1,k_{n+1}} h_{n,k_{n+1}}} X_{n+1,k_{n+1}} + Z_n, \end{aligned} \tag{2.3}$$

$$\begin{aligned} Y_{n,k_n} = \sqrt{P_{n,k_n} h_{n,k_n}} X_{n,k_n} + \alpha \sqrt{P_{n-1,k_{n-1}} h_{n-1,k_n}} X_{n-1,k_{n-1}} \\ + \alpha \sqrt{P_{n+1,k_{k+1}} h_{n+1,k_n}} X_{n+1,k_{n+1}} + Z_{n,k}. \end{aligned} \tag{2.4}$$

The Wyner model was then used for analysing the uplink throughput of cellular networks both in Single-Cell Processing (SCP) and Two-Cell-Site Processing (TCSP) in [30] and [31], respectively. The authors of [32, 33] used the Wyner model for the information-theoretic analysis of relying on pseudo-noise direct-sequence code-division multiple-access (DS-CDMA). The uplink sum capacity of Multiple-Input-Multiple-Output (MIMO) systems was derived under the Wyner model in [34]. Recently, the Wyner model was extended to incorporate shadowing in [35].

Turning our attention to the downlink channel, the authors of [36] invoked the Wyner model for the analysis of the attainable average rates in the high Signal-to-Noise Ratio (SNR) region, where a simple low-complexity transmit preprocessing scheme, relying on the knowledge of the anticipated downlink Channel Impulse Response (CIR) was invoked for eliminating the interference at the MT with the aid of signal processing at the downlink BS transmitter.

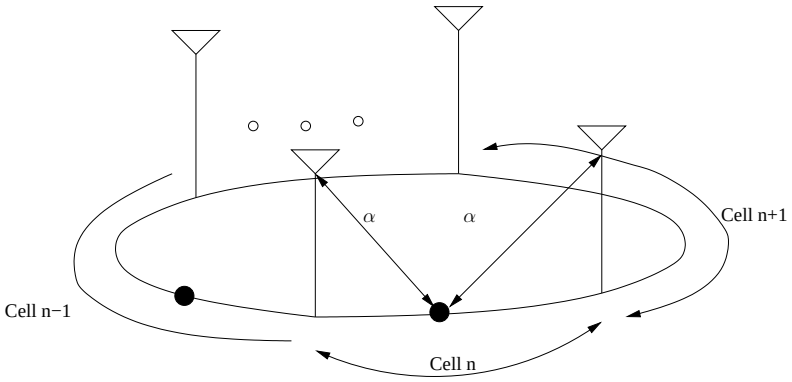

Figure 2.3: The modified circular array based Wyner model derived from its 1-D counterpart.

Later, a modified Wyner model was introduced in [37], in order to derive the average per-cell sum-rate attained with the aid of joint multicell processing, while considering both non-fading and flat-fading channels. The modified Wyner model is depicted in Fig. 2.3, where the authors assume that the cells are arranged along a circle. Furthermore, it is assumed that the cellular BSs are located at the boundaries of the cells and the MTs receive the signals transmitted by the two BSs, which are located at their cell edges. The key difference with respect to the original Wyner model of [26] is that the users are concentrated at the boundaries of the cells, where no single dominant BS can be identified. As a result, the users are hence in what is referred to as a ”soft-handoff” situation between these two BSs. Later, the Wyner model and the modified Wyner model were widely used for evaluating different constrained coordination strategies involved in cellular networks [38–41].

More recently, the authors of [42] verified the accuracy of the Wyner model by considering both uplink and downlink transmissions. The authors utilized a pair of performance metrics in cellular systems, namely the outage and average throughput for evaluating the accuracy of the Wyner model. It was demonstrated that the Wyner model's parameter α can be accurately tuned for characterizing the key trends of both the uplink outage and the average uplink throughput, when

considering a sufficiently high number of simultaneous MTs. However, the Wyner model becomes inaccurate in the downlink analysis, even in the presence of numerous simultaneous MTs. The authors' conclusion [42] was that the Wyner model, which itself models the average interference conditions, can be adapted to the handling of mean-based metrics, such as the sum or the average of the throughput. By contrast, it became inaccurate in handling metrics that depend on the overall statistics of the intercell interference, such as the outage probability. However, the Wyner model is nonetheless capable of capturing the outage behavious of the CDMA uplink system in the presence of a sufficiently high number of simultaneous users, which is an explicit benefit of the law of large numbers.

We summarize the aforementioned history of the Wyner model used in analysing cellular networks in Table 2.1.

Year	Authors	Contributions
1994	Wyner [26]	Proposed a one-dimensional cellular network model for characterizing the capacity of the cellular uplink.
1997	Shamai and Wyner [30, 31]	Analysed the uplink throughput of cellular networks for both single-cell and twin-cell.
2001	Shamai and Zaidel [36]	Analysed the attainable average downlink rates in the high-SNR region of cellular networks by using Wyner model.
2006	Aktas *et al.* [34]	Derived the uplink sum capacity of cellular networks under the Wyner model relying on MIMO transceivers.
2007	Somekh *et al.* [37]	Proposed a modified Wyner model, where the cells are assumed to be arranged on a circle.
2010	Kaltakis *et al.* [35]	Extended the Wyner model by considering of the effects of shadowing.
2011	Xu *et al.* [42]	Verified the accuracy of the Wyner model by considering both uplink and downlink transmissions.

Table 2.1: Brief history of the Wyner model and of the research inspired by it in analysing cellular networks.

2.1.2 Grid-based Network

Recall from Eq. (2.1)-Eq. (2.4) that, the Wyner model only considers the interference arriving from two adjacent cells, where the users are randomly located and the path loss is ignored. Hence

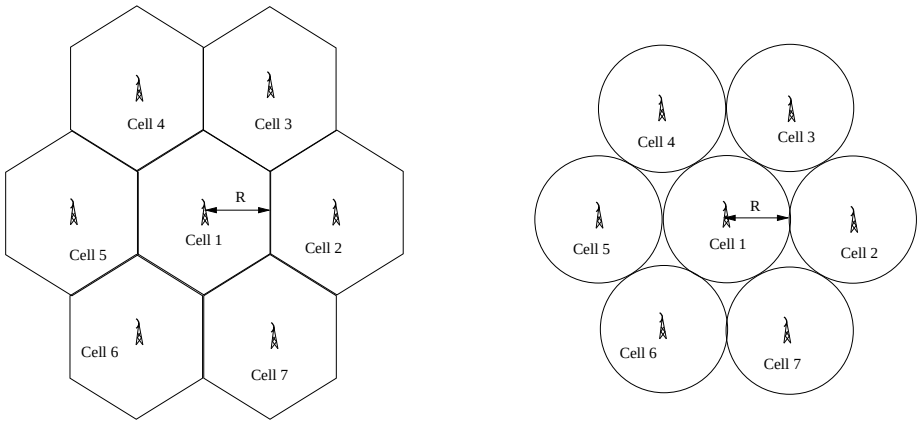

Figure 2.4: Regular grid based cellular networks.

the Wyner model is quite inaccurate in capturing the random position of MTs, especially during downlink transmissions. Practising systems engineers and researchers need more realistic models relying on a 2-D network of BSs positioned on a regular hexagonal grid, or slightly more simply, on a regular grid of circles, as seen in Fig. 2.4. The BSs are regularly distributed and the coverage area of each BS is modelled either as a hexagon or as a circle.

In contrast to the Wyner model, here we do actively consider the path-loss effects between the BS and the MT. There are two main models conceived for characterizing the path loss, namely the empirical models and the site-specific model [23]. Empirical models are based on the statistical characterization of the received signal, while site-specific model rely on a certain physical basis as well as on a vast amount of data regarding the geometry and location of the buildings, etc.. Since these deterministic models may require an excessive amount of computations, most of the researchers invoke stochastic processes for modelling the wave-propagation. The simplest model for a transmission channel is the path loss, which is inversely proportional to the distance between the transmitter and the receiver [43, 44]. If we denote the distance from the transmitter to a receiver as d, the path-loss L is given by:

$$L = Ad^{-\gamma}, \tag{2.5}$$

where A is a function of carrier frequency f_c, and we assume that it is constant for all paths between a MT and a BS. Furthermore, γ is the Path Loss Exponent (PLE), which is typically in the range of 2 to 6 [43, 45]. It had been confirmed by measurements that the path-loss model of Eq. (2.5) is reasonably accurate for distances spanning from 1 to 20 km for BS antenna heights in exceed of 30 m in areas with little terrain profile variation [12]. Hence, this path loss model is reasonable for the family of conventional cellular networks. Empirical results have illustrated [45] that the specific value of A may be different for outdoor and indoor transmission channels. In this treatise, the empirical results of [46, 47] are employed, where the path-loss of the outdoor channel is $A_{out} = \frac{f_c^{3.326}}{10^{7.986}}$ and that of the indoor channel is $A_{in} = 10^{3.7}$, respectively. Furthermore, the multi-path

fading effects will also be taken into account, which are modelled by uncorrelated Rayleigh fading model. In conclusion, the wireless radio frequency channel is subject to the path loss, as well as the uncorrelated Rayleigh fading having a unity average power. When considering a typical CDMA system, in contrast to the Wyner model, we should consider the interference emanating from all cells around the serving cell. Again, it is assumed that the MT set in cell n and the kth MT in cell n are denoted by $\mathcal{K}_n$ and k_n, respectively. As a result, the received uplink signal Y_n at cell n is given by:

$$Y_n = \sum_{k_n \in \mathcal{K}_n} \sqrt{P_{n,k_n} L_{n,k_n} h_{n,k_n}} X_{n,k} + \sum_{n' \neq n} \sum_{k_{n'} \in \mathcal{K}_{n'}} \sqrt{P_{n',k_{n'}} L_{n,k_{n'}} h_{n,k_{n'}}} X_{n',k_{n'}} + Z_n, \quad (2.6)$$

where L_{n,k_n} and h_{n,k_n} denote the path loss of the channel spanning from the transmitter (MT k_n) to the BS receiver in cell n as represented by Eq. (2.5) and the uncorrelated Rayleigh fading channel between the transmitter of MT k_n to BS n, respectively. Similarly, the signal Y_{n,k_n} received at MT k_n in cell n in the downlink, is written as:

$$Y_{n,k_n} = \sqrt{P_{n,k_n} L_{n,k_n} h_{n,k_n}} + \sum_{n' \neq n} \sqrt{P_{n',k_{n'}} L_{n',k_n} h_{n',k_n}} X_{n',k_{n'}} + Z_{n,k_n}. \quad (2.7)$$

Although the 2-D grid based network model is capable of capturing the random locations of MTs by considering the path-loss, the ICI represented by the second term of Eq. (2.6) and Eq. (2.7) remains a challenge to model accurately, owing to the sum of infinite variables.

The first analysis on the ICI was provided by Cooper and Nettleton in [48]. The paper studied the uplink of a frequency-hopped system and analysed the performance of this system in terms of its Signal to Interference Ratio (SIR). The total interference imposed by a cell other than the desired one was calculated by integrating the interference expression by considering a continuous and uniform geographic distribution over a circular region approximating a hexagonal cell. However, the analytic results derived in [48] was only for restricted values of the PLE and hence the authors used numerical integration for calculating the interference levels. Later, this integral based approach was also used for analysing other systems, such as the DS-CDMA system [49], where the PLE γ was fixed to be 4 and the circular cellular layout was assumed. An extension of [48] was published in [50] which included the effects of shadowing. The uplink of a CDMA system was considered and the propagation loss from a MT to a BS was subject to both path-loss and lognormal shadowing. The total interference encountered in the presence of lognormal shadowing is a random variable which is approximated by a Gaussian distribution, which was also assumed in [51]. Another analytical approximation of the ICI under the fixed SIR power control mechanism was presented in [52], where an iterative method was proposed for determining the ICI distribution, which was shown to obey a log-normal distribution in the scenario investigated. When considering a practical power control mechanism designed for maintaining a constant SINR, the ICI was characterized in [53, 54], where the SIR of each MT was considered to be identical. The authors of [55] relied on numerical integration approach for analysing the interference in DS/CDMA cellular networks, where the interference imposed by the grey shaded area of Fig. 2.5 was considered. By

contrast, the interference arriving from outside of the grey area was ignored. Then this analytical model was used for characterizing a call admission control scheme [55].

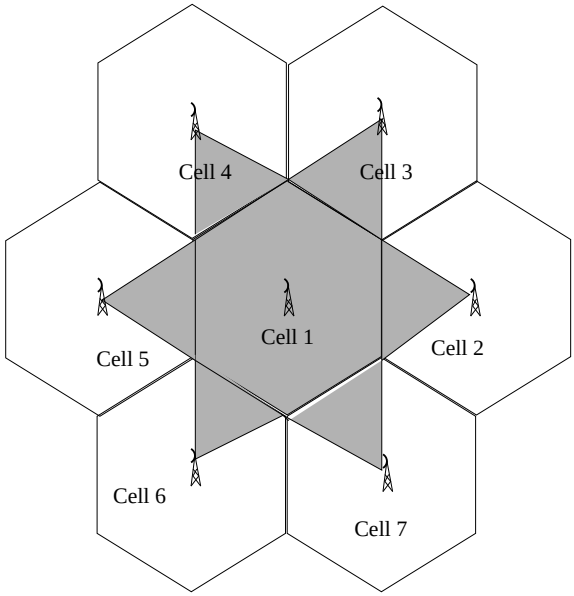

Figure 2.5: A regular grid based cellular network, where the interfering area is denoted by the grey shade [55].

The authors of [56] considered the effects of shadowing and analytically derived an upper bound expression for the ICI factor, defined as the ratio of inter-cell interference to the intra-cell interference. This parameter can be conveniently used in cellular planning calculations. In [57], specific values of the ICI factor were derived by simulations for diverse practical according scenarios, which were also compared to the upper bound of the ICI factor derived in [56]. The randomness of user location within a cell was then considered in [45], where the distribution of the interference arriving from a randomly located MT in another cell of the network was derived. As a further advance, the authors of [58] investigated the effect of mobile locations on the Erlang cell capacity using a simulation approach. The performance analysis of the uplink in a multi-cellular MIMO systems was studied in [59], where the distribution of the intra-cell interference was approximated by the Gamma distribution, while the ICI was calculated by numerical integration.

Turning to the downlink channel, the authors of [60] considered the downlink of orthogonal resource based multiple access systems, such as the downlink of a Time Division Multiple Access (TDMA) system or the downlink of an Orthogonal Frequency Division Multiple Access (OFDMA) system. As a result, the intra-cell interference was entirely avoided. It was assumed in [60] that the path-loss between an interfering BS and the target MT was a fixed value, which was equal to the inter-cell interference intensity α. As a result, if we assume that the target MT k_n is in cell n, we have $L_{n',k_n} = \alpha L_{n,k_n}$, $\forall n' \neq n$. This approach is capable of reducing the complexity of calculating the sum of the ICI and the results become tractable. However, similar to the Wyner model,

this approach does not take the randomness of MT locations into account. Hence this approach is inaccurate in downlink analysis. Later, the authors of [61] extended this approach to the analysis of the ICI in multiple-antenna aided broadcast channels. Then, the sum rate of random beamforming was derived for downlink multiple-antenna aided systems in the presence of ICI, for a large number of MTs.

Then, in contrast to the ICI factor based approach used in [60, 61], Kelif et al. proposed a 'Fluid Model' [20, 62, 63] for characterizing the ICI in the downlink of cellular systems, where the discrete BSs of the cellular networks were modelled as a continuum. The outage probability of downlink transmissions in an Orthogonal Frequency Division Multiple Access (OFDMA) system was derived in [62]. The simulation results illustrated the reasonable accuracy of the 'Fluid Model' in characterizing the downlink ICI. Hence, in this treatise, the 'Fluid Model' is used for analysing the performance of cellular networks. Therefore, we will introduce the principles of the 'Fluid Model' in the following.

2.1.3 The Fluid Model of Inter-Cell-Interference

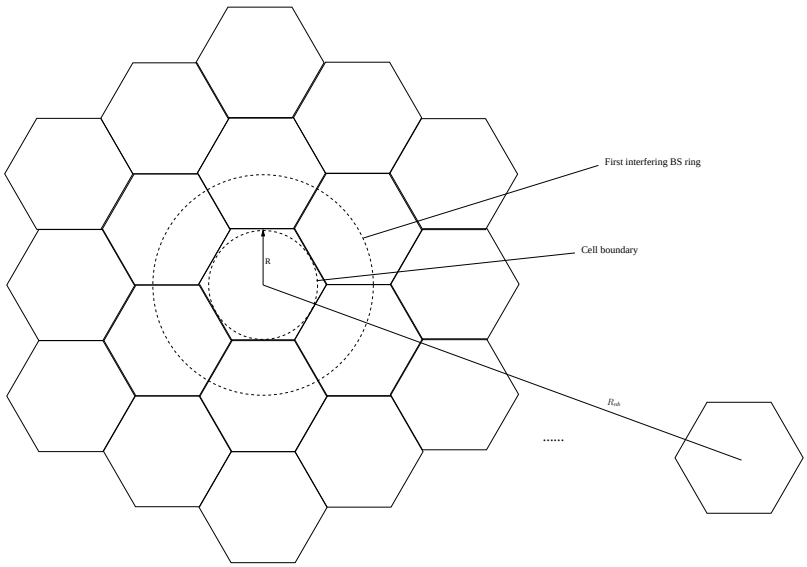

Figure 2.6: A Hexagonal cell-based network, where the Fluid Model is used for analysing the downlink interference.

The key characteristic of the Fluid Model is that it replaces a given finite number of interfering BSs by an equivalent continuum of BSs, which are spatially distributed in the network. Since the BSs are regularly located in the classic grid-based networks, it is reasonable to assume having spatially distributed BSs. We consider a regular hexagonal grid based cellular network, where each BS is located in the centre of a hexagonal, as seen in Fig. 2.4. As a result, the density of BSs ρ_{BS}

may be expressed as: $\rho_{BS} = \frac{\sqrt{3}}{6R^2}$ [1]. Let us consider a MT u at a distance d_u from its serving BS. Then the power of the received signal P_r may be written as $P_r = P_t A d_u^{-\gamma}$. Given a distance z from MT u, the area of the elementary surface may be formulated as $zdzd\theta$. Hence, the equivalent number of the interfering BSs is $\rho_{BS} zdzd\theta$ and their contribution to the downlink interference is given by $P_t A z^{-\gamma} \rho_{BS} zdzd\theta$. For analytical convenience, the cell boundary is approximated as the circle, which is represented by the inner circle printed in dashed line in Fig. 2.6. The first-tier of interfering BSs is represented by the outer circle printed in dashed line in Fig. 2.6. Then the distance from the first-tier of interfering BSs to the MT u is $2R - d_u$. We also assume that the network boundary is characterized by a ring of BSs at a distance of r_{nb} and hence the distance from the network boundary BSs to the MT u is $(R_{nb} - d_u)$. The MT u may suffer from the interference imposed by the BSs located in the first BS ring of Fig. 2.6. Then, the total downlink interference I_{dl} received by a MT at a distance d_u may be written as:

$$\begin{aligned} I_{dl} &= \int_0^{2\pi} \int_{2R-d_u}^{R_{nb}-d_u} P_t A z^{-\gamma} \rho_{BS} z dz d\theta \\ &= \frac{2\pi P_t A \rho_{BS}}{\gamma - 2} \left[(2R - d_u)^{2-\gamma} - (R_{nb} - d_u)^{2-\gamma} \right]. \end{aligned} \tag{2.8}$$

Since the PLE γ may be larger than 2 in practical scenarios and the network boundary radius R_{nb} tends to infinity, then the Eq. (2.8) may be further approximated by:

$$I_{dl} = \frac{2\pi P_t A \rho_{BS}}{\gamma - 2} (2R - d_u)^{2-\gamma}. \tag{2.9}$$

As a result, the signal to interference ratio (SIR) may be approximated by:

$$SIR = \frac{(\gamma - 2)\, d_u^{-\gamma}}{2\pi \rho_{BS} (2R - d_u)^{2-\gamma}}. \tag{2.10}$$

Let us now verify the accuracy of Fluid Model in approximating the downlink received SIR. The simulator assumes having a regular hexagonal network constituted by several rings around a central cell. Fig. 2.7 illustrates the SIR of a target MT as a function of the distance from the MT to the serving BS, when we assume that the transmission power P_c equals to $46dBm$, the carrier frequency is 2GHz and the radius of the cell is 1 km. Observe from Fig. 2.7 that as expected, the SIR of the target MT decreases when this MT moves away from the serving BS. The SIR of the MT becomes higher, when the PLE γ is higher, because the desired signal's link is always shorter than the interfering link. It is clear that Eq. (2.10) derived by the Fluid Model is quite accurate for all the considered. Hence, the Fluid Model is capable of tracking the characteristical of the downlink ICI quite accurately. Later, Kelif *et al.* extended the Fluid Model to sectored wireless networks in [64], where the outage probability was validated by Monte Carlo simulations. In [65, 66] the effects of log-normal distributed shadowing were considered relying on the Fluid Model.

Similar with the Section 2.1.1, we summarize the key contributions on analysing the ICI using the grid-based model in cellular networks in the context of Table 2.2 and Table 2.3

[1] In the Chapter 3, we will simplify our macrocell model as the circle model, as a result the density of BSs ρ_{BS} equals to $\frac{1}{\pi R^2}$.

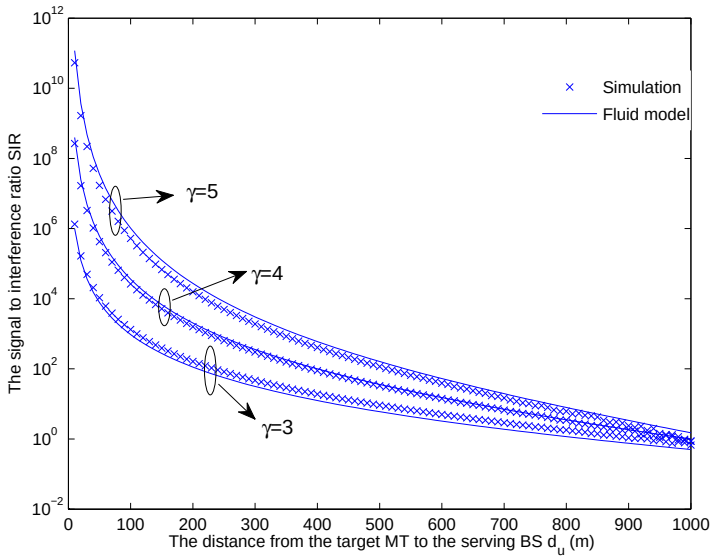

Figure 2.7: The SIR of a target MT versus the distance between the serving BS and the target MT, for the cell radius of $R = 1km$.

2.1.4 The Stochastic Geometry Based Poisson Point Process Model

Instead of assuming the regular grid based macrocell BSs, the network is now assumed to obey a convenient Poisson point process (PPP) which captures the network properties. In probability theory, a PPP is defined as a particular random process characterizing a set of isolated points scattered along a line or across a Two-Dimensinal (2-D) plane or in a Three-Dimensional (3-D) space, where the number of points within any compact set is a Poisson distributed random variable and the numbers of points in disjoint sets are independent of each other [67]. As a result, the cellular network model consists of BSs arranged according to a homogeneous PPP Υ of intensity λ in the Euclidean plane [27]. Fig. 2.8 illustrates a realization of a PPP based network in a 20km $\times$ 20km region having an intensity of 0.2 points/km^2, where the dots denote the macrocell BSs. Hence, the total number of BSs is a variable, with its expectation value being equal to $400 \times 0.2 = 80$. Assuming that the MTs are only associated with the nearest Bs, the cell boundaries are shown, which forms a Voronoi diagram in Fig. 2.8.

The stochastic geometry based approach conceived for cellular network BS modelling has been considered as early as 1997 [68], where two independent Poisson processes representing the MTs and the BSs were considered. However, the key metric constituted by coverage has not been investigated. Subsequently, the PPP based abstraction model was also advocated in [69], and it was shown that the PPP model results in lower bounds of the attainable cellular performance, while the traditional hexagonal systems provide an upper performance bound. The PPP model of the BS positions of the BSs has been attracting more and more attention. In [27], PPP model based cel-

Year	Authors	Contributions
1978	Cooper and Nettleton [48]	Analysed the performance of an uplink frequency-hopped system, where the total ICI is calculated by integrating the interference expression considering a continuous and uniform user density over a circular region.
1991	Gilhousen *et al.* [50]	Extended the contribution of [48] by considerating the effects of lognormal shadowing.
1994	Viterbi *et al.* [56]	Obtained an upper bound for the uplink ICI factor, which denotes the ratio of ICI to intra-cell interference.
1999	Evans and Everitt [45]	Derived the distribution function of the uplink interference imposed by a randomly located mobile terminal in a interfering macrocell. Hence, the effects of random user locations within a cell were studied.
2001	Ho *et al.* [55]	Proposed an alternative approach for calculating the ICI, where only the interference emerging from the most significant interference area is taken into account.
2002	Staehle *et al.* [52]	Proposed an iterative method for approximating the uplink ICI under a power control mechanism.
2003	Elayoubi *et al.* [51]	Extended the contribution of [50], and the total interference was approximated by a Gaussian distribution.

Table 2.2: Brief history of the analysis of ICI for cellular networks using grid-based model: Part I.

lular networks were analysed, where a comprehensive framework was conceived for deriving the coverage and the average rate of single-tier cellular networks under the assumption that the downlink channel was subject to Rayleigh fading. Recently, the validation of the PPP model for real BSs deployments was provided in [70], where the actual locations of the BSs were collected from Ofcom, the independent regulator and competition authority in the UK. The authors applied the maximum pseudo-likelihood goodness-of-fit technique to fit them to show that the PPP model was as accurate as the regular grid model [71]. Inspired by these results, numerous researchers started to use the PPP-based abstraction model for studying the cellular networks. The authors of [72] considered the PPP-based cellular networks and the associated handover probability. The effect of the BS density on the attainable downlink performance of PPP-based cellular networks was investigated in [73]. Later, the authors of [74] extended the contribution of [27] and the outage probability

Year	Authors	Contributions
2004	Kolahi *et al.* [57]	Used the method of [56] and the specific values of the ICI factor were derived by simulations for diverse scenarios.
2006	Tokgoz and Rao [59]	Analysed the uplink performance of multi-cellular MIMO systems, where the distribution of the intra-cell interference is approximated by the Gamma distribution and the inter-cell interference is calculated by numerical integration.
2007	Kim *et al.* [60]	Analysed the downlink performance of cellular networks. The path loss between the serving BS and the target MT which was equal to the inter-cell interference intensity α.
2007	Kelif *et al.* [20, 63]	Proposed a 'Fluid Model' for characterizing the ICI in the downlink cellular, where the discrete BSs of the cellular networks were replacing by an equivalent continuum of BSs.
2008	Kelif *et al.* [64]	Extended the 'Fluid Model' to sectored wireless networks, where the outage probability was validated by the Monte Carlo simulations.
2009	Kelif *et al.* [66]	Evaluated the effects of log-normal distributed shadowing relied on 'Fluid Model'.
2011	Moon *et al.* [61]	Extended the approach of [60] for analysing the downlink ICI in multiple-antenna broadcast channels.

Table 2.3: Brief history of the analysis of ICI for cellular networks using grid-based model: Part II.

was derived under the consideration of the user density. In order to mitigate the ICI, the authors of [75, 76] studied the benifit of interference coordination in PPP-based cellular networks, where a random clustering model was proposed and each cluster exploited the intercell interference nulling technique. More recently, the authors of [77] considered MIMO-aided cellular networks, where the macrocells were subject to the PPP model. The average error probability of PPP based cellular networks was analysed therein. Turning our attention to the uplink, the coverage probability was derived for a randomly chosen mobile user relying on power control in [78]. The brief history of the PPP model used in analysing cellular networks is summarized in Table 2.4.

Although the interference statistics can not be readily obtained, the exact distribution of $\mathrm{SIR}_{i,j}$ is obtainable, upon assuming the presence of Rayleigh fading on the downlink. Then we will present the technique of analysing the cellular network performance, relying on PPP-based ab-

Year	Authors	Contributions
1997	Baccelli *et al.* [68]	Proposed the stochastic geometry based approach for cellular network modelling, where the MTs and BSs were modelled as two independent Poisson processes.
2000	Brown [69]	Proposed the PPP based abstraction model.
2011	Andrews *et al.* [27]	Analysed the downlink PPP model based cellular networks, where the coverage and the average rate of downlink cellular networks was derived.
2012	Vu *et al.* [72]	Evaluated the handover probability of PPP model based cellular networks.
2012	Lee *et al.* [73]	Analysed the optimal tradeoff between the performance gain by increasing the BS density and the resultant network cost accounting for energy consumption, BS hardware and backhaul cables.
2013	Yu and Kim [74]	Extended the contribution of [27] by considering thes effect of user density.
2013	Akoum and Heath [76]	Investigated the interference coordination in PPP-based cellular networks, where a random clustering model was proposed and each cluster exploited intercell interference nulling technique.
2013	Renzo and Guan [77]	Analysed the downlink performance of the multi-cellular MIMO systems, where the average error probability of PPP based cellular networks is derived.
2013	Novlan *et al.* [78]	Derived the uplink coverage probability for a randomly chosen MT with power control in PPP model based cellular networks.

Table 2.4: Brief history of the PPP model used in analysing cellular networks.

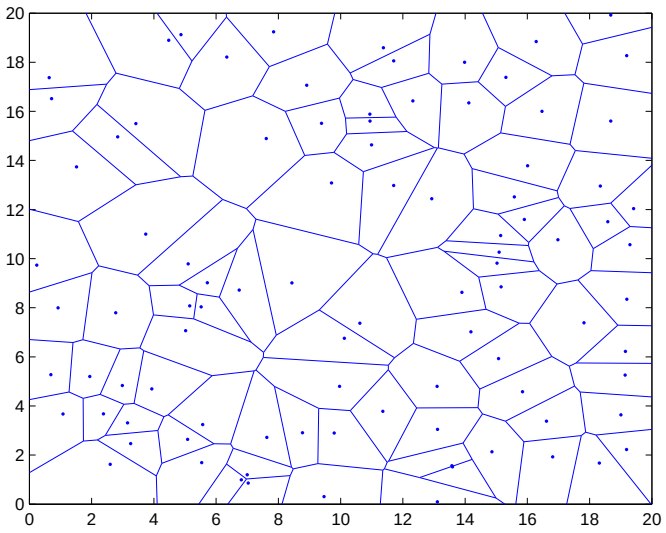

Figure 2.8: PPP based network in a 20km×20km region with intensity 0.2 point/km^2. The macrocell BSs are denoted by the dots and the cell boundaries are constituted by a Voronoi diagram.

straction model.

Consider the cellular network model illustrated in Fig. 2.8, where the BSs are arranged according to a PPP Υ of intensity λ, while each of the MTs is associated with the closest base station. We assume that the cellular BS set is denoted as Φ. The downlink channel is subjected to uncorrelated Rayleigh fading having a unity average power and the path-loss. Then the power P_r received at a MT at a distance of r from its BS is $P_t A h r^{-\gamma}$, where the random variable h follows an exponential distribution with unity mean. The SIR of the target MT i served by BS j is formulated as:

$$\text{SIR}_{i,j} = \frac{h_{i,j} r_{i,j}^{-\gamma}}{\sum_{k \in \Phi/j} h_{i,k}^2 r_{i,k}^{-\gamma}}. \tag{2.11}$$

Then, the cumulative distribution function (CDF) of $\text{SIR}_{i,j}$ may be written as:

$$\begin{aligned} F_{\text{SIR}_{i,j}}(\theta) &= \mathbb{P}\left(\text{SIR}_{i,j} \leq \theta\right) \\ &= \mathbb{P}\left(\frac{h_{i,j} r_{i,j}^{-\gamma}}{\sum_{k \in \Phi/j} h_{i,k} r_{i,k}^{-\gamma}} \leq \theta\right) \\ &= \mathbb{P}\left[h_{i,j} \leq \theta r_{i,j}^{\gamma} \left(\sum_{k \in \Phi/j} h_{i,k} r_{i,k}^{-\gamma}\right)\right]. \end{aligned} \tag{2.12}$$

We assume that $I = \sum_{k \in \Phi/j} h_{i,k} r_{i,k}^{-\gamma}$. Exploiting the fact that h follows an exponential distribution

with unity mean, as a result, Eq. (2.12) may be rewritten as:

$$\begin{aligned} F_{\mathrm{SIR}_{i,j}}(\theta) &= \mathbb{P}\left(h_{i,j} \leq \theta r_{i,j}^{\gamma} I\right) \\ &= 1 - \mathbb{P}\left(h_{i,j} \leq \theta r_{i,j}^{\gamma} I\right) \\ &= 1 - \int_{-\infty}^{\infty} \mathbb{P}\left(h_{i,j} \leq \theta r_{i,j}^{\gamma} I \mid I\right) f_I(I)\, dI \\ &= 1 - \mathbb{E}_I\left[\mathbb{P}\left(h_{i,j} \leq \theta r_{i,j}^{\gamma} I \mid I\right)\right] \\ &= 1 - \mathbb{E}_I\left[\exp\left(-\theta r_{i,j}^{\gamma} I\right)\right] \\ &= 1 - \mathcal{L}_I\left(-\theta r_{i,j}^{\gamma}\right), \end{aligned} \tag{2.13}$$

where $f_I(I)$ denotes the Probability Density Function (PDF) of the variable I, and $\mathcal{L}_I$ represents the Laplace transform of the variable I, which may be expressed as:

$$\begin{aligned} \mathcal{L}_I\left(-\theta r_{i,j}^{\gamma}\right) &= \mathbb{E}_I\left[\exp\left(-\theta r_{i,j}^{\gamma} I\right)\right] \\ &= \mathbb{E}_{\Phi,|h_{i,k}|^2}\left[\exp\left(-\theta r_{i,j}^{\gamma} \sum_{k\in\Phi/j} h_{i,k} r_{i,k}^{-\gamma}\right)\right] \\ &= \mathbb{E}_{\Phi,h_{i,k}} \prod_{k\in\Phi/j} \exp\left(-\theta r_{i,j}^{\gamma} h_{i,k} r_{i,k}^{-\gamma}\right) \\ &\overset{a}{=} \mathbb{E}_{\Phi} \prod_{k\in\Phi/j} \mathbb{E}_h\left[\exp\left(-\theta r_{i,j}^{\gamma} h r_{i,k}^{-\gamma}\right)\right] \\ &\overset{b}{=} \exp\left[-\lambda \iint_{\mathbb{R}} \left(1 - \mathbb{E}_h\left[\exp\left(-\theta r_{i,j}^{\gamma} h r^{-\gamma}\right)\right] r dr\right)\right], \end{aligned} \tag{2.14}$$

where the equality of (a) follows from the i.i.d. distribution of $|h_{i,k}|^2$ and from its further independence of the point process Φ. The equality of (b) follows from the Probability Generating Functional (PGFL) [79] of the PPP and the integration region $\mathbb{R}$ denotes the interfering region. Then the Laplace transform of the variable I may be rewritten as:

$$\begin{aligned} \mathcal{L}_I\left(-\theta r_{i,j}^{\gamma}\right) &= \exp\left[-2\pi\lambda \int_0^{\infty} \left(1 - \int_0^{\infty} \exp\left(-\theta r_{i,j}^{\gamma} r^{-\gamma} x\right) \exp(-x)\, dx\right) r dr\right] \\ &= \exp\left[-2\pi\lambda \int_0^{\infty} \left(1 - \frac{1}{1 + \theta r_{i,j}^{\gamma} r^{-\gamma}}\right) r dr\right] \\ &= \exp\left[-\pi\lambda C_{\gamma} r_{i,j}^2 \theta^{\frac{2}{\gamma}}\right], \end{aligned} \tag{2.15}$$

where we have $C_{\gamma} = \int_0^{\infty} \frac{1}{1+s^{\frac{\gamma}{2}}} ds$. As a result, the CDF of $\mathrm{SIR}_{i,j}$ is given by:

$$F_{\mathrm{SIR}_{i,j}}(\theta) = 1 - \exp\left[-\pi\lambda C_{\gamma} r_{i,j}^2 \theta^{\frac{2}{\gamma}}\right]. \tag{2.16}$$

Recall from Eq. (2.16) that the CDF of a MT's SIR, assuming a distance $r_{i,j}$ from the serving BS, is subject to the BS density of PPP based abstraction model and the outdoor PLE.

Having introduced the above three modelling methods of traditional cellular networks, we will then shift our attention to the emerging subject of small-cell techniques, which have shorter transmission link, lower transmission power and hence tend to provide higher network capacity.

2.2 Introduction of Femtocell

Both the topology and architecture of cellular networks are undergoing a major paradigm shift from being voice-centric, circuit switched and centrally optimized for coverage towards becoming data-centric, packet switched and capacity-oriented [80]. The traditional methods of increasing the amount of spectrum or deploying more macro base stations may fail to keep pace with the data explosion. One of the effective techniques of improving the coverage and enhancing the capacity and data rate in cellular wireless networks is to reduce the cell size and hence the transmission distance. In recent years, enormous gains have been reaped from the efficient spatial reuse of the spectrum by increasing the higher area spectral efficiency. As a result, one of most logical trends emerging from the cellular evolution are constituted by femtocells [81, 82]. Femtocells are small and they are covered by inexpensive, low-power base stations that are generally consumer-deployed and connected to the operators, core network through the users' Digital Subscriber Line (DSL), optical fibre or cable broadband internet connection [80,81,83]. A typical femtocell is shown in Fig. 2.9, where different femtocell subscribed MTs are capable of connecting to the femtocell access point for both uplink and downlink service provision. In the following, we will firstly introduce the brief history of femtocells, then the modelling methods for femtocells are highlighted, followed by the technical challenges and existing solutions.

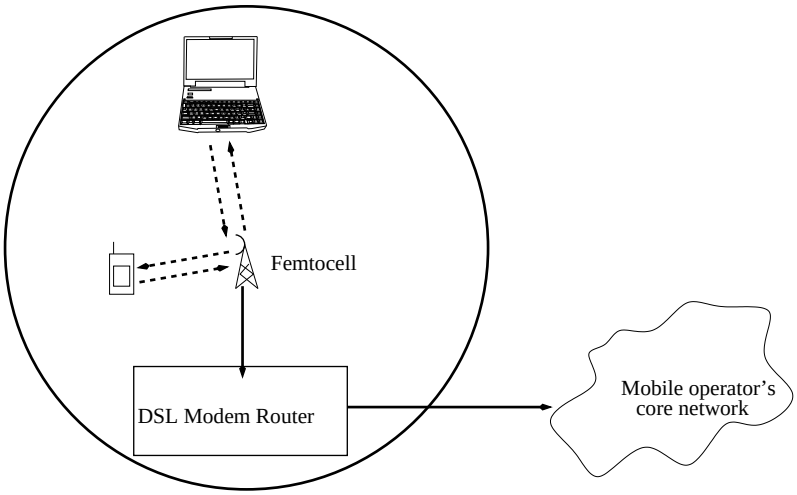

Figure 2.9: A typical femtocell

2.2.1 Brief History of Femtocells

The concept of femtocells evolved from the idea of small cells, where a macrocell would be split into a number of smaller cells having a reduced transmit power and a radius of perhaps a few hundred meters [84]. The birth of contemporary femtocells emerged in the early 1990s, when South-

west Bell and Panasonic developed an indoor femtocell solution that reuses the same spectrum as the macrocells [85]. Later, Alcatel announced a Global System for Mobile Communications (GSM) based home base station to be brought to the market in 2000 [86]. In recent years, different types of femtocells have been developed and promoted based on various air interface technologies, services, standards and access control strategies. For example, 3G femtocells use the Wideband Code Division Multiple Access (WCDMA) based air interface of Universal Mobile Telecommunication System (UMTS), which is also referred to as the UMTS Terrestrial Radio Access (UTRA). These femtocells are capable of communicating through IP based networks, which make it more applicable to femtocells. More recently, the Worldwide Interoperability for Microwave Access (WiMAX) and Long Term Evolution (LTE) femtocells opted for OFDMA as their physical layer technology. These femtocell are capable of providing a variety of high data rate services for the MTs [87] and the LTE femtocells are referred to as Home evolved Node BSs (HeNBs) [88]. In 2007, the Femto Forum (now called Small cell Forum) [89] was formed in order to promote the standardisation and wide scale deployment of femtocells all around the world. It accelerates small cell (femtocell) adoption in order to change the shape of mobile networks and to maximise the potential of mobile services. It is predicted that the future LTE and LTE-A networks would rely on femtocells for the provision of high-quality indoor cellular coverage. As a result, femtocells are likely to be deployed on a large scale in the near future.

2.2.2 Femtocell Network Modeling

The femtocells are overlaid onto the traditional cellular macrocells, hence, forming a two-tier cellular network. The addition of femtocells requires an evolution of the traditional cellular model. Generally, four two-tier cellular network modelling approaches have been deployed [80]. We will then briefly introduce these approaches.

The first model simply consider all the channel gains (including those of the interfering channels), without specifying the precise spatial model for the various BSs [90–93]. This model simplifies the channel model of the two-tier cellular network and may invoke game theory, power control and resource allocation. In some studies [90, 91], these channel gains obey Rayleigh distribution and to a first order they are determined by the locations of the transmitting sources. However, this model is inaccurate for system performance analysis, since the path-loss is inaccurately modelled.

The second approach assumes that a single femtocell is dropped in a single macrocell [94–96], which leads to a fairly sparse femtocell deployment, as seen in Fig. 2.10. In the downlink, the interference imposed on the femtocell MTs is assumed to be arriving only from the traditional macrocell BSs, while the interference between the femtocells is neglected. In the uplink, the interference is bound to come impinge neighbouring MTs transmitting to the macrocell BSs. The main limitation of this model is that the performance of macrocell MTs may not be accurately characterized, because both the femtocell interference and the inter-cell interference imposed by other macrocells is

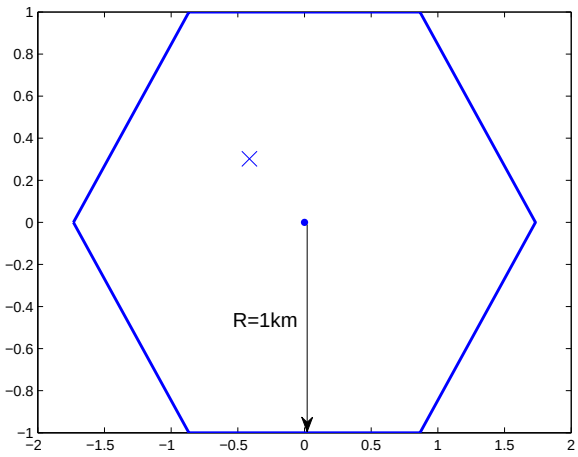

Figure 2.10: A single femtocell BS is 'dropped' in a single hexagonal macrocell, where the radius of the macrocell is 1km. The macrocell BS and the femtocell BS are denoted by the dot and the cross, respectively.

ignored, even though in practice the macrocell MTs' performance is significantly affected by the interference generated by the femtocell.

Another approach is to assume the regular grid model for macrocell BSs, and assume that the femtocells are randomly placed within the macrocells [97–103], as shown in the Fig. 2.11. In the downlink, the interference imposed on the femtocell MTs emerges from both the macrocells and the neighbouring femtocells. The interference inflected upon the macrocell MTs emerges from both the neighbouring macrocells and the neighbouring femtocells. Similarly, in the uplink, the interference measured at the femtocell BSs arrives from both the neighbouring marcocell MTs and the neighbouring femtocell MTs. This model is capable of characterizing the interference of this two-tier cellular network.

The fourth model assumes that both the macrocells and femtocells are randomly placed. More specifically, both the macrocell BSs and the femtocells are assumed to be PPP based [104–108]. Fig. 2.12 illustrates this model. An appealing aspect of this approach is that the random locations of the femtocells actually allows significantly improved mathematical tractability and the SINR distribution can be found explicitly [80]. This may allow the fundamental impact of different PHY and MAC designs to be theoretically evaluated in the future.

2.2.3 Technical Challenges in Femtocells

The deployment of femtocells will economically benefit both end-users and network operators. On the one hand, the end users accessing femtocells can achieve an improved signal quality owing to

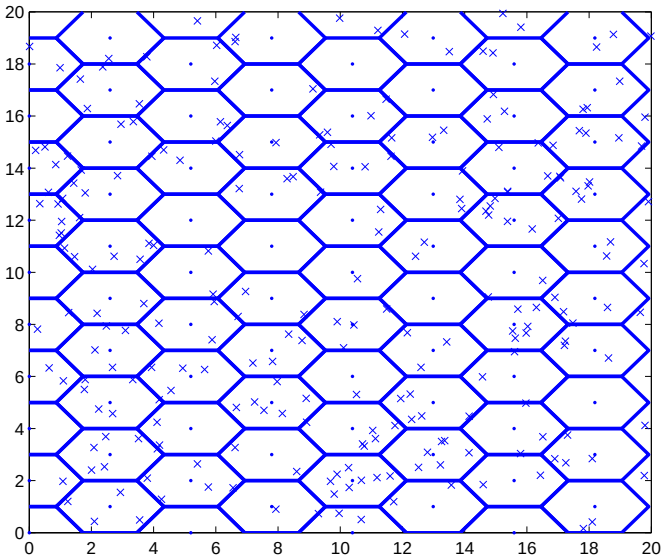

Figure 2.11: The PPP model based femtocell BSs are randomly distributed across the regular hexagonal macrocell BS grid in a 20km $\times$ 20 km region, where the intensity of the femtocell BS deployment is 0.6 point/km^2. The macrocell BSs and the femtocell BSs are denoted by the dots and the crosses, respectively.

the reduced transmit-receive distance. On the other hand, from the operators' point of view, femtocells will improve the indoor coverage, hence conveying a large amount of indoor traffic. Having good channel conditions enables the femtocells to provide high data rate services for the users by using higher-throughput modulation and coding schemes. Furthermore, a femtocell usually serves a small number of users compared to a macrocell. Hence this enables the femtocells to provide a better QoS for their users, compared to the macrocells. From a business perspective, femtocells can provide an excellent platform for the operators to maximise their revenue and to increase their network capacity without any further investment in macro-cellular network upgrades. Furthermore, there would be no need to lease land for new BS sites and the electricity cost no longer affects the operators. These savings reduce the overall network costs.

However, femtocells also pose a number of design challenges related to the choice of access modes, mobility management, handovers, self-organisation, security and interference management, as depicted in Fig. 2.13. These challenges will be more important when the deployments of femtocells becomes denser in urban environments. In this section, we briefly discuss the above technical challenges.

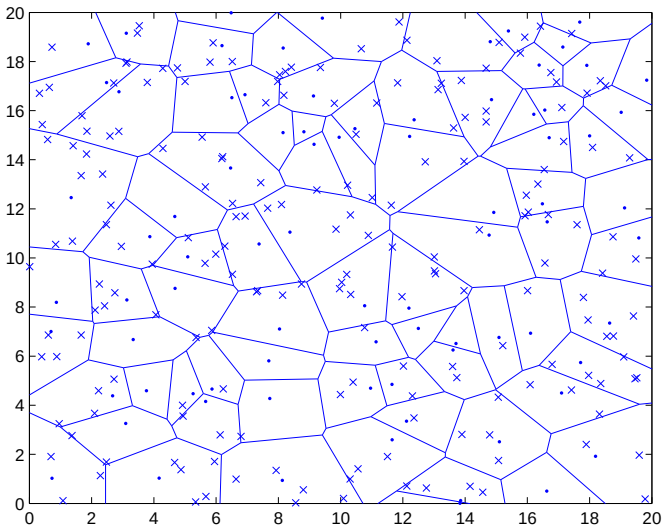

Figure 2.12: The PPP model based femtocell BSs are randomly distributed across the PPP model based macrocell BSs in a 20km $\times$ 20km region, where the intensity of the macrocell BSs and the femtocell BSs is 0.2 and 0.6 point/km^2, respectively. The macrocell BSs and the femtocell BSs are denoted by the dots and the crosses, respectively.

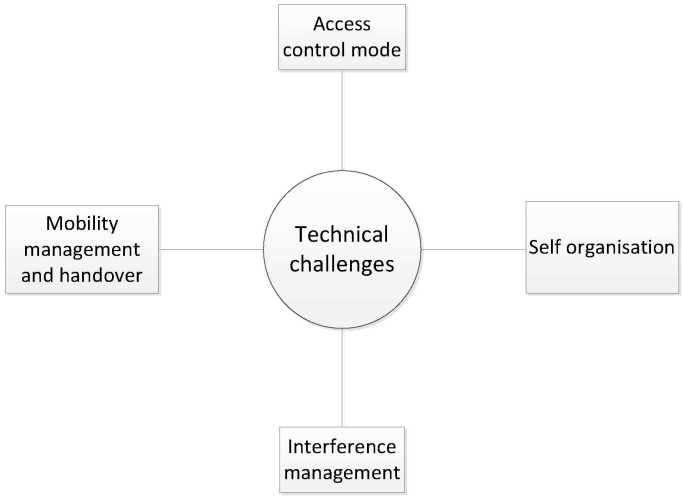

Figure 2.13: The key technical challenges in Femtocell systems.

2.2.3.1 Femtocell Access Control Mode

Femtocells are capable of supporting several MTs, and hence one of their important issue is the design of femtocell access control. Three popular access control modes have been defined in [81]: Open Access mode, Closed Access mode and Hybrid Access mode, which are described below:

- *Open Access mode*: In this mode, the MTs may unconditionally access the femtocell and all MTs are treated equally from a camping perspective and also from a charging perspective.
- *Closed Access mode*: This access control mode allows femtocell access to a restricted set of MTs, which is referred to as a Closed Subscriber Group (CSG). Normal service is only expected for the set of MTs belonging to the CSG.
- *Hybrid Access mode*: This access control mode only allows a limited amount of the femtocell resources to be assigned to all MTs. However, the MTs who are subscribed to the femtocell may be able to get preferential charging in comparison to users who are not subscribed to the cell.

In general, the choice of access modes has a direct impact on the interference in the system. The open access mode constitutes a superior approach from a network capacity point of view, and it provides the potential solution for sophisticated interference coordination.It was shown in [109] that the open access induced improves the overall capacity of the network, mainly because the macrocell users are capable of connecting to nearby femtocells, when its performance under the macrocell is deficient. However, this mode may complicate the handoff and security issues. Moreover, from the femtocell end users' view, the owner who purchased the femtocell access point and pays both for the back-haul and electricity, might not want its femtocell resources to be shared with everyone. As a result, the closed access mode is more likely to be deployed in the home environment. In this treatise, we assume that the indoor femtocells rely on the closed access mode, hence, only the subscribed MTs are capable of accessing their serving femtocell. Hybrid approaches allow the connectivity of non-subscribers with the explicit permission of femtocell subscribers, while restricting the amount of available resource. The femtocells may reserve part of the capacity for their subscribers. It has been shown in [110, 111] that the hybrid access mode is capable of providing an improved overall network performance while maintaining the QoS of the femtocell users. The comparison of these access modes was provided in [94, 112] for the uplink and downlink, respectively. More details on the access modes and on their impact were given in [113, 114].

2.2.3.2 Mobility Management and Handover

Since the coverage area of an individual femtocell is small and the deployment of femtocells may be unplanned, it would be impossible for a femtocell to keep track of its neighbours for supporting handovers. Hence, the provision of mobility management is one of the most challenging issues.

Handover scenarios may include femtocell-to-macrocell, macrocell-to-femtocell and femtocell to femtocell handovers. Although femtocells may rely on existing mobility procedures, a number of unique challenges arise that require special consideration. One of the most difficult aspect of femtocell mobility is that they are typically not directly connected into the core networks where the mobility procedures are usually coordinated. The lack of a low-delay connection to the core network may result in significant handover signalling delays.

The available literature studied various handover decision algorithms for the two-tier macrocell-femtocell network [115–123]. More specificity, the handover mechanisms between macrocells and femtocells based on the signal strength were proposed in [115–117, 120]. The handover decision algorithms were adjusted according to the traffic-type criteria in [118, 119]. Furthermore, handover algorithms based on the velocity of MTs were conceived in [121–123]. A summary of mobility management and handover solutions is provided in [124].

2.2.3.3 Self Organisation

Since femtocells are installed by end users or private enterprises often in an *ad hoc* manner and the locations of femtocells can with vary time, this makes the traditional network planning and tools designed for configuring and optimising a femtocell network unusable. As a result, the femtocells have to be able to self-configure and optimise without importing a substantial impact on the existing cellular system. Due to these features, femtocells are also referred to as a specific type of Self-Organised Network (SON) [82].

Numerous efficient self-organization techniques have been designed for femtocell networks. In [125] a coverage adaptation technique was proposed for femtocell deployments in UMTS networks that exploited the knowledge of mobility events of indoor users for optimizing the femtocell coverage. Each femtocell sets its transmission power to a value that on average minimizes the total number of attempts of roaming users to connect to such a femtocell. The results illustrated that the self-optimization technique was capable of improving the indoor coverage for femtocells and resulted in a reduced number of 'mobility events' in the core network. An efficient self-organisation approach was proposed in [126] for OFDMA femtocell networks, where the femtocells were capable of dynamically sensing the air interface and of tuning the sub-channel allocation. This approach provides a good solution for the sub-channel assignment problem. Similarly, the related power control and channel assignment allocation problems were considered and solved based on self-organisation approaches in [106, 127–129]. The authors of [130] investigated the benefits of femtocell placement optimization. A range of researchers also considered the benefits of having cognitive capabilities for the femtocells that were able to dynamically sense the prevalent spectrum usage by the macrocell and carefully adapt their transmissions for optimizing the overall usage of the spectrum [96, 131, 132]. However, purely cognitive approaches are known to exhibit low convergence speeds and precision [80]. As the number of femtocells increases, the problem of

self-organisation would become more challenging and hence the community needs more research in this area.

2.2.3.4 Interference Management

Perhaps one of the most significant challenges imposed by the dense deployment of femtocells is the possibility of stronger, and less predictable interference. Basically, there are two main modes of femtocell deployment: the orthogonal channel deployment and the co-channel deployment [133]. In the orthogonal channel deployment, a unique channel is allocated for the femtocells, which is a dedicated channel and hence it is not used by the macrocell MTs. However, in the co-channel deployment, the femtocells may reuse the same spectrum as the macrocells. Due to the high cost of licensed spectrum, the co-channel deployment is much favoured by the operators. As a result, there is a risk that the macrocell and femtocell MTs impose interference on each other. Fig. 2.14 illustrates the interference scenario in a two-tier macro-femto network for the uplink and downlink, where the solid lines denote the desired signal, while the dashed lines represent the interference.

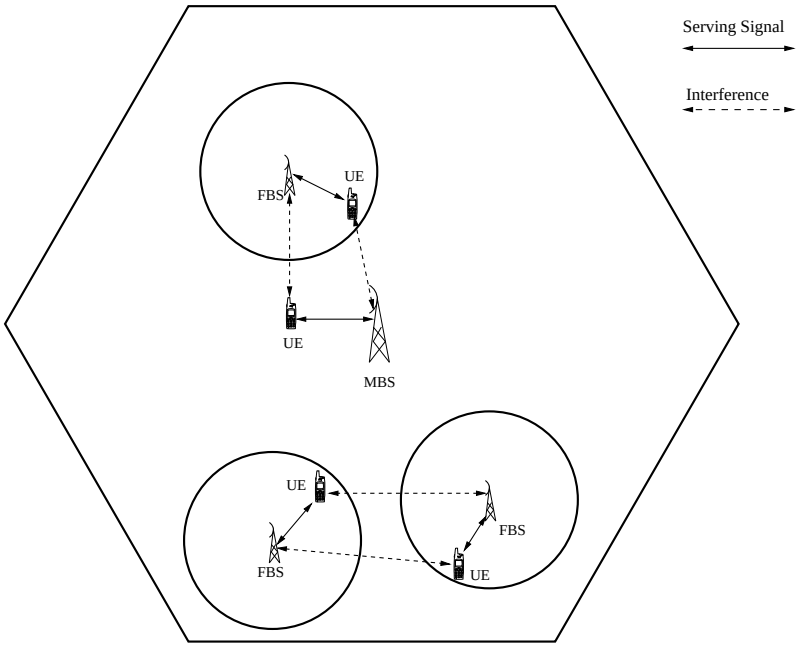

Figure 2.14: Interference scenarios in the macro-femto two-tier networks for the uplink and downlink.

As shown in Fig. 2.14, two different types of interference are defined in this two-tier network architecture:

- Co-tier interference: This type of interference occurs among network elements that belong to the same tier in the network. As depicted in Fig. 2.14, the cross-tier interference occurs between neighbouring femtocells. To be more explicit, a femtocell MT may cause uplink

co-tier interference to the neighbouring femtocell BSs. On the other hand, a femtocell MT may also suffer from the downlink interference from the neighbouring femtocell BSs.

- Cross-tier interference: This type of interference occurs among network elements that belong to different tiers in the network. As depicted in Fig. 2.14, the co-tier interference occurs between femtocells and macrocells. To be more explicit, a femtocell MT may impose uplink co-tier interference to
  on the macrocell BSs. On the other hand, a macrocell MT may also suffer from the downlink interference arriving from the neighbouring femtocell BSs.

Unlike the macrocells, which are designed for predetermined geographic locations and are typically modelled as a regular tessellated hexagonal lattice, femtocells are dispersed rather randomly. Owing to the femtocells' unplanned deployment, some femtocells may be situated close to a MBS and hence the Femtocell Base Station (FBS) subscribers might suffer from a high cross-tier interference from the MBS. The opposite also happens, when macrocell users roam in the vicinity of a FBS and these MBS subscribers will suffer from a high cross-tier interference imposed by the FBS. The former problem is referred to in the literature as the Cell-Centre Region (CCR) problem, while the latter is termed as the Cell-Edge Region (CER) problem. We collectively refer to them as the classical near-far problem [134].

Recognizing these challenges, sophisticated techniques have been proposed for mitigating the interference in two-tier networks, which are summarized in Fig. 2.15.

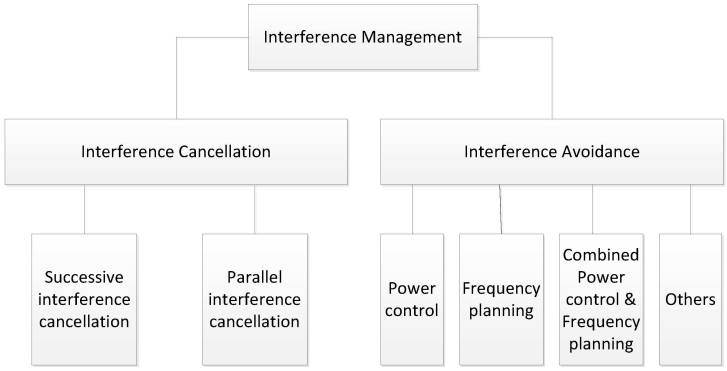

Figure 2.15: The summary of interference management techniques conceived for femtocells.

Two popular interference management approaches have been defined in [81], as seen in Fig. 2.15. Interference cancellation techniques allows the receivers subtract the interference with the aid of jointly signal processing between multiple cells. However, the interference is avoided/reduced when the system relying on interference avoidance techniques.

Different types of IC techniques have been adopt to cope with the interference encountered in two-tier macro-femto networks [135–142]. The authors of [135] considered a dense femtocell scenario and proposed a successive interference cancellation (SIC) method in order to cope with the uplink co-tier interference, where the femtocells cooperated through the joint processing of all the femtocells' signal using the same frequency band. The simulation results illustrated that the bit error rate (BER) of the system improved significantly with the aid of the cooperative interference cancellation technique. A similar SIC method was used in [136] to cope with the downlink co-tier interference. By contrast, SIC method was used in [137, 138] for mitigating the uplink cross-tier interference, while the downlink cross interference was cancelled by SIC in [139, 142]. These simulation results illustrated that the SIC techniques were capable of improving the performance of the two-tier network. Both the SIC and parallel interference cancellation (PIC) methods were investigated for coping with the cross-tier interference in [143]. The majority of the IC techniques require some knowledge of the interference characteristics. As a result, these algorithms can be complex and hence may be more suitable for BSs, which suggests their employment for uplink interference management [83]. We summarize the key contributions of IC techniques in Tables. 2.5

Year	Authors	Contributions
2010	Branco *et al.* [142]	Deployed both the SIC and PIC methods for the sake of mitigating the downlink cross-tier interference.
2010	Alade *et al.* [135]	Proposed the SIC method for mitigating the downlink co-tier interference, where the femtocells cooperated through joint processing for all the femtocells' signals using the same frequency band.
2011	Hu and Mao [136]	
2011	Kaufman *et al.* [137]	Proposed the SIC method in order to cope with the uplink cross-tier interference.
2013	Ghani *et al.* [143]	Used the IC techniques in the MIMO based macro femto two-tier networks.

Table 2.5: Key contributions of interference cancellation techniques.

In addition to IC, interference avoidance compose an important interference mitigation approach. Power control constitutes a key technique in interference avoidance by carefully adjusting the transmission power of femtocells. Dynamic power adjustment setting can be performed either in an open loop power setting (OLPS) or closed loop power setting (CLPS) mode. In the OLPS mode, a transmitter adjusts its transmission power based on its measurement results or predetermined system parameters. In the CLPS mode, the femtocell adjusts its transmission power based on its coordination with the macrocell.

For the downlink scenario, if the power of a FBS is controlled and optimised, the nearby macrocell MT can be sufficiently protected well. The authors of [144, 145] used this idea for reducing the downlink cross-tier interference, where the transmission power of a FBS was set according to its position. To be more specific, the FBSs placed near a MBS may transmit at a higher power, while those far away from a MBS may assign a lower transmission power. This approach only relies on topological/positional information. There are also some power control approaches adjust the transmission FBS power relying on the QoS requirements of their MTs, such as the SINR requirement [146, 147] and the outage probability (OP) requirement [148]. However, these contributions only focused on single femtocell configurations and did not consider any cooperation between the femtocells and macrocells.

In order to characterize this interaction, game theoretic models were used for designing the power control in the downlink of two-tier macro-femto networks [149–154]. The broad categories of game theoretic models are the non-cooperative and cooperative game models. In a non-cooperative game, every BS (both FBS and MBS) selfishly maximizes its own utility function. Hence, solving a non-cooperative game constitute a OLPS approach. By contrast, the MBS acts as a leader, while the FBSs act as followers in a cooperative game and this represent a CLPS approach. In [149, 150], the downlink power control problem of two-tier networks was modelled by a so-called Stackelberg game, which is a cooperative game. The game was formulated as a mathematical program relying on equilibrium constraints, and the best response constituted for a single leader-multiple follower game was derived. In [151], both non-cooperative and cooperative games (Stackelberg game) were proposed for solving the resultant distributed power control problem. It was shown that there exists an optimal number of FBSs to be deployed in the network covering a fixed area. Later, the author of [152] suggested the idea of a non-cooperative game and modeled the power control problem by using a utility function, where differentiated classes of MTs having distinct access priorities and design requirements were considered and modelled. Similarly, each femtocell maximized its utility function under the consideration of the associated queue stability constraints in [153], and a distributed algorithm was proposed for femtocells to decide their downlink transmission power.

Apart from game theory techniques, Reinforcement Learning (RL) was also used to solve the power control problem. In [154], the authors proposed a distributed power management based on a specific form of multi-agent RL, which was also known as distributed Q-learning. The decisions about power allocation were made in a distributed manner, based on the paradigm of independent learning, where the agents were unaware of the other agents' actions.

Turning to the uplink, power control techniques are also capable of optimising the transmission power of MTs for the sake of mitigating the co-tier and cross-tier interference. Similar to the ideas in [146], in [155], the MTs of each femtocell estimated the interference imposed on the neighbouring MBSs and adjusted their transmission power so that the estimated interference did not exceed a pre-defined threshold. Game theory techniques have also been used for solving the

uplink power control issues. The authors of [156] assumed that the macrocell and femtocell MTs participated in a non-cooperative power control game and modeled the utility function evaluated for the femtocell MTs as a reward function plus a penalty function. By solving the maximization problem, the paper derived a relationship which finds the highest feasible cellular SINR values for the femtocells. However, instead of implementing interference power constraints at the femtocell MT, in [95], the authors assumed that such constraints were imposed by the MBS, which controlled the interference received from the femtocell MTs through pricing the interference. Then a distributed interference-price bargaining algorithm was proposed for this Stackelberg game. Furthermore, the utility function was modified by taking ito consideration the MT's QoS requirements in [157], and an iterative algorithm was proposed for deriving the optimal power for both the femtocell MTs and macrocell MTs. We summarize the key contributions of power control in Tables. 2.6

Year	Authors	Contributions
2007	Claussen [144]	Proposed an OLPS mode to control the transmission power of femtocells, where the power was adjusted according to their positions.
2009	Chandrasekhar *et al.* [156]	Proposed a non-cooperative power control game and model the utility function as a reward function plus a penalty function, where the uplink cross-tier interference issue was solved.
2010	Galindo-Serrano *et al.* [154]	Proposed a distributed power management method based on a form of multi-agent RL, where the decisions were made based on the paradigm of independent learning.
2011	Bennis and Perlaza [149]	Modelled the downlink power control problem as a cooperative Stackelberg game, and the best response for this one leader-multiple follower game was derived.
2013	Guruacharya [150]	
2012	Ngo [152]	Induced the idea of non-cooperative game for solving the downlink cross-tier interference issue, where differentiated classed of users design requirements were considered.
2012	Kang *et al.* [95]	Assumed the interference power constraints were imposed by the MBS, which controls the received interference through pricing processes. A distributed interference price bargaining algorithm was proposed.

Table 2.6: Key contributions of power control techniques.

Apart from power control, frequency band planning is also an important interference avoidance technique in two-tier networks. This approach is basically used when the macrocells also rely on some frequency reuse techniques. The basic mechanism of this method divides the entire frequency band into several sub-bands, which may be assigned to the macrocells and femtocells so that the interference can be reduced. In [158, 159], the authors defined a so-called interference-limited coverage area, where orthogonal channel deployment was operated. By contrast, co-channel deployment was used beyond this area. As a result, the uplink/downlink interference arriving from the MBS at the femtocell MTs was reduced. However, the cell edge macrocell MTs were not protected in this approach. The authors of [160] extended this idea for the sake of mitigating the uplink interference in OFDMA femtocell networks. The cross-tier interference was reduced by forcing the macrocell MTs interfering with the femtocell to use only some dedicated subcarriers. Furthermore, the co-tier interference was mitigated by an auction algorithm.

Frequency band planning techniques have become more sophisticated and their design is more challenging, when the femtocells deploy multi-carrier techniques. The authors of [161] considered having a 100 MHz LTE-Advanced bandwidth consisting of five carriers, where an autonomous carrier selection scheme was proposed. Each femtocell firstly chose one and only one primary component carrier. The allocation of an additional secondary component carrier was possible, if and only if its performance impact on the neighbouring cells was estimated to be acceptable. This approach relied on existing MT measurement reports, hence the MTs have to be capable of spectrum sensing. Similar MT measurement reports were exploited for dynamic frequency planning in OFDMA based two-tier macro-femto networks in [161–163].

Clustering algorithms were recently used in coping with the co-tier interference by assigning different subcarriers to the neighbouring femtocells. The authors of [164, 165] proposed a cluster-based resource allocation scheme, where the clusters were determined by the topology-related information on the femtocells. In each cluster, a specific femtocell was elected to act as the cluster head according to the MT measurement reports, while the other femtocells in this cluster were cluster members. The cluster head carried out the subcarrier allocation in its cluster. Graph-colouring algorithms were also used for mitigating the co-tier interference, while minimizing the number of colours, under the assumption that the number of subcarriers was larger than the number of femtocells [166, 167]. We summarize the key contributions of frequency planning in Tables. 2.7

In OFDMA systems, the researchers always combine the dynamic frequency planning with power control schemes in order to further mitigate the interference. In [169], a fixed transmission power was assumed and the optimal subcarrier assignment was derived. Then, given the optimal subcarrier assignment, the optimal transmission power was derived subsequently. After several iterations between optimizing these objective functions both, the optimal power allocation and subcarrier assignment were derived. The authors of [170–172] carried out the subcarrier assignment and power allocation separately, where cluster-based algorithms were proposed for solving the subcarrier assignment problem and the resultant transmission power was then adjusted in order to

Key frequency planning techniques		
Year	Authors	Contributions
2008	Kim and Lee [168]	Proposed a frequency reuse approach for macrocell, where the femtocells used the frequency band that are orthogonal to the overlaid macrocells.
2009	Bai *et al.* [159]	Defined a interference-limited coverage area, where orthogonal channel deployment was employed in this area.
2009	Garcia *et al.* [161]	Proposed an autonomous component carrier scheme, where each femtocell chose one primary component carrier. The allocation of the secondary component carriers was based on the performance impact on neighbouring cells.
2012	Liang *et al.* [167]	Proposed the graph-colouring algorithm by minimizing the number of total colors.
2014	Hatoum *et al.* [165]	Proposed a cluster-based resource allocation scheme, where the clusters are determined by the femtocells' position. One femtocell was elected to be as cluster head and this femtocell applied subcarrier allocation within each cluster.

Table 2.7: Key contributions of frequency planning techniques.

guarantee the QoS constraint. A cognitive approach was pursued for femtocells in [131] and [173] in order to sense the unused subcarriers. Then, opportunistic subcarrier selection algorithms were proposed. The femtocells relies on a sophisticated power control approach designed for fulfilling the QoS constraints. We summarize the key contributions of frequency planning in Tables. 2.8

Apart from the power control and frequency planning solutions, some researchers proposed MIMO-aided two-tier macro-femto networks and used the MIMO transmission techniques as a interference avoidance solution. For example, a beam selection algorithm was proposed in [174], where the cross-tier interference was reduced by adaptively reducing the number of transmission beams. The technique of interference alignment was employed in [175] and [176] in order to cope with both the cross-tier and co-tier interference both with and without considering use-selection, respectively. The authors of [177] relied on the CoMP concept and proposed downlink MIMO-aided transmit pre-coding cooperation between macrocell and femtocells.

There are also a range of other interference avoidance techniques used in literatures. For example, the authors of [98] proposed a time-hopped CDMA-based physical layer and sectored antenna techniques for CDMA femtocell networks for reducing outage probability. Cross polarization

Year	Authors	Contributions
2010	Lien *et al.* [173]	Used the cognitive approach for femtocells for sensing the spare subcarriers and an opportunistic subcarrier selection algorithm was proposed. The femtocells further operate power control approach to fulfil the QoS constraints.
2014	Ngo *et al.* [169]	Proposed an iteration algorithm, where optimal subcarrier assignment was derived with the fixed power assumption, and then the optimal power was determined with the derived subcarrier allocation. After several iteration the jointly optimal resource allocation was presented.
2014	Abdelnasser *et al.* [171]	Proposed a joint resource allocation algorithm, where cluster-based algorithms were proposed to solve the subcarrier assignment problem and the transmission power was adjusted according to the QoS constraint.

Table 2.8: Key contributions of combined power control and frequency planning techniques.

aided techniques were used in [178], where the femtocells rely on right-hand circular polarization (RHCP), and macrocell make use of left-hand circular polarization (LHCP). The results illustrated that the employment of cross-polarized assisted transmission was capable of increasing the attainable system capacity. We summarize other key interference management techniques in Tables. 2.9.

Albeit there are numerous open challenges, femtocells constitute an efficient approach in improving the indoor coverage and providing high-data-rate services [88]. Having introduced the rudimentary concepts of femtocells, let us now turn our attention in the next section to a less well-explored area of wireless communications, namely to VLC systems.

Year	Authors	Contributions
2009	Chandrasekhar and Andrews [98]	Proposed a time-hopped CDMA aided physical layer and sectorized antenna techniques for CDMA femtocell networks.
2013	Jacob *et al.* [178]	Used cross polarized techniques, where femtocells rely on RHCP and macrocell makes use of LHCP.
2014	Guler and Yener *et al.* [176]	Considered MIMO based two-tier networks and used the technique of interference alignment for the sake of mitigating both cross-tier and co-tier interference.
2014	Elsherif *et al.* [177]	Induced the concept of CoMP and proposed a downlink MIMO pre-coding cooperation between macrocell and femtocells

Table 2.9: Other key interference management techniques.

2.3 The Visible Light Communication Systems

In the time of writing, there is an increasing requirement for increased data transmission rates. Wireless access networks constitute a key element of achieving this goal. However, the availability of RF bandwidth at frequencies which support a reasonable spatial coverage is a limiting factor. As a result, alternative wireless transmission techniques have to be explored. The increasing interest in the VLC system is justified by its significantly wider spectrum, compared to the rather congested RF spectrum used by state-of-the-art wireless communications systems [179]. As depicted in Fig. 2.16, the available optical bandwidth is about 10 000 times higher than the entire RF spectrum. Furthermore, the optical frequency band is unlicensed and hence free, which may further reduce the service-provision costs of the operators. As a result, optical wireless communications systems have been one of the technologies complementary to the traditional RF systems.

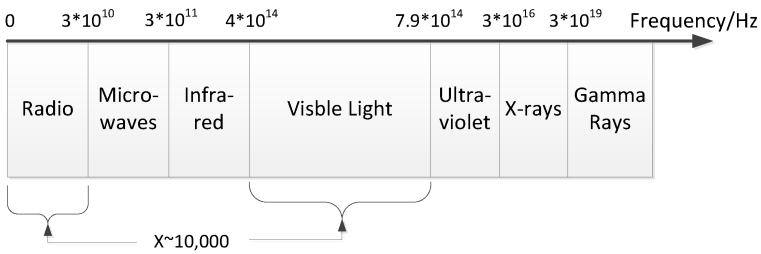

Figure 2.16: The electromagnetic spectrum [179].

The idea of using optical signals for communication may go back to 1880, when Bell proposed the idea of a ”photophone” [180], which allowed for the transmission of sound via optical signals between two buildings. However this idea only became more practical after 1966, when Kao and Hockham demonstrated that glass fibres ’may’ be used as transmission lines for light, akin to coaxial cables used for electronic signals [181]. Later, Gfeller and Bapst [182] motivated contemporary optical wireless communications research in 1979, with the promise of gaining access to thousands of Terahertz of bandwidth.

A typical optical communication system consists of a transmitter, which encodes a message into an optical signal, a channel, which carriers the signal and a receiver, which decodes the message from the received optical signal [183]. The most commonly used components of optical wireless communication transmitters are laser diodes and Light Emitting Diodes (LED). Compared to LDs, LEDs are cheaper and they have a longer lifetime. Furthermore, the high optical output power of LDs poses potential risks for human eyes. As a result, LED lights based VLC systems attracted substantial attentions and may more feasibly be operated in indoor scenarios. For VLC, typically high-power white light sources are used, which is generated by yellow and blue lights. The yellow emission has a slow time constant compared to the direct modulation of the blue emitter drive current, hence only the blue ”channel” is used for communications. At the receiver side, typically a filter is used to pass only the blue light from the LED’s emission. The lights is then focussed onto a photodetector using some optical components. Then the photodetector converts the wireless optical power to a current. This current is finally converted to a voltage, which is then amplified before data recovery.

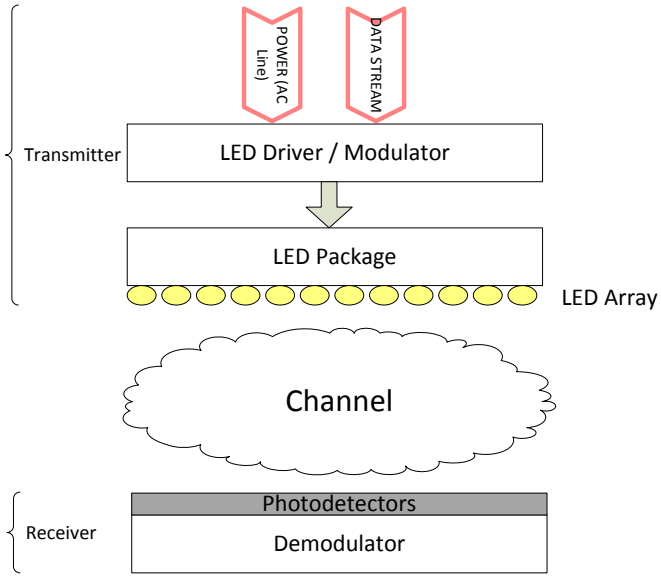

Figure 2.17: A stylized VLC system architecture.

Since white LED lights are capable of providing high-brightness illumination, the associated VLC systems may have a wide area of applications in indoor scenarios. In this treatise, we will focus our attention on indoor VLC systems. An indoor VLC channel can be characterized by the optical wireless channel discussed in [184]. The channel gain of the VLC channel consists of lines of sight (LOS) from the LED chips as well as of the reflections of the walls or objects in the room [185, 186]. The multiple copies of the transmitted signal impinging at the receiver will have different propagation delays and the power in each of them will be summed by the photodetector at the receiver. These delays may cause Inter-Symbol Interference (ISI). The amount of ISI depends on the transmission scenario influenced by the room properties, distribution of LED lights and LED properties. For example, it was assumed in [186] that all signals arriving at the receiver with a delay of more than half of the symbol period after the first signal contribute to ISI. Hence, if the bandwidth of the transmitted signal is limited to 20 MHz, the Nyquist symbol period is limited to 25 ns. As a result, ISI will occur, only if the transmitted data symbols experience delays larger than 12.5 ns.

A stylized VLC system architecture is illustrated in Fig. 2.17, where the transmitter consists of a conventional wireless communication system and an additional optical driver, while the receiver uses photodetectors in order to convert the optical signal to current. In practice, the transmitter is an LED array, which is mounted on the ceiling of a room, as depicted in Fig. 2.18, for example, and the receiver is a VLC enabled device.

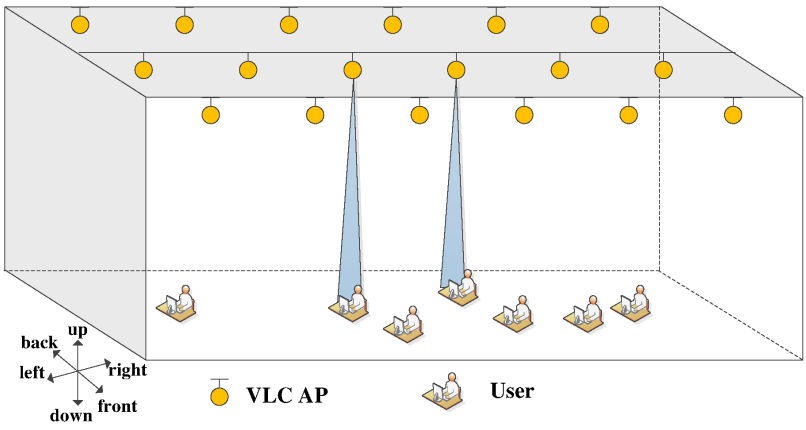

Figure 2.18: Example of a indoor LED light based VLC system.

We summarise the advantages of LED based VLC systems over RF communication systems as follows [187]:

- The virtually unlimited bandwidth of over 350 THz.
- Unregulated spectrum available for immediate exploitation.
- White LED lights currently penetrate many areas of our daily life. They are replacing the

incandescent light bulbs.

- The existing power line communication system can be potentially used as its backbone.
- Since the wall-penetration of light waves can be ignored, it is inherently secure.
- Transmitters and receivers are of low cost.
- Visible light with limited intensity is free of any health concerns. As a result, VLC can be used in hospitals, private homes, etc.
- No interference with RF based operational systems.

Although VLC systems exhibit several advantages over the traditional RF systems in indoor scenarios, a range of future challenging tasks have to be resolved. Firstly, VLC using illumination sources is naturally suited to broadcast applications, but supporting an uplink transmissions might be problematic [2]. Secondly, it has been shown that the predominately line-of-sight (LOS) optical wireless systems exhibit a poor performance in the presence of obstructing objects. Thirdly, the coverage of each optical access point is limited compared to cellular RF networks.

2.3.1 State-of-the-Art in VLC Technologies

Early research on the LED light based VLC systems focused on the simply simulation of the received SNR, which was analysed in [185, 188], but the associated modulation schemes were not considered. However, modulation constitutes an essential part of the physical layer design, since the signal modulation required for communication directly affects the illumination. At the current state of the off-the-shelf illumuniation components and photodetectors, VLC is readily realizable as an intensity modulation and direct detection (IM/DD) based scheme [189], where only the signal intensity is used for conveying information. In [190], the BER performance was characterized under the consideration of a on-off keying (OOK), where binary 1s and 0s were transmitted as the presence or absence of light. This meant that the LED was turned on and off constantly. More sophisticated modulation techniques were explored for VLC systems later [186, 191, 192]. Pulse-Amplitude Modulation (PAM) was invoked for baseband transmission in [186], where the received SNR and the achievable transmission rate were also evaluated. Furthermore, Colour Shift Keying (CSK) was standardised in the IEEE 802.15.7 [191] and might be an important potential future modulation scheme in VLC systems. The performance of the IEEE 802.15.7 CSK physical layer was evaluated in [192]. More recently, Jiang, Zhang and Hanzo studied an uncoded *M*-CSK scheme relying on a joint Maximum Likelihood (ML) Hard-Detection (HD) based VLC system, where both simulation-based and anlytical BER results were derived [193]. Pulse Position Modulation (PPM) is another option proposed for indoor VLC systems [184], where the modulating signal is encoded into 2^M legitimate time-slots for $M-$array PPM. Furthermore, a generalized form of PPM termed expurgated PPM (EPPM) was introduced into a VLC system [194].

In order to provide higher data transmission rates, multiple-carrier techniques have also been used in VLC systems. In [186], quadrature-amplitude-modulation (QAM) based discrete multi-tone (DMT) transmissions were developed and the BER performance was evaluated. OFDM has also been extensively studied, which was shown to achieve data rates exceeding 500 Mb/s using a single LED [195]. There are two popular types of IM/DD aided optical OFDM (OOFDM) systems, namely the Direct Current-biased Optical OFDM (DCO-OFDM) [196] and ACO-OFDM [197]. Later, ACO-OFDM and DCO-OFDM were compared in [198]. Higher order phase shift keying (PSK) and QAM have also been considered in OOFDM aided VLC systems. The attainable BER performance was evaluated for quadrature phase shift keying (QPSK) based OOFDM VLC systems in [187], where realistic channel estimation, time synchronisation and forward error correction (FEC) coding was used. Recently, Zhang and Hanzo conceived multi-layer modulation (MLM)-aided OOFDM, where a double turbo receiver was proposed for jointly detecting the MLM signal and a genetic-algorithm-aided weight optimization was pursued for seeking an increased MLM bits per symbol throughput [199].

Apart from the physical-layer studies, the realization of a mobile communication system requires efficient networking solutions. Optical propagation naturally creates confined ”cells” of which are either limited by the beamshape or the walls and partitions within buildings. The early study in [185] simply assumed that all LEDs in the room constitute a single transmission cell and they active only a single LED light for transmission according to the MTs’s position. As a result, the exploitation of the LED lights is inefficient, since only a single MT is scheduled for each transmission slot. Alternatively, the same information may be sent in the downlink from all LEDs. A straightforward way of improving the exploitation of LED lights is to simply transmit a different signal simultaneously from every LED light. Hence, these LED lights formulated as a single transmission ”cell”. This idea was employed in [200] and the authors referred to the VLC solution based network as a Light Fidelity (Li-Fi) network. However, a major problem of this cell formulation is the interference amongst the neighbouring LED lights. In order to cope with this issue, more sophisticated cell formulation schemes should be employed.

There is a paucity of studies on the cell formulation of VLC cells. The authors of [200,201] proposed a Fractional Frequency Reuse (FFR) cell formulation for indoor LED based VLC systems. A key issue of this cell formulation approach is the handover, since switching between frequencies every few meters during the MT’s movement degrades the user’s experience. Another approach appeared recently, which employs the idea of Coordinated Multi-Point (CoMP) of RF wireless systems. Chen *et al.* proposed a joint transmission scheme, where the same frequency was employed to all regions [202], and a MT was served by multiple nearby LED lights. Later, Li *et al.* employed Zero-Forcing Beamforming in an indoor VLC system in order to reduce the interference imposed [203].

Another important issue in indoor VLC architectures is its resource management mechanism. When multiple MTs are under the coverage of a given VLC system, RA has to be carefully per-

formed based on prevalent QoS requirements. The RA problem was discussed in [204], where multiple-carrier techniques were employed and the simple transmission model of [185] was used. In Chapter 5, we will investigate the RA issues when the indoor LED based VLC system relies on various transmission models, including the radical UFR transmission, Frequency Reuse transmission and the more sophisticated cell coordination transmission.

Furthermore, it is of paramount importance to develop cooperative techniques, which can be combined with optical systems for providing a seamless data service. The early study of [205] mentioned the potential cooperation of VLC and RF systems, while the benefits of cooperative optical communications were studied in terms of various technical aspects in [203, 206–211]. Hou and O'Brien proposed a fuzzy-logic (FL)-based decision-making algorithm for vertical handovers in an integrated optical wireless and RF systems [206]. Then the authors of [207] used the RF signal for the localization of MTs. Later, the widely used Wireless Fidelity (WiFi) network was considered to be a complementary element of VLC system in [208], where a simplified vertical handover mechanism was proposed. Similarly, Chowdhury and Katz [209] considered a hybrid VLC and WiFi scheme in an indoor scenario, where the mobility issues of MTs were investigated. Later, the authors of [211] proposed a protocol supporting both horizontal and vertical handover mechanisms for the MTs. The associated load balancing and cell formulation issues were investigated in [203]. In Chapter 4, we will investigate the relevant RA issues under delay-guarantee constraints in a hybrid VLC and femtocell system. We summarize the key contributions on VLC techniques in Tables 2.10-2.12.

Early exploration of VLC techniques		
Year	Authors	Contributions
1880	Bell [180]	Proposed the idea of "photophone", which allowed for the transmission of sound via optical signal.
1966	Kao and Hockham [181]	Demonstrated that glass fibres would be used as transmission lines for light akin to coaxial cables for electrical signals.
1979	Gfeller and Bapst [182]	Motivated contemporary optical wireless communications research with the promise of gaining access to thousands of terahertz of bandwidth.
1997	Kahn and Barry [184]	Presented the advantages and drawbacks of the infrared medium, comparing to those of radio and microwave media.

Table 2.10: Key contributions of VLC techniques: Part I.

Key contributions in VLC system		
Year	Authors	Contributions
1996	Carruthers and Kahn [196]	Proposed the Direct Current-biased Optical OFDM scheme for VLC system.
2001	Tanakat *et al*. [190]	Characterized the BER performance under the OOK modulation scheme for VLC system.
2004	Komine and Nakagawa [185, 188]	Evaluated the received SNR and illumination without the consideration of modulation schemes at the network level.
2007	Elgala *et al*. [187]	Demonstrated the BER performance for QPSK based optical OFDM VLC system.
2008	Grubor *et al*. [186]	Derived the BER performance for QAM based DMT transmission aided VLC system.
2009	Liang and Evans [197]	Proposed the asymmetrically clipped optical OFDM scheme for VLC system.
2010	Vucic *et al*. [195]	Demonstrated the achievable data rates for optical OFDM based VLC system.
2011	IEEE standard [191]	The Colour Shift Keying modulation scheme was standardised in IEEE 802.15.7.
2011	Mesleh *et al*. [198]	Compared the ACO-OFDM and DCO-OFDM schemes, and it was shown that ACO-OFDM typically requires a lower average optical power than DCO-OFDM.
2013	Singh *et al*. [192]	Evaluated the performance of IEEE 802.15.7 CSK physical layer of VLC system.
2013	Zhang and Hanzo [199]	Proposed a multi-layer modulation scheme for intensity-modulated direct-detection optical OFDM aided VLC system.
2014	Noshad and Brandt-Pearce [194]	Proposed a generalized form of pulse position modulation (PPM) scheme called expurgated PPM in VLC system.
2015	Jiang *et al*. [193]	Proposed an uncoded M-CSK scheme relying on the joint Maximum Likelihood Hard-Detection VLC system.

Table 2.11: Key contributions of VLC techniques: Part II.

Key contributions in VLC system		
Year	Authors	Contributions
1998	Heatley *et al.* [205]	Proposed the idea of the potential cooperation of VLC and RF systems.
2006	Hou and O'Brien [206]	Proposed a fuzzy-logic based decision-making algorithm for vertical handover in the integrated system of optical wireless and RF technologies.
2010	Wang *et al.* [207]	Used the RF signal for the localization of MTs in the hybird VLC and RF systems.
2011	Rahaim *et al.* [208]	Proposed a vertical handover mechanism in a hybrid WiFi and VLC system.
2013	Chen *et al.* [201]	Proposed a Fractional Frequency Reuse cell formulation scheme for indoor LED lights based VLC system.
2013	Tsonev *et al.* [200]	
2013	Chen *et al.* [202]	Proposed a joint transmission scheme for indoor VLC system, where the same frequency was employed to all conflicting regions.
2013	Chowdhury and Katz [209]	Investigated the mobility issues of MTs in a hybrid VLC and WiFi indoor scenario.
2014	Jin *et al.* [210]	Investigated the resource allocation issues in a hybrid VLC and femtocell indoor scenario, under the consideration of diverse QoS requirements.
2014	Bao *et al.* [211]	Proposed a protocol combined with horizontal, and vertical handovers mechanisms for MT, under the consideration of the mobility of MTs.
2015	Li *et al.* [203]	Investigated the load balancing and cell formulation issues in a hybrid VLC and WiFi system.

Table 2.12: Key contributions of VLC techniques: Part III.

2.4 Chapter Summary and Conclusions

A heterogeneous network relies on multiple access techniques, which may contain the existing cellular network and new small-cell technologies, such as femtocells and VLC systems. In this chapter, we introduced the modelling of these technologies, while the modelling of the traditional cellular network was developed in Section 2.1, where three different modelling methods were discussed. The Wyner model is a simple model conceived for analysing the performance of cellular networks for both the uplink and downlink. The brief history of the Wyner model used in analysing cellular networks was summarized in Table 2.1. While the Wyner model is widely used in information-theoretic performance analysis, researchers popularly use the grid-based model for characterizing a more realistic cellular network scenario. However, a specific drawback of the grid-based model is that the analysis of ICI is untractable. Early researchers calculated the other cell interference using integration based approaches. In 2007, Kelif *et al.* proposed the Fluid Model for deriving a tractable expression of other cell interference, when using the grid-based cellular network model. We introduced this method and evaluated its accuracy in Fig. 2.7. Since the Fluid Model is capable of characterizing the grid-based cellular network quite accurately, we use this model in the analysis of two-tier heterogeneous networks in Chapter 3. More recently, the stochastic geometry based PPP model was proposed for analysing the cellular networks or small cells. The key difference with respect to the above two models is the random position of the BSs. The advantage of this model is that analysis of ICI becoming tractable. We also presented the derivation of received SINR by using the PPP based model.

Compared to the traditional cellular networks, the research of small cells has attract growing attention. Femtocells constitute an efficient technique of improving the throughput of indoor scenarios and hence may be seen as an important complement of the traditional cellular networks. In Section 2.2, we touched upon several key aspects of femtocells, commencing from the history of femtocells, their modelling and the technical challenges. There are three popular femtocell network modelling methods. The layout of these three models are illustrated in Fig. 2.10, Fig. 2.11 and Fig. 2.12, respectively. The proliferation of femtocells may impose further challenges upon the existing networks and hence requires further research. The technical challenges of femtocell networks and the associated key contribution were listed in Tables 2.5-2.9. Apart from the RF solutions, the optical wireless techniques also constitute network important small-cell solutions. In Section 2.3 we briefly introduced the features of LED based VLC systems and provided overview of current VLC technologies.

Chapter 3

Fractional Frequency Reuse Aided Two-Tier Femtocell Networks: Analysis, Design and Optimization

3.1 Introduction

In Chapter 2, we introduced several key elements of heterogeneous networks, including the topology and the modelling of macrocell networks, femtocells and VLC systems. These wireless communication systems may provide overlapping coverage in some areas, hence forming a heterogeneous network. In this chapter, we consider an RF heterogeneous network scenario, where the femtocells are overlaid onto the traditional macrocells. Furthermore, we consider an advanced frequency planning arrangement technique, where the macrocells rely on the FFR.

The main limitation of cellular networks is the ubiquitous ICI, which is particularly damaging in the CER of systems employing the radical UFR, which the research community aspires to in the context of both the UMTS and in its LTE. In the open literature, several solutions have been proposed to cope with ICI, such as time-domain techniques. The so called, Almost Blank Subframe (ABSF), is one of the proposed time-domain techniques. Naturally, it is a straightforward practical solution for avoiding the strong ICI is to allocate orthogonal frequency bands within adacent cells and reuse them in a certain pattern, leading to traditional FR. A more sophisticated technique of exploiting the available frequency band is constituted by the FFR, where each macrocell is divided into a CCR having acess to the cell-centre's frequency band F_c and the CER having access to the cell-edge's frequency band F_e. A typical FFR frequency allocation structure is depicted in Fig.

3.1, where the entire frequency band is divided into four frequency bands. Since the FFR scheme is capable of significantly reducing the ICI for the CER, FFR has been adopted in the 3GPP LTE initiative [212] and in the WiMax [213] system.

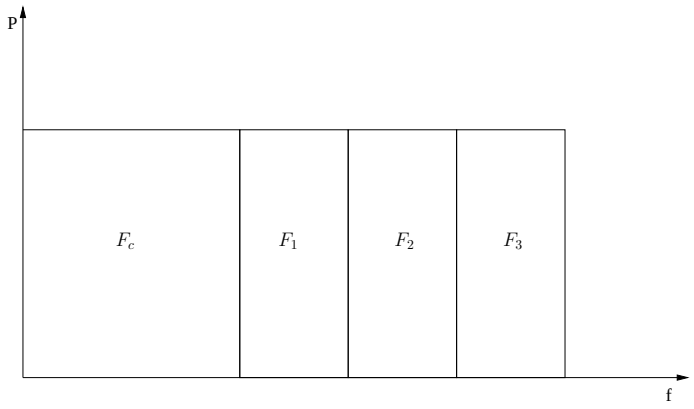

Figure 3.1: The spectrum partition for FFR scheme, where the whole frequency band is divided into four frequency bands. The CCR has access to the frequency band F_c, and the CER has access to the frequency bands F_1, F_2 or F_3.

As we stated in Chapter 2, femtocells, which constitute an economical solution conceived for improving the indoor coverage, may be overlaid onto the traditional cellular, forming a two-tier cellular networks. In this chapter, we will investigate and design our two-tier cellular networks, when the new incoming femtocells are overlaid on the FFR scheme aided macrocells. Prior research on twin-layer cellular structures characterized both the UpLink and DownLink scenarios. Some of these contributions [98, 134] derived the OP relying on the shared spectrum access policy by considering the coverage issues. In contrast to the shared spectrum access policy, several authors [214, 215] considered assigning orthogonal spectral resources to the central macrocells and to be nomadic femtocells in order to eliminate their cross-layer interference. In addition to the above-mentioned centralized approaches, the authors of [91, 170] proposed a distributed and self-organizing femtocell management scheme conceived for OFDMA-based cellular networks. However, most of the contributions in the literature stipulated the implicit assumption of UFR aided macrocells. Recently, some of these contributions [78, 216, 217] considered the FFR aided two-tier network system. Specifically, the authors of [216] analysed the cross-layer interference aspects and proposed a power allocation scheme. However, the inter-macrocell and inter-femtocell interference effects were not considered. The authors of [78, 217] provided valuable analytical results, however the consideration of cross-layer interference was beyond their scope. In this chapter, we consider a multi-cell OFDMA network [84], where the femtocells are overlaid onto the static FFR aided macrocells, rather than focusing on the conventional widely investigated UFR aided macrocell.

The FFR scheme does not have to be time-invariant, it can be implemented statically or dynamically controlled. According to the time-invariant strategy, all parameters are configured in advance

and are fixed for a certain period. By contrast, for the dynamic FFR scheme, some of the parameters are adjusted according to the instantaneous channel and traffic information related to the network. In this chapter, we focus our attention on the static FFR scheme. In the static FFR scheme, the selection of some critical system parameters, such as the frequency reuse factors and the SINR or distance threshold used for identifying the CCR and CER, may significantly affect the attainable system performance. Several contributions were focused on the optimal parameter design issues of FFR aided cellular networks [218–222]. The contributions [220] and [221] studied the overall performance of cellular networks relying on the distance threshold based FFR scheme, where the effect of distance threshold on the average cellular throughput was evaluated. By contrast, the authors of [218] and [222] investigated the overall performance of cellular networks relying on the SINR threshold based FFR scheme. Again, the effect of the distance threshold on the average cellular throughput was evaluated. These contributions studied the optimization problems by invoking an exhaustive search. Later, the authors of [219] focused their attention on finding the optimal distance threshold, where the average cellular throughput was formulated as a function of the distance threshold. However, these contributions only discussed the FFR design issues of single-tier networks or only touched upon the experimental design aspects. To the best of our knowledge, the performance of FFR aided two-tier femtocell networks has not been analysed and the FFR parameter design issues of these two-tier networks have not been studied.

Against the above background, in this chapter, we consider a downlink multi-cell OFDMA network [84], where the femtocells are overlaid onto the static FFR aided macrocells, rather than focusing on the conventional widely investigated UFR aided macrocell. A range of important questions arise in this specific context, such as the interference aspects of the twin-layer network and the FFR-related design parameters. To answer these questions,

- we employ stochastic geometry [68, 79] for modelling the random distribution of femtocells and derive the approximate per-layer OP in a FFR environment. We also involve the interference imposed by other macrocells, which was not considered in [98, 134].
- we study the impact of femtocells on the existing FFR aided macrocells, where the per-tier OP and the per-tier ASE are derived. Furthermore, we optimize the FFR-related parameters in order to achieve the maximum macrocell ASE with the consideration of our own QoS constrains.
- In order to reduce the cross-tier interference, we propose a Spectrum Swapping Allocation (SSA) for the femtocells over-sailed by the FFR aided macrocells for the sake of overcoming both the adverse near-far effects and the cross-layer interference. Similarly, the corresponding optimal parameter design issues are also investigated and presented.

This chapter is organized as follows. In Section 3.2, we present the review of the classical static FFR scheme, where the performance of the FFR scheme is illustrated. In Section 3.3, we

describe our FFR aided two-tier network model. Section 3.4 elaborates on the FFR aided two-tier network relying on Full Spectrum Access (FSA) and then the corresponding optimization problems are presented. The proposed SSA will be studied in Section 3.5. Finally, our numerical results are provided in Section 3.6 and our conclusions are offered in Section 3.6.

3.2 Review of the Classical FFR Scheme

In this section, we will review the classical static FFR scheme, where the topology model, the downlink OP and the performance of the FFR aided macrocells are investigated.

3.2.1 Cellular Topology

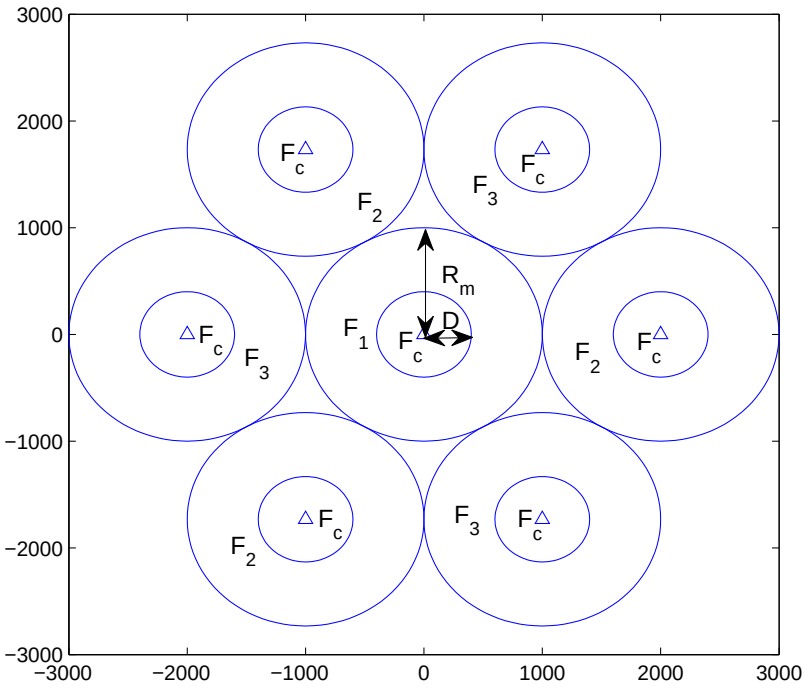

Figure 3.2: The topology of the FFR aided cellular network, where the radius of the macrocells is 1km and the macrocell BSs are denoted by the triangles.

We adopt the regular grid-based cellular network model shown in Fig. 2.4 of Chapter 2. The topology of a FFR aided multicell cellular network is illustrated in Fig. 3.2. For analytical convenience, we model the macrocells as a circle with a radius of R_m and coverage area of $|\mathcal{C}| = \pi R_m^2$, where the central target macrocell base station (MBS) is surrounded by a single ring of adjacent MBSs. We denote the MBS set as Φ. In this chapter, we assume that the CCR and CER are iden-

tified by a predefined distance threshold D, as depicted in Fig. 3.2. Furthermore, we denote the distance threshold ratio by $\omega = \frac{D}{R_m}$, which is the ratio of the interior cell centre radius to the cell radius. The total available bandwidth F is partitioned into four orthogonal frequency bands, F_c, F_1, F_2 and F_3, obeying $F = F_c + F_1 + F_2 + F_3$, where F_c represents the bandwidth of the CCR, while $F_i, i \in [1, 2, 3]$ represents the bandwidth of the CER of one of the three adjacent cells. We also assume that the same transmission power is assigned to the CCR MTs and to the CER MTs, where each MBS transmits at its maximum power allowance P_m.

As we mentioned in the Chapter 2, we assume that the down link (DL) channel is subject to uncorrelated Rayleigh fading with a unity average power and propagation loss, where we adopt the COST231 model [47] for characterizing the propagation path-loss. Given a MT k_m located at a distance from its serving MBS m, the received signal Y_{k_m} may be written as:

$$Y_{k_m} = \sqrt{P_m L_{m,k_m}} h_{m,k_m} X_{m,k_m} + \sum_{m' \in \mathcal{I}_m} \sqrt{P_{m'} L_{m',k_m}} h_{m',k_m} X_{m',k_{m'}} + Z_{k_m}, \tag{3.1}$$

where L_{m,k_m} and h_{m,k_m} denotes the propagation path loss and the uncorrelated Rayleigh fading channel spanning from the MBS m to the target MT k_m, respectively. The pathloss L_{m,k_m} is calculated by Eq. (2.5) of Chapter 2. The MT k_m may suffer from the interference imposed by the neighbouring MBSs, where the interfering MBS set is denoted as $\mathcal{I}_m$. Furthermore, X_{m,k_m} and Z_{k_m} denote the signal transmitted from MBS m to MT k_m and the mutually independent zero-mean AWGN with variance σ^2. Owing to the power constraint, we may have $\mathbb{E}\left[|X_{m,k_m}|^2\right] = 1$. As a result, the SINR ξ_{m,k_m} of the MT k_m served in macrocell m is given by:

$$\xi_{m,k_m} = \frac{P_m L_{m,k_m} |h_{m,k_m}|^2}{P_{m'} L_{m',k_m} |h_{m',k_m}|^2 + \sigma^2}. \tag{3.2}$$

Let us now employ continuous rate adaptation and let ϖ be the SINR discrepancy between the SINR experienced and the SINR required for meeting the target BER, which is given by: $\varpi = \frac{-1.5}{\log(5\text{BER})}$ [223]. We opted for BER $= 10^{-5}$ in this chapter. Then the instantaneous transmission rate r_{m,k_m} for MT k_m served by MBS m is written as:

$$r_{m,k_m} = \log_2 \left(1 + \frac{\xi_{m,k_m}}{\varpi}\right). \tag{3.3}$$

3.2.2 Downlink Performance of the FFR Scheme

In this section, we present some downlink performance results for FFR aided macrocell networks. It is assumed that OFDM is employed so that intra-cell interference is avoided. As we stated in Subsection 3.2.1, the transmission power of each MBS is fixed. When using the FFR scheme, the CCR and CER are identified by a predefined distance threshold D. The main system parameters adopted in our simulations are summarized in Table 3.1.

Firstly, we characterize the OP of the outdoor MTs. We assume that an outage occurs, when the instantaneous received SINR of a transmission falls below a predefined SINR threshold. As

Table 3.1: Notations and System parameters of the FFR aided two-tier femtocell networks

Symbol	Description	Value
f_c	Carrier frequency	2 GHz
N_0	Thermal noise density	-174 dBm/Hz
$\mathcal{B}_0$	Bandwidth of a subcarrier	15 kHz
R_m	Radius of the Macrocell	1000 m
R_f	Radius of the Femtocell	20 m
A_O	Fixed outdoor pathloss	$\frac{f_c^{3.326}}{10^{7.986}}$
A_I	Fixed indoor pathloss	$10^3.7$
γ_1	Outdoor pathloss exponent	4
γ_2	Indoor pathloss exponent	2
W_{dB}	Wall penetration loss	5 dB
$P_{m,dB}$	MBS transmit power	46 dBm
$P_{f,dB}$	FBS transmit power	13 dBm

illustrated in Fig. 3.3, the OP increases when the distance from the serving MBS is increased, approaching 0.6, when the MT is located in the cell edge, when the networks employ traditional UFR. In general, employing the FFR scheme enhances the CER MTs' SINR. As a result, the OP is reduced for the outdoor CER MTs compared to that of the UFR scheme. In more detail, the OP recorded for a MT located at 1km from the serving MBS (the boundary of a macrocell) reduces from 0.6 to 0.12, when the FFR regime is employed in our simulations.

Furthermore, we also compare the downlink long-term throughput of the outdoor MTs in Fig. 3.4. Since we assume that OFDMA is used in our scenario, the variance of the received noise σ^2 equals to $B_{W_0}N_0$, where B_{W_0} and N_0 denote the bandwidth of a subcarrier and the thermal noise density, respectively. Similar to the OP, it is observed that the outdoor MTs benefit to a certain degree from using the FFR scheme for the CER MTs. In more detail, the long-term throughput of a MT located at 1km from the serving MBS (the boundry of a macrocell) increases from 0.2 bit/s to 2 bit/s, when the FFR is employed in our simulations.

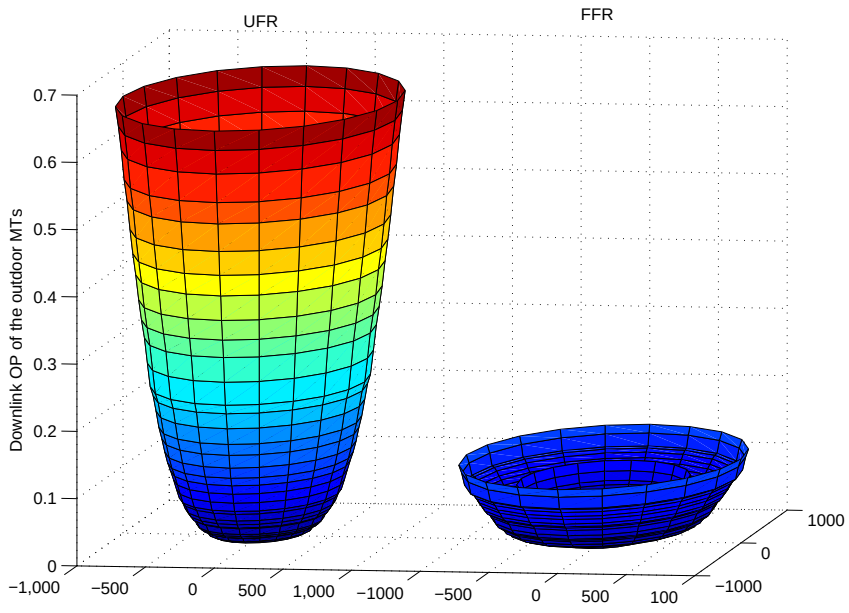

Figure 3.3: The downlink OP of the outdoor MTs, where the SINR threshold is set to be $0dB$. The OP results are characterized by the color, where the distribution of OP of the UFR aided networks is illustrated on the left and that of FFR aided networks is illustrated on the right. The simulation parameters are listed in Table 3.1.

3.3 System Model of FFR Aided Two-Tier Femtocell Networks

The topology model of a two-tier multicell OFDMA cellular network using the FFR strategy is illustrated in Fig. 3.5, where the over-sailing macrocells are overlaid on top of the femtocells. Similar with the parameter setting in Sec. 3.2, we model the macrocells as a circle with a radius of R_m and coverage area of $|\mathcal{C}| = \pi R_m^2$, where the central target MBS B_{m_0} is surrounded by a single ring of adjacent MBSs B_{m_i}, $i \in [1, ..., 6]$. Again, we denote the MBS set as Φ. The FBSs are represented by the small circles having a radius of R_f in Fig. 3.5, which are randomly distributed obeying a homogeneous Spatial Poisson Point Process (SPPP) according to an area-density of λ. Hence, the average number of femtocells per macrocell N_f is $\lambda|\mathcal{C}|$. We denote the FBS set by ψ_i which is overlaid onto macrocell i. The union of the FBS set is denoted by Ψ. In addition to the above BS configuration, we assume the outdoor macrocell MTs to be independently and uniformly distributed in each cell. Similarly, the indoor femtocell MTs are independently and uniformly distributed in each femtocell coverage. The MBSs and FBSs invoke the classic Round Robin (RR) scheduling strategy. Furthermore, the MBSs and FBSs will transmit their signals at their maximum power allowance, which are denoted as P_m and P_f, respectively.

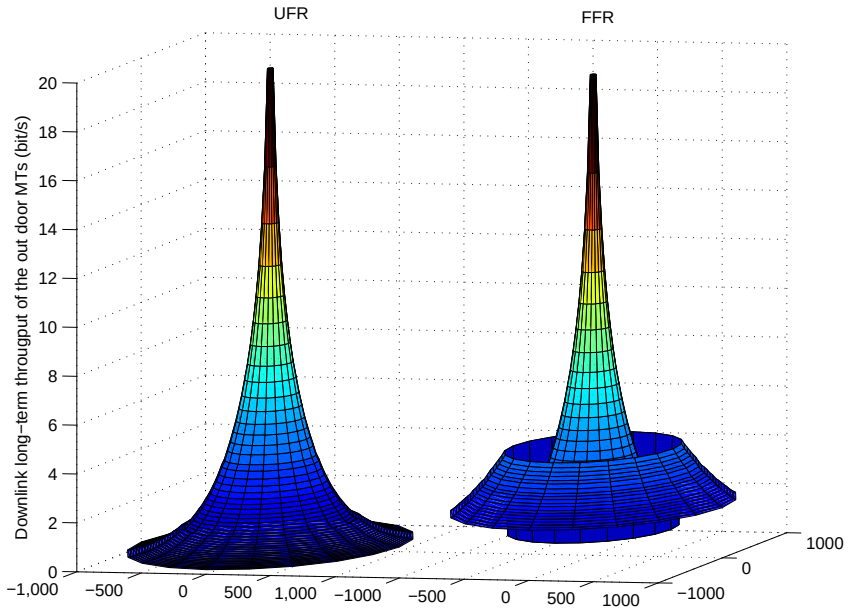

Figure 3.4: The downlink long-term throughput of the outdoor MTs. In more details, the long-term throughput results are characterized by the colour, where the distribution of downlink long-term throughput of the UFR aided networks is illustrated on the left and that of FFR aided networks is illustrated on the right. The simulation parameters are listed in Table 3.1.

Again, We opted for the FFR strategy for the macrocells. The total available bandwidth F is partitioned into four orthogonal frequency bands, F_c, F_1, F_2 and F_3, obeying $F = F_c + F_1 + F_2 + F_3$, where F_c represents the bandwidth available for the CCR, while $F_i, i \in [1, 2, 3]$ represents the bandwidth available for the CER of one of the three adjacent cells. We assume that $F_c = \rho F$ and $F_e = F_1 = F_2 = F_3 = \frac{1-\rho}{3}F$. We also assume that the same transmission power is assigned to the CCR MTs and to the CER MTs. As we stated in Chapter 2, the co-channel developed two-tier networks may suffer from serious interference. In this chapter, we consider two different spectrum access (SA) schemes. In Section 3.4, a straightforward full spectrum access (FSA) scheme is invoked for this FFR aided two-tier femtocell network, where the femtocells reuse the entire available frequency bandwidth F. However, in order to reduce the cross-tier interference, a spectrum swapping access (SSA) scheme is proposed in Section 3.5, where the femtocells use the specific frequency bands, which are orthogonal to those of the outdoor macrocell MTs. More explicitly, the femtocells opt for using the frequency band that was not assigned in its hosting macrocell. For the cell-centre region of the macrocell of Fig. 3.5, F_c and F_1 are available for CCR and CER outdoor macrocell MTs, respectively. Then the frequency bands F_2 and F_3 become available for femtocell transmission. The detailed SSA strategy is elaborated in the context of Fig.

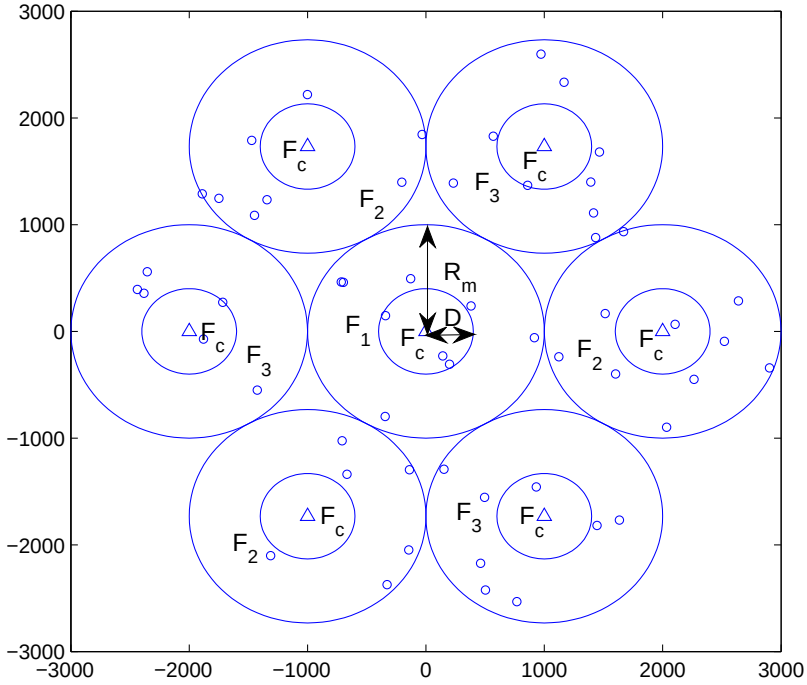

Figure 3.5: The topology of the FFR aided two-tier cellular network, where the radius of the macrocells and that of the femtocells are 1km and 20m. The MBSs and femtocells are denoted by the triangles and small circles.

3.6.

In this chapter, we assume that the down link (DL) channel is subject to uncorrelated Rayleigh fading with a unity average power, as well as to wall-penetration loss and propagation loss. Since the technique of OFDMA is employed, the effect of noise is negligible comparing to the interference. The thermal noise is neglected for analytical simplicity. However, the effects of noise will be taken into account in presenting the simulation results. Let d_m^O and d_f^O denote the distance from an outdoor macrocell MT to the mth MBS B_m and to the fth FBS B_f, respectively, while d_m^I and d_f^I denote the distance from an indoor home MT to the mth MBS B_m and to the fth FBS B_f. We also denote the distance from FBS B_f to MBS B_m by d_m^f.

Note that we have $R_m \gg R_f$, hence we can make the assumption: $d_m^f \approx d_m^I$, as depicted in Fig. 3.7. We can readily derive the relationship: $d_m^f - d_f^I \leq d_m^I \leq d_m^f + d_f^I$. Since the radius of indoor area R_f is relatively small compared to the macrocell size, our assumption holds for $d_f^l \ll d_m^I$.

The DL propagation loss between a BS transmitter and a MT is modelled as we stated in Chapter 2: $L = Ad^\gamma$, where A is a constant that depends on the carrier frequency f_c, d denotes

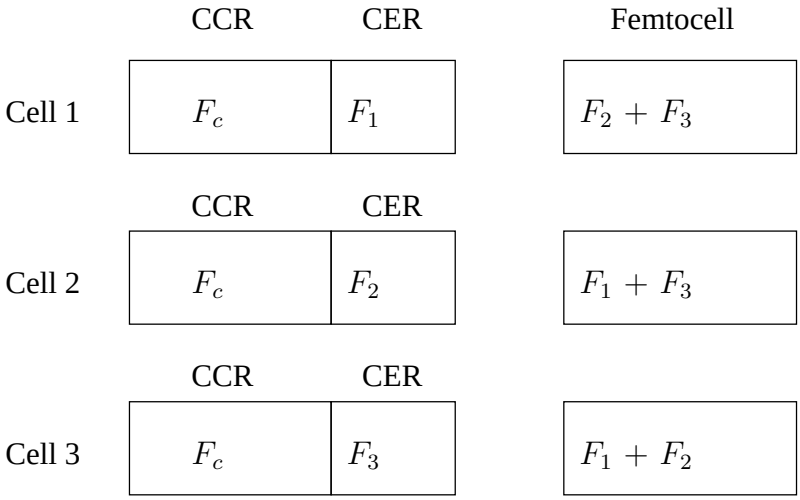

Figure 3.6: An example of the spectrum-swapping scheme.

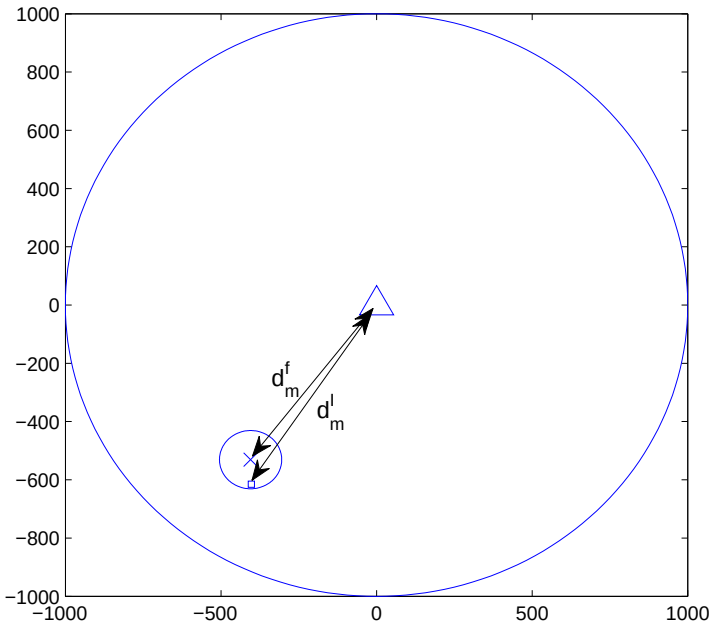

Figure 3.7: A femtocell which is denoted by the small circle is overlaid onto a macrocell denoted by the larger circle. The MBS, FBS and a indoor femtocell MT are denoted by the triangle, the cross and the square, respectively. The distance between the FBS and the MBS is d_m^f, and the distance between the indoor femtocell MT and the MBS is d_m^I. Since the radius R_f of the femtocell is much smaller than the macrocell radius R_m, we may have $d_m^f \approx d_m^I$.

the length of this transceiver link, while γ is the pathloss exponent. Furthermore, we denote the outdoor and indoor fading constant by A_O and A_I, respectively. Finally, we denote the outdoor and indoor pathloss exponent by γ_1 and γ_2. The detailed channel model parameters are summarized in Table 3.1.

3.4 FFR aided two-tier femtocell networks with FSA

In this section, we will investigate the FFR aided two-tier network combined with FSA. As we stated in the Sec. 3.3, femtocells reuse the whole available frequency bandwidth F in FSA. The per-tier OP of both the outdoor macrocell MTs and the indoor femtocell MTs will be derived first, where an outage occurs, when the instantaneous received SIR of a transmission falls below the SIR threshold x. Then the long-term spatially averaged macrocell throughput will be formulated. Finally, we characterize our optimal network design in terms of the attainable macrocell throughput.

3.4.1 Per-tier Outage Probability

3.4.1.1 Outdoor Macrocell MTs' OP

The outdoor MTs roaming in the macrocell m suffer from the interference imposed by the interfering MBSs $\Phi \setminus B_m$, which use the same sub-band, as well as from the interfering FBSs Ψ. As a result, the associated SIR ξ_m of this outdoor macrocell MT located at a distance of d_m^O from the MBS B_m, is given by:

$$\xi_m = \frac{\frac{P_m}{A_O}\left(d_m^O\right)^{-\gamma_1} h_m}{\sum\limits_{m' \neq m} \frac{P_{m'}}{A_O}\left(d_{m'}^O\right)^{-\gamma_1} h_i + \sum\limits_{f \in \Psi} \frac{P_f}{A_O W}\left(d_f^O\right)^{-\gamma_1} g_f}, \tag{3.4}$$

where h and g denote the exponentially distributed channel attenuation of unity mean w.r.t. the MBS and FBS, respectively. Here W denotes the wall-penetration loss. With the aid of Lemma 1, we can derive the approximated OP of outdoor macrocell MTs in our FFR aided two-tier cellular network relying on FSA.

Lemma 1. We consider an outdoor macrocell MT, at a distance of $d_m^O = l$ from the serving MBS. The OP of this outdoor MT is then approximated as:

$$\begin{aligned} \mathcal{F}_{m_1}(x|l) &= 1 - \exp\left[-\zeta_1 x - \pi\lambda C_{\gamma_1} l^2 (Kx)^{\frac{2}{\gamma_1}}\right], \text{if } \ l \leq D, \\ \mathcal{F}_{m_2}(x|l) &= 1 - \exp\left[-\zeta_2 x - \pi\lambda C_{\gamma_1} l^2 (Kx)^{\frac{2}{\gamma_1}}\right], \text{if } \ l > D, \end{aligned} \tag{3.5}$$

where we have $\zeta_1 = \frac{2l^{\gamma_1}}{(\gamma_1-2)R_m^2(2R_m-l)^{(\gamma_1-2)}}$, $\zeta_2 = \frac{2l^{\gamma_1}}{3(\gamma_1-2)R_m^2(2\sqrt{3}R_m-l)^{(\gamma_1-2)}}$, $C_{\gamma_1} = \int_0^\infty \frac{1}{1+s^{\frac{\gamma_1}{2}}} ds$ and $K = \frac{P_f}{P_m W}$, respectively.

Proof. Recall the Eq. (3.4), we may rewrite the SIR of a outdoor MT as:

$$\begin{aligned}\xi_m &= \frac{\frac{P_m}{A_O}\left(d_m^O\right)^{-\gamma_1} h_m}{\sum\limits_{m'\neq m}\frac{P'_m}{A_O}\left(d_{m'}^O\right)^{-\gamma_1} h_{m'} + \sum\limits_{f\in\Psi}\frac{P_f}{A_O W}\left(d_f^O\right)^{-\gamma_1} g_f} \\ &= \frac{h_0}{I_1+I_2},\end{aligned} \tag{3.6}$$

where we have $I_1 = \left(d_m^O\right)^{\gamma_1}\sum_{m'\neq m}\left(d_{m'}^O\right)^{-\gamma_1} h_{m'}$ and $I_2 = \left(d_m^O\right)^{\gamma_1}\sum_{f\in\Psi}\frac{P_f}{P_m W}\left(d_f^O\right)^{-\gamma_1} g_f$. The Eq. (3.6) holds since we assumed that each MBS transmits equal power.

The OP of an outdoor MT is the probability that its SIR is below a threshold x, given by:

$$\begin{aligned}F(x) &= \mathbb{P}\left[\xi_m\left(d_m^O\right) \leq x\right] \\ &= 1-\mathbb{P}\left[h_m \geq x(I_1+I_2)\right] \\ &= 1-\mathbb{E}_{I_1+I_2}\left\{\mathbb{P}\left[h_m \geq (I_1+I_2)\,|I_1+I_2\right]\right\} \\ &= 1-\mathbb{E}_{I_1+I_2}\left[\exp\left(-x\left(I_1+I_2\right)\right)\right] \\ &= 1-\mathbb{E}_{I_1}\left[\exp\left(-xI_1\right)\right]\mathbb{E}_{I_2}\left[\exp\left(-xI_2\right)\right] \\ &= 1-\mathcal{L}_{I_1}(x)\mathcal{L}_{I_2}(x),\end{aligned} \tag{3.7}$$

where $\mathcal{L}_{I_1}$ and $\mathcal{L}_{I_2}$ denote the Laplace transform of the variable I_1 and I_2, respectively. We will then derive the Laplace transform of I_1 and I_2, separately. The Laplace transform of the variable I_1 is given by:

$$\begin{aligned}\mathcal{L}_{I_1}(x) &= \mathbb{E}_{I_1}\left[\exp\left(-xI_1\right)\right] \\ &\geq \left[\exp\left(-x\mathbb{E}(I_1)\right)\right] \\ &= \exp\left(-x\left(d_m^O\right)^{\gamma_1}\sum_{m'\neq m}\left(d_{m'}^O\right)^{-\gamma_1}\right)\end{aligned} \tag{3.8}$$

Recall from the results derived in Chapter 2, the sum received downlink interference is evaluated by employing 'Fluid Model' when the cellular macrocells developing UFR, as stated in Eq. (2.9). As a result, we may have the following equality for CCR MTs ($d_m^O \leq D$):

$$\begin{aligned}\left(d_m^O\right)^{\gamma_1}\sum_{m'\neq m}\left(d_{m'}^O\right)^{-\gamma_1} &= \left(d_m^O\right)^{\gamma_1}\int_0^{2\pi}\int_{2R_m-d_m^O}^{\infty} z^{-\gamma_1}\rho_{MBS} z\,dz\,d\theta \\ &= \left(d_m^O\right)^{\gamma_1}\frac{2\pi\rho_{MBS}}{\gamma_1-2}\left(2R_m-d_m^O\right)^{2-\gamma_1},\end{aligned} \tag{3.9}$$

where $\rho_{MBS} = \frac{1}{\pi R_m^2}$ denotes the density of the grid-based MBSs [1]. However, when the MTs roam to the CER, the density of interfering MBSs is $\frac{1}{3\rho_{MBS}}$. As a result, we may have the following equality of CER MTs ($d_m^O > D$):

$$\begin{aligned}\left(d_m^O\right)^{\gamma_1} \sum_{m' \neq m} \left(d_{m'}^O\right)^{-\gamma_1} &= \left(d_m^O\right)^{\gamma_1} \int_0^{2\pi} \int_{2R_m - d_m^O}^{\infty} z^{-\gamma_1} \frac{\rho_{MBS}}{3} z dz d\theta \\ &= \left(d_m^O\right)^{\gamma_1} \frac{2\pi\rho_{MBS}}{3\left(\gamma_1 - 2\right)} \left(2R_m - d_m^O\right)^{2-\gamma_1}.\end{aligned} \tag{3.10}$$

Substituting the Eq. (3.9) and the Eq. (3.10) into the Eq. (3.8), the Laplace transform of I_1 is given by:

$$\begin{aligned}\mathcal{L}_{I_1}(x) &\geq \exp\left[\left(d_m^O\right)^{\gamma_1} \sum_{m \neq m'} \left(d_{m'}^O\right)^{-\gamma_1}\right] \\ &= \exp\left[-\frac{2l^{\gamma_1} x}{G(\gamma_1 - 2) R_m^2 (2\sqrt{G} R_m - l)^{(\gamma_1 - 2)}}\right],\end{aligned} \tag{3.11}$$

where we have $G = 1$ when $d_m^O \leq D$ and $G = 3$ when $d_m^O > D$ under the FFR scheme. As a results, the lower bound of $\mathcal{L}_{I_1}$ is derived. In this chapter, we approximate the real $\mathcal{L}_{I_1}$ by its lower bound of $\mathcal{L}_{I_1}$ for the sake of deriving the OP. Hence we made the approximation that: $\mathcal{L}_{I_1} \approx \exp\left[-\frac{2l^{\gamma_1} x}{G(\gamma_1 - 2) R_m^2 (2\sqrt{G} R_m - l)^{(\gamma_1 - 2)}}\right]$.

Meanwhile, the Laplace transform of the Poissonian shot-noise process I_2 is given by:

$$\begin{aligned}\mathcal{L}_{I_2} &= \mathbb{E}_{I_2}\left[\exp\left(\left(d_m^O\right)^{\gamma_1} \sum_{f \in \Psi} \frac{P_f}{P_m W} \left(d_f^O\right)^{-\gamma_1} g_f\right)\right] \\ &= \mathbb{E}_{\Psi, g_f} \prod_{f \in \Psi} \mathbb{E}_{g_f}\left[\exp\left(-\left(d_m^O\right)^{\gamma_1} K x g_f \left(d_f^O\right)^{-\gamma_1}\right)\right] \\ &= \mathbb{E}_{\Psi} \prod_{f \in \Psi}\left[\frac{1}{1 + \left(d_m^O\right)^{\gamma_1} K x \left(d_f^O\right)^{-\gamma_1}}\right] \\ &\overset{a}{=} \exp\left[-\lambda \iint_{\mathbb{R}} \left(1 - \frac{1}{1 + \left(d_m^O\right)^{\gamma_1} K x t^{-\gamma_1}}\right) t dt\right] \\ &= \exp\left[-2\pi\lambda \int_0^{\infty} \left(1 - \frac{1}{1 + \left(d_m^O\right)^{\gamma_1} K x t^{-\gamma_1}}\right) t dt\right]\end{aligned} \tag{3.12}$$

The equalitly of a in Eq. (3.12) follows from the Probability Generating Functional (PGFL) of the SPPP [224] and $\mathbb{R}$ denotes the FBS interference region. Assuming that

[1] As we stated in Chapter 2, when the hexagonal model is used, we have $\rho_{MBS} = \frac{\sqrt{3}}{6R_m^2}$.

$\left(d_m^O\right)^{\gamma_1} Kxt^{-\gamma_1} = s^{\frac{\gamma_1}{2}}$, we may futher derive the Laplace transform of I_2, which is written as:

$$\mathcal{L}_{I_2} = \exp\left[-\pi\lambda C_{\gamma_1}\left(d_m^O\right)^2 (Kx)^{\frac{2}{\gamma_1}}\right], \tag{3.13}$$

where $C_{\gamma_1} = \int_0^\infty \frac{1}{1+s^{\frac{\gamma_1}{2}}} ds$ and $K = \frac{P_f}{P_m W}$, respectively. Substituting Eq. (3.11) and Eq. (3.13) into Eq. (3.7), we arrive at Lemma 1. □

3.4.1.2 Indoor Femtocell MTs' OP

The indoor MTs served by the FBS B_f suffer from the interference imposed by the surrounding MBS set Φ and the neighbouring FBS set $\Psi \setminus B_f$. Owing to the near-far effects, femtocells suffer from serious interference only in the scenario, when they are located near the over-sailing MBS. As a result, the MBS's interference is dominated by the over-sailing macrocell [98]. In this chapter, we will ignore the MBS interference arriving from the other macrocells. However, the effect of other MBS's interference will be considered in the simulations.

Considering the FBS B_f at a distance of d_m^f from the MBS B_m, the SIR ξ_f of the associated indoor MT located at a distance of d_f^I, is given by:

$$\xi_f = \frac{\frac{P_f}{A_I}\left(d_f^I\right)^{-\gamma_2} g_f}{\frac{P_m}{A_O}\left(d_m^f\right)^{-\gamma_1} h_m + \sum\limits_{f' \neq f} \frac{P_f}{A_O W^2}\left(d_{f'}^I\right)^{-\gamma_1} g_{f'}}. \tag{3.14}$$

We can now derive the OP of the indoor femtocell MTs with the aid of Lemma 2.

Lemma 2. Let us consider an indoor femtocell MT, given the distance of $d_m^f = l$ from the reference FBS B_f to the MBS B_m. The OP of the indoor home MT may be expressed as:

$$\mathcal{F}_f(x|l) = 1 - \frac{2}{R_f^2}\int_0^{R_f} \frac{\exp\left(-\pi\lambda C_{\gamma_1} r^{\gamma_2/2} (Jx)^{\frac{2}{\gamma_1}}\right)}{1 + x\frac{J}{K} l^{-\gamma_1} r^{\gamma_2}} r dr, \tag{3.15}$$

where we have $J = \frac{A_I}{A_O W^2}$. Specifically, assuming outdoor and indoor pathloss exponents of $\gamma_1 = 4$ and $\gamma_2 = 2$ [2], respectively, the OP of the indoor home MT is formulated as:

$$\mathcal{F}_f(x|l) = 1 - \frac{\mathcal{H}(x,l)}{R_f^2 z(x,l)}, \tag{3.16}$$

where $z(x,l) = xl^{-4}\frac{J}{K}$, and $\mathcal{H}(x,l)$ can be derived from [225], which may be written as:

[2] Here, $\gamma_2 = 2$ is assumed in order to derive the closed-form OP. In reality, the indoor path-loss exponent is larger than 2. We will opt $\gamma_2 = 3$ for our simulation results.

$$\begin{aligned}\mathcal{H} = e^{\frac{iy(x)}{\sqrt{z(x,l)}}}&\left[Ei\left(y(x)R_f - \frac{iy(x)}{\sqrt{z(x,l)}}\right) - Ei\left(\frac{-iy(x)}{\sqrt{z(x,l)}}\right)\right]\\ + e^{\frac{-iy(x)}{\sqrt{z(x,l)}}}&\left[Ei\left(y(x)R_f + \frac{iy(x)}{\sqrt{z(x,l)}}\right) - Ei\left(\frac{iy(x)}{\sqrt{z(x,l)}}\right)\right],\end{aligned} \tag{3.17}$$

where Ei is the exponential integral function, with $y(x) = -\frac{\pi^2}{2}\lambda\sqrt{Jx}$.

Proof. Let us now consider an indoor femtocell MT. Similarly, given the distance $d_m^f = l$, $d_f^I = r$, the SIR $\xi_f\left(d_m^f, d_f^I\right)$ of Eq. (3.14) is rewritten as:

$$\xi_f\left(l, r\right) = \frac{g_f}{I_3 + I_4}, \tag{3.18}$$

where we have $I_3 = \frac{P_m A_I}{P_f A_O} l^{-\gamma_1} r^{\gamma_2} h_m$ and $I_4 = \frac{A_I}{A_O W^2} r^{\gamma_2} \sum_{f' \neq f} d_{f'}^I g_{f'}$. The OP of an indoor home user is given as:

$$\begin{aligned}\mathcal{F}_f\left[x|(l,r)\right] &= 1 - \mathbb{P}\left[g_f \geq x(I_3 + I_4)\right]\\ &= 1 - \mathcal{L}_{I_3}(x)\mathcal{L}_{I_4}(x),\end{aligned} \tag{3.19}$$

where $\mathcal{L}_{I_3}$ and $\mathcal{L}_{I_3}$ are similarly derived from Eq. (3.11) and Eq. (3.13), yielding:

$$\mathcal{L}_{I_3}(x) = \frac{1}{1 + x\frac{P_m A_I}{P_f A_O W} l^{-\gamma_1} r^{\gamma_2}} \tag{3.20}$$

$$\mathcal{L}_{I_4}(x) = \exp\left[-\pi C_{\gamma_1} r^{\frac{\gamma_2}{2}} \left(\frac{A_I}{A_O W^2} x\right)^{\frac{2}{\gamma_1}}\right]. \tag{3.21}$$

Assuming that the femtocell MTs are uniformly distributed, $\mathcal{F}_f(x|l)$ is given by:

$$\mathcal{F}_f(x|l) = \frac{2}{R_f^2} \int_0^{R_f} \mathcal{F}\left[x|(l,r)\right] r dr. \tag{3.22}$$

Substituting Eq. (3.19), Eq. (3.20) and Eq. (3.21) into the Eq. (3.22), we arrive at Lemma 2. □

3.4.2 Long-Term Spatially Averaged Macrocell Throughput

Let us denote the total number of MTs per macrocell by U_m and the number of macrocell users located in the CCR and CER by U_{m_1} as well as U_{m_2}, respectively. Hence, we have $U_m = U_{m_1} + U_{m_2}$. Since we assumed that the macrocell users are uniformly distributed in the circular region of Fig 3.5, the probability that a user lies in the CCR $\mathbb{P}\left(U_{m_1} = 1\right)$ or in the CER $\mathbb{P}\left(U_{m_2} = 1\right)$ is

given by: ω^2 and $1-\omega^2$, while the average number of users located in the CCR and CER is given by: $\overline{U}_{m_1} = \omega^2 U_m$ and $\overline{U}_{m_2} = \left(1-\omega^2\right) U_m$, respectively. As a result, the probability that there is at least one user in the CCR is given by:$\sum_{k=1}^{U_m} \mathbb{P}\left[U_{m_1} = k\right] = 1 - \left(1-\omega^2\right)^{U_m}$. Similarly, the probability that there is at least one user in the CER is given by:$1-\omega^{2U_m}$.

We note that the OP corresponding to the distance formulas of Eq. (3.5) is the conditional cumulative distribution function (CDF) of the users' SIR. Hence the joint CDF of the SIR and the distance may be written as $\mathcal{F}(x,l) = \mathcal{F}(x|l)\mathbb{P}\left(d_m^O = l\right)$. As a result, the CDF of the spatially averaged SIR is given by:

$$\begin{aligned}
\mathcal{F}_{m_1}(x,\omega) &= \left[1-\left(1-\omega^2\right)^{U_m}\right] \int_0^D \mathcal{F}_{m_1}(x|l)\frac{2l}{D^2}dl, \text{if } l \le D, \\
\mathcal{F}_{m_2}(x,\omega) &= \left(1-\omega^{2U_m}\right) \int_D^{R_m} \mathcal{F}_{m_2}(x|l)\frac{2l}{R_m^2 - D^2}dl, \text{if } l > D.
\end{aligned} \tag{3.23}$$

Hence, the probability density function (PDF) of the spatially averaged SIR for the CCR and CER users is directly given by the derivative of the CDF, written as:

$$\mathrm{f}_m(x) = \begin{cases} \mathrm{f}_{m_1}(x,\omega) = \frac{d\mathcal{F}_{m_1}(x,\omega)}{dx}, & \text{if } l \le D, \\ \mathrm{f}_{m_2}(x,\omega) = \frac{d\mathcal{F}_{m_2}(x,\omega)}{dx}, & \text{if } l > D. \end{cases} \tag{3.24}$$

According to the Eq. (3.3) in Section 3.2, the long-term spatially averaged macrocell throughput T_m is expressed as:

$$T_{m_1}(\omega) = \int_0^\infty log_2(1+\frac{x}{\varpi})\mathrm{f}_{m_1}(x,\omega)dx. \tag{3.25}$$

$$T_{m_2}(\omega) = \int_0^\infty log_2(1+\frac{x}{\varpi})\mathrm{f}_{m_2}(x,\omega)dx. \tag{3.26}$$

In the next subsection, we will move our attentions to discuss the parameter design issues for the FFR aided two-tier femtocell networks.

3.4.3 Optimal Design of FFR Aided Two-Tier Network Using FSA

We will then focus on the optimal design of the FFR aided two-tier system using FSA. Specifically, we will optimize the spectrum allocation factor ρ and distance threshold factor ω. The appropriate selection of these parameters is expected to significantly affect the performance of the network. We will determine the parameters in order to achieve the maximum ASE $\mathcal{S}_m$ of macrocell, which may be formulated as:

$$\mathcal{S}_m(\rho,\omega) = \frac{\rho T_{m_1}(\omega) + \frac{1-\rho}{3}T_{m_2}(\omega)}{\pi R_m^2}. \tag{3.27}$$

3.4.3.1 Area-Proportional Design

The authors of [217,218,221] selected a fixed distance threshold factor and the spectrum allocation factor was determined by so-called 'area-proportional design ', where have $\rho = \omega^2$, when the

macrocell users are uniformly distributed in the macrocells. Under this criterion, the spectrum allocated to the CCR users is proportional to the CCR area. The optimization problem using this design may be formulated as:

Problem 1:

$$(\rho^*, \omega^*) = \underset{(0\leq\rho,\omega\leq 1)}{\arg\max}\, \mathcal{S}_m(\rho, \omega) \tag{3.28}$$

$$\text{subject to } \rho = \omega^2. \tag{3.29}$$

Upon eliminating the constraint of Eq. (3.28), the optimization Problem 1 may be rewritten as:

$$\omega^* = \underset{(0\leq\omega\leq 1)}{\arg\max}\, \omega^2 T_{m_1}(\omega) + \frac{1-\omega^2}{3} T_{m_2}(\omega). \tag{3.30}$$

3.4.3.2 QoS-Constrained Design

In addition to the area-proportional design, we also present a QoS-constrained design approach, where we stipulate a QoS requirement η that the guaranteed long-term spatially averaged CER throughput per MT is at least η w.r.t CCR throughput per MT. Hence, the system parameters may be adjusted to trade the data-rates required by the CCR macrocell users against those of the CER macrocell users. As a result, the optimization problem using this design approach may be formulated as:

Problem 2:

$$(\rho^*, \omega^*) = \underset{(0\leq\rho,\omega\leq 1)}{\arg\max}\, \mathcal{S}_m(\rho, \omega) \tag{3.31}$$

$$\text{subject to } T_{m_2,u} \geq \eta T_{m_1,u}, \tag{3.32}$$

where $T_{m_1,u} = \frac{\rho T_{m_1}(\omega)}{\omega^2 U_m}$ and $T_{m_2,u} = \frac{(1-\rho) T_{m_2}(\omega)}{3(1-\omega^2) U_m}$ denote the long-term spatially averaged throughput (bit/s) per subchannel per CCR MT and per CER MT, respectively.

Note that the constraint imposed by Inequality (3.32) is a linear constraint, hence the problem can be solved by the method of Lagrange multipliers. The optimum ρ^* is located at the extremal points of Inequality (3.32), which may be written as:

$$\rho^* = \left[1 + 3\eta \frac{\left(1-\omega^2\right)}{\omega^2} \frac{T_{m_1}(\omega)}{T_{m_2}(\omega)}\right]^{-1}. \tag{3.33}$$

Upon substituting Eq. (3.33) into Eq. (3.31), the optimization Problem 2 is rewritten as:

$$\omega^* = \arg \max_{(0\leq\omega\leq 1)} \rho^* T_{m_1}(\omega) + \frac{1-\rho^*}{3} T_{m_2}(\omega). \tag{3.34}$$

Here we note that if we set $\eta = \frac{T_{m_2}(\omega)}{3T_{m_1}(\omega)}$, then we get $\rho^* = \omega^2$ from Eq. (3.33). As a result, our design becomes equivalent to the area-proportional design. Hence we may say that the area-proportional design is a specific case of our QoS-constrained design.

3.4.3.3 Solving Problems of Eq. (3.30) and Eq. (3.34)

Since no closed-form equations have been found for T_{m_1} and T_{m_2}, we solve the optimization problems of Eq. (3.30) and Eq. (3.34) using a Genetic Algorithm (GA), which attempts to mimic computationally the processes by natural selection operation in order to solve the optimization problems. Developed by J. Holland in the 1960s and 1970s [226] genetic algorithms provide a framework for studying the effects of such biologically inspired factors as mate selection, reproduction, mutation, and crossover of genetic information [227]. The GA constitutes an attractive adaptive global search method, where the fitness of every individual within the population of solutions is evaluated, then multiple individuals are randomly selected from the current population of candidate solutions (based on their fitness), and are appropriately modified (recombined and possibly randomly mutated) to form a new population. The new population of the next generation of candidate solutions is then used in the next iteration of the algorithm. The GA process hence leads to the gradual evolution of the population to better solutions of the problem to be solved than solutions that they were created from, just as in natural evolution. The basic framework of a genetic algorithm is adpted from M. Mitchell [228] in her interesting book as follows:

- *Step 0*: Initialization. Assuming that the data are encoded in bit strings. Specify a crossover probability or crossover rate, and a mutation probability or mutation rate.
- *Step 1*: The population is chosen, consisting of a set of chromosomes.
- *Step 2*: The fitness function is calculated for each chromosome in the population.
- *Step 3*: Iterate through the following steps until reaching the maximum allowance.
  - *Step 3a*: Selection. Using the values from the fitness function from step 2, assign a probability of selection to each chromosome, with higher fitness providing a higher probability of selection.
  - *Step 3b*: Crossover. Select a randomly chosen crossover point for where to perform the crossover with the crossover probablility. Then perform crossover with the parents selected in Step 3a, thereby forming two new offspring. If the crossover is not performed, clone two exact copies of the parents to be passed on to the new generation,
  - *Step 3c*: Mutation. With the predefined mutation probability, perform mutation on each of the two offspring at each crossover point. The chromosomes then take their place in the new population.
- *Step 4*: The new population of chromosomes replaces the current population.
- *Step5*: Check whether termination criteria have been met. If convergence is achieved, stop the iterations and report results; otherwise, go to Step 2.

We will then use such framework of the GA to solve our problems of Eq. (3.30) and Eq. (3.34). The optimization process using the GA is briefly summarized as follows:

1. Initialization. The GA randomly generates a number of potential solutions, hosted by a so-called population, which may be composed of N_{ind} number of L-bit (candidate solutions) chromosomes and each chromosome represents an individual distance threshold ω. In the simulations, we used $N_{ind} = 40$ and $L = 12$.

2. Calculate the fitness function $F(\omega)$ of each chromosome ω in the population. The individual fitness $F(\omega_i)$ is computed as the individual's performance relative to that of the entire population, which may be formulated as:

$$F(\omega_i) = \frac{\rho^*(\omega_i)T_{m_1}(\omega_i) + \frac{1-\rho^*(\omega_i)}{3}T_{m_2}(\omega_i)}{\sum_{i=1}^{N_{ind}}\left[\rho^*(\omega_i)T_{m_1}(\omega_i) + \frac{1-\rho^*(\omega_i)}{3}T_{m_2}(\omega_i)\right]}, \tag{3.35}$$

   where T_{c_1} and T_{c_2} are given by Eq. (3.25) and Eq. (3.26) for FSA, respectively. If we opt for the 'area-proportional design', ρ^* satisfies Eq. (3.29). If we opt for the 'QoS-constrained design', ρ^* satisfies Eq. (3.33)

3. Repeat the steps (a)-(c) below, until N offspring have been created:

   (a) Select a pair of parent chromosomes from the current population, with the probability of selection being an increasing function of fitness.

   (b) With probability p_c, arrange for the cross-over of the pair at a randomly chosen point to form two offspring for the two 'parent' individuals. We set the so-called cross-over probability to $p_c = 0.7$ in our simulations.

   (c) Mutate i.e. 'deliberately perturb' the two offspring with a probability of p_m, and then place the resultant chromosomes in the new population. We used a mutation probability of $p_m = 0.05$ for avoiding premature convergence to a suboptimum value.

4. Replace the current population with the new population.

5. Go to step 2.

3.5 FFR Aided Two-Tier Network with SSA

To mitigate the cross-layer interference, SSA scheme, which is described in Section 3.3, is proposed in the FFR aided two-tier femtocell networks. The OP arrived at with the aid of our solution will be then derived. The corresponding optimal network design will also be presented.

3.5.1 Spectrum Swapping Access

As we discussed in Section 3.3, both the outdoor and indoor MTs may suffer from cross-layer interference in conjunction with FSA. In the SSA, the femtocells will reuse the specific frequency bands, which are orthogonal to the over-sailing macrocells. For example, for the center macrocell seen in Fig. 3.5, the MBS may assign F_c and F_1 to the outdoor CCR MTs. To avoid the cross-layer interference emanating from over-sailing macrocells, the femtocells in macrocell 0 may access frequency bands F_2 and F_3. With the aid of our SSA, the cross-layer interference is substantially reduced. Specifically, the cross-layer interference is avoided for the outdoor CCR macrocell MTs. The outdoor CER macrocell MTs only suffer from the interference arriving from the femtocells located within other macrocells. For the indoor femtocell MTs, the cross-layer interference emanating from the over-sailing MBS is avoided.

3.5.2 Per-Layer Outage Probability

3.5.2.1 Outdoor Macrocell MTs' OP

When employing the proposed SSA strategy, the outdoor macrocell MTs roaming in the CCR of macrocell m suffers from the interference imposed by the neighboring MBS set $m' \neq m,\ m' \in \mathcal{I}_m$. Hence, the SIR ξ_m of a CCR MT located at a distance of d_m^O from the MBS B_m is given by:

$$\xi_m = \frac{\frac{P_m}{A_O}\left(d_m^O\right)^{-\gamma_1} h_m}{\sum\limits_{m' \in \mathcal{I}_m} \frac{P_m}{A_O}\left(d_{m'}^O\right)^{-\gamma_1} h_{m'}}. \tag{3.36}$$

The outdoor macrocell MTs roaming in the CER may suffer from the interference imposed by the interfering MBS set $\mathcal{I}_m$, which share the same frequency band within the CER MTs, and by the FBS set located within the other macrocells $\mathcal{I}_f$. Hence we may formulate the SIR γ_m of a CER MT located at a distance of d_m^O from the MBS B_m as:

$$\xi_m = \frac{\frac{P_m}{A_O}\left(d_m^O\right)^{-\gamma_1} h_m}{\sum\limits_{m' \in \mathcal{I}_m} \frac{P_m}{A_O}\left(d_m^O\right)^{-\gamma_1} h_{m'} + \sum\limits_{f \in \mathcal{I}_f} \frac{P_f}{A_O W}\left(d_f^O\right)^{-\gamma_1} g_f}. \tag{3.37}$$

The OP of the outdoor macrocell MTs is formulated in Lemma 3 for our proposed solution.

Lemma 3. Given the distance of $d_m^O = l$ from the MBS B_m, the OP of this outdoor user for our proposed spectrum-swapping solution is written as:

$$\begin{aligned} \mathcal{F}_{m_1}^p(x|l) &= 1 - \exp\left(-\zeta_1 x\right), \text{if } \ l \leq D, \\ \mathcal{F}_{m_2}^p(x|l) &= 1 - \exp\left(-\zeta_2 x - \lambda l^2 \sqrt{Kx} S\right), \text{if } \ l > D, \end{aligned} \tag{3.38}$$

where we have $S = \left(\frac{\pi^2}{2} - \int_0^{\pi} \arctan \frac{\left(\sqrt{R_m^2 - l^2 \sin^2\theta} - l\cos\theta\right)^2}{d^2\sqrt{Kx}} d\theta\right)$, assuming $\gamma_1 = 4$.

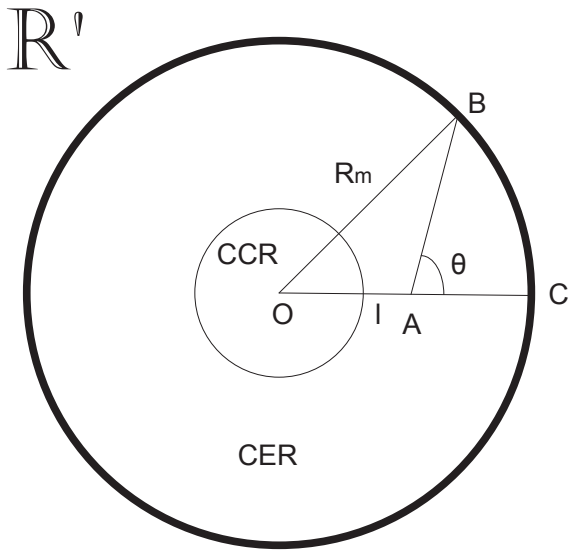

Figure 3.8: The topology of the FBS interference analysis when the outdoor MT marked by 'A' is roaming towards the CER, where the interfering FBS region is denoted as $\mathbb{R}'$.

Proof. We first consider an outdoor macrocell MT. Comparing Eq. (3.36) to Eq. (3.4), the OP of an outdoor macrocell MT located in the CCR is simply derived by removing $\mathcal{L}_{I_2}$ of Eq. (3.7).

However, as for the CER users, they suffer from the FBS interference imposed by the FBSs located upon the neighbouring macrocells. Here we denote the FBS interference region $\mathbb{R}'$. Similarly to I_2, we assume $I_5 = \sum_{j\in\Psi\setminus\psi_0} \frac{P_f}{P_m W}\left(d_{f_j}^O\right)^{-\alpha_1} g_j$, and the Laplace transform of I_5 is given by:

$$\mathcal{L}_{I_5} = \exp\left[-\lambda \iint_{\mathbb{R}'} \left(1 - \frac{1}{1+\left(d_{m_0}^O\right)^{\alpha_1} K x t^{-\alpha_1}}\right) t dt d\theta\right]. \tag{3.39}$$

Let us now discuss the integral interval $\mathbb{R}'$. If a CER MT roams at a distance l from the MBS, as shown in Fig. 3.8, given the angle $\angle BAC = \theta$, we have $AB = \sqrt{R_m^2 - l^2\sin^2\theta} - l\cos\theta$, hence the distance from the CER user to the FBSs varies from AB to ∞. As a

result, $\mathcal{L}_{I_5}$ is rewritten as:

$$\mathcal{L}_{I_5} = \exp\left[-\lambda \int_0^{2\pi} \int_{\sqrt{R_m^2 - l^2 \sin^2\theta} - l\cos\theta}^{\infty} \left(1 - \frac{1}{1 + (d_m^O)^{\gamma_1} Kxt^{-\gamma_1}}\right) tdtd\theta\right]. \tag{3.40}$$

Hence, assuming $\gamma_1 = 4$, the OP of the CER MT is given by Eq. (3.38) and Lemma 3 follows. □

3.5.2.2 Indoor Femtocell Users' OP

Under the SSA scheme, the target femtocell's indoor home user endures interference from the nearby FBS set denoted by $\mathcal{I}_f$. As a result, when considering the target FBS at a distance of $d_m^f = l$ from the target MBS, the SIR ξ_f of the associated indoor home MT located at a distance of d_f^I from the target FBS B_f may be expressed as:

$$\xi_f\left(d_m^f, d_f^I\right) = \frac{\frac{P_f}{A_I}\left(d_f^I\right)^{-\gamma_2} g_f}{\sum_{f' \in \mathcal{I}_f} \frac{P_f}{A_O W^2}\left(d_{f'}^I\right)^{-\gamma_1} g_{f'}}. \tag{3.41}$$

As a result. We use the Lemma 4 characterizing the OP of the indoor home MT of the proposed spectrum-swapping solution in the FFR scenario.

Lemma 4. Given the distance $d_m^f = l$ from the reference femtocell f to the macrocell f and the target SIR threshold of x, the OP of the indoor home user involving our spectrum-swapping in the FFR environment is given by:

$$\mathcal{F}_f^p(x) = \mathcal{F}_f^p(x|l) = 1 - \frac{2}{R_f^2 t} A(x)^{-\frac{2}{t}} \Gamma\left[\frac{2}{t}, A(x) R_f^t\right], \tag{3.42}$$

where we have $t = \frac{2\gamma_2}{\gamma_1}$, $A(x) = \pi\lambda C_{\gamma_1} (Jx)^{\frac{2}{\gamma_1}}$, and also $J = \frac{A_I}{A_O W^2}$. Furthermore, $\Gamma(s, x)$ is the incomplete gamma function, which is written as:

$$\Gamma(s, x) = \int_0^x t^{s-1} e^{-t} dt. \tag{3.43}$$

Proof. Now we consider an indoor femtocell MT located at a distance r from its serving FBS. Observing that its SIR under our proposed solution is independent of the distance d_m^f, Eq. (3.41) may be rewritten as:

$$\xi_f(r) = \frac{g_f}{r^{\gamma_2} J I_5}, \tag{3.44}$$

where we have $d_f^I = r$, $I_5 = \sum_{f' \in \mathcal{I}_f} d_{f'}^{I})^{-\gamma_1} g_{f'}$ and $J = \frac{A_I}{A_O W^2}$. Then the OP of the indoor home MT's SIR under our proposed solution may be expressed as:

$$\mathcal{F}_f^p(x|r) = 1 - \mathbb{P}\left[\gamma_f(r) \geq x\right] = 1 - \mathcal{L}_{I_5}\left(xr^{\gamma_2} J\right), \tag{3.45}$$

where $\mathcal{L}_{I_5}(\cdot)$ is similarly given by:

$$\mathcal{L}_{I_5}\left(xr^{\gamma_2} J\right) = \exp\left(-\pi\lambda C_{\gamma_1} r^{\frac{2\gamma_2}{\gamma_1}} (Jx)^{\frac{2}{\gamma_1}}\right). \tag{3.46}$$

Since we assumed that the indoor home MTs tend to be uniformly distributed in the coverage region of their FBS, the OP of an indoor home MT benefiting from our proposed solution may be written as:

$$\begin{aligned}
\mathcal{F}_f^p(x) &= \mathbb{E}_r\left[\gamma_f(r) < x | 0 \leq r \leq R_f\right] \\
&= 1 - \frac{2}{R_f^2} \int_0^{R_f} r \exp\left(-\pi\lambda C_{\gamma_1} r^{\frac{2\gamma_2}{\gamma_1}} (Jx)^{\frac{2}{\gamma_1}}\right) dr \\
&\text{Assume } t = \frac{2\gamma_2}{\gamma_1} \text{ and } A(x) = \pi\lambda C_{\gamma_1} (Jx)^{\frac{2}{\gamma_1}} \\
&= 1 - \frac{2}{R_f^2} \int_0^{R_f} r e^{-A(x) r^t} dr \\
&= 1 - \frac{2}{R_f^2 t} A^{(-\frac{2}{t})} \Gamma\left(\frac{2}{t}, A R_f^t\right),
\end{aligned} \tag{3.47}$$

□

3.5.3 Long-Term Spatially Averaged Macrocell Throughput with SSA Scheme

3.5.3.1 CCR Throughput

We note that the OP of Eq. (3.38) is the conditional CDF of the CER MTs' SIR. Similarly the Section 3.4.2, the long-term spatially averaged throughput is given by:

$$T_{m_1}(\omega) = \left[1 - \left(1 - \omega^2\right)^{U_m}\right] \int_0^{\omega R_m} \frac{2l}{\left(\omega R_m\right)^2} \left[\int_0^{\infty} log_2\left(1 + \frac{x}{\varpi}\right) \mathrm{f}_{m_1}^p(x) dx\right] dl. \tag{3.48}$$

We assume that $\mathcal{T} = \frac{2l^{\gamma_1} x}{(\gamma_1 - 2) R_m^2 (2R_m - l)^{(\gamma_1 - 2)}}$, Eq. (3.48) may be rewritten as:

$$\begin{aligned}
T_{m_1}(\omega) &= \left[1 - \left(1 - \omega^2\right)^{U_m}\right] \int_0^{\omega R_m} \frac{2l}{\left(\omega R_m\right)^2} \left[\int_0^{\infty} log_2\left(1 + \frac{1}{V} t\right) e^{-\mathcal{T}} d\mathcal{T}\right] dl \\
&= \left[1 - \left(1 - \omega^2\right)^{U_m}\right] \int_0^{\omega R_m} -\frac{2l}{\left(\omega R_m\right)^2 ln2} \exp(V) Ei(-V) dl,
\end{aligned} \tag{3.49}$$

where $V = \frac{2\varpi l^{\gamma_1}}{(\gamma_1-2)R_m^2(2R_m-l)^{(\gamma_1-2)}}$. The integral (3.49) is difficult to solve. Noting that $V \ll 1$, we may invoke the approximation that $\exp(V) \approx 1$. The Taylor series of the exponential integral term in Eq. (3.49) is given by:

$$Ei(V) \approx \epsilon + \ln V - V, \tag{3.50}$$

where ϵ is the Euler-Mascheroni constant [225]. When assuming $\alpha = 4$, the long-term spatially averaged CCR throughput under the SSA is approximated as:

$$\begin{aligned} T_{m_1}(\omega) \approx \left[1 - \left(1-\omega^2\right)^{U_m}\right] \Bigg[& 2\log_2 \frac{2-\omega}{\omega^2} + \frac{8}{\omega^2}\log_2 \frac{2}{2-\omega} + \frac{\omega(1-\epsilon)-4}{\omega \ln 2} \\ & - \log_2 \varpi + \frac{1}{6\varpi\omega^4 \ln 2}\, {}_2F_1(2,6,7,\frac{3}{R_m})\Bigg], \end{aligned} \tag{3.51}$$

where ${}_2F_1(a,b,c,z)$ denotes the Gauss hypergeometric function [225]. Furthermore, the ASE of CCR MTs using SSA regime S_{m_1} is given by $\frac{T_{m_1}}{\pi R_m^2}$.

3.5.3.2 CER Throughput

We note that the OP of Eq. (3.38) is the conditional CDF of the CER MTs' SIR. As a result, the spatially averaged CDF of the SIR for the CER MTs is given by:

$$\mathcal{F}_{m_2}^p(x) = \left(1-\omega^{2U_m}\right) \int_D^{R_m} \mathcal{F}_{m_2}^p(x|l) \frac{2l}{(R_m^2 - D^2)} dl, \tag{3.52}$$

where $\mathcal{F}_{m_2}^p(x|l)$ is given by Eq. (3.38). Similarly to Section 3.4.2, the long-term spatially averaged macrocell throughput (bit/s/Hz) in the CER is expressed as:

$$T_{m_2}(\omega) = \int_0^\infty log_2(1+\frac{x}{\varpi}) \mathrm{f}_{m_2}^p(x) dx, \tag{3.53}$$

where $\mathrm{f}_{m_2}^p(x) = \frac{d\mathcal{F}_{m_2}^p(x)}{dx}$ denotes the PDF of the spatially averaged SIR for the CER MTs. Furthermore, the ASE of CER MTs using SSA regime S_{m_2} is given by $\frac{T_{m_2}}{\pi R_m^2}$.

3.5.4 Optimal Design of the FFR Aided Two-Tier Network with SSA

In this subsection, we will focus our attention on the optimal design of the FFR aided two-tier system using SSA. Similar to Section 3.4, we also consider the area-proportional design and the QoS-constrained design relying on our SSA strategy in order to achieve the maximum ASE of macrocell. We also use a GA to solve the above pair of optimization problems, where T_{m_1} and T_{m_2} will be numerically evaluated from Eq. (3.51) and Eq. (3.53), respectively. The optimization process using the GA is briefly summarized as follows:

1. Initialization. The GA randomly generates a number of potential solutions, hosted by a so-called population, which may be composed of N_{ind} number of L-bit (candidate solutions) chromosomes and each chromosome represents an individual distance threshold ω. In the simulations, we used $N_{ind} = 40$ and $L = 12$.

2. Calculate the fitness function $F(\omega)$ of each chromosome ω in the population. The individual fitness $F(\omega_i)$ is computed as the individual's performance relative to that of the entire population, which may be formulated as:

$$F(\omega_i) = \frac{\rho^*(\omega_i)T_{m_1}(\omega_i) + \frac{1-\rho^*(\omega_i)}{3}T_{m_2}(\omega_i)}{\sum_{i=1}^{N_{ind}}\left[\rho^*(\omega_i)T_{m_1}(\omega_i) + \frac{1-\rho^*(\omega_i)}{3}T_{m_2}(\omega_i)\right]}, \tag{3.54}$$

where T_{c_1} and T_{c_2} are given by Eq. (3.51) and Eq. (3.53) for SSA, respectively. If we opt for the 'area-proportional design', ρ^* satisfies Eq. (3.29). If we opt for the 'QoS-constrained design', ρ^* satisfies Eq. (3.33)

3. Repeat the steps (a)-(c) below, until N offspring have been created:

   (a) Select a pair of parent chromosomes from the current population, with the probability of selection being an increasing function of fitness.

   (b) With probability p_c, arrange for the cross-over of the pair at a randomly chosen point to form two offspring for the two 'parent' individuals. We set the so-called cross-over probability to $p_c = 0.7$ in our simulations.

   (c) Mutate i.e. 'deliberately perturb' the two offspring with a probability of p_m, and then place the resultant chromosomes in the new population. We used a mutation probability of $p_m = 0.05$ for avoiding premature convergence to a sub-optimum value.

4. Replace the current population with the new population.

5. Go to step 2.

3.6 Numerical Results and Discussions

3.6.1 Simulation Assumptions

In this section, the downlink performance of the FFR aided two-tier network is characterized by simulations. The system topology considered is illustrated in Fig. 3.5, where the macrocells and femtocells are represented by a circle having a radius of R_m and R_f, respectively. Again, it is assumed that the transmission power of the MBSs and FBSs is fixed to their maximum. As a result, the power allocation problem is not considered. As we stated in Section 3.3, the effect of the noise is ignored in the OP analysis, since the noise power is negligible compared to the interference. However, the effect of noise will be taken into account in our simulations. The distance threshold based FFR scheme is considered. Hence the macrocell MTs are located in the CCR, when the distance from its serving MBS is shorter than the distance threshold. Otherwise, the MTs are located in the CER. The per-layer OP is investigated first, where the performance of both the UFR aided two-tier networks, as well as that of the FSA based FFR aided two-tier networks and that of

the SSA based FFR aided two-tier networks are considered. The SIR threshold for the macrocell MTs and that for the femtocell MTs is set to be $0dB$ and $20dB$, respectively. Then the long-term spatially averaged macrocell throughput formulas of Eq. (3.25), Eq. (3.26), Eq. (3.51) and Eq. (3.53) are verified by simulations. Later, the optimal parameters are found, where the performance of both the area-proportional design and that of the QoS-constrained design are presented. The distance threshold D is assumed to be spanning from $0.05R_m$ to $0.95R_m$. Again, the system parameters are summarized in Table 3.1.

3.6.2 Per-Layer OP for Both the Outdoor Macrocell MTs and the Indoor Femtocell MTs

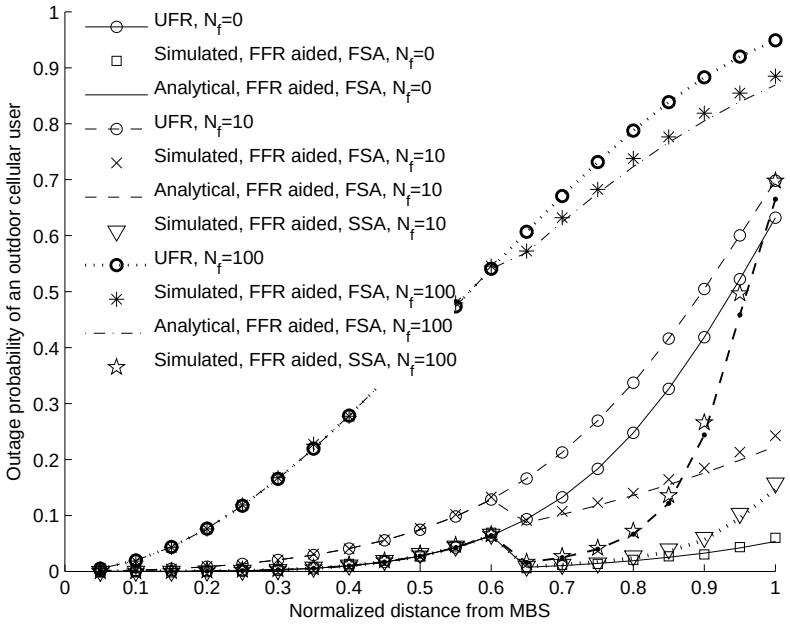

Figure 3.9: The OP of an outdoor cellular MT versus the normalized distance from the MBS, for the target SIR threshold of $x = 0$ dB. The OP performance of UFR aided two-tier networks, FFR aided two-tier networks using FSA and FFR aided two-tier networks using SSA are compared. Three scenarios are considered, where a) no femtocell is overlaid onto the macrocells, b) low density of femtocells are overlaid onto the macrocells ($N_f = 10$ per macrocell), as well as c) high density of femtocells are overlaid onto the macrocells ($N_f = 100$ per macrocell). All system parameters were summarized in Table 3.1.

Fig. 3.9 illustrates the OP for an outdoor macrocell MT as a function of the distance from the MT to the serving MBS B_m, when we set the target SIR threshold to 0dB. Observe from Fig.3.9 that as expected, the OP increases, when the user moves from the CCR to the CER. In general, employing the FFR scheme enhances the CER MTs' SIR. As a result, the OP is reduced for the CER outdoor users compared to the UFR scheme. With the aid of FFR, the interference emanating from other MBS is reduced. As a result, there is an OP reduction, when the outdoor user moves from the CCR to the CER. Naturally, introducing femtocells will impose additional interference on the outdoor macrocell MTs. More explicitly, when the two-tier network employing the FSA strategy, as an increasing number of femtocells, the advantage of the FFR scheme gradually erodes for the CER users, especially for the MTs located far from the serving MBS. By contrast, the OP of an outdoor macrocell MT is significantly reduced in both the CCR and CER with the aid of the proposed SSA strategy. Additionally, we also verified the formulas of Eq. (3.5) and Eq. (3.38) in Section 3.4 and Section 3.5, respectively. We demonstrated that our theoretical results are accurate for both the FSA and SSA strategies.

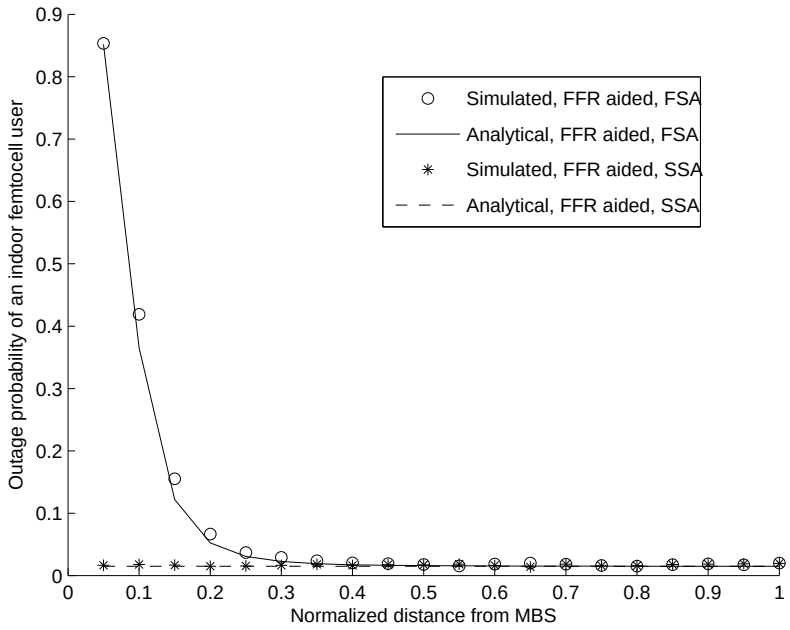

Figure 3.10: The OP of indoor MTs versus the distance from serving FBS to the MBS, for the target SIR threshold of $x = 20dB$ and $N_f = 10$. The OP performance of FFR aided two-tier networks using FSA and FFR aided two-tier networks using SSA are compared. All system parameters were summarized in Table 3.1.

Fig. 3.10 shows the OP of an indoor femtocell MT as a function of the distance from the FBS to the central MBS B_m, when we set the target SIR threshold to 20dB and the averaged number of femtocells per cell to 100. For the FSA, the indoor MTs may suffer from a high OP, when

their serving FBS is near to the MBS, especially for the distance range ($l \leq 0.1R_m$) owing to the high MBS interference. However, when the FBS is sufficiently far away from the MBS, the OP is rapidly reduced. On the other hand, the OP of the indoor MTs supported by our SSA remains low, because the interference emanating form the neighbouring FBSs is significantly reduced owing to the attenuation of walls. It is also observed that the analytical OP formulae accurately predict the OP, as confirmed by the simulations. It is noted that the SSA results in an constant OP trend for the femtocell MTs, which is independent of their positions. This is because that the femtocell MTs using SSA scheme suffer the interference which is domainated by the femtocells overlaided onto the neighbouring macrocells. As a result, the overall interference suffered by the femtocell MTs may be independent with the distance from its serving FBS to the underlaided MBS.

3.6.3 Long-Term Spatially Averaged Macrocell Throughput

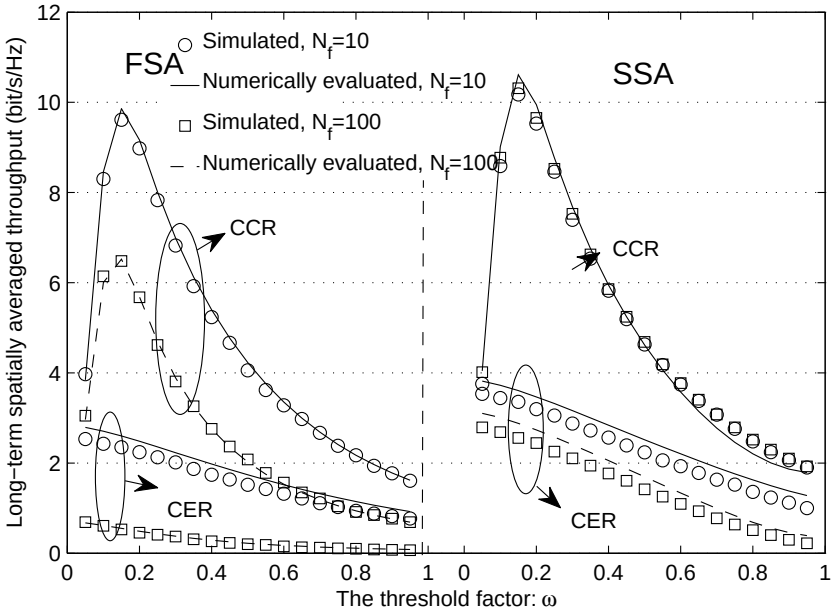

Figure 3.11: The long-term spatially averaged macrocell throughput. The performance according to the threshold factor of FFR aided two-tier networks using FSA and FFR aided two-tier networks using SSA are compared. Two scenarios are considered, where a) low density of femtocells are overlaid onto the macrocells ($N_f = 10$ per macrocell), and b) high density of femtocells are overlaid onto the macrocells ($N_f = 100$ per macrocell). All system parameters were summarized in Table 3.1.

Let us now verify the numerically evaluated macrocell long-term results given in Eq. by simu-

lations in Fig. 3.11. As expected, the performance in the CCR is consistently higher than that in the CER for both dense and sparse femtocell deployments for FSA scheme. This is because that the received SIR of CCR MTs may always much higher than that of CER MTs, which leading higher throughput for CCR MTs. Since the probability that at least one MT is located in the CCR is low when ω is small, the throughput will be low along with a low ω. The CCR related curve exhibits a peak at a point around $\omega = 0.15$, while the CER related curve is monotonic as a function of ω. Similar trends are also valid for SSA. The ASE of CCR is independent with the femtocell density. This is because that CCR macrocell MTs may only suffer the interference from the neigbouring MBSs as well as the FBSs which are located overlaid onto the neighbouring macrocells, when the SSA shceme is employed. As a result, the throughput of CCR is independent of the femtocell density. On the other hand, the difference between the FSA and SSA is that for the FSA, dense femtocells will result in a higher ASE degradation in comparison to sparse femtocells. By contrast, the variation of the femtocell density has a less pronounced effect. Furthermore, for both the FSA and the SSA, the numerically evaluated results derived in Section 3.4 and Section 3.5 are quite accurate, as decipted in Fig. 3.11.

3.6.4 Optimal Design for the Two-Tier Network

In order to highlight the importance of optimal parameter design, the performance of the FFR aided two-tier network having several different system configurations are compared, based on both the area-proportional design and on the QoS-constrained design, respectively. More explicitly, the following system configurations are considered: *System 1 (S1)*: It is assumed that S1 opts for the FSA strategy and the parameters ω of S1 are fixed. Two parameter sets are considered: S1(a): $\omega = 1/3$ and S1(b): $\omega = 2/3$. *System 2 (S2)*: It is assumed that S2 opts for the FSA strategy. When the femtocells are overlaid onto existing macrocells, two different approaches are assumed in handling the femtocells in the context of the area-proportional design *S2(a): Femtocell unaware*– In this system, the parameters are optimized assuming that the MBS is unaware of the femtocells. More explicitly, the optimal parameters are determined assuming that no femtocell is overlaid onto the macrocells. *S2(b): Femtocell awareness*–The parameters are optimized according to the number of femtocells in this system. By contrast, only the femtocell aware scenario is considered in the context of the QoS-constrained design, since ω and ρ are determined under the constraint of Eq. (3.32), which requires the system to have the knowledge of T_{m_1} and T_{m_2}. *System 3 (S3)*: It is assumed that S3 opts for the SSA strategy and the parameters are optimized in order to achieve the highest throughput, also assuming that the system is femtocell aware.

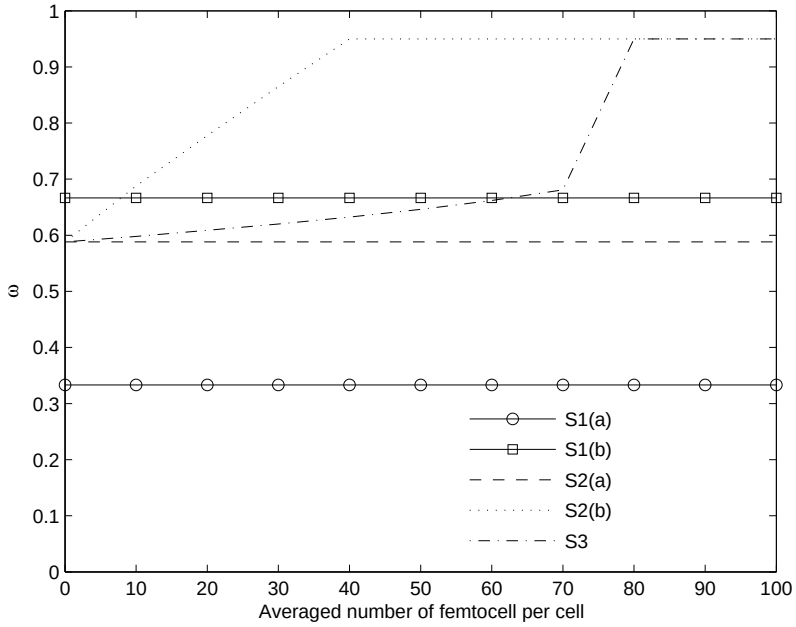

Figure 3.12: The optimal threshold ω in the area-proportional design. The following system configurations are considered:a) S1: The FSA strategy and the parameters ω are fixed. Two parameter sets are considered: S1(a): $\omega = 1/3$ and S1(b): $\omega = 2/3$. b) S2: FSA strategy is assumed and two different approaches are assumed in handling the femtocells in the context of the area-proportional design S2(a): Femtocell unaware, and S2(b): Femtocell awareness. c) S3: SSA strategy is assumed and Femtocell awareness is employed. All system parameters were summarized in Table 3.1.

3.6.4.1 Area-Proportional Design

Fig. 3.12 and Fig. 3.13 illustrate the dependence of the system parameters for the three systems on the number of femtocells. Owing to the system configuration of S1, ρ and ω are set to be fixed and independent with the averaged number of femtocell per cell. Furthermore, it is constrained by the characterization of area-proportional design and $\rho = \omega^2$ follows. The system parameters of ρ^* and ω^* are optimized for S2(a), assuming no femtocells are overlaid. Then the optimal parameters are derived according to Eq. (3.29) with $\lambda = 0$. Since femtocell unaware configuration is assumed for S2(a), the optimal parameters are independent with the averaged number of femtocell per cell. On the other hand, ω tends to increase upon increasing the number of femtocells for S2(b) and S3, which are aware of the number of femtocells. We note that the CCR will extend to the maximum tolerance level ($\omega = 0.95$), when we have $N_f \geq 40$ for the FSA and $N_f \geq 70$ for the SSA. As

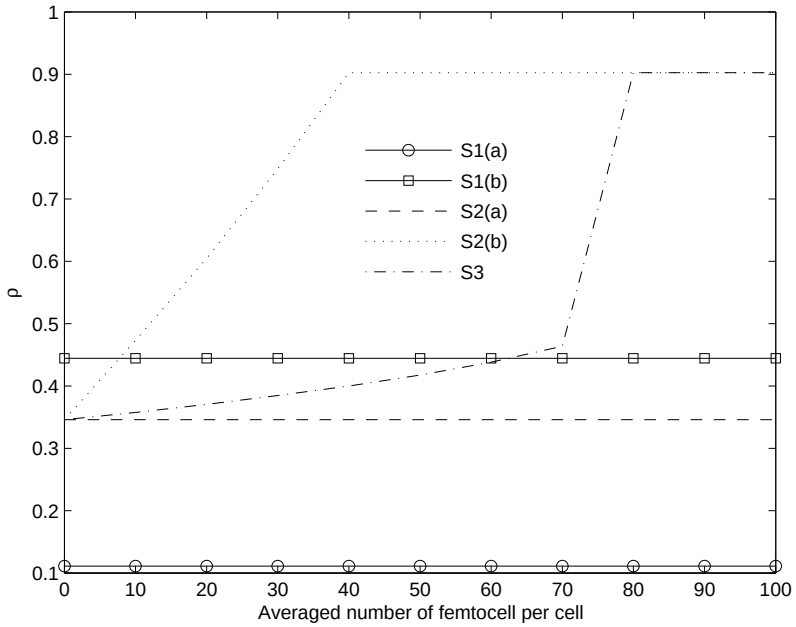

Figure 3.13: The optimal spectrum allocation ρ in the area-proportional design. The following system configurations are considered:a) S1: The FSA strategy and the parameters ω are fixed. Two parameter sets are considered: S1(a): $\omega = 1/3$ and S1(b): $\omega = 2/3$. b) S2: FSA strategy is assumed and two different approaches are assumed in handling the femtocells in the context of the area-proportional design S2(a): Femtocell unaware, and S2(b): Femtocell awareness. c) S3: SSA strategy is assumed and Femtocell awareness is employed. All system parameters were summarized in Table 3.1.

a result, we may conclude that the optimized system tends towards the UFR aided network in a dense-femtocell scenario. This is because that the CER performance degrades significantly in the dense-femtocell scenario. As a result, the system is willing to allocate more resource to the CCR. Finally, the ρ obeys similar trends to ω owing to their fixed relationship of Eq. (3.29).

Fig. 3.14 compares the ASE of macrocell for these systems. It is shown that the specific selection of system parameters may significantly affect the macrocell's ASE. For the traditional single-layer network ($N_f = 0$), the optimized systems (S2 and S3) attain a higher ASE than the fixed parameter based system (S1). Hence our GA based optimization is capable of achieving a high ASE. Similar trends were also noted in [218]. For the two-tier network ($N_f > 0$), the optimal design which ignores the number of femtocells (S2(a)) will be inefficient and its performance may even be worse than the fixed parameter based design (S1(b)). By contrast, the optimal design,

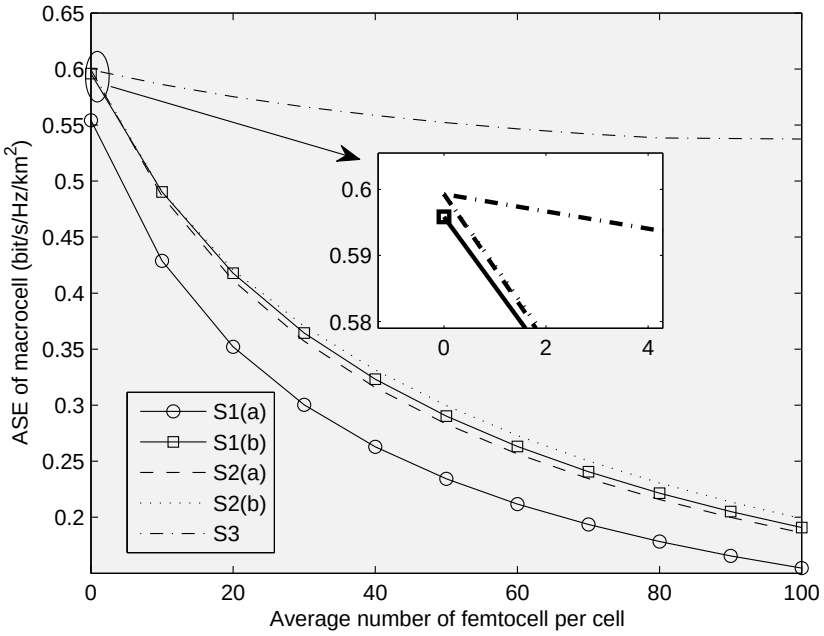

Figure 3.14: The ASE of macrocell in the area-proportional design. The following system configurations are considered:a) S1: The FSA strategy and the parameters ω are fixed. Two parameter sets are considered: S1(a): $\omega = 1/3$ and S1(b): $\omega = 2/3$. b) S2: FSA strategy is assumed and two different approaches are assumed in handling the femtocells in the context of the area-proportional design S2(a): Femtocell unaware, and S2(b): Femtocell awareness. c) S3: SSA strategy is assumed and Femtocell awareness is employed. All system parameters were summarized in Table 3.1.

which is aware of the number of femtocells (S2(b)) is capable of achieving a higher ASE than the fixed parameter based design (S1). However, the S2(b) system's performance may be sensitive to the number of femtocells, where the ASE reduces significantly upon increasing N_f owing to the high level FBS interference. Hence the effect of femtocells should be taken account into the optimization design. On the other hand, our proposed SSA strategy attains the highest ASE among all of our systems, guaranteeing a high macrocell ASE even in the high-density femtocell deployment scenario of $N_f = 100$.

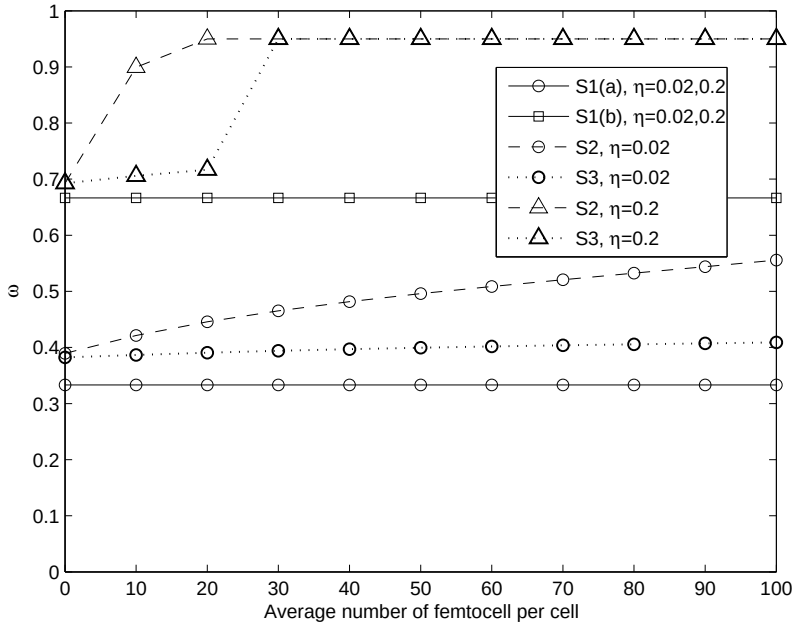

Figure 3.15: The optimal threshold ω in QoS-constrained design. The QoS requirements of $\eta = 0.02$ and $\eta = 0.2$ are considered, respectively. The following system configurations are considered:a) S1: The FSA strategy and the parameters ω are fixed. Two parameter sets are considered: S1(a): $\omega = 1/3$ and S1(b): $\omega = 2/3$. b) S2: FSA strategy and femtocell awareness is assumed. c) S3: SSA strategy is assumed and Femtocell awareness is employed. All system parameters were summarized in Table 3.1.

3.6.4.2 QoS-Constrained Design

To model the different data-rates sought by the CCR macrocell MTs relative to the CER macrocell MTs, the QoS requirements of $\eta = 0.02$ and $\eta = 0.2$ are considered, corresponding to either a 50 times higher throughput per CCR macrocell MT than per CER macrocell MT or five times higher, respectively. Fig. 3.15 and Fig. 3.16 illustrate the system parameters ω and ρ versus the number of femtocells for the above three systems. Apart from the parameter design of S1, the range of CCR should be extended upon increasing the number of femtocells in order to achieve the maximum macrocell throughput, regardless of the specific spectrum access strategy. It is observed that the optimal ω increases slower if a lower QoS requirement η is chosen. As far as ρ is concerned, in general, the denser the femtocells, the lower ρ has to become, with the exception of high η values in both the S2 and S3 scenarios, where the relationship is not monotonic. Another feature observed for S1 is that lower η values result into requiring higher ρ values. By contrast, these trends are

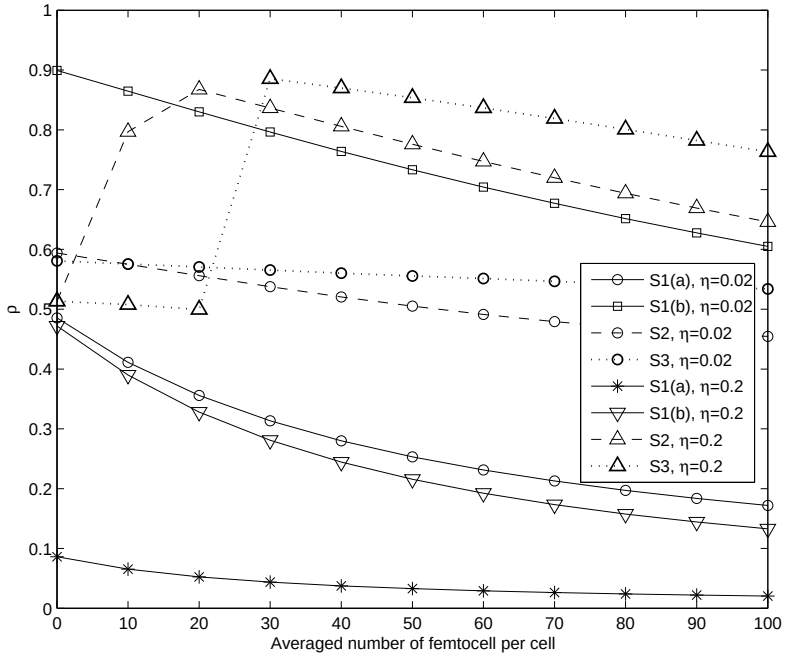

Figure 3.16: The optimal spectrum allocation ρ in QoS-constrained design. The QoS requirements of $\eta = 0.02$ and $\eta = 0.2$ are considered, respectively. The following system configurations are considered:a) S1: The FSA strategy and the parameters ω are fixed. Two parameter sets are considered: S1(a): $\omega = 1/3$ and S1(b): $\omega = 2/3$. b) S2: FSA strategy and femtocell awareness is assumed. c) S3: SSA strategy is assumed and Femtocell awareness is employed. All system parameters were summarized in Table 3.1.

reversed for the S2 and S3 system configurations.

Fig. 3.17 compares the ASE of the macrocells for these systems. It is shown that the specific selection of system parameters may significantly affect the macrocells' ASE. It is observed that the macrocells' ASE is reduced for all the scenarios considered, when the averaged number of femtocell per cell is increased. Also, the GA based optimized designs are capable of achieving a higher ASE for both $\eta = 0.02$ and $\eta = 0.2$ than the fixed parameter based design. Furthermore, when considering the effects of η, the ASE of the macrocell will be reduced for higher η values (higher data rate per CER user demand), since the CER throughputs is obviously lower than the CCR throughput. Observe in Fig. 3.17 that our proposed SSA strategy achieved the highest ASE among all the systems for the QoS-constrained design and it is more resilient against the impact of femtocells.

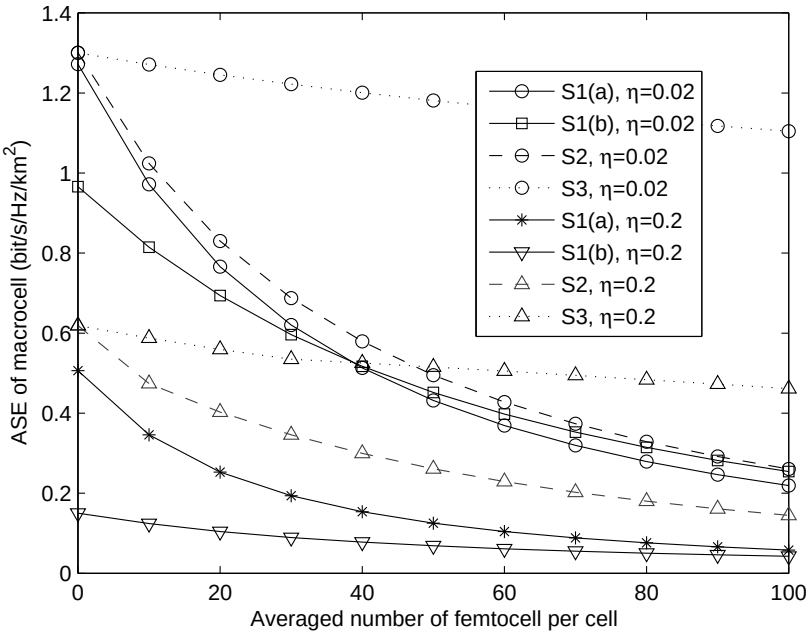

Figure 3.17: The ASE of macrocell in QoS-constrained design. The QoS requirements of $\eta = 0.02$ and $\eta = 0.2$ are considered, respectively. The following system configurations are considered:a) S1: The FSA strategy and the parameters ω are fixed. Two parameter sets are considered: S1(a): $\omega = 1/3$ and S1(b): $\omega = 2/3$. b) S2: FSA strategy and femtocell awareness is assumed. c) S3: SSA strategy is assumed and Femtocell awareness is employed. All system parameters were summarized in Table 3.1.

3.6.5 The Impact of the Proposed SSA on the Femtocell Performance

The numerical results of Subsection 3.6.4 demonstrate that the macrocell MTs benefit from the proposed SSA strategy. However, this benefit comes at the expense of partitioning the spectrum of femtocells. As a result, the femtocell throughput (bit/s) may be degraded under the SSA. Fig. 3.18 compares the long-term femtocell-throughput (bit/s) and femtocell ASE under FSA and SSA, respectively. Since the femtocells reuse the entire available frequency band for FSA, the femocell-throughput and ASE obey the same trends, where the femtocells situated in the vicinity of the MBS (for example for $l < 100$) tend to suffer from a high MBS interference and hence may exhibit a poor performance. By contrast, the femtocells situated far away from the MBS may attain a high throughput. On the other hand, the proposed SSA strategy eliminates the fluctuation of the femtocell throughput, which hence may become independent of its position. Observe in Fig. 3.18 that the femtocell's throughput reaches about 6 bit/s for SSA, which is lower than that recorded at

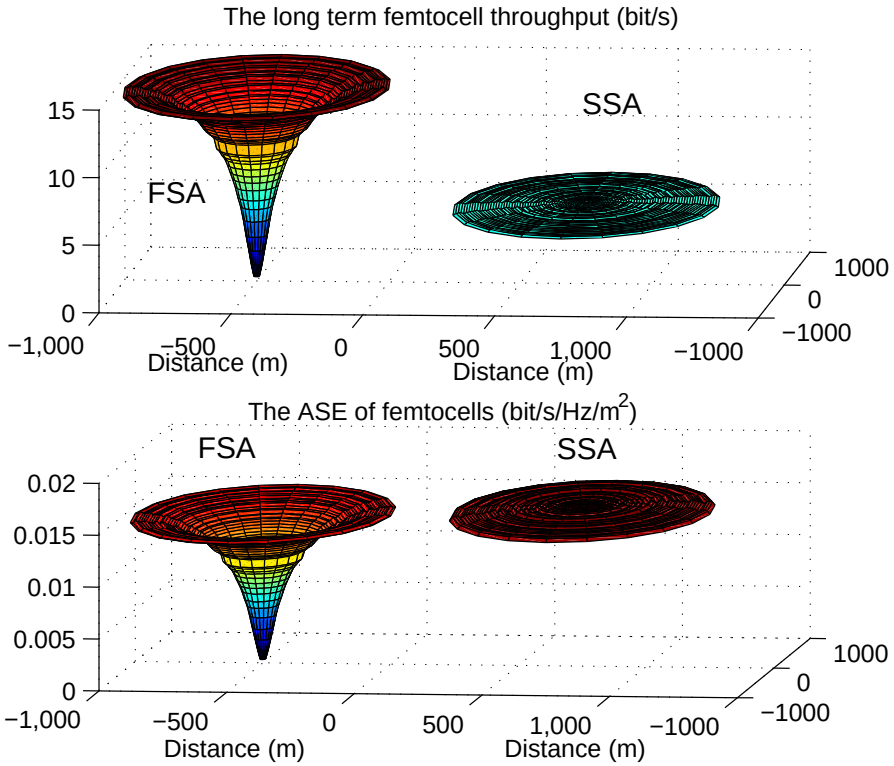

Figure 3.18: The long-term spatially averaged femtocell throughput and ASE. The system parameters of ω and ρ for the network employing FSA and SSA are derived separately by GA, according to the area-proportional design. Furthermore, the femtocell awareness approach is employed for the area-proportional design. All system parameters were summarized in Table 3.1.

the distance of $l > 200$ for FSA. The ASE of femtocells using SSA is higher than that of FSA in the entire cell, as seen in Fig. 3.18. This is because that the ASE quantifies the achievable bit rate per Hz per area. As a result, the ASE of SSA is higher owing to the reduced interference. Hence, the SSA may be treated as a ASE-oriented femtocell solution, which remains fairly unaffected by the FFR aided macrocell, albeit at the cost of delivering a limited peak throughput. By contrast, the FSA may be treated as a throughput-oriented femtocell design, which acts selfishly by disregarding both the macrocell's ASE and its own ASE.

3.7 Chapter Summary and Conclusions

In Section 3.2, we reviewed the concept of the classical FFR shceme and characterized the downlink performance of cellular networks using the classical FFR scheme in comparison to the traditional

UFR scheme. More specifically, the topology of the FFR aided cellular networks of Fig. 3.2 was introduced, where the distance based CCR/CER identification was adopted. The downlink OP and the downlink long-term throughput were investigated and the corresponding simulation results were portrayed in Fig. 3.3 and Fig. 3.4 of Section 3.2. As expected, the simulation results confirmed that the FFR scheme is capable of significantly reducing the OP of macrocell MTs. However, the outdoor MTs benefit from the FFR scheme for the CER MTs, and the performance of the FFR recorded both for the CCR MTs is similar to that of the UFR scheme. We have summarized the downlink performance of the FFR scheme and of the UFR scheme of Fig. 3.3 and Fig. 3.4 in Table 3.2.

Table 3.2: Downlink performance comparison of cellular macrocell MTs for UFR and FFR

	UFR	FFR
Distance threshold	N/A	$0.6R_m$
SINR threshold	0dB	0dB
Outage probability	$0 \sim 0.65$	$0 \sim 0.12$
Throughput	$0.18 \sim 19.7$ bit/s/Hz	$1.12 \sim 19.7$ bit/s/Hz

In Section 3.3, the system model of FFR aided two-tier femtocell networks was presented, where the topology of the two-tier networks, the downlink channel model and the associated spectrum allocation strategies were introduced. Two different spectrum allocation strategies were considered, where the system may employ either the FSA or SSA regimes. The performance of FSA based two-tier networks was investigated in Section 3.4. The per-tier OP was derived analytically, followed by finding the optimal parameters for the FSA based two-tier networks. Based on the simulation results illustrated in Fig. 3.9 and Fig. 3.10, the CER macrocell MTs and the CCR femtocell MTs suffered from the interference inflicted and as a result, the performance significantly degraded, when the system invoked FSA. In order to mitigate the cross-tier interference, the SSA scheme of Fig. 3.6 was proposed for this FFR aided two-tier network in Section 3.5. Again, the per-tier OP was derived analytically, followed by finding the optimal parameters of the SSA based two-tier networks. Recall the simulation results of Fig. 3.9 and Fig. 3.10, where the SSA scheme is seen to be capable of reducing the OP of both the macrocell MTs and of the femtocell MTs, whilst achieving an increased throughput. We have summarized the attainable performance of both the FSA and SSA of Fig. 3.9, Fig. 3.10 and Fig. 3.11 in Table 3.3, including the macrocell MTs' OP, the femtocell MTs' OP, as well as the spatially averaged CCR throughput of the macrocells and the spatially averaged CER throughput of macrocells.

Table 3.3: Downlink performance comparison of FFR aided two-tier femtocell networks for FSA and SSA

	FSA		SSA	
N_f	10	100	10	100
Macrocell MTs' OP	$0 \sim 0.21$	$0 \sim 0.87$	$0 \sim 0.12$	$0 \sim 0.68$
Femtocell MTs' OP	$0.01 \sim 0.87$		0.01	
CCR throughput (bit/s/Hz)	$1.98 \sim 10$	$0.8 \sim 6.2$	$1.99 \sim 10.6$	$1.99 \sim 10.6$
CER throughput (bit/s/Hz)	$0.7 \sim 2.6$	$0 \sim 0.6$	$1.1 \sim 3.9$	$0.1 \sim 3.5$

In order to improve the performance of the system, the choice of the optimal system parameters was discussed in Section 3.4 for FSA based two-tier networks, while in Section 3.5 for SSA based two-tier networks. In Section 3.6.4, the so-called area-proportional design and QoS-constrained design were studied. The optimal distance threshold ω^* and the optimal spectrum allocation ρ^* were derived with the aid of GA. The optimal system parameters taking into account the average number of femtocells per cell are illustrated in Fig. 3.12, Fig. 3.13, Fig. 3.16 and Fig. 3.15. The simulation results of Fig. 3.14 and Fig. 3.17 demonstrated that the GA based optimization process is capable of achieving an increased ASE of the macrocells. Furthermore, an increased macrocell's ASE was achieved by our SSA using a jointly optimized spectrum allocation and distance threshold policy. However, it is observed from the long-term spatially averaged femtocell throughput simulation results of Fig. 3.18 that the benefit of the SSA scheme is achieved at the expense of partitioning the spectrum of femtocells. As a result, the femtocell throughput is degraded for the SSA scheme, as depicted in Fig. 3.18. It is concluded that the SSA may be treated as a ASE femtocell solution, which remains fairly unaffected by the FFR aided macrocell at the cost of delivering a limited peak throughput. By contrast, the FSA may be treated as a throughput-oriented femtocell design, which is a selfish owing to disregarding both the macrocell's and its own ASE.

Chapter 4

Resource Allocation for Heterogeneous Visible-Light and RF Femtocell

4.1 Introduction

In Chapter 3, an outdoor heterogeneous network scenario was investigated, where the femtocells are overlaid onto the traditional macrocells. Apart from the outdoor scenario, indoor cells may also form part of a HetNet. In this chapter, we consider an indoor scenario, where femtocells and LED light based VLC are used for providing indoor coverage. The related Resource scheme is investigated in this Chapter, where diverse QoS requirements, such as the achievable data rate, the fairness and the statistical delay specifications are considered.

As stated in Chapter 2, optical wireless systems using visible light exhibit several advantages, including license-free operation, immunity to electro-magnetic interference, network security and a high bandwidth potential [24]. The optical access point is referred to as an attocell in [200]. However, the performance of VLC systems is degraded in the absence of line-of-sight (LOS) propagation. Hence we may combine VLC with a complementary network for providing a seamless data service. An optical attocell not only improves indoor coverage, it is able to enhance the capacity of the RF wireless networks, since it does not generate any additional interference. Here, we consider an indoor scenario, where a VLC system is combined with a classic RF femtocell system [229] and investigate the associated RA problems.

For a HetNet, an important component of the integrated architecture is its Resource Management (RM) mechanism. To access the Internet through a HetNet, the terminals such as laptops and cellphones are usually equipped with multiple wireless access network interfaces. There are two basic types of terminals. The conventional multi-mode mobile terminals are unable to support IP

mobility or multi-homing. Hence, these multi-mode terminals typically opt for the specific network providing the best radio-coverage. By contrast, the family of more sophisticated terminals is equipped with IP-based mobility and multi-homing functionalities, which have the capability of aggregating radio resources from different networks. Numerous contributions have studied the RA problem in a HetNet scenario [230–233]. Multi-homing RA mechanisms are studied in [230], which allocate the radio bandwidth to different tele-traffic types based on the specific utility of the service supported. However, this required a central resource manager for controlling the RA process. On the other hand, the authors of [231–233] proposed a distributed algorithm for solving the RA problem. However, these contributions only focus on maximizing the data rate, while QoS requirements formulated in terms of the delay requirements of mobile terminals were not considered in these contributions. Furthermore, these contributions considered a pure RF HetNet model, while our paper considered the RA problem of a combined VLC and RF Femtocell HetNet.

Future broadband wireless networks are expected to support a wide variety of communication services having diverse QoS requirements. Applications such as voice transmission as well as real-time lip-synchronized video streaming are delay-sensitive and they require a minimum guaranteed throughput. On the other hand, applications such as file transfer and email services are relatively delay-tolerant. As a result, it is important to consider the delay as a performance metrics in addition to the classic Physical layer performance metric in cross-layer optimization. Diverse approaches may be conceived for delay-aware resource control in wireless networks [13–19]. For example, the average delay-constraint may be converted into an equivalent average rate-constraint using the large deviation theory approach of [14–18]. In order to satisfy the QoS requirements, we apply the *effective capacity* [14] based approach for deriving the optimal RA algorithm, which guarantees meeting the statistical delay target of HetNets.

4.1.1 Main Contributions

In this chapter, the optimal RA in the DL of a HetNet is addressed, while meeting both the bit rate and statistical delay targets of delay-sensitive traffic. The contributions of this chapter are summarized as follows:

- We consider an indoor scenario, where a combined VLC attocell and RF femtocell system is employed for providing indoor coverage. For a given position of the MT, the received optical power of a MT is constituted by the sum of the direct LOS optical power and of the first reflected optical power. Hence the resultant VLC channel has two different rates, a higher one for the non-blocked LOS channel-scenario, and a reduced rate in the blocked LOS channel-scenario, when only the reflected ray is received. The RF channel is modelled as a classic Rayleigh fading channel. We investigate the VLC vs. RF activation and RA problem in this HetNet scenario.

- A limited-delay RA problem is formulated for the indoor HetNet considered. In contrast to the RA solutions of [16, 17, 232, 233], we apply the effective capacity approach of [14] for converting the statistical delay constraints into equivalent average rate constraints. Furthermore, we formulate our fairness-problem as an α-proportional fairness utility function, as defined in [234–237].

- The RA problem is formulated as a NLP problem for the multi-homing MTs. We show mathematically that this NLP problem is concave with respect to the RA probability matrix $\boldsymbol{\beta}$, which hence can be solved by convex optimization techniques, such as the barrier method of [238]. A distributed algorithm using the dual decomposition approach of [22] is proposed for RA in HetNets. It is demonstrated that this distributed algorithm approaches the optimal solution within a low number of iterations, where the optimal solution is that found by a centralized controller.

- We also demonstrate that the RA problem is formulated as a MINLP problem for multi-mode MTs, which is mathematically intractable. In order to make the problem more tractable, a relaxation of the integer variables is introduced. Then, we formally prove that the relaxed problem is concave with respect to both the relaxed network selection matrix $\boldsymbol{x}$ and to the RA probability matrix $\boldsymbol{\beta}$. Finally, a distributed algorithm is conceived using the dual decomposition approach for RA in our HetNet for the specific family of MTs having a multi-mode capability, but no multi-homing facility.

The chapter is organized as follows. In Section 4.2, the system model of VLC using LED lights is presented. In Section 4.3, the indoor heterogeneous network is described, where a combined VLC attocell and RF femtocell system is employed for providing indoor coverage. The formulation of our RA problems is described in Section 4.4 for both multi-homing MTs and multi-mode MTs. The proposed distributed algorithms are outlined in Section 4.5. Finally, our numerical results are provided in Section 4.6 and our conclusions are offered in Section 4.7.

4.2 The System Model of VLC Using LED Lights

As stated in Chapter 2, white LED lights are capable of providing high-brightness illumination, whilst additionally supporting down-link coverage in indoor scenarios. In this chapter, the link characteristics of LED light based VLC system is introduced. An example of a three-dimensional (3D) indoor LED light based VLC system is illustrated in Fig. 2.18, where the LED lights are uniformly distributed on the ceiling of the room, assuming that the length of the room equals to the width of this room. The crossover of the room is illustrated in Fig. 4.1, where the MTs are receiving both the LOS rays and the reflected rays. We assume that the set of MTs located or roaming in the indoor region is denoted by $\mathcal{N} = \{1, ..., n, ..., N\}$, while the set of LED lights is

denoted by $\mathcal{U} = \{1, ..., u, ..., U\}$.

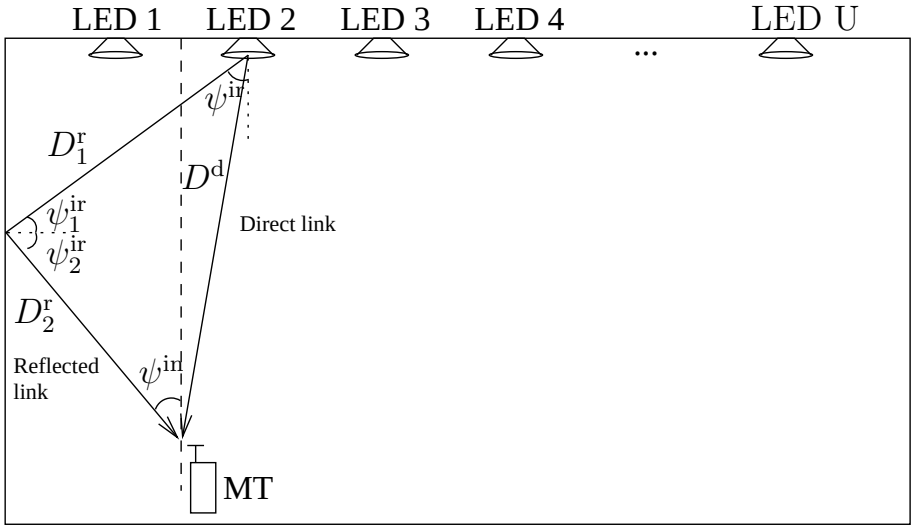

Figure 4.1: The crossover of the room using the LED lights based VLC system considered, where the LED lights are uniformly distributed on the ceilling.

4.2.1 Link Characteristics

The indoor VLC channel can be characterized by the optical channel, where the VLC channel consists of the line of sight (LOS) path spanning from the LED lights as well as the reflections from the walls in the room [185, 186]. It was shown in [185] that the sum power of the reflected path is dominated by the first-reflection path. Hence, only the first-reflection path is considered in this thesis.

Let us assume that ψ^{ir} is the angle of irradiation of the LED lights, ψ^{in} is the angle of incidence, and D^d is the distance between the transmitter and receiver. In an optical link the channel's direct current (DC) gain H^d on the direct LOS path is given by [182]:

$$H^d = \begin{cases} \dfrac{(q+1)\tilde{\pi}\kappa O}{2\pi (D^d)^2}\mathcal{G}, & \text{if } \psi^{in} \leq \Psi_c, \\ 0, & \text{if } \psi^{in} > \Psi_c, \end{cases} \tag{4.1}$$

where q is the order of Lambertian emission, which is given by the semi-angle $\phi_{1/2}$ at half illumination of an LED as $q = \frac{\ln 2}{\ln(\cos \phi_{1/2})}$. Furthermore, $\tilde{\pi}$ is the physical area of the photo-detector (PD), O is the gain of the optical filter used, and Ψ_c denotes the width of the field of view (FOV) at the receiver. Eq. (4.1) indicates that once the angle of irradiation of a receiver is higher than the Field of View (FOV), the receiver's LOS would be blocked. We assume that $\mathcal{G} = \cos^q\left(\psi^{ir}\right) g^{oc}(\psi^{in}) \cos(\psi^{in})$, where $g^{oc}(\psi^{in})$ is the gain of an optical concentrator [185],

which can be characterized as [184]:

$$g^{oc}(\psi^{in}) = \begin{cases} \dfrac{q^2}{\sin^2 \Psi_c}, & \text{if } \psi^{in} \leq \Psi_c, \\ 0, & \text{if } \psi^{in} > \Psi_c. \end{cases} \tag{4.2}$$

Owing to the obstructions, the LOS propagation path of the VLC system might be blocked. Here, a random variable κ is used for characterizing the VLC LOS blocking events, which are assumed to random and unpredictable. In line with [210], we assume that the LOS blocking events obey the *Bernoulli distribution*, which indicates whether the VLC LOS reception is blocked or not. Its probability mass function may be expressed as:

$$f(\kappa) = \begin{cases} 1-p, & \text{if } \kappa = 1 \\ p, & \text{if } \kappa = 0 \end{cases}, \tag{4.3}$$

where p denotes the VLC LOS blocking probability.

Apart from the VLC LOS reception, the MTs also receive the VLC path reflected by the wall. The channel gain owing to the reflection consists of the sum of all the channel gains of the reflected path, which may be written as:

$$H^r = \int_{\text{walls}} dH^{ref}, \tag{4.4}$$

where dH^{ref} denotes the first reflection from a small area of the wall, which is given by [185]:

$$dH^{ref} = \begin{cases} \dfrac{(q+1)AO\tilde{\rho}}{2\pi^2 \left(D_1^r D_2^r\right)^2} \cos(\psi_1^{ir}) \cos(\psi_2^{ir}) \mathcal{G} dA_{\text{wall}}, & \text{if } \psi^{in} \leq \Psi_c, \\ 0, & \text{if } \psi^{in} > \Psi_c \end{cases}, \tag{4.5}$$

where D_1^r is the distance between an LED light and a reflecting surface, D_2^r denotes the distance between a reflective point and a MT receiver, $\tilde{\rho}$ is the reflectance factor, whilst dA_{wall} is a small reflective area. Furthermore, it is assumed that ψ_1^{ir} and ψ_2^{ir} denote the angle of irradiance to a reflective point and the angle of irradiance to a MT's receiver, respectively.

Based on the above discussions, the VLC channel gain $H_{m,n}$ of the link spanning from the mth LED light to MT n is expressed as: $H_{m,n} = H_{m,n}^d + H_{m,n}^r$. The VLC channel gain matrix H is constituted by $M \times N$ elements. Having received the optical radiation, the photodetector converts the optical signal into electronic current.

The dominant noise contribution is assumed to be the shot noise due to ambient light emanating from the windows. We also take the thermal noise into account. Hence, the receiver filter's output contains Gaussian noise having a total variance of σ^2 given by the sum of contributions from both the shot noise and the thermal noise, which is expressed as:

$$\left(\sigma^{VLC}\right)^2 = \sigma_{\text{shot}}^2 + \sigma_{\text{thermal}}^2. \tag{4.6}$$

According to [185], the variance of shot noise σ_{shot}^2 is given by:

$$\sigma_{\text{shot}}^2 = 2\tilde{e}\varsigma P_r^{VLC} \mathcal{B}^{VLC} + 2\tilde{e} I_{bg} I_1 \mathcal{B}^{VLC}, \tag{4.7}$$

where $\tilde{e}$ is the electronic charge and ς is the detector's responsivity. P_r^{VLC} denotes the received optical power of the VLC system, $\mathcal{B}^{VLC}$ is the equivalent noise bandwidth of our VLC system and I_{bg} is the background current induced by the background light. Furthermore, the variance of thermal noise is given by [185]:

$$\sigma^2_{thermal} = \frac{8\pi\tilde{n}_1\tilde{T}}{\tilde{G}}\tilde{\eta}\tilde{\pi}I_1\left(\mathcal{B}^{VLC}\right)^2 + \frac{16\pi^2\varrho\tilde{T}\tilde{n}_2}{\tilde{n}_3}\tilde{\eta}^2\tilde{\pi}^2I_2\left(\mathcal{B}^{VLC}\right)^3, \tag{4.8}$$

where $\tilde{n}_1$ is the Boltzmann's constant, $\tilde{T}$ is the absolute temperature, $\tilde{G}$ is the open-loop voltage gain, $\tilde{\eta}$ is the fixed capacitance of the PD per unit area, $\tilde{n}_2$ is the FET channel noise factor, and finally, $\tilde{n}_3$ is the FET transconductance. The noise bandwidth factors I_1 and I_2 are constant experimental values. Here, we opt for the typical values used in the literature [184, 185], namely for $I_1 = 0.562$ and $I_2 = 0.0868$.

4.2.2 Transmission Strategy Assumptions

In this chapter, a Single Cell Multi-point Transmission (SCMT) scheme [185] is assumed, where all LED lights in the room operate as a single transmission cell, which is referred to as an attocell [200]. The MTs receive the same single from all the LED lights during their DL transmission, as depicted in Fig. 4.2.

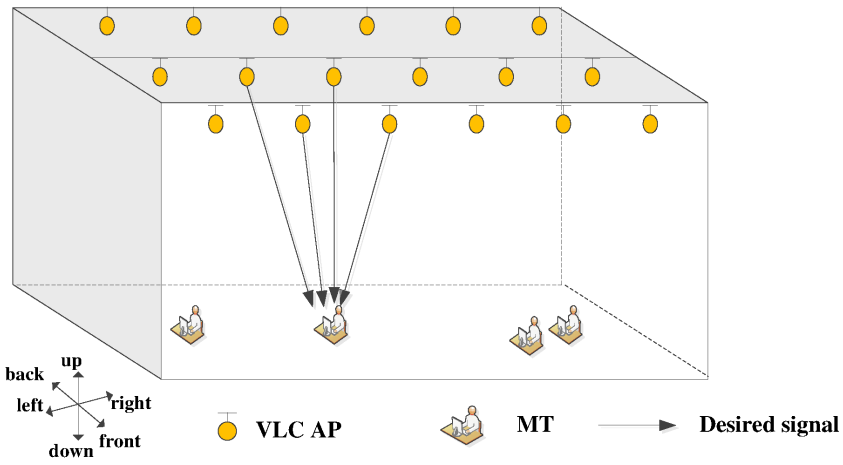

Figure 4.2: The 3-D model of the room using the LED light based VLC system, where all the LED lights in the room operate as a single transmission cell.

Additionally, it is assumed that ACO-OFDM is employed [197], which eliminates the effects of the a power multipath propagation in the LED light based VLC system considered. When an ACO-OFDM scheme is used in our VLC system, the relationship between the transmitted electronic

power $P_t^{VLC,e}$ and the transmitted optical power $P_t^{VLC,o}$ is defined as [239]:

$$P_t^{VLC,e} = \pi \left(P_t^{VLC,o} \right)^2 . \tag{4.9}$$

As a result, the MTs receive both the desired signal as well as the noise, and the received SNR ξ_n^{VLC} of MT n served by the VLC system is given by:

$$\xi_n^{VLC} = \frac{\pi \left(\varsigma P_t^{VLC,o} \sum_u H_{u,n} \right)^2}{\left(\sigma^{VLC} \right)^2}, \tag{4.10}$$

where the VLC channel gain $H_{u,n}$ of the link spanning from the uth LED light to MT n is given by Eq. (4.1) and Eq. (4.5), while the variance of noise σ^2 is given by Eq. (4.6), Eq. (4.7) and Eq. (4.8).

In this thesis, we assume that the square Quadrature Amplitude Modulation (QAM) is used in our ACO-OFDM aided VLC system. As a result the Bit Error Ratio (BER) may be given by [198]:

$$BER_n^{VLC} = \frac{\sqrt{M_{QAM}}}{\sqrt{M_{QAM}} \log_2 \sqrt{M_{QAM}}} erfc \left(\sqrt{\frac{3\xi_n^{VLC}}{2\left(M_{QAM}-1\right)}} \right), \tag{4.11}$$

where M_{QAM} represents the constellation size.

Since ACO-OFDM is capable of processing complex value symbols, according to [240], the achievable rate of the ACO-OFDM aided VLC system could be characterised by the channel capacity, which is written as [239]:

$$R_n^{VLC} = \frac{\mathcal{B}^{VLC}}{4} \log_2 \left(1 + \xi_n^{VLC} \right), \tag{4.12}$$

where the factor four reduction is due to the so-called Hermitian Symmetry property [241]. Then, the distribution of both the received SNR in dB and that of the achievable rate of the ACO-OFDM aided VLC system are evaluated.

4.2.3 Downlink Performance of VLC system

Fig. 4.3 illustrates the spatial distribution of the received SNR in dB for the VLC system investigated. We consider three different LED light scenarios, where the main system parameters adopted in our simulations are summarized in Table 4.1. Observe from Fig. 4.3 that the received SNR is significantly affected by the number of LED lights. When the number of LED light is $U = 2 \times 2$, which implies the density of LED lights is 0.01, the VLC system is only capable of covering some of the indoor area. However, there are still some areas which suffer from poor coverage. The MTs located in these dead zones may be unable to receive the direct link or the reflected links, since the angle of incidence may be wider than the width of the FOV. However, for the MTs located at the edge of the room, it is possible to receive the reflected links. As a result, they are still capable of receiving downlink transmissions from the VLC system, though the received SNR may be

Table 4.1: Main system parameters of VLC system

Length of room	20 [m]
Width of room	20 [m]
Height of room	3 [m]
Desity of MT	1 per m^2
Height of MT	0.85
Height of LED	2.5 [m]
Power of LED	20 [w]
Semi-angle at half power	70 [deg.]
Width of the field of view	120 [deg.]
Detector physical area of a PD	1.0 $[cm^2]$
Refractive index of a lens at a PD	1.5
O/E conversion efficiency	0.53 [A/W]
Available bandwidth for VLC system	10 [MHz]
Reflectance factor	0.8
Electronic charge	1.6×10^{-19} [C]
Background current	5.1×10^{-3} [A]
Open-loop voltage gain	10
Fixed capacitance of the PD per unit area	1.12×10^{-6}
FET channel noise factor	1.5
FET transconductance	3×10^{-2}

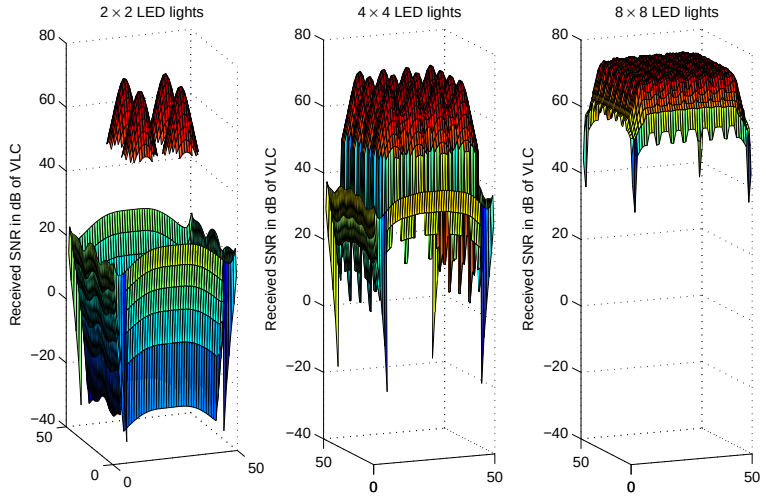

Figure 4.3: The received SNR in dB for the VLC system using different number of LED lights in the room. The simulation parameters are listed in Table 4.1.

low. When the number of LED lights is increased, the area of the dead zone becomes smaller. More specifically, all the MTs are covered by the VLC system, when the density of LED lights U is higher than 0.04, as seen in Fig. 4.3. It is observed however that there are SNR fluctuations, especially for MTs that are located at the edge of the room, when the number of LED lights is set to $U = 4 \times 4$. This is because the performance of these MTs is dominated by the reflected rays. By contrast, the performance of other MTs may be dominated by the direct rays arriving from the LED lights. It is also remarkable that the received SNR becomes near-constant, when the number of LED lights $U = 8 \times 8$ in our simulations.

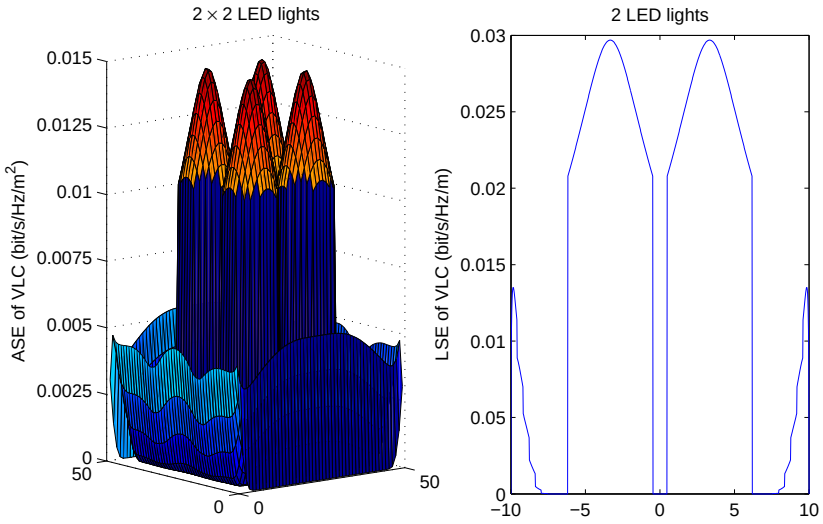

Figure 4.4: The ASE and LSE, with 2×2 LED lights for 3-D model and 2 LED lights for 2-D model. The simulation parameters are listed in Table 4.1.

In this thesis, we further simplify the VLC system model using a 2-D indoor model, where U LED lights are uniformly distributed on the ceiling. This 2-D model is the crossover of the 3-D model, as shown in Fig. 4.1. We will then verify the 2-D model by comparing the ASE of our VLC system. In a 3-D VLC model, the ASE of VLC is typically measured in (bit/s/Hz) per unit area. Here, we induce a concept of Line Spectrum Efficiency (LSE) for our 2-D VLC system, which is measured in (bit/s/Hz) per unit length. Then the LSE of the simplified 2-D model aided VLC is compared with the ASE of the 3-D model aided VLC in Fig. 4.4-4.6, relying on different LED ligths densities. It is observed that there are some dead-zone areas in the room, if insufficient LED lights are employed as shown in Fig. 4.4. When the number of LED lights increases, the entire indoor area is under the coverage of VLC system and the ASE of the indoor MTs becomes more flat. It is illustrated that the LSE of our 2-D model is 20 times of that of the crossover of ASE of 3-D model. This is because that we only divide the length of the room in calculating LSE. It is also verified that the LSE of 2-D model aided VLC has the same trend with the crossover of ASE of 3-D model aided VLC. Hence, the 2-D model is capable of capturing the feature of ASE of 3-D model

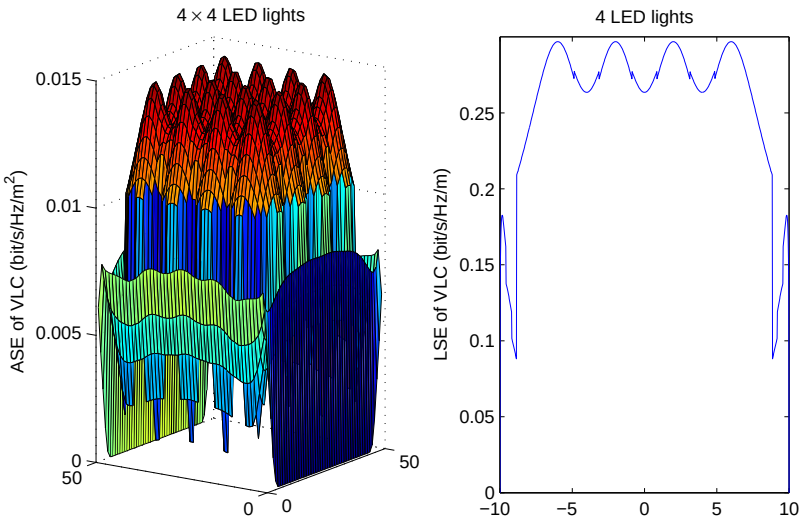

Figure 4.5: The ASE and LSE, with 4×4 LED lights for 3-D model and 4 LED lights for 2-D model. The simulation parameters are listed in Table 4.1.

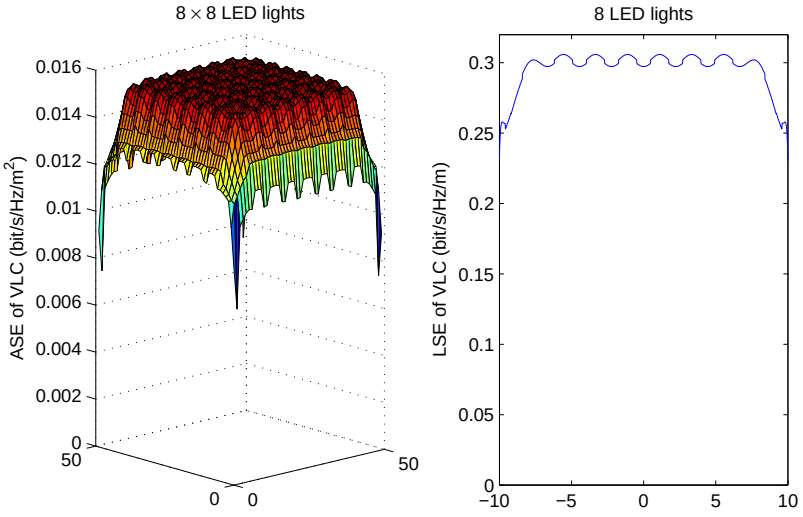

Figure 4.6: The ASE and LSE, with 8×8 LED lights for 3-D model and 8 LED lights for 2-D model. The simulation parameters are listed in Table 4.1.

in the scenarios considered. We will use 2-D VLC model of Fig. 4.1 in the following simulations, owing to its simplicity.

4.3 System Model of Heterogeneous VLC and RF Femtocell

According to the conclusion in [24], the performance of VLC systems is degraded in the absence of line-of-sight (LOS) propagation. In this chapter, we consider a heterogeneous indoor network, where a combined VLC and a RF femtocell network are employed in a room, where the 2-D room is illustrated in Fig. 4.7.

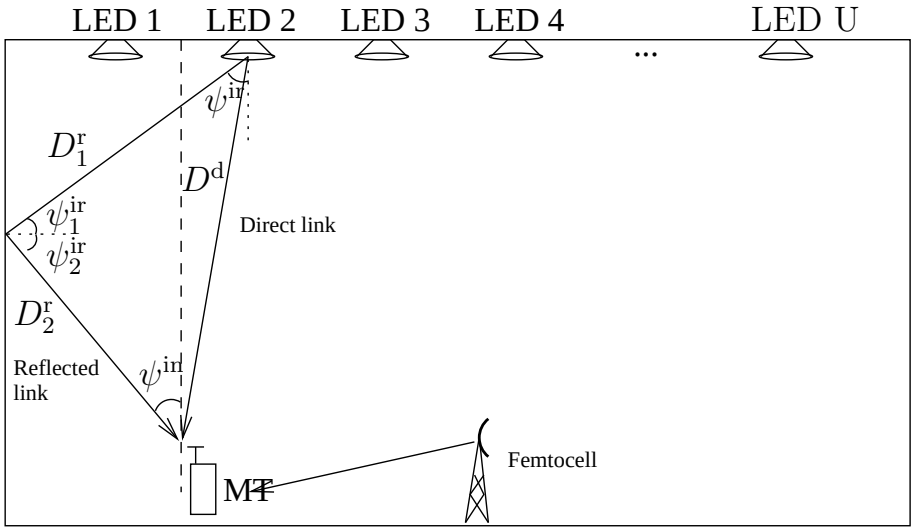

Figure 4.7: The 2D model of the room using both the VLC system and the RF femtocell system

.

The network set is denoted as: $\mathcal{M} = \{1, 2\}$, where $m = 1$ and $m = 2$ represent the ACO-OFDM aided VLC and the RF femtocell network, respectively. It is assumed that both the VLC and the RF femtocell system are supported either by an optical fibre or power-line backbone for exchanging their roaming-related signalling information, which is unproblematic in a indoor scenario.

Similar with the definition in Section 4.2, the set of MTs located or roaming in the indoor region is denoted by $\mathcal{N} = \{1, \cdots, n, \cdots, N\}$. We assume that the N MTs are uniformly distributed in the room. Each MT for $n \in \mathcal{N}$, is capable of accessing both the VLC and the femtocell network with the same priority. Again, we consider two types of MTs, namely multi-mode MTs and multi-homing MTs. Again, the multi-mode MTs are assigned to a single network at a time, hence each multi-mode MT has to appropriately set its network selection index $x_{m,n}$, where $x_{m,n} = \{1, 0\}$

indicates whether the MT n is assigned to the network m. By contrast, for the multi-homing MTs, both the VLC and the femtocell provide resource blocks simultaneously. We denote the instantaneous transmission probability of the network m transmitting to MT n as $\beta_{m,n}$. Here $\beta_{m,n}$ may also be interpreted as the specific fraction of the normalized serving duration, during which network m supports MT n. Furthermore, we use $\boldsymbol{x}$ and $\boldsymbol{\beta}$ to represent the network assignment matrix and RA probability matrix, respectively. The achievable throughput of MT n supported by network m is expressed as: $\beta_{m,n}r_{m,n}$, where $r_{m,n}$ denotes the instantaneous transmission bit rate in the DL of network m to MT n. The VLC system has a rather different transceiver model and channel model than the traditional RF communication networks. We will now briefly introduce the achievable instantaneous transmission bit rate of both the VLC and of the RF femtocell network.

4.3.1 VLC Using LED lights

The link characteristic of the VLC system is presented in Section 4.2.1, where the VLC channel gain is constituted by the sum of the direct link gain and the first-reflection link gain. Furthermore, the received SNR and the achievable bit rate from the ACO-OFDM aided VLC system to the MT n is given by Eq. (4.10) and Eq. (4.12), respectively.

4.3.2 Channel model of the RF femtocell

Similar with the assumption in Chapter 3, it is assumed that the DL channel of the femtocell to a MT is subject to uncorrelated Rayleigh fading [1] obeying a unity average power constraint and inverse-$gamma$th power path-loss. As a result, given a MT n located at a distance d_n^F from the serving RF femtocell, the received SNR ξ_n^F is given by:

$$\xi_n^F = \frac{P_t^F A_I \left(d_n^F\right)^{-\gamma} h_n^F}{\left(\sigma^F\right)^2}, \tag{4.13}$$

where P_t^F, A_I and γ denote the downlink transmission power of FBS, the indoor path-loss constant and the indoor path-loss exponent, respectively. The uncorrelated Rayleigh fading is characterized by h_n^F, while $\left(\sigma^F\right)^2$ denote the variance of the noise, which is given by: $\left(\sigma^F\right)^2 = \mathcal{B}^F N_0$, where $\mathcal{B}^F$ and N_0 are denote the available bandwidth of femtocell and the thermal noise density, respectively. Furthermore, the instantaneous transmission bit rate R_n^F of MT n served by the RF femtocell is given by the classical Shannon capacity of:

$$R_n^F = \mathcal{B}^F \log_2\left(1 + \frac{\xi_n^F}{\varpi}\right), \tag{4.14}$$

[1] Since we may not be able to guarantee line of sight transmission for the RF femtocell system, here we consider the worst-case scenario, where the DL channel of the RF femtocell system is modelled as the widely used Rayleigh channel.

where ϖ denotes the received SNR discrepancy from the continuous input memoryless channel's capacity at the target BER, which is also used in Chapter 3.

4.3.3 Effective Capacity

In next-generation networks, it is essential to consider a range of QoS metrics, such as the achievable data rate, the tolerable delay and the delay-violation probability. During the early 90's, statistical QoS guarantees have been extensively studied in the context of effective bandwidth theory of [242–244]. The theory states that for a dynamic queueing system having stationary ergodic arrival and service processes, the probability of exceeding a certain queue length decays exponentially. Inspired by the effective bandwidth theory, the authors of [14] proposed a link-layer metric termed as the effective capacity, which characterizes the effect of delay on the system. Owing to its advantages, the effective capacity has been widely adopted [14–18] for studying the steady-state delay-target violation probability. According to [14], for a dynamic queueing system where the arrival and service processes are stationary and ergodic, the probability that the queue length $D(t)$ at an instant t of a service exceeds the maximum tolerable delay bound $D_{\max}$ is given by:

$$\mathbb{P}\left\{D(t) \geq D_{\max}\right\} \approx \gamma(t) e^{-\theta D_{\max}}, \tag{4.15}$$

where $\gamma(t) = \Pr\left\{D(t) \geq 0\right\}$ is the probability that the transmission queuing buffer is non-empty at a randomly selected instant t. Note from Eq. (4.15) that $\theta \geq 0$ is a crucial parameter, directly characterizing the exponential decaying rate of the probability that the delay exceeds D_{max}. As a result, θ may be referred to as delay-related QoS exponent of a connection.

The effective capacity may also be interpreted as the maximum constant packet-arrival rate that the system is capable of supporting, without violating a given delay-related QoS requirement indicated by the QoS exponent θ. For uncorrelated block fading channels wherein the service process is uncorrelated, the effective capacity is defined as [14, 245]:

$$\Delta(\theta) = -\frac{1}{\theta} \ln \mathbb{E}\left[\exp\left(-\theta r\right)\right], \tag{4.16}$$

where $\mathbb{E}(\cdot)$ is the expectation operator and r denotes the throughput.

4.3.3.1 Effective Capacity of VLC

Given the position of a MT n, if the angle of irradiation of a receiver is higher than the FOV, the effective capacity of VLC Δ_n^{VLC} is equal to 0. However, if the angle of irradiation of a receiver is lower than the FOV, the instantaneous transmission rate r_n^{VLC} obeys a Bernoulli distribution, with the probability mass function of:

$$f(r_{1,n}) = \begin{cases} 1-p, & \text{if } r_{1,n} = R_{1,n}^{VLC} \\ p, & \text{if } r_{1,n} = R_{2,n}^{VLC} \end{cases}, \tag{4.17}$$

where $R_{1,n}^{VLC}$ and $R_{2,n}^{VLC}$ denote the achievable transmission rate from VLC system to MT n with and without VLC LOS reception, respectively. As a result, the VLC transmission channel is modelled as a two-rates channel.

Based on the above discussions, the VLC system's effective capacity, which is again the maximum constant packet-arrival rate that the service is capable of supporting under the statistical delay limit of the MT n specified by θ_n, may be expressed as:

$$\Delta_{1,n} = \begin{cases} -\frac{1}{\theta_n} \ln p e^{-\theta_n \beta_{1,n} R_{2,n}^{VLC}} + (1-p) e^{-\theta_n \beta_{1,n} R_{1,n}^{VLC}}, & \text{if } \psi_{in} \leq \Psi_c, \\ 0, & \text{if } \psi_{in} > \Psi_c. \end{cases} \tag{4.18}$$

4.3.3.2 Effective Capacity of the RF Femtocell

According to Eq. (4.14), and Eq. (4.16), the effective capacity of the RF femtocell system to MT n is given by:

$$\begin{aligned} \Delta_{2,n} &= -\frac{1}{\theta_n} \ln \int_0^\infty e^{-\theta_n \beta_{2,n} \mathcal{B}^F \log_2\left(1+\xi_n^F\right)} f\left(\xi_n^F\right) d\xi_n^F \\ &= -\frac{1}{\theta_n} \ln \left[\frac{1}{\mathcal{Q}} \int_0^\infty (1+x)^{-\frac{\theta_n \beta_{2,n} \mathcal{B}^F}{\ln 2}} e^{-\frac{x}{\mathcal{Q}}} dx \right] \\ &= -\frac{1}{\theta_n} \ln \left[\mathcal{Q}^{-\frac{\theta_n \beta_{2,n} \mathcal{B}^F}{2 \ln 2}} e^{\frac{1}{2\mathcal{Q}}} \mathcal{W}_{-\frac{\theta_n \beta_{2,n} \mathcal{B}^F}{2 \ln 2}, \frac{\ln 2 - \theta_n \beta_{2,n} \mathcal{B}^F}{2 \ln 2}} \left(\frac{1}{\mathcal{Q}}\right) \right] \\ &= \frac{\beta_{2,n} \mathcal{B}^F}{2 \ln 2} \ln \mathcal{Q} - \frac{1}{2\theta_n \mathcal{Q}} - \frac{1}{\theta_n} \ln \mathcal{W}_{-\frac{\theta_n \beta_{2,n} \mathcal{B}^F}{2 \ln 2}, \frac{\ln 2 - \theta_n \beta_{2,n} \mathcal{B}^F}{2 \ln 2}} \left(\frac{1}{\mathcal{Q}}\right), \end{aligned} \tag{4.19}$$

where $\mathcal{Q} = \frac{P_t^F A_I \left(d_n^F\right)^{-\gamma}}{\varpi \left(\sigma^F\right)^2}$, and $\mathcal{W}_{\cdot,\cdot}(\cdot)$ represents the Whittaker functions [225].

Note from the Eq. (4.18) and Eq. (4.19), the effective capacity of the network m to MT n is the function of $\beta_{m,n}$. In the following sections, we will use $\Delta_{m,n}$ to represent $\Delta_{m,n}\left(\beta_{m,n}\right)$.

4.4 Problem Formulation

In this section, the RA problem formulation is presented for both multi-homing MTs and multi-mode MTs in the indoor HetNet considered. Let us now adopt a utility function based perspective, assuming that the MT n obtains utility $U_{m,n}\left(\beta_{m,n}\right)$ from network m.

4.4.1 Utility Function: α-proportional Fairness Approach

In this paper, we consider the RA problem under the consideration of the concept fairness. The mathematical concept of fairness is formulated as an optimization problems. The fairness optimization problem may be interpreted as a throughput maximization problem [21], as a max-main fairness problem [21] and as a proportional fairness problem [246]. Here a generic fairness notion

referred to α-proportional fairness [234–237] is introduced, which embodies a number of fairness concepts, including the above-mentioned three problems by appropriately adjusting the values of the parameter α. We define the utility $U_{m,n}\left(\beta_{m,n}\right)$ as:

$$U_{m,n}\left(\beta_{m,n}\right)=\varphi_{\alpha}\left(\Delta_{m,n}\right), \tag{4.20}$$

where $\varphi_{\alpha}\left(\cdot\right)$ denotes the α-proportional fairness defined in [235], where $\varphi_{\alpha}\left(\cdot\right)$ is a monotonically increasing, strictly concave and continuously differentiable function, which may be expressed as:

$$\varphi_{\alpha}(x)=\begin{cases}\log(x), & \text{if } \alpha=1\\ \dfrac{x^{1-\alpha}}{1-\alpha}, & \text{if } \alpha\geq 0,\ \alpha\neq 1.\end{cases} \tag{4.21}$$

We note that for different values of α, maximizing our utility function $U_{m,n}\left(\beta_{m,n}\right)$ reduces to several well-known fairness concepts. For example, the *maximum effective capacity* is achieved for $\alpha=0$ [21], *proportional fairness* is achieved for $\alpha=1$ [246] and *max-min fairness* [21] is obtained, when we have $\alpha\rightarrow\infty$.

4.4.2 Problem Formulation for Multi-Homing MTs

When the MTs are capable of multi-homing, both the VLC and the RF femtocell networks may allocate resource blocks for simultaneously supporting the MTs. We set out to maximize the overall effective capacity of all indoor MTs. As a result, the corresponding RA problem may be formulated as:

$$\textit{Problem 1}: \quad \underset{\boldsymbol{\beta}}{\text{maximize}} \sum_{n\in\mathcal{N}}\varphi_{\alpha}\left(\sum_{m\in\mathcal{M}}\Delta_{m,n}\right) \tag{4.22}$$

$$\text{subject to:} \quad \sum_{m\in\mathcal{M}}\Delta_{m,n}\geq\mathcal{R}_{n},\ \forall\, n\in\mathcal{N}, \tag{4.23}$$

$$\sum_{n\in\mathcal{N}}\beta_{m,n}\leq 1,\ \forall\, m\in\mathcal{M}, \tag{4.24}$$

$$0\leq\beta_{m,n}\leq 1. \tag{4.25}$$

The effective capacity $\Delta_{1,n}$ of the VLC and $\Delta_{2,n}$ of the femtocell is given by Eq. (4.18) and Eq. (4.19), respectively. Physically, the constraint (4.23) ensures that the HetNet is capable of satisfying the bit-rate $\mathcal{R}_n$ of the MT n, while the constraint (4.24) guarantees that the total transmission probability for each of the networks should always be less than 1. Finally, the constraint (4.25) describes the feasible region of the optimization variables.

Lemma 5. The RA problem described by (4.22), (4.23), (4.24) and (4.25) is a concave optimization problem.

Proof. Firstly, we prove that the effective capacity $\Delta_{m,n}\left(\beta_{m,n}\right)$ of the link spanning from network m to MT n is a concave function of $\beta_{m,n}$. The first derivative of the effective

capacity $\Delta_{1,n}(\beta_{1,n})$ from the VLC link to MT n is given by:

$$\frac{d\Delta_{1,n}}{d\beta_{1,n}} = \frac{R_{2,n}^{VLC} p e^{-\theta_n R_{2,n}^{VLC}\beta_{1,n}} + R_{1,n}^{VLC}(1-p)\, e^{-\theta_n R_{1,n}^{VLC}\beta_{1,n}}}{p e^{-\theta_n R_{2,n}^{VLC}\beta_{1,n}} + (1-p)\, e^{-\theta_n R_{1,n}^{VLC}\beta_{1,n}}}. \tag{4.26}$$

Then the second derivative of the effective capacity $\Delta_{1,n}$ from the VLC link to MT n is given by:

$$\begin{aligned}\frac{d^2\Delta_{1,n}}{d\beta_{1,n}^2} &= -\frac{(R_{1,n}^{VLC} - R_{2,n}^{VLC})^2 \theta_n p(1-p)\, e^{-\theta_n \beta_{1,n}(R_{1,n}^{VLC}+R_{2,n}^{VLC})}}{\left[p e^{-\theta_n R_{2,n}^{VLC}\beta_{1,n}} + (1-p)\, e^{-\theta_n R_{1,n}^{VLC}\beta_{1,n}}\right]^2} \\ &\leq 0, \quad \text{for } \theta_n \geq 0,\ 0 \leq p \leq 1.\end{aligned} \tag{4.27}$$

The second derivative of the effective capacity $\Delta_{2,n}$ from the RF femtocell link to MT n is given by:

$$\begin{aligned}\frac{d^2\Delta_{2,n}(\beta_{2,n})}{d\beta_{2,n}^2} &= \frac{\theta_n \left(\mathcal{B}^F\right)^2}{\ln^2 2}\Bigg\{\frac{\left[\int_0^\infty (1+x)^{\frac{-\theta_n \mathcal{B}^F \beta_{2,n}}{\ln 2}} e^{\frac{-x}{\mathcal{Q}}} \ln(1+x)\, dx\right]^2}{\left[\int_0^\infty (1+x)^{\frac{-\theta_n \mathcal{B}^F \beta_{2,n}}{\ln 2}} e^{\frac{-x}{\mathcal{Q}}} dx\right]^2} \\ &\quad - \frac{\int_0^\infty (1+x)^{\frac{-\theta_n \mathcal{B}^F \beta_{2,n}}{\ln 2}} e^{\frac{-x}{\mathcal{Q}}} \ln^2(1+x)\, dx \int_0^\infty (1+x)^{\frac{-\theta_n \mathcal{B}^F \beta_{2,n}}{\ln 2}} e^{\frac{-x}{\mathcal{Q}}} dx}{\left[\int_0^\infty (1+x)^{\frac{-\theta_n \mathcal{B}^F \beta_{2,n}}{\ln 2}} e^{\frac{-x}{\mathcal{Q}}} dx\right]^2}\Bigg\} \\ &\overset{a}{\leq} 0,\end{aligned} \tag{4.28}$$

where inequality a holds, according to the Cauchy-Schwarz inequality property presented in [247].

Assuming that we have $f_1(\beta_{m,n}) = \varphi_\alpha\left(\sum_{m\in\mathcal{M}} \Delta_{m,n}\right)$, the second partial derivative of $f_1(\beta_{m,n})$ may be written as:

$$\begin{aligned}\frac{\partial^2 f_1(\beta_{m,n})}{\partial \beta_{m,n}^2} &= \frac{\Delta_{m,n}'' \sum_{m\in\mathcal{M}} \Delta_{m,n}(\beta_{m,n}) - (\Delta_{m,n})^2}{\left(\sum_{m\in\mathcal{M}} \Delta_{m,n}\right)^2} \\ &\leq 0.\end{aligned} \tag{4.29}$$

As a result, the objective function (4.22) of Problem 1 is a concave function with respect to $\beta_{m,n}$. The linear transformations of a concave function still constitue a function, hence the problem described by (4.22), (4.23), (4.24) and (4.25) is a concave problem. □

While the Problem 1 of Eq. (4.22)-(4.25) may be solved in a centralized manner with the aid of a central resource manager, this is not a viable practical solution, when the available networks are operated by different service providers.

4.4.3 Problem Formulation for Multi-Mode MTs

When multi-mode MTs are considered, only a single network supports the MT at a time. Then, the RA problem may be formulated as that of maximizing the total utility $U_{m,n}\left(\beta_{m,n}\right)$ under the constraint of the QoS requirements expressed in terms of each MT's overall effective capacity, fairness and delay as follows:

$$\textit{Problem 2}: \quad \max_{\boldsymbol{x},\,\boldsymbol{\beta}} \sum_{n\in\mathcal{N}} \varphi_\alpha\left(\sum_{m\in\mathcal{M}} x_{m,n}\Delta_{m,n}\right) \tag{4.30}$$

$$\text{subject to:} \quad \sum_{m\in\mathcal{M}} x_{m,n}\Delta_{m,n} \geq \mathcal{R}_n,\ \forall\, n\in\mathcal{N}, \tag{4.31}$$

$$\sum_{n\in\mathcal{N}} x_{m,n}\beta_{m,n} \leq 1,\ \forall\, m\in\mathcal{M}, \tag{4.32}$$

$$\sum_{m\in\mathcal{M}} x_{m,n} = 1, \tag{4.33}$$

$$x_{m,n} = \{1,0\}, \quad 0\leq\beta_{m,n}\leq 1. \tag{4.34}$$

The effective capacity of VLC $\Delta_{1,n}$ and femtocell $\Delta_{2,n}$ is given by Eq. (4.18) and Eq. (4.19), respectively.

Under this formulation, the variables to be optimized are $x_{m,n}$ and $\beta_{m,n}, \forall\, m,n$. Physically, the constraint (4.31) ensures that the HetNet is capable of satisfying the bit-rate R_n of the MT n, while the constraint (4.32) guarantees that the total transmission probability for each of the networks should always be less than 1. Furthermore, the constraint (4.33) guarantees that each MT should always select only one of the networks for its transmissions. Finally, the constraint (4.34) describes the feasible region of the optimization variables.

We note that Problem 2 is a MINLP problem that involves both binary variables $x_{m,n}$ and real-valued positive variables $\beta_{m,n}$ during optimization. In general, MINLP problems are mathematically intractable. Nonetheless, recently serveral optimization tools have been developed for solving MINLP problems. The BONMIN solver [248] is for example capable of solving smooth, twice differentiable, mixed integer nonlinear programs, which was deployed for providing the upper-bound benchmark solution.

4.5 Decentralized Sub-optimal Resource Allocation Schemes

Problem 1 and Problem 2 may be solved with the aid of centralized optimization tools. However, in order to reduce the computational complexity and to make the problem tractable, in this section we propose decentralized sub-optimal RA schemes.

4.5.1 Decentralized Solution for Multi-Homing MTs

Since the problem is a concave one, convex duality implies that the optimal solution to this problem may be found from the Lagrangian formulation [238]. The Lagrangian function for (4.22) under the constraints of (4.23), (4.24) and (4.25) can be expressed as:

$$\begin{aligned}\mathbb{L}\left(\boldsymbol{\beta}, \boldsymbol{\upsilon}, \boldsymbol{\mu}\right) = \sum_{n\in\mathcal{N}} \Bigg[\varphi_\alpha\left(\sum_{m\in\mathcal{M}} \Delta_{m,n}\right) - \sum_{m\in\mathcal{M}} \upsilon_m \beta_{m,n} \\ + \sum_{m\in\mathcal{M}} \mu_n \Delta_{m,n}\Bigg] + \sum_{m\in\mathcal{M}} \upsilon_m - \sum_{n\in\mathcal{N}} \mu_n \mathcal{R}_n,\end{aligned} \tag{4.35}$$

where we have $\mathbf{0} \leq \boldsymbol{\beta} \leq \mathbf{1}$, while μ_n and υ_m are the Lagrange multipliers or prices associated with the nth inequality constraint (4.23) and with the mth inequality constraint (4.24), respectively. The dual objective function $g\left(\boldsymbol{\upsilon}, \boldsymbol{\mu}\right)$ is defined as the maximum value of the Lagrangian over $\boldsymbol{\beta}$, which is expressed as:

$$g\left(\boldsymbol{\upsilon}, \boldsymbol{\mu}\right) = \sup_{\boldsymbol{\beta}} \mathbb{L}\left(\boldsymbol{\beta}, \boldsymbol{\upsilon}, \boldsymbol{\mu}\right). \tag{4.36}$$

The dual variables $(\boldsymbol{\upsilon}, \boldsymbol{\mu})$ are dual feasible if we have $\boldsymbol{\upsilon} \geq 0, \boldsymbol{\mu} \geq 0$. The dual function can then be maximized for finding an upper bound on the optimal value of the original problem (4.22):

$$\begin{aligned}&\min_{\boldsymbol{\upsilon},\boldsymbol{\mu}} g\left(\boldsymbol{\upsilon}, \boldsymbol{\mu}\right) \\ &sub \quad \boldsymbol{\upsilon} \geq 0, \boldsymbol{\mu} \geq 0,\end{aligned} \tag{4.37}$$

which is always a convex optimization problem. The difference between the optimal primal objective and the optimal dual objective is referred to as the duality gap, which is always non-negative. A central result in convex analysis showed that when the problem is convex, the duality gap reduces to zero at the optimum [238, 249]. Hence, the primal problem of Eq. (4.22) can be equivalently solved by solving the dual problem of (4.37). In principle, the dual problem may be readily solved using standard routines, such as the Newton method and the barrier method [238]. However, these algorithms generally involve centralized computation and require global knowledge of all parameters. Hence, we propose an optimal decentralized RA algorithm for solving the problem using full dual decomposition [22].

Recall that in Eq. (4.36) we defined a dual objective function $g_n\left(\upsilon_m, \mu_n\right)$ for MT n, which may be written as:

$$g_n\left(\upsilon_m, \mu_n\right) = \varphi_\alpha\left(\sum_{m\in\mathcal{M}} \Delta_{m,n}\right) - \sum_{m\in\mathcal{M}} \upsilon_m \beta_{m,n} + \sum_{m\in\mathcal{M}} \mu_n \Delta_{m,n}. \tag{4.38}$$

Our primal problem described by (4.22),(4.23), (4.24) and (4.25) may be separated into two levels of optimization. At the lower level, we decouple the problem of Eq. (4.36) into N subproblems, where the nth subproblem may be written as:

$$\beta^\star_{m,n} = \underset{0\leq\beta_{m,n}\leq 1}{\text{argmax}} \; g_n\left(\upsilon_m, \mu_n\right), \quad \forall\, m \in \mathcal{M}. \tag{4.39}$$

It may be shown that $g_n(\upsilon_m, \mu_n)$ is concave with respect to the variable $\beta_{m,n}$. Hence the maximization of $g_n(\upsilon_m, \mu_n)$ may be achieved by finding the partial derivative of $g_n(\upsilon_m, \mu_n)$ with respect to $\beta_{m,n}$, which is given by:

$$\frac{\partial g_n(\upsilon_m, \mu_n)}{\partial \beta_{m,n}} = \frac{\Delta'_{m,n}}{\sum\limits_{m\in\mathcal{M}} \Delta_{m,n}} + \mu_n \Delta'_{m,n} - \upsilon_m, \tag{4.40}$$

where $\Delta'_{m,n} = \frac{d\Delta_{m,n}}{d\beta_{m,n}}$. Furthermore, the second partial derivative of $g_n(\upsilon_m, \mu_n)$ is given by:

$$\frac{\partial^2 g_n(\upsilon_m, \mu_n)}{\partial \beta^2_{m,n}} = \mu_n \Delta''_{m,n} + \frac{\Delta''_{m,n} \sum\limits_{m\in\mathcal{M}} \Delta_{m,n}}{\left(\sum\limits_{m\in\mathcal{M}} \Delta_{m,n}\right)^2} - \frac{\left(\Delta'_{m,n}\right)^2}{\left(\sum\limits_{m\in\mathcal{M}} \Delta_{m,n}\right)^2} \leq 0, \tag{4.41}$$

$$\frac{\partial^2 g_n(\upsilon_m, \mu_n)}{\partial \beta_{i,n} \partial \beta_{j,n}} = -\frac{\Delta'_{i,n}\Delta'_{i,n}}{\left(\sum_{m\in\mathcal{M}} \Delta_{m,n}\right)^2} \leq 0, \tag{4.42}$$

where we have $\Delta''_{m,n} = \frac{d^2\Delta_{m,n}}{d\beta^2_{m,n}}$. As a result, $\frac{\partial g_n(\upsilon_m,\mu_n)}{\partial \beta_{m,n}}$ is a monotonically decreasing function with respect to $\beta_{m,n}$ for all m. If we have $\left[\frac{\partial g_n(\upsilon_m,\mu_n)}{\partial \beta_{m,n}} | \beta_{m,n} = 0\right] \leq 0$, then we may have $\beta^\star_{m,n} = 0, \forall\ m$. By contrast, if we have $\left[\frac{\partial g_n(\upsilon_m,\mu_n)}{\partial \beta_{m,n}} | \beta_{m,n} = 1\right] \geq 0$, then we may have $\beta^\star_{m,n} = 1, \forall\ m$. Otherwise, $\beta^\star_{m,n}$ may be derived by solving the following Equation for each network m:

$$\frac{\Delta'_{m,n}}{\sum_{m\in\mathcal{M}} \Delta_{m,n}} + \mu_n \Delta'_{m,n} - \upsilon_m = 0, \tag{4.43}$$

which may be solved by the steepest descent method [238].

At the higher level, we have the master dual problem, which may be expressed as:

$$\min_{\boldsymbol{\upsilon},\boldsymbol{\mu}} g(\boldsymbol{\upsilon}, \boldsymbol{\mu}), \tag{4.44}$$

where we have $g(\boldsymbol{\upsilon}, \boldsymbol{\mu}) = \sum\limits_{m\in\mathcal{M}} \sum\limits_{n\in\mathcal{N}} g_{m,n}\left(\beta^\star_{m,n}, \upsilon_m, \mu_n\right) + \sum\limits_{m\in\mathcal{M}} \upsilon_m - \sum\limits_{n\in\mathcal{N}} \mu_n R_n$, and $\beta^\star_{m,n}$ denotes the optimal value derived from the lower level optimization problem of Eq. (4.39). Since the function $g(\boldsymbol{\upsilon}, \boldsymbol{\mu})$ is concave and differentiable, we can use a gradient method for solving the master dual problem, as a benefit of its simplicity. Instead of minimizing the function directly with respect to $\boldsymbol{\upsilon}$ and $\boldsymbol{\mu}$, it can be minimized over a single set of Lagrange multipliers first, and then over the remaining one, which may be formulated as $\min\limits_{\boldsymbol{\mu}\geq\mathbf{0}} \left[\min\limits_{\boldsymbol{\upsilon}\geq\mathbf{0}} g(\boldsymbol{\upsilon}, \boldsymbol{\mu})\right]$.

Firstly, we solve the minimization problem for a given $\boldsymbol{\mu}$. Then the derivative of $g(\boldsymbol{\upsilon}, \boldsymbol{\mu})$ with respect to $\boldsymbol{\upsilon}$ is written as:

$$\frac{\partial g(\boldsymbol{\upsilon}, \boldsymbol{\mu})}{\partial \boldsymbol{\upsilon}} = 1 - \sum_{n\in\mathcal{N}} \beta^\star_{m,n}. \tag{4.45}$$

As a result, the price parameter $\boldsymbol{\upsilon}$ is updated according to:

$$\upsilon_m(t+1) = \left[\upsilon_m(t) - \xi_\upsilon(t)\left(1 - \sum_{n\in\mathcal{N}} \beta^\star_{m,n}\right)\right]^+, \tag{4.46}$$

where $[\cdot]^+$ is a projection on the positive orthant to account for the fact that we have $\upsilon_m \geq 0$. Furthermore, $\xi_\upsilon(t)$ denotes the step-size taken in the direction of the negative gradient for the

price parameter $\boldsymbol{\upsilon}$ at iteration t. In order to guarantee convergence, where we have to satisfy $\lim_{t\to\infty} \xi_\upsilon(t) = 0$ and $\sum_{t=0}^{\infty} \xi_\upsilon(t) = \infty$. In this paper, we set $\xi_\upsilon(t) = \xi t^{-\frac{1}{2}+\epsilon}$, ξ and ϵ are positive constants.

Then, the price parameter $\boldsymbol{\mu}$ is similarly updated according to:

$$\mu_n(t+1) = \left[\mu_n(t) - \xi_\mu(t)\left(\sum_{m\in\mathcal{M}} \Delta_{m,n} - R_n\right)\right]^+. \tag{4.47}$$

Based on the above discussions, the decentralized optimal RA scheme is constituted by an iterative algorithm, which determines the optimal transmission probability in the DL of network m to MT n based on the update of a pair of price parameters υ_m and μ_n, over a number of iterations, until the optimal solution is found. Each of the networks m is initialized to a feasible price value υ_m, while each MT n is initialized to a feasible price value μ_n. Each MT broadcasts its price value to all the available networks. Then each MT calculates the optimal transmission probability based on the price information $(\boldsymbol{\upsilon}, \boldsymbol{\mu})$ and the optimal transmission probability is derived during the last iteration. Each of the networks m updates its price value υ_m based on the newly derived optimal transmission probability $\boldsymbol{\beta}$ and then broadcasts the optimal transmission probability to the MTs. Similarly, each MT updates its price value μ_n based on the optimal transmission probability. The MTs broadcast their new price values $\boldsymbol{\mu}$ to the networks and the process continues, until the algorithm converges. The decentralized optimal RA algorithm is formally described in Algorithm 1.

4.5.2 Decentralized Solution for Multi-Mode MTs

Problem 2 of Eq. (4.30) to Eq. (4.34) is formulated as a MINLP and may be computationally intractable. A potentially straightforward solution may be to derive firstly the optimal resource block $\boldsymbol{\beta}$ for a specific $\boldsymbol{x}$, then to exhaustive search through the entire set of all the possible $\boldsymbol{x}$ values. For a system having access to M networks and N MTs, there are M^N combinations for the network selection indicator variables $\boldsymbol{x}$. Therefore, a simpler solution may be found by relaxing the binary constraint imposed on the network selection indicator variables $x_{m,n}$, so that they may assume continuous values from the interval $[0, 1]$. Naturally, the original problem is not actually solved by the relaxation of the binary constraint. However, it has been shown in [250] that solving the dual of the relaxed problem provides solutions that are arbitrarily close to the original, non-relaxed problem.

Since $x_{m,n}$ assumes either the values of 0 or 1, there is exactly one $x_{m,n} = 1$ value for each MT n. If we denote such a specific network by the index m', we have $\varphi_\alpha\left(\sum_{m\in\mathcal{M}} x_{m,n}\Delta_{m,n}\right) = \varphi_\alpha\left(\Delta_{m',n}\right)$. Thus, the objective function in Eq. (4.30) is equivalent to the following function:

$$\max_{\boldsymbol{x},\,\boldsymbol{\beta}} \sum_{n\in\mathcal{N}}\sum_{m\in\mathcal{M}} x_{m,n}\varphi_\alpha\left(\Delta_{m,n}\right). \tag{4.48}$$

Table 4.2: Decentralized algorithm for Problem 1

Algorithm 1
Input
θ_n: Delay requirement of each MT n $\forall n$,
R_n: Rate requirement of each MT n $\forall n$
Initialization
$t \leftarrow 1$;
Price value for each network: $\boldsymbol{\upsilon}(t) = \{\upsilon_1(t), ..., \upsilon_M(t)\} = 0$
Price value for each MT: $\boldsymbol{\mu}(t) = \{\mu_1(t), ..., \mu_N(t)\} = 0$
step size: positive ξ and ϵ
While t does not reach its maximum
Get optimal $\boldsymbol{\beta}$
For each MT $n \in \mathcal{N}$
Each MT solves the problem presented in Eq. (4.39);
End for
Update price values
For $m \in \mathcal{M}$
Price value υ_m updates according to Eq. (4.46)
End for
For $n \in \mathcal{N}$
Price value μ_n updates according to Eq. (4.47)
End for
$\xi \leftarrow \xi t^{-\frac{1}{2}+\epsilon}$
$t \leftarrow t + 1$
End
Output $\boldsymbol{\beta}^{\star}(t)$

The equivalent relaxed optimization problem of Eq. (4.30) to Eq. (4.34) is reformulated as follows:

$$\textit{Problem 3}: \quad \max_{\boldsymbol{x},\,\boldsymbol{\beta}} \sum_{m\in\mathcal{M}} \sum_{n\in\mathcal{N}} x_{m,n}\varphi_{\alpha}\left(\Delta_{m,n}\right) \tag{4.49}$$

$$\text{subject to:} \quad \sum_{m\in\mathcal{M}} x_{m,n}\Delta_{m,n} \geq R_n, \ \forall\, n \in \mathcal{N}, \tag{4.50}$$

$$\sum_{n\in\mathcal{N}} x_{m,n}\beta_{m,n} \leq 1, \ \forall\, m \in \mathcal{M}, \tag{4.51}$$

$$\sum_{m\in\mathcal{M}} x_{m,n} = 1, \tag{4.52}$$

$$0 \leq x_{m,n} \leq 1, \quad 0 \leq \beta_{m,n} \leq 1. \tag{4.53}$$

In this formulation, the variables to be optimized are $x_{m,n}$ and $\beta_{m,n}$, $\forall\, m, n$.

Lemma 6. The RA problem described by (4.49), (4.50), (4.51), (4.52) and (4.53) is a concave

optimization problem with respect to the variables $x_{m,n}$ and $\beta_{m,n}$.

Proof. Firstly, we assume that $f_2\left(x_{m,n},\beta_{m,n}\right)=x_{m,n}\varphi_\alpha\left(\Delta_{m,n}\right)$. Let us now use the Hessian matrix for examining the concavity of the function $f_2\left(x_{m,n},\beta_{m,n}\right)$, which is given by:

$$\mathcal{H}\left(f_2\right)=\begin{bmatrix}\frac{\partial^2 f_2}{\partial\beta_{m,n}^2} & \frac{\partial^2 f_2}{\partial\beta_{m,n}\partial x_{m,n}}\\ \frac{\partial^2 f_2}{\partial x_{m,n}\partial\beta_{m,n}} & \frac{\partial^2 f_2}{\partial x_{m,n}^2},\end{bmatrix}, \tag{4.54}$$

where $\frac{\partial^2 f_1}{\partial\beta_{m,n}^2}$ and $\frac{\partial^2 f_1}{\partial x_{m,n}^2}$ are the principle minors of the Hessian matrix. Recalling the proof of Lemma 5 in Section 4.4.2, it may be readily seen that the effective capacity of each MT $\Delta_{m,n}$ is concave functions with respect to $\beta_{m,n}$. As a result, $\frac{\partial^2 f_2}{\partial\beta_{m,n}^2}=\frac{x_{m,n}\Delta''_{m,n}-x_{m,n}\left(\Delta'_{m,n}\right)^2}{\left(\Delta_{m,n}\right)^2}$ is non-positive. Furthermore, we have $\frac{\partial^2 f_1}{\partial x_{m,n}^2}=0$. Hence all the principle minors of the Hessian matrix are non-positive, and therefore the function $f_2\left(x_{m,n},\beta_{m,n}\right)$ is concave with respect to the variables $x_{m,n}$ and $\beta_{m,n}$.

Similarly, we can readily show that the constraint described by (4.50) is concave with respect to the variables $x_{m,n}$ and $\beta_{m,n}$. The constraints described by (4.51), (4.52) and (4.53) are linear. As a result, Problem 3 is a concave optimization problem. □

Since Problem 3 is also based on a concave function, the optimal solution may be found from the Lagrangian formulation, which may be written as:

$$\begin{aligned}\mathbb{L}\left(\boldsymbol{x},\boldsymbol{\beta},\boldsymbol{\upsilon},\boldsymbol{\mu}\right)=\sum_{m\in\mathcal{M}}\sum_{n\in\mathcal{N}}\Big[&x_{m,n}\varphi_\alpha\left(\Delta_{m,n}\right)\\&-\upsilon_m\beta_{m,n}+\mu_n x_{m,n}\Delta_{m,n}\Big]+\sum_{m\in\mathcal{M}}\upsilon_m-\sum_{n\in\mathcal{N}}\mu_n R_n,\end{aligned} \tag{4.55}$$

where we have $\mathbf{0}\leq\boldsymbol{x}\leq\mathbf{1}$, $\mathbf{0}\leq\boldsymbol{\beta}\leq\mathbf{1}$ and $\sum_{m\in\mathcal{M}}x_{m,n}=1$. Furthermore, μ_n and υ_m are the Lagrange multipliers or prices associated with the nth inequality constraint of (4.50) and with the mth inequality constraint of (4.51), respectively. The optimal RA variables $\boldsymbol{x}$, $\boldsymbol{\beta}$ may be obtained by solving:

$$\min_{\boldsymbol{\upsilon},\boldsymbol{\mu}}\max_{\boldsymbol{x},\boldsymbol{\beta}}\mathbb{L}\left(\boldsymbol{x},\boldsymbol{\beta},\boldsymbol{\upsilon},\boldsymbol{\mu}\right). \tag{4.56}$$

Similarly to Section 4.5.1, a decentralized optimal RA algorithm can be proposed for solving the problem using full dual decomposition.

We define a dual objective function $g_n\left(x_{m,n},\beta_{m,n}\right)$ for MT n, which may be written as:

$$g_n\left(x_{m,n},\beta_{m,n}\right)=\sum_{m\in\mathcal{M}}x_{m,n}\varphi_\alpha\left(\Delta_{m,n}\right)-\sum_{m\in\mathcal{M}}\upsilon_m\beta_{m,n}+\sum_{m\in\mathcal{M}}\mu_n x_{m,n}\Delta_{m,n}. \tag{4.57}$$

At the lower level, we have the subproblems, one for each n, which may be written as:

$$\left\{x^{\star}_{m,n}, \beta^{\star}_{m,n}\right\} = \underset{0\leq x_{m,n}\leq 1, 0\leq \beta_{m,n}\leq 1}{\text{argmax}} g_n\left(x_{m,n}, \beta_{m,n}\right). \tag{4.58}$$

Similarly, $g_n\left(x_{m,n}, \beta_{m,n}\right)$ is concave with respect to the variable $x_{m,n}$ and $\beta_{m,n}$. Hence the maximization of $g_n\left(x_{m,n}, \beta_{m,n}\right)$ may be derived by finding the partial derivative of $g_n\left(x_{m,n}, \beta_{m,n}\right)$, which is given by:

$$\frac{\partial g_n}{\partial x_{m,n}} = \varphi_{\alpha}\left(\Delta_{m,n}\right) + \mu_n \Delta_{m,n} - \upsilon_m \beta_{m,n} \tag{4.59}$$

$$\frac{\partial g_n}{\partial \beta_{m,n}} = x_{m,n}\left(\frac{\Delta'}{\Delta_{m,n}} + \mu_n \Delta'_{m,n} - \upsilon_m\right). \tag{4.60}$$

We will firstly derive the optimal RA probability $\beta^{\star}_{m,n}$ according to Eq. (4.60). Since we relaxed the binary constraint in Ploblem 3, here we will map the relaxed x back to the binary limit.

If we assume that $x_{m,n} = 0$, then $\beta_{m,n}$ is readily derived as $\beta_{m,n} = 0$; If we have $x_{m,n} \neq 0$, since the second partial derivative of $g_n\left(x_{m,n}, \beta_{m,n}\right)$ with respect to $\beta_{m,n}$ is non-positive, $\beta^{\star}_{m,n}$ is derived according to the following criterion:

1. If $\frac{\Delta'_{m,n}(1)}{\Delta_{m,m}(1)} + \mu_n \Delta'_{m,n}(1) - \upsilon_m \geq 0$, then $\beta^{\star}_{m,n} = 1$;
2. If $\frac{\Delta'_{m,n}(0)}{\Delta_{m,m}(0)} + \mu_n \Delta'_{m,n}(0) - \upsilon_m \leq 0$, then $\beta^{\star}_{m,n} = 0$;
3. Else, the optimal RA probability $\beta^{\star}_{m,n}$ from network m and MT n is derived by solving the equation $\frac{\Delta'_{m,n}(\beta^{\star}_{m,n})}{\Delta_{m,m}(\beta^{\star}_{m,n})} + \mu_n \Delta'_{m,n}(\beta^{\star}_{m,n}) - \upsilon_m = 0$.

The optimal network selection index $x^{\star}_{m,n}$ is then determined according to the $\beta^{\star}_{m,n}$ derived. Each MT n calculates the partial derivative of $g_n\left(x_{m,n}, \beta^{\star}_{m,n}\right)$ in the direction of $x_{m,n}$ for all the networks. Then MT n chooses the specific network m' associated with the highest value, which may be written as:

$$\begin{aligned} &x^{\star}_{m',n} = 1, \text{ if } m' = \underset{\forall\ m}{\text{argmax}} \frac{\partial g_n\left(x_{m,n}, \beta^{\star}_{m,n}\right)}{\partial x_{m,n}}; \\ &x^{\star}_{m,n} = 0, \text{ if } m \neq m'. \end{aligned} \tag{4.61}$$

At the higher level, we have the master dual problem, which may be expressed as:

$$\min_{\boldsymbol{\upsilon},\boldsymbol{\mu}} g\left(\boldsymbol{\upsilon}, \boldsymbol{\mu}\right), \tag{4.62}$$

where we have $g\left(\boldsymbol{\upsilon}, \boldsymbol{\mu}\right) = \sum_{n\in\mathcal{N}} g_n\left(x^{\star}_{m,n}, \beta^{\star}_{m,n}\right) + \sum_{m\in\mathcal{M}} \upsilon_m - \sum_{n\in\mathcal{N}} \mu_n R_n$, and $x^{\star}_{m,n}, \beta^{\star}_{m,n}$ denotes the optimal value derived from the lower level optimization problem Eq. (4.58). Similar to the solution provided in Section 4.5.1, the price parameters $\boldsymbol{\upsilon}$ and $\boldsymbol{\mu}$ are updated according to:

$$\upsilon_m(t+1) = \left[\upsilon_m(t) - \xi_{\upsilon}(t)\left(1 - \sum_{n\in\mathcal{N}} \beta^{\star}_{m,n}\right)\right]^{+}, \tag{4.63}$$

$$\mu_n(t+1) = \left[\mu_n(t) - \xi_\mu(t)\left(x^\star_{m,n}\sum_{n\in\mathcal{N}}\Delta_{m,n}\left(\beta^\star_{m,n}\right) - R_n\right)\right]^+. \tag{4.64}$$

Similarly, our decentralized optimal RA algorithm is an iterative algorithm, which performs an optimal network selection and finds the corresponding resource block probability from network m to MT n based on the update of the price parameters υ_m and μ_n, over a number of iterations, until the optimal solution is reached. Each of the networks m starts with an feasible initial price value υ_m, while each MT n starts with an feasible initial price value μ_n. Each MT broadcasts its price value to all networks. Then each network calculates the optimal network selection $x^\star_{m,n}$ and transmission resource block probability $\beta^\star_{m,n}$ based on the price information $(\boldsymbol{\upsilon}, \boldsymbol{\mu})$. Each network m updates its price value υ_m and then broadcasts the optimal transmission resource block to the MTs. Similarly, each MT updates its price values μ_n. The MTs broadcast their new price values $\boldsymbol{\mu}$ to the networks and the process continues, until the algorithm converges. The decentralized optimal RA algorithm is formally described in Algorithm 2.

4.6 Results and Discussions

In this section, we present numerical performance results for characterizing the proposed RA algorithms in the context of the indoor HetNet of Fig. 4.7, where the ACO-OFDM aided VLC system and femtocell are employed in order to provide indoor coverage. Again, it is assumed that the transmission power of the optical VLC system and that of the FBS are fixed to their maximum. Here we consider a straightforward transmission strategy for the VLC system, where all the LED lights in the room operate as a single transmission cell and hence no inter-LED interference is generated. Furthermore, the 'twin-rate' transmission channel model is used for the VLC system, while the RF femtocell channel is subjected to uncorrelated Rayleigh fading with a unity average power and to the ubiquitous propagation loss. We assume that $N = 10$ MTs are randomly distributed in the room and all experience the same delay exponent. Furthermore, the MTs are divided into two groups, where four guaranteed-rate MTs are in one of the groups, while no guaranteed rate is maintained for the MTs in the other group. Firstly, the convergence behaviour of the proposed distributed algorithm is verified. Then, we evaluate the effect of the VLC system's parameters on the overall effective capacity. In this chapter, two different types of MTs, namely the multi-homing MTs and multi-mode MTs defined in Section .4.3 are considered. We will then compare the effective capacity of these two different types of MTs. The effects of the statistical delay and the LOS blocking probability are also investigated in this Section. The effect of the MTs' geographic distribution is also studied, where the MTs are located at the room-centre and room-edge, respectively. Our main system parameters are summarised in Table 4.4.

Table 4.3: Decentralized algorithm for Problem 2

Algorithm 2
Input
θ_n: Delay requirement of each MT n $\forall n$,
R_n: Rate requirement of each MT n $\forall n$
Initialization
$t \leftarrow 1$;
Price value for each network: $\boldsymbol{\upsilon}(t) = \{\upsilon_1(t), ..., \upsilon_M(t)\} = 0$
Price value for each MT: $\boldsymbol{\mu}(t) = \{\mu_1(t), ..., \mu_N(t)\} = 0$
step size: positive ξ and ϵ
While t does not reach its maximum
Get optimal $\boldsymbol{\beta}^\star$ and $\boldsymbol{x}^\star$
For each MT $n \in \mathcal{N}$
Each MT solves the problem presented in Eq. (4.58);
End for
Update price values
For $m \in \mathcal{M}$
Price value υ_m updates according to Eq. (4.63)
End for
For $n \in \mathcal{N}$
Price value μ_n updates according to Eq. (4.64)
End for
$\xi \leftarrow \xi t^{-\frac{1}{2}+\epsilon}$
$t \leftarrow t + 1$
End
Output $\boldsymbol{x}^\star(t)$ and $\boldsymbol{\beta}^\star(t)$

4.6.1 Convergence of the Iterative Distributed Algorithm

Fig. 4.8 illustrates the convergence behaviour of our distributed RA algorithm for both the sophisticated multi-homing MTs and for the multi-mode MTs defined in Section 4.3 at a zero VLC blocking probability of $p = 0$, in conjunction with $\theta = 0.01$ and $\alpha = 1$. For comparison, we use the BONMIN solver [248] in order to derive the optimal solution for our RA problem. As shown in Fig. 4.8, our distributed RA algorithm converges to the optimal value within 100 iterations for both the multi-homing MTs and for the multi-mode MTs. This result demonstrates that the distributed RA algorithm indeed finds the optimal RA probability for multi-homing MTs as well as the optimal RA probability and network selection for the multi-mode MTs, respectively. Observe furthermore from Fig. 4.8 that the objective function value is higher for multi-homing MTs than that for the multi-mode MTs. This is because the multi-homing MTs are supported by both the

Table 4.4: Notations and System parameters

2D indoor scenario	
Length of room	20m
Height of room	3m
Number of indoor MT	10
Height of MT	0.85m
Number of rate guaranteed MT	4
BER target of MTs	10^{-5}
Guaranteed effective capacity	10/20 (Mbit/s)
Number of iteration	100
VLC System	
Height of LED	2.5 [m]
Power of LED	20 [w]
Semi-angle at half power	70 [deg.]
Width of the field of view	60 [deg.]
Detector physical area of a PD	1.0 $[cm^2]$
Refractive index of a lens at a PD	1.5
O/E conversion efficiency	0.53 [A/W]
Available bandwidth for VLC system	10 [MHz]
Reflectance factor	0.8
Electronic charge	1.6×10^{-19} [C]
Background current	5.1×10^{-3} [A]
Open-loop voltage gain	10
Fixed capacitance of the PD per unit area	1.12×10^{-6}
FET channel noise factor	1.5
FET transconductance	3×10^{-2}
Femtocell System	
Position of the indoor femtocell	$(0, 0)$
Transmission power of the femtocell BS	0.02 [w]
Indoor path-loss exponent	3
Carrier frequency	2 [GHz]
Indoor path-loss constant	37 [dB]
Available bandwidth for femtocell system	5 [MHz]

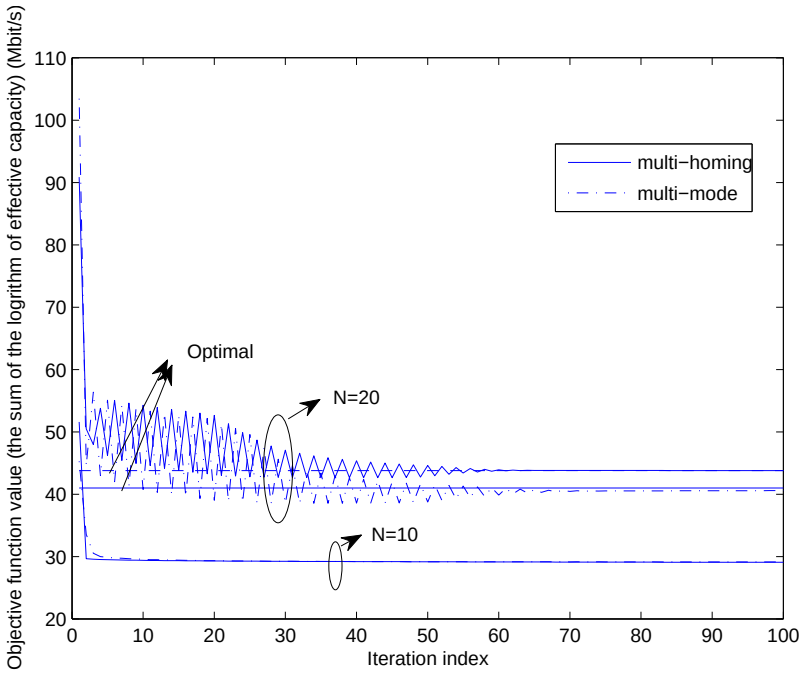

Figure 4.8: Objective function (OF) values versus the total number of iterations for the proposed decentralized algorithms for both multi-homing MTs and multi-mode MTs, in conjunction with $\alpha = 1$, $\theta = 0.01$ and $p = 0$

.

the VLC system and the femtocell. By contrast, multi-mode MTs are only supported by one of the avaiable networks. It is also observed that the objective function value converges after 8 iterations, when the total number of MTs is set to 10. However, the speed of convergence becomes slower, when we increase the number of MTs. The objective function value converges after 60 iterations in our simulations, when the total number of MTs is set to be 20.

4.6.2 Effective Capacity of MTs: Multi-Homing versus Multi-Mode MTs

Let us now compare the performance of multi-homing MTs and multi-mode MTs for different values of α. It is observed that the performance of the multi-homing MTs is better than that of the multi-mode MTs. Again, this is because the multi-mode transmission may be viewed as a specific scenario of multi-homing. Hence, the performance of multi-mode MTs may be interpreted as the lower bound of the maximum achievable capacity of multi-homing MTs. When we set $\alpha = 0$, as shown in Fig. 4.9, the RA problem is reformulated as the maximization of the total effective capacity. Since user 5 and user 6 are located in the middle of the room and are capable of achieving a better performance for the RF femtocell, the femtocell system is willing to allocate more resources to these two MTs in the multi-homing scenario.

Furthermore, owing to the rate constraint, the guaranteed-rate MTs always satisfy the minimum rate requirement. For the multi-homing scenario, the VLC system and the RF femtocell system may simultaneously transmit to MT 4 in order to satisfy the rate requirement. However, for the multi-mode scenario, the femtocell system may allocate the resource to MT 4 in order to satisfy its rate requirement This is because the VLC system may not be able to simultaneously satisfy all of the four MTs' rate requirement. For the non-rate-guranteed MTs, no resource will be allocated, when $\alpha = 0$. This is because the VLC system prefers to allocate resources to the guaranteed-rate MTs, and the femtocell system may allocate resources to the centrally located MTs, in order to achieve the maximum total effective capacity.

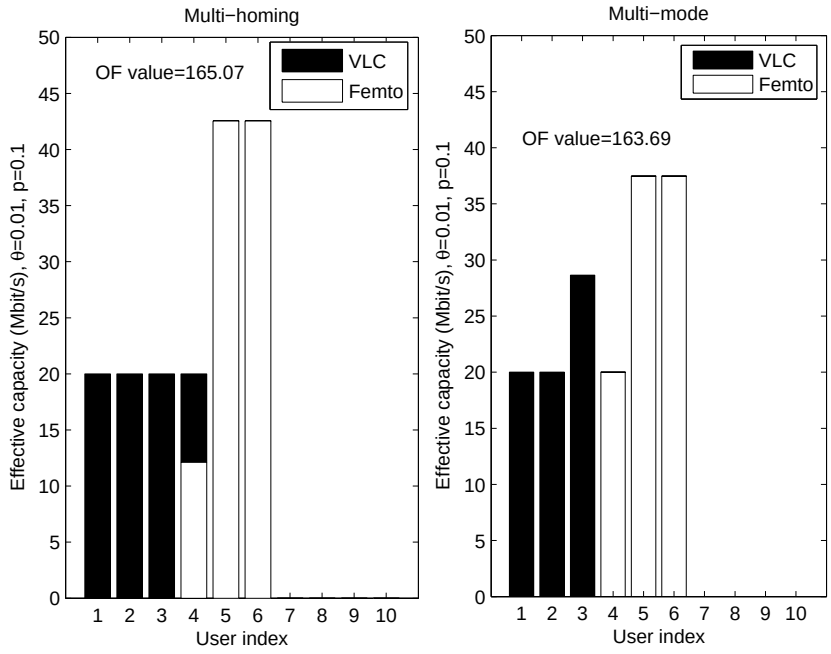

Figure 4.9: The effective capacity of both multi-homing MTs and multi-mode MTs, along with $\alpha = 0$, $\theta = 0.01$ and $p = 0.1$

.

When we set $\alpha = 1$, observe in Fig. 4.10 that the RA problems are formulated under the proportional fairness constraint. It is illustrated that the objective function value for MT-homing MTs is higher than that for MT-mode MTs. The rate guaranteed MTs have higher priority and their rate requirements are satisfied for both the multi-homing and the multi-mode scenarios. It may be observed in Fig. 4.10 that the MTs located in the middle of the room may achieve a higher effective capacity for multi-homing MTs. This is because the MTs in the middle of the room are capable of achieving a better performance, when communicating with the RF femtocell system. In contrast to the scenario of $\alpha = 0$, the system may allocate resources to the non-guaranteed-rate MTs under the consideration of fairness to all MTs. Hence MT 7, 8, 9, 10 also receive their signals from the VLC

system or from the femtocell system. When the MTs are of the multi-mode type, the centre MTs may choose the RF femtocell system for their transmission, while the VLC system may transmit to the edge MTs. Furthermore, observe in Fig. 4.11 that when we increase the value of α, the differences of effective capacity upon receiving from a specific network between the different MTs are smaller than that when we set $\alpha = 1$. As a result, we believe that having a higher α results in a higher grade of fairness.

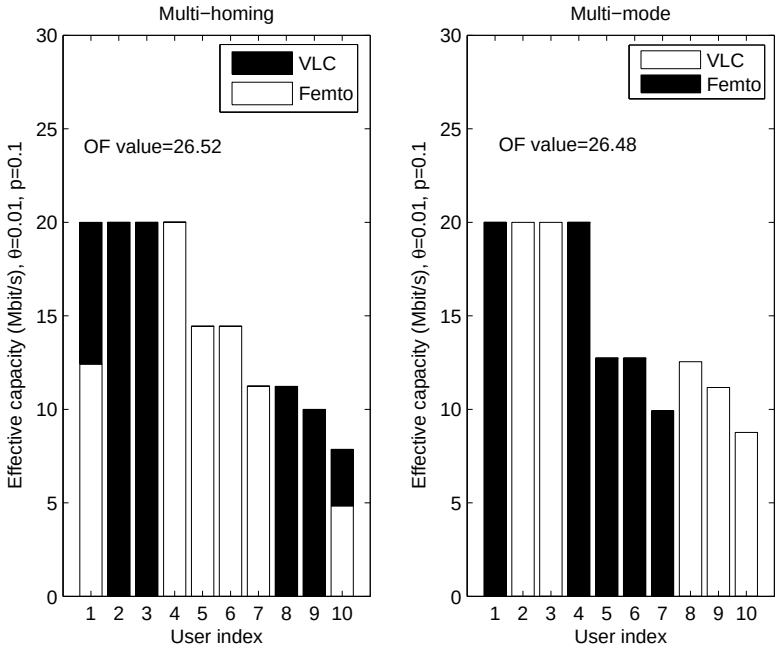

Figure 4.10: The effective capacity of both multi-homing MTs and multi-mode MTs, with $\alpha = 1$, $\theta = 0.01$ and $p = 0.1$

.

4.6.3 Effect of the Delay Statistics

Fig. 4.12 illustrates the effect of the delay exponent θ on the overall effective capacity of the MTs for the blocking probabilities of $p = 0$ and $p = 0.1$, respectively. Observe from the figure that the overall effective capacity is reduced upon increasing the delay exponent θ. However, the overall effective capacity of both the VLC and of the RF femtocell system is fairly insensitive to the delay exponent, when the exponent is relatively small. This is because when the delay exponent is low, the resultant delay requirement is loose and the overall effective capacity is close to the Shannon capacity, which depends on the wireless channel, but is independent of the delay of the packet-arrival process. However, the overall effective capacity of the RF femtocell decreases substantially, when the delay exponent is increased. Furthermore, when the delay exponent is relatively high, the

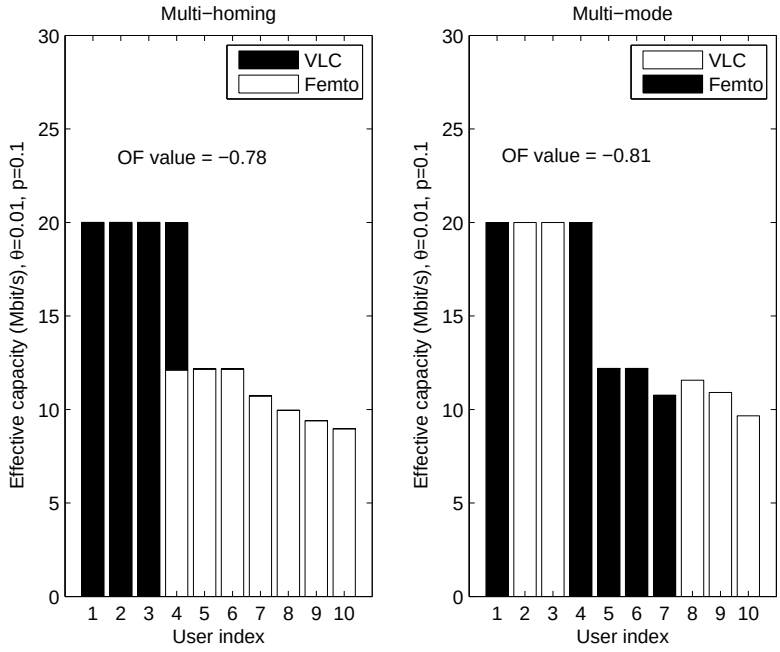

Figure 4.11: The effective capacity of both multi-homing MTs and multi-mode MTs, with $\alpha = 2$, $\theta = 0.01$ and $p = 0.1$

.

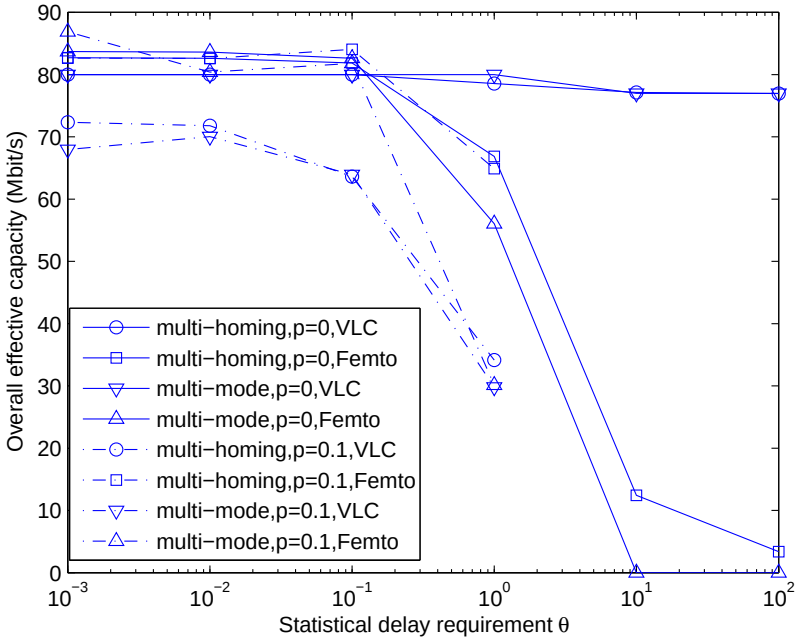

Figure 4.12: The overall effective capacity of MTs versus the statistical delay parameter θ , for $\alpha = 1$

.

overall effective capacity tends to zero. However, it is shown in Fig. 4.12 that the overall effective capacity of the VLC remains almost unchanged for the entire delay exponent region considered for $p = 0$. The DL effective capacity between the VLC LEDs and MT n is expressed as: $\Delta_{1,n}(\beta_{1,n}) = \beta_{1,n} R_{1,n}^{VLC}$, which is independent of the delay exponent θ. Observe from Fig. 4.12 that the effective capacity gleaned from the VLC system decreases only slightly, while the effective capacity of the RF femtocell decreases rapidly. This is because the VLC system increases the amount of resources allocated to the guaranteed-throughput MTs, at the cost of decreasing the overall effective capacity. Hence, the VLC system benefiting from a zero blocking probability is more reliable than the RF femtocell link, when the MTs have to satisfy a certain delay constraint.

When we assume that the blocking probability of the VLC system equals to 0.1, its performance degrades rapidly for $\theta \geq 0.1$. Hence naturally, the VLC system is more sensitive to the delay constraints in the presence of a non-zero blocking probability. As a result, the RF femtocell has to increase its RA probability, especially to the MTs operating under a strict bit rate guarantee. When we have $\theta > 1$, it is observed in Fig. 4.12 that our system fails to fulfil the bit rate requirement. In this case, no optimal solution can be found. It is also observed in Fig. 4.12 that the attainable performance is similar for multi-homing MTs and multi-mode MTs, when the delay requirement is loose.

4.6.4 Effect of the VLC System's Blocking Probability

Let us now quantify the effect of the VLC system's blocking probability on the overall effective capacity of the MTs, when using a delay exponent of 1. It is illustrated in Fig. 4.13 that the VLC system's effective capacity decreases, when the blocking probability is increased. However, as seen in Fig. 4.13, the effective capacity of the RF femtocell system is slightly reduced for the multi-homing MTs. The RF femtocell system should increase the amount of resources allocated to the MTs, if they have to satisfy a certain guaranteed throughput, which is achieved at the price of decreasing the overall effective capacity. When the MTs are multi-mode terminals, we observe that the overall effective capacity of the VLC system and RF femtocell system substantially decreases at $p = 0.1$. This is because when the VLC LOS reception is blocked with a certain probability, the effective capacity is substantially reduced according to Eq. (4.18) and the first reflected ray may only contribute to the MTs located near the wall. As a result, the RF femtocell system may have to allocate resources to the guaranteed-rate MTs, even if their RF channel quality is not particularly good. When the LOS reception blocking probability increases from $p = 0.1$ to $p = 1$, the overall effective capacity of the RF femtocell system remains constant. This is because the femtocell system may allocate most of its resources to the guaranteed-rate MTs. Increasing p results in decreasing the performance of the VLC system. As a result, the overall effective capacity of the VLC system keeps on decreasing. When $p = 1$, the LOS ray is blocked, hence the MTs may only receive a reduced optical power due to the first reflected ray. Hence, it is plausible that when the

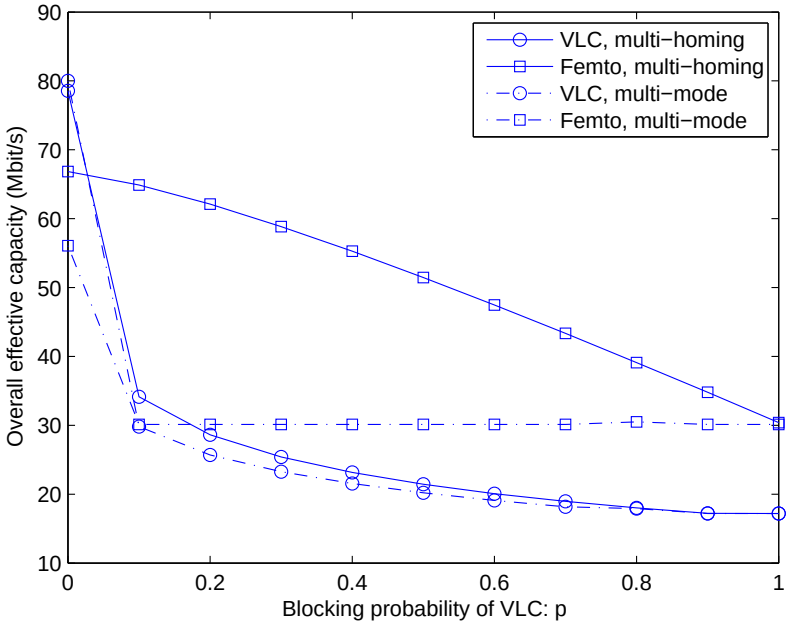

Figure 4.13: The overall effective capacity of MTs versus the blocking probability of the VLC system p , for $\alpha = 1$ and $\theta = 1$

.

blocking probability of the VLC system is high, the RF femtocell system becomes more reliable.

4.6.5 Effect of the User Distribution

In the above simulations, we assume that the MTs are randomly located in the room. Fig. 4.14 compares the overall effective capacity, when all the MTs are located in the center (center cluster) or at the edge (edge cluster). Observe that the performance of the RF femtocell system of center-cluster MTs is better than that of the edge-cluster MTs. This is because we assume that the RF femtocell BS is positioned in the center of the room. As a result, the center-cluster MTs benefit from a shorter transmission distance and a lower pathloss. We also observe that the overall effective capacity of the VLC system decreases upon increasing the VLC LOS reception blocking probability p. When the MTs are center-clustered, the effective capacity of the VLC system is substantially reduced, as p increases from 0 to 0.1. Then it starts to decay towards 0 for larger p values. The performance of the VLC system is sensitive to the LOS reception blocking, especially when the MTs are located in the center of the room. However, when the MTs are edge-clusted, the VLC system may still be capable of supporting an approximately 30 Mbit/s transmission rate, even if the VLC LOS blocking probability becomes 1, because the edge MTs may still benefit from the reflected optical power.

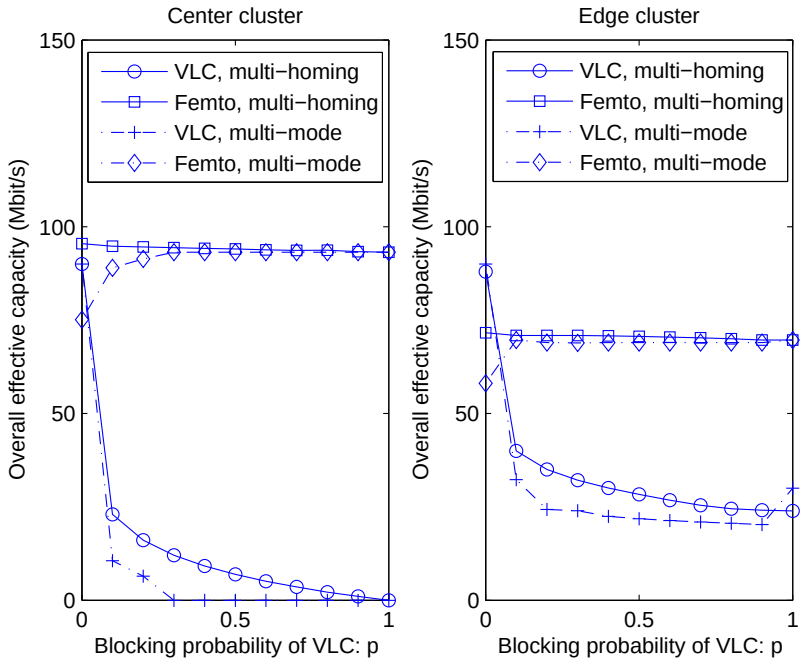

Figure 4.14: The overall effective capacity of MTs versus the blocking probability of p, when the MTs are located at the room-center and room-edge, for $\alpha = 1$ and $\theta = 1$

.

4.7 CONCLUSIONS

In Section 4.2, we outlined the model of a VLC system relying on LED lights, where both the link characteristics and the transmission strategy were presented. More specifically, the topology of the VLC system is illustrated as Fig. 4.1. The received SNR and the achievable bit rate was formulated in Eq. (4.10) and Eq. (4.12). The corresponding simulation results were portrayed in Fig. 4.3 and in Fig. 4.4-4.6 of Section 4.6, where the distribution of the indoor received SNR, and that of the ASE were illustrated. It was observed that there is a coverage dead-zone, when the number of LED lights is not sufficient, but the received SNR and ASE becomes near-constant, when the number of LED lights is increased.

In Section 4.3, the system model of the indoor heterogeneous network was characterized, where the effective capacity of VLC system and of the RF femtocell system were expressed in Eq. (4.18) and Eq. (4.19). Later, the RA problems of both the multi-homing MTs and the multi-mode MTs were formulated in Section 4.4, where their fairness, statistical delay constraints and their bit rate requirements were also taken into account. In order to solve the associated RA problems efficiently, distributed RA algorithms were proposed in Section 4.5. The convergence behaviour of the distributed algorithms was illustrated in Fig. 4.8, where the performance of the distributed algo-

rithm was verified by comparing the related simulation results to those of the optimal centralized solution.

We also compared the performance of multi-homing MTs to that of the multi-mode MTs, for different fairness factors, as depicted in Fig. 4.9, Fig. 4.10 and Fig.4.11. Observe in these figures that the proposed distributed solution is indeed capable of guaranteeing the associated bit requirements. As expected, multi-homing MTs are capable of achieving a better performance than multi-mode MTs, since multi-homing MTs have access to multiple networks. Furthermore, it is observed in Fig. 4.9, Fig. 4.10 and Fig. 4.11 that having a higher α results in a higher grade of fairness. In order to evaluate the effects of statistical delay parameters and that of the LOS blocking probability, the overall effective capacity was studied in Fig. 4.12 and in Fig. 4.13. We have summarized the overall effective capacity of MTs extracted from Fig. 4.12 and Fig. 4.13 and summarized them in Table 4.6 and in Table 4.5, respectively.

Table 4.5: Performance summary of the indoor HetNet of Fig. 4.12, for different statistical delay exponent θ and for $\alpha = 1$.

	VLC, $p = 0$		Femtocell,$p = 0$	
MT type	Multi-homing	Multi-mode	Multi-homing	Multi-mode
$\theta = 10^{-3} \sim 10^{-1}$	79 Mbit/s	79 Mbit/s	82 Mbit/s	82 Mbit/s
$\theta = 1$	79 Mbit/s	79Mbit/s	68 Mbit/s	58 Mbit/s
$\theta = 10$	78 Mbit/s	78 Mbit/s	11 Mbit/s	0 Mbit/s
$\theta = 10^2$	78 Mbit/s	78 Mbit/s	2 Mbit/s	0 Mbit/s
	VLC, $p = 0.1$		Femtocell,$p = 0.1$	
MT type	Multi-homing	Multi-mode	Multi-homing	Multi-mode
$\theta = 10^{-3}$	71 Mbit/s	69 Mbit/s	82 Mbit/s	86 Mbit/s
$\theta = 10^{-2}$	70Mbit/s	69Mbit/s	82 Mbit/s	80 Mbit/s
$\theta = 10^{-1}$	66 Mbit/s	66 Mbit/s	82 Mbit/s	80 Mbit/s
$\theta = 1$	32 Mbit/s	29 Mbit/s	67 Mbit/s	29 Mbit/s
$\theta = 10$	N/A	N/A	N/A	N/A
$\theta = 10^2$	N/A	N/A	N/A	N/A

It is observed from Fig. 4.12 that the overall effective capacity is reduced upon increasing the delay exponent. However, the system performance remains fairly insensitive to the delay exponent, in the range spanning from 10^{-3} to 10^{-1}. It is remarkable that the VLC system remains independent of the statistical delay parameter, provided that the LOS blocking probability is set to 0. However, if there is an non-negligable blocking probability for indoor MTs, the system performance is significantly degraded, especially when the delay exponent is relatively high. As a result, the indoor HetNet may not be capable of satisfying the QoS requirements of indoor MTs.

As expected, the performance of a VLC system is significantly affected by the LOS blocking probability. When we have $p = 1$, the LOS ray is blocked, hence the MTs may only receive a

Table 4.6: Performance summary of the indoor HetNet of Fig. 4.13, for different blocking probability p, for $\alpha = 1$ and $\theta = 1$.

	VLC		Femtocell	
MT type	Multi-homing	Multi-mode	Multi-homing	Multi-mode
$p = 0$	79 Mbit/s	79 Mbit/s	68 Mbit/s	58 Mbit/s
$p = 0.2$	29Mbit/s	26Mbit/s	62 Mbit/s	30 Mbit/s
$p = 0.4$	24 Mbit/s	23 Mbit/s	58 Mbit/s	30 Mbit/s
$\theta = 0.6$	20 Mbit/s	19.5 Mbit/s	50 Mbit/s	30 Mbit/s
$\theta = 0.8$	19 Mbit/s	19 Mbit/s	40 Mbit/s	30 Mbit/s
$\theta = 1$	18 Mbit/s	18 Mbit/s	30 Mbit/s	30 Mbit/s

reduced optical optical power due to the first reflected ray. In order to satisfy a particular bit rate requirement, the femtocell has to allocate its resources to the rate guarantee MTs, at the price of decreasing the overall effective capacity. Hence it is plausible that when the VLC LOS blocking probability is high, the RF femtocell system becomes more reliable.

Additionally, the effect of the MT distribution was investigated, as characterized in Fig. 4.14. Central MTs benefit from a shorter transmission distance, when the blocking probability is 0. However, it is observed that the edge MTs benefit from the reflected ray when there is a non-negligible blocking probability.

Chapter 5

Resource Allocation for Indoor HetNet Relying on Different VLC Transmission Strategies

5.1 Introduction

In Chapter 4 an indoor Heterogeneous Network HetNet was considered, where femtocells and LED light based VLC was used for providing indoor coverage. The optimal Resource Allocation RA in the DL of this HetNet was addressed, while meeting diverse QoS requirements. It was assumed that a SCMT scheme was employed, where all LED lights in the room provide coverage for a single transmission cell, as depicted in Fig. 4.2. Hence the signal received from a MT is characterized by the sum of the signals transmitted from all the LED lights according to Eq. (4.10). A specific drawback of this approach is that the resultant ASE of the LED lights is low, since only a single LED MT is supported in a specific DL transmission slot. In order to overcome this drawback, we study the RA problems of this indoor HetNet under the consideration of various transmission strategies in the context of ACO-OFDM aided VLC. A straightforward technique of improving the ASE of the LED lights is to simply transmit different DL signals simultaneously from every LED light. As a result, each LED light creates a transmission cell. A major impairment imposed by this cell formulation is the interference between neighbouring LED lights of the adjacent attocells. The performance of VLC system is mainly dominated by the received LOS component, hence the more distant cell edge MTs may suffer from severe interference. A In order to cope with this impairment, sophisticated transmission strategies have to be designed, but at the time of writing, there is a paucity of studies on the transmission strategies of VLC cells. A cooperation transmission

scheme was proposed in [203], where two neighbouring LED lights operate as a transmission cell and transmit identical signals, namely, Combined Transmission for two LED lights (CT-2). As a result, the potential ICI is benefically turned into useful signals. Furthermore, the authors of [201] discussed FFR invoked for VLC cells and subsequently a joint multi-LED transmission regime was derived in [202, 203]. In this chapter, these transmission strategies are introduced and the performance of ACO-OFDM aided VLC is compared. Furthermore, we still consider the indoor HetNet scenario considered in Chapter 4, the Resource Allocation (RA) problems are solved.

In this chapter, we still address the optimal RA in the DL of HetNet, where ACO-OFDM aided VLC combined with an RF femtocell scenario is employed. Four different transmission strategies are conceived for VLC, and their performance is compared. Then, the optimal RA is found different transmission strategies, while meeting the statistical delay targets of delay-sensitive traffic. The contributions of this chapter are summarized as follows:

- In contrast to the SCMT scheme used in Chapter 4, we introduce another three transmission strategies for our ACO-OFDM aided VLC system. In the radical UFR, each LED light provides coverage for a single transmission cell, hence creating an attocell of its own. By contrast, the merged Combined Transmission (CT) scenario, several neighbouring LED lights can be merged into a multi-LED aided transmission cell and in order to mitigate the inter-cell interference of the VLC system considered. For example, in the CT-2 transmission scenario, two neighbouring LED lights transmit identical signals. In this context, Frequency Reuse (FR) aided transmission is invoked, where the LED lights of the neighbouring attocells use a different frequency band, hence forming a VLC system having a frequency reuse factor 2. The performance of these transmission strategies is compared and investigated.

- The RA problems are formulated, under the consideration of the various transmission strategies of the VLC system. Similar to Chapter 4, the RA problems are formulated as non-linear programming problems and a distributed algorithm is proposed for solving the RA problems.

This chapter is organized as follows. In Section 5.2, we describe both our system model as well as the transmission strategies of the VLC system. The achievable bit rate of VLC under these transmission strategies is compared in Section 5.3. The formulation of our RA problems and the proposed distributed algorithms are outlined in Section 5.4. Finally, our performance results are provided in Section 5.5 and our conclusions are offered in Section 5.6.

5.2 Transmission Strategies in ACO-OFDM Aided VLC

5.2.1 The Topology Model

Similar with the indoor model employed in Chapter 4, the 2-dimensional (2D) indoor room model is used, as depicted in Fig. 4.1. Again, the set of MTs is denoted by $\mathcal{N} = \{1, \cdots, n, \cdots, N\}$. Similarly, the set of LED lights is denoted by $\mathcal{U} = \{1, \cdots, u, \cdots, U\}$. The cell set is denoted as: $\mathcal{M} = \{1, \cdots, m, \cdots, M\}$, where m denotes the mth accessible cell. Since it was illustrated in Fig. 4.8 that the multi-homing MTs are capable of achieving a better performance than the multi-mode MTs, in this chapter, only multi-homing MTs are considered.

The link characteristic of the VLC system was presented in Section 4.2.1, where the VLC channel gain is constituted by the sum of the direct link gain and the first-reflection link gain. Furthermore, the received SNR and the achievable bit rate of the ACO-OFDM aided VLC system at MT n is given by Eq. (4.10) and Eq. (4.12), respectively. Again, ACO-OFDM is employed for our VLC system and, the achievable rate of the ACO-OFDM aided VLC system is characterised by Eq. (4.12), where we denote the instantaneous transmission probability of the cell m transmitting to MT n as $\beta_{m,n}$. The achievable throughput of MT n supported by cell m is expressed as: $\beta_{m,n} r_{m,n}$, where $r_{m,n}$ denotes the instantaneous transmission bit rate in the DL of cell m to MT n.

5.2.2 Transmission Strategy

5.2.2.1 Single Cell Multi-point Transmission

In the Chapter 4, the SCMT philosophy was used, where all LED lights in the room illuminate a single transmission cell, as depicted in Fig. 4.2. As a result, the received SNR ξ_n^{VLC} of MT n served by the VLC system is given by:

$$\xi_n^{SCMT} = \frac{\pi \left(\varsigma P_t^{VLC,o} \sum_u H_{u,n} \right)^2}{\left(\sigma^{VLC}\right)^2}, \tag{5.1}$$

where the VLC channel gain $H_{u,n}$ of the link spanning from the uth LED light to MT n is given by Eq. (4.1) and Eq. (4.5), while the variance σ^2 of the noise is given by Eq. (4.6), Eq. (4.7) and Eq. (4.8). The achievable rate R_n^{SCMT} of the VLC system under the SCMT for MT n is given by Eq. (4.12).

Since all the LED lights illuminate as a single cell, indoor MTs are capable of accessing both the VLC cells and the RF femtocell. As a result, we may have $M = 2$, where $m = 1$ and $m = 2$ represent the ACO-OFDM aided VLC and the RF femtocell network, respectively.

5.2.2.2 Unity Frequency Reuse

Again, a straightforward way of constructing a VLC cell is to simply assume that each VLC light illuminates an individual attocell, which corresponds to adopting Unity Frequency Reuse (UFR) across all VLC cells, as depicted in Fig. 5.1. Hence, apart from receiving the desired signal, a MT may also suffer from the interference impinging from the neighbouring LED lights.

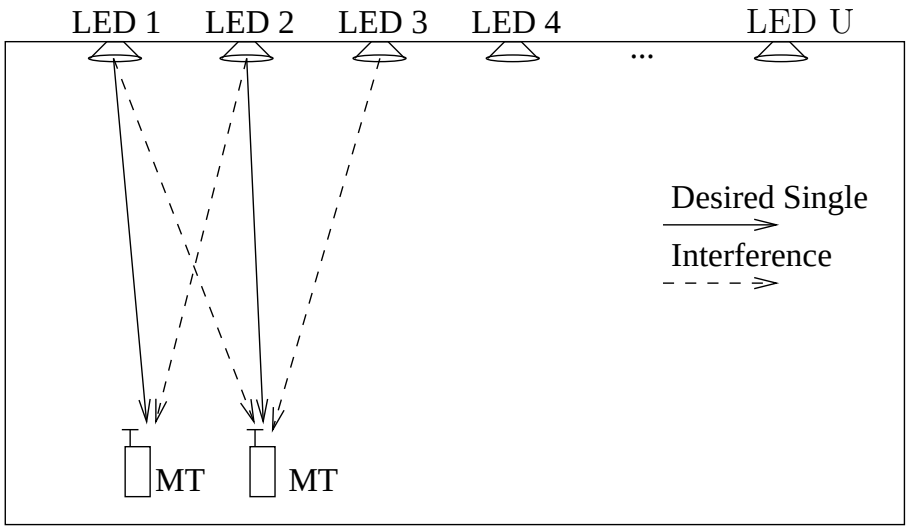

Figure 5.1: The 2D model of the room using the LED light based VLC system, where the UFR transmission is assumed.

Here each LED light operates as a single cell. Hence, there are U attocells for the DL VLC transmission. As a result, the set of cells accessible for our indoor MTs is constituted by M VLC attocells plus the femtocell, where we have $M = U + 1$. We assume that $m = \{1, \cdots, m, \cdots, U\}$ denote the mth VLC attocell, whilst $m = U + 1$ represents the RF femtocell. The received SINR $\xi_{m,n}^{UFR}$ of MT n served by cell m is given by:

$$\xi_{m,n}^{UFR} = \frac{\pi \left(\varsigma P_t^{VLC,o} H_{m,n}\right)^2}{(\sigma^{VLC})^2 + \pi\varsigma^2 \sum_{m' \neq m} \left(P_t^{VLC,o} H_{m',n}\right)^2}, \tag{5.2}$$

where again the VLC channel gain $H_{m,n}$ of the link spanning from the mth LED light to MT n is given by Eq. (4.1) and Eq. (4.5), and the variance σ^2 of noise is given by Eq. (4.6), Eq. (4.7) and Eq. (4.8). The instantaneous transmission rate $R_{m,n}^{UFR}$ of the VLC under UFR supported by the VLC attocell m for MT n is given by Eq. (4.12). Again, the bit rate achieved by MT n becomes $\beta_{m,n} r_{m,n}$, where $r_{m,n}$ denotes the instantaneous transmission bit rate according to Eq. (4.12).

5.2.2.3 Combined Transmission

In this CT arrangement, each individual VLC light of a multi-LED cell conveys the same information on the same carrier frequency. In this chapter, we assume that the neighbouring two LED lights are merged into a CT-2 transmission cell and transmit identical signals, as depicted in Fig. 5.2 [1].

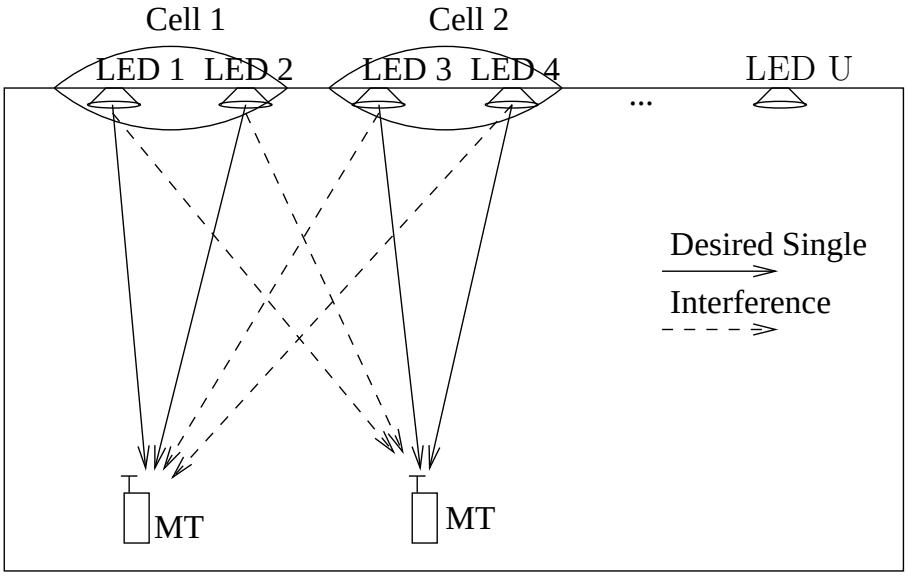

Figure 5.2: The 2D model of the room using the LED light based VLC system, where the CT-2 transmission is assumed.

Under the CT-2 transmission, there are $\frac{U}{2}$ attocells for DL VLC transmission. As a result, the set of cells accessible for our indoor MTs are $\frac{U}{2}$ VLC attocells plus the femtocell. We assume that $m = \left\{1, \cdots, \frac{U}{2}\right\}$ denote the mth VLC attocell, whilst $m = \frac{U}{2} + 1$ represents the RF femtocell. The received SINR $\xi_{m,n}^{CT-2}$ of MT n served by cell m is given by:

$$\xi_{m,n}^{CT-2} = \frac{\pi \left[\varsigma P_t^{VLC,o} \left(H_{2m-1,n} + H_{2m,n}\right)\right]^2}{\left(\sigma^{VLC}\right)^2 + \pi\varsigma^2 \sum_{m' \neq m} \left(P_t^{VLC,o} H_{m',n}\right)^2}. \tag{5.3}$$

Then, the instantaneous transmission rate of the VLC under UFR $R_{m,n}^{CT-2}$ from VLC virtual cell m to MT n is given by the Eq. (4.12). Again, the bit rate achieved by MT n becomes $\beta_{m,n} r_{m,n}$, where $r_{m,n}$ denotes the instantaneous transmission bit rate according to Eq. (4.12).

[1] Since two LED lights are merged into an attocell in this chapter, we assume that the number of indoor LED lights U is even, for simplicity.

5.2.2.4 Frequency Reuse Aided Transmission

Again, following the traditional RF cellular design principle, FR aided transmission may be employed for reducing the inter-cell interference (ICI). Here we invoke this classic idea in our VLC system, where the neighbouring LED lights use a different frequency band, hence forming a VLC system having frequency reuse factor equalling to 2, as depicted in Fig. 5.3. We refer to this transmission strategy as FR-2. The entire available frequency band of VLC is divided into two frequency band, namely F_1 and F_2, where we have $|F_1| = |F_2|$. It is reasonable to stipulate this frequency reuse assumption in our VLC system. This is because that there are two popular techniques of constructing white LEDs, namely either by mixing the Red-Green-Blue frequencies using three chips, or by using a single blue LED chip having a phosphor layer. We consider the latter one, which is the favoured commercial version. Although the terminology of 'white' LED gives the impression of having all frequency components across the entire visible light spectrum, in fact only the blue frequency-range is detected. More precisely, not even the entire blue frequency-range is detected, since the less responsive phosphorescent portion of the frequency-band is ignored. Hence, the modulation bandwidth is typically around 20 MHz, albeit this measured bandwidth depends on the specific LED product used. Given this 20 MHz bandwidth, we are now ready to employ ACO/DCO-OFDM and partition its bandwidth into arbitrary frequency reuse patterns.

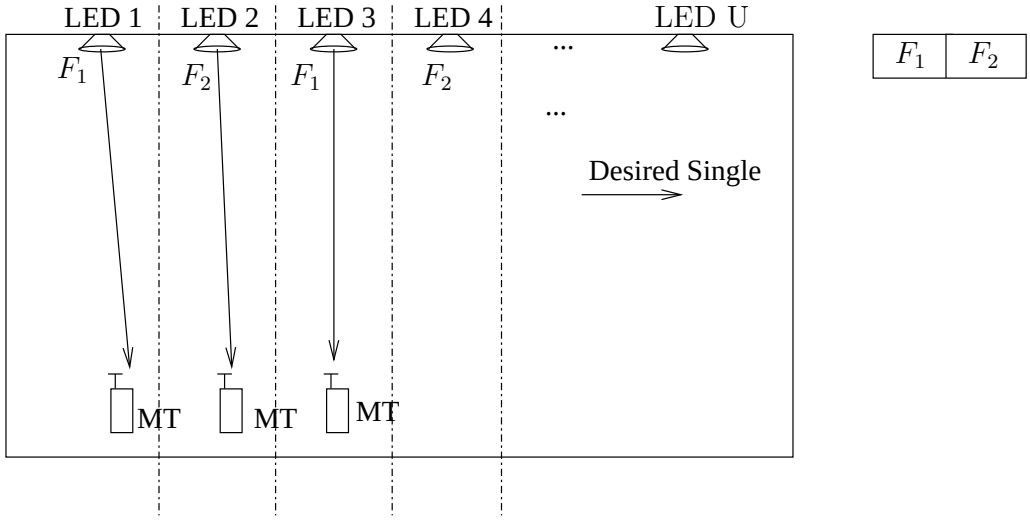

Figure 5.3: The 2D model of the room using the LED light based VLC system, where the FR-2 transmission is assumed.

Similar to the UFR transmission of Fig. 5.1, each LED light operates as a single attocell, hence, there are U VLC attocells for downlink transmission. As a result, the set of cells accessible for our indoor MTs is U VLC transmission attocells plus the RF femtocell. We assume that $m = \{1, \cdots, m, \cdots, U\}$ denote the mth virtual VLC cell, whilst $m = U+1$ represents the RF femtocell. Furthermore, We assume that the VLC attocells of $\mathcal{M}_1 = \{1, 3, \cdots, U-1\}$ use the frequency band F_1, whilst the attocells of $\mathcal{M}_2 = \{2, 4, \cdots, U\}$ develop the frequency band F_2. The received

SINR $\xi_{m,n}^{FR-2}$ of MT n served by cell $m \in \mathcal{M}_1$ is given by:

$$\xi_{m,n}^{FR-2} = \frac{\pi \left(\varsigma P_t^{VLC,o} H_{m,n}\right)^2}{\left(\sigma^{VLC}\right)^2 + \pi\varsigma^2 \sum_{m' \in \mathcal{M}_2} \left(P_t^{VLC,o} H_{m',n}\right)^2}. \tag{5.4}$$

Again, the bit rate achieved by MT n becomes $\beta_{m,n} r_{m,n}$, where $r_{m,n}$ denotes the instantaneous transmission bit rate according to Eq. (4.12).

It is remarkable that the ICI imposed by the direct link is completely avoided when employing a frequency reuse factor equalling to 2 in the 2-D indoor scenario considered. We do not consider the FFR scheme employed in [202], because the FFR imposes a high complexity, hence, it is unrealistic for adoption in VLC systems.

5.3 Simulation Results

In this section, the achievable bit rate of the considered ACO-OFDM aided VLC is presented, relying on the four transmission strategies introduced. Similar system configurations of VLC system is opted, as listed in Table 4.1. Again, it is assumed that the transmission power of the optical VLC system is fixed. Firstly, the achievable bit rate distribution and BER of the ACO-OFDM aided VLC is compared. Then, we assume that $N = 10$ MTs are randomly distributed in the room and the classical round robin scheduling scheme [251] is used in our simulations, where each MT is allocated the same resource. The Cumulative Distribution Function (CDF) of the achievable bit rate is presented. Furthermore, the effects of the FOV and that of the semi-angle at half power is evaluated.

5.3.1 The Downlink performance of VLC

Let us now compare the performance of the ACO-OFDM aided VLC using the parameters listed in Table 4.1 under the four transmission strategies introduced in Section 5.2.2. The achievable bit rate and BER of our VLC system are demonstrated in Fig. 5 Observed from the Fig. 5.4 that SCMT regime is capable of achieving the highest bit rate, since all the LED lights transmit an identical signal which results in a near-uniformly distributed received SNR. However, as we stated in Section 5.2, the achievable bit rate is expected to be significantly reduced, when multiple MTs are in the room, since only a single MT is served for SCMT regime. As expected, The indoor MTs suffer from the interference, relying on UFR regime. As a result, the bit rate decays in most of the indoor areas (-7 to 7). Although, UFR transmissions activate all the LEDS for transmission as individual attocells, it is still unwise to employ UFR transmissions owing to the poor performance of the indoor centrally located MTs. The CT-2 regime improves the indoor coverage in Fig. 5.4 by jointing the neighbouring pair of LED lights. However, there are still some areas, which suffer

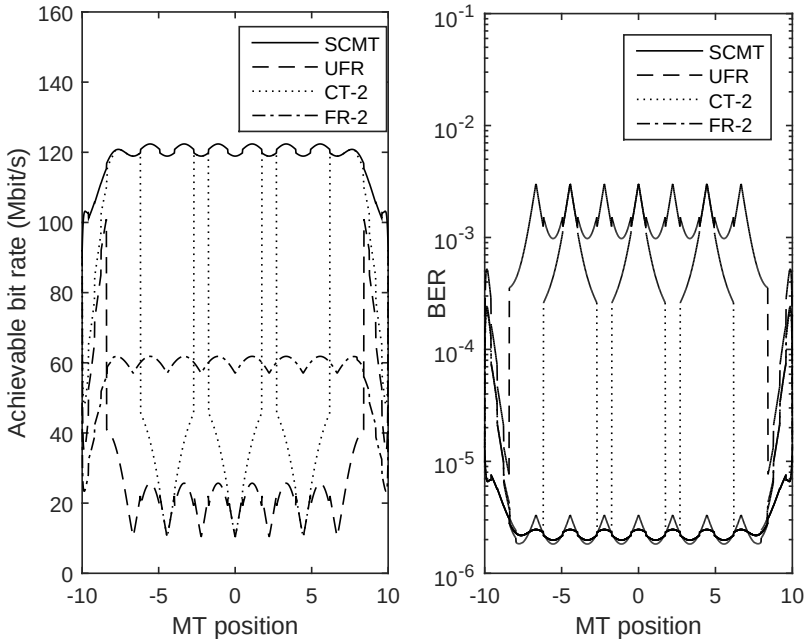

Figure 5.4: The achievable bit rate and the BER of our VLC system, under the SCMT, UFR transmission, CT-2 and FR-2 Transmission. The number of LED light is set to 8, and the other simulation parameters are listed in Table 4.1.

from the inter-cell interference. This erodes the achievable bit rate, because CT-2 is unable to avoid the inter-cell interference. In contrast to CT-2 regime, FR-2 transmission scheme is capable of maintaining a near-constant bit rate. This is because that the interference is avoided amongst the neighbouring cells, since different frequency bands are used for the neighbouring attocells. However, the achievable bit rate is limited by the reduced bandwidth, when the MTs relying on FR-2.

We also demonstrate the BER of indoor MTs in the right of Fig. 5.4. As expected, SCMT regime exhibit the lowest BER, where most of indoor MTs are capable of the downlink transmission with a BER of 10^{-5}. FR-2 regime is capable of achieving the similar BER with SCMT regime, because the inter-cell interference is avoided when MTs is relying on FR-2 in our 2-D VLC system. The UFR regime exhibit the worst BER performance, where the BER of indoor central MTs may become to 10^{-2}.

Furthermore, when the LOS rays are blocked, i.e. $p = 1$, the achievable bit rate of indoor MTs is compared in Fig. 5.5. It is observed that the central MTs in the range spanning from -7.8m to 7.8m are unable to maintain a useful transmission bit rate. The angle of incidence of the reflected rays may be wider than the value of FOV, when the MTs are located in the central region. By contrast, the edge MTs are capable of achieving a beneficial DL transmission rate, owing to the reflected rays. Observed from Fig. 5.5 that the SCMT outperforms the other three transmission

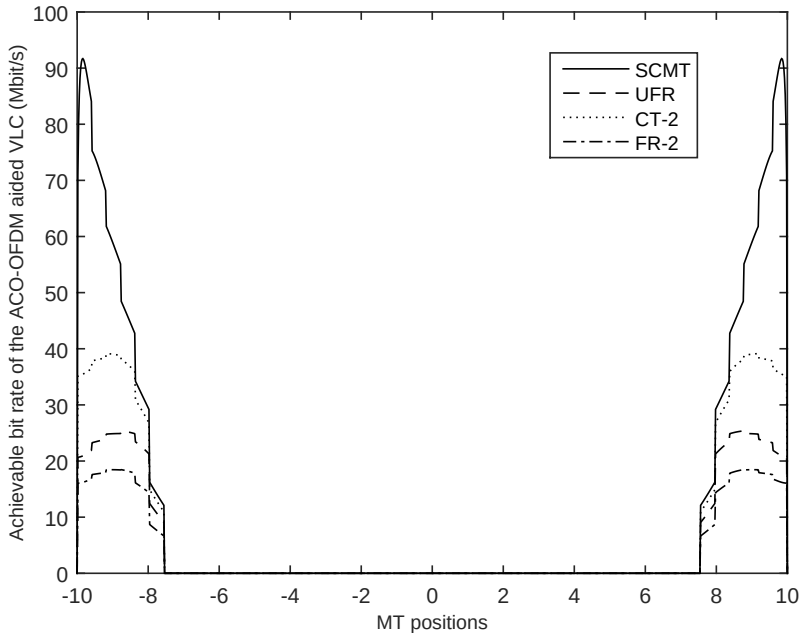

Figure 5.5: The bit rate distribution of our VLC system relying on the SCMT, UFR transmission, CT-2 and FR-2 transmission, when the LOS ray is blocked. The number of LED light is set to $U = 8$, and the other simulation parameters are listed in Table 4.1.

strategies in this scenario, since there is no interference under the SCMT regime and the desired signals are constituted by the sum of all the LED lights. It is somewhat unexpected that the FR-2 transmission regime exhibits the lowest available bit rate.

5.3.2 Cumulative Distribution Function of The Achievable Bit Rate

Fig. 5.6 compares the Cumulative Distribution Function (CDF) of the for different transmission strategies, in conjunction with $U = 8$ LED lights, a half field of view $\Phi_c = 60^o$ and $N = 10$ indoor MTs. The indoor MTs are randomly distributed and the classic round robin scheduling scheme is assumed. Hence each MT is allocated the same resource. Observe from the figure that the MTs maintain a bit rate ranging from 10 Mbit/s to 15 Mbit/s, when the SCMT regime is employed. By contrast, the achievable bit rate of MTs fluctuates dramatically both for the UFR and CT-2 transmission, spanning from 5 Mbit/s to 120 Mbit/s. About of the 50% MTs under CT-2 maintain a bit rate more than 20 Mbit/s, but this is reduced to 30% for the UFR regime. Furthermore, the FR-2 transmission regime may support the highest transmission bit rate according to Fig. 5.6, since the interference is avoided in the scenarios considered. It is remarkable that 60 Mbit/s the maximum transmission bit rate of FR-2 is much lower than that of the UFR and CT-2 transmission.

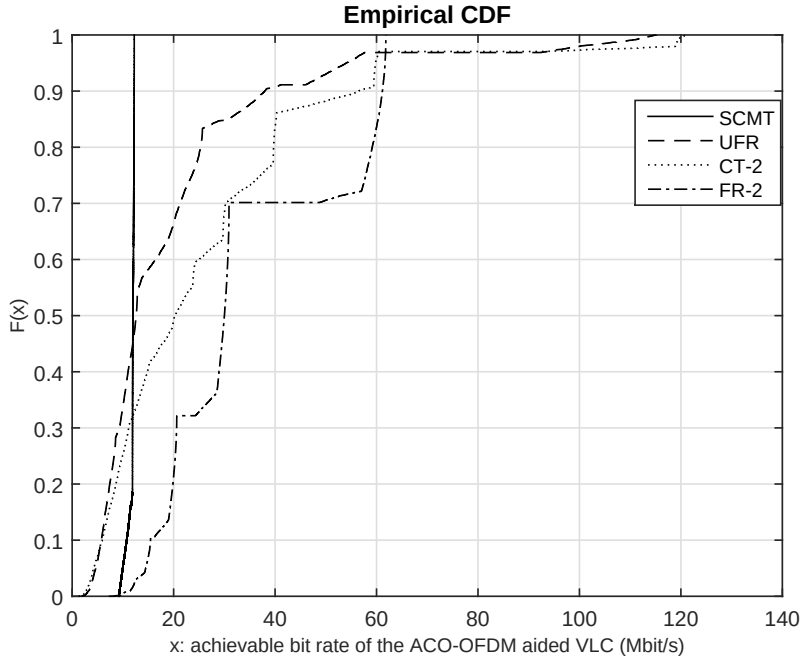

Figure 5.6: The CDF of the achievable bit rate of our VLC system of Fig. 4.1, under SCMT, UFR, CT-2 and FR-2 transmission. The number of LED lights is set to $U = 8$, and the other simulation parameters are listed in Table 4.1.

5.3.3 Effect of The Field of View Angle

Let us now focus our attention on the effect of the FOV of MTs. Increasing the FOV leads to the expansion of the areas contaminated by interference. Furthermore, the value of the FOV may affect the gain of an optical concentrator, according to Eq. (4.2) and it is also expected to affect the channel gain of the VLC system. Firstly, it is observed from Fig. 5.7 that the achievable rate of the MTs is near-constant under the SCMT, because the FOV does not substantially affect the channel gain of the VLC, owing to the logarithm in Eq. (4.12). By contrast, the achievable bit rate gracefully decays under the UFR and CT-2 regime, since the MTs suffer from the interference generated by more LED lights, which erodes the achievable bit rate. The CT-2 regime outperforms the UFR transmission in the scenario considered. By contrast, the achievable bit rate of the MTs under the FR-2 transmission regime remains near-constant, when we have a FOV of $\Phi_c \leq 125^o$. This is because the MTs may not suffer from any interference as a benefit of the frequency reuse. However, the achievable bit rate is reduced when we further increase the FOV of MTs. The reason for this phenomenon is that the the indoor MTs may still suffer from the interference generated by the LED lights using the same frequency band, if the FOV is wide.

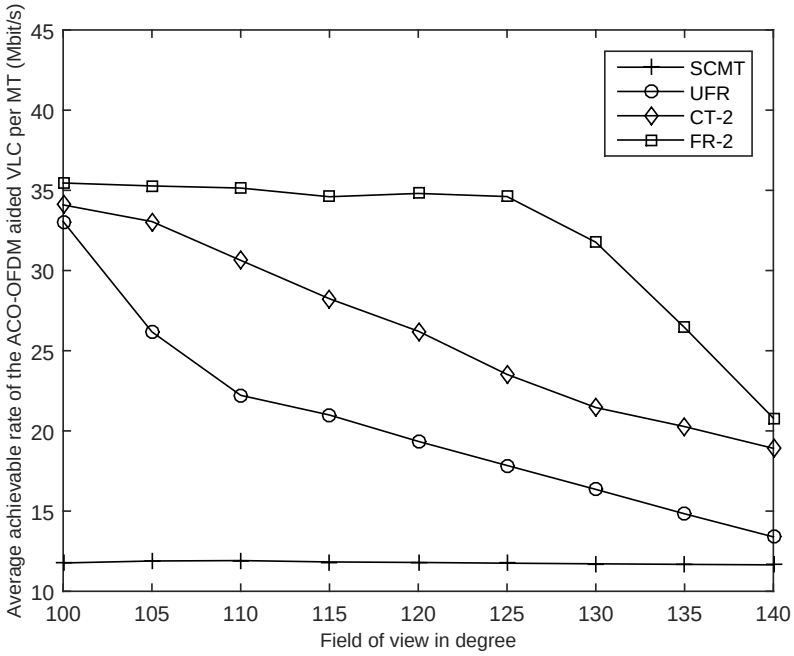

Figure 5.7: The achievable bit rate of the VLC system of Fig. 4.7, for different FOV angles, under the SCMT, UFR, CT-2 and FR-2 transmission. The number of LED lights is set to $U = 8$, and the other simulation parameters are listed in Table 4.1.

5.3.4 Effect of The Semi-Angle at Half Power

Fig. 5.8 illustrates the effect of the value of semi-angle at half power on the available bit rate of indoor MTs, in conjunction with $U = 8$ LED lights, a half field of view $\Phi_c = 60^o$, and $N = 10$ indoor MTs. As shown in the figure, the bit rate decreases as a function of the semi-angle. Explicitly, the semi-angle at half power may affect the order of Lambertian emission q, which may be written as: $q = \frac{\ln 2}{\ln(\cos \phi_{1/2})}$. To expound further, a wider value of semi-angle at half power reduces the order of Lambertian emission and hence further decreases the received SNR. It is remarkable that the SCMT remains fairly insensitive to the value of the semi-angle at half power. By contrast, the UFR transmission is seen to be more sensitive to the value of the semi-angle at half power in Fig. 5.8.

5.4 Resource Allocation for The Indoor HetNet

In this section, the RA problem formulation is formulated for indoor multi-homing MTs in the context of the HetNet considered, and then the problems are solved by the distributed algorithm

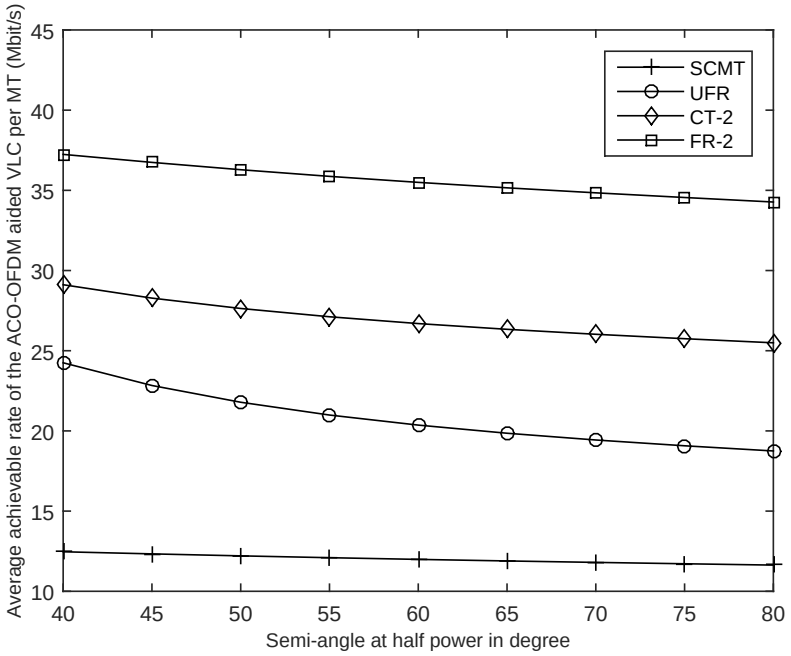

Figure 5.8: The achievable bit rate of the VLC system of Fig. 4.7, for different semi-angle at half power, under the SCMT, UFR, CT-2 and FR-2 transmission. The number of LED light is set to $U = 8$, and the other simulation parameters are listed in Table 4.1.

introduced in Section 4.4. Similar to the scenario considered in Chapter 4, the ACO-OFDM aided VLC and a RF femtocell are used for providing indoor coverage. The RA problems are formulated relying on proportional fairness, while satisfyingthe specific statistical delay constraints. Again, we invoke the effective capacity approach for converting the statistical delay constraints into equivalent average rate constraints. The effective capacity $\Delta_{m,n}$ of the indoor MT n supported by cell m is given by the Eq. (4.18), whilst the effective capacity of the femtocell is formulated in the Eq. (4.19).

5.4.1 Problem Formulation

Our objective is to find the optimal RA per network by maximizing the sum of all MT's utility function. In this chapter, the utility function of MT n served by the cell m is defined as $\log\left[\Delta_{m,n}\left(\beta_{m,n}\right)\right]$, where the logarithm is used for guaranteeing fairness amongst the MTs served.

As a result, the corresponding RA problem may be formulated as:

$$\textit{Problem 1}: \quad \underset{\boldsymbol{\beta}}{\text{maximize}} \sum_{m\in\mathcal{M}}\sum_{n\in\mathcal{N}} \log\left[\Delta_{m,n}\left(\beta_{m,n}\right)\right] \tag{5.5}$$

$$\text{subject to:} \quad \sum_{n\in\mathcal{N}} \beta_{m,n} \leq 1, \ \forall\, m \in \mathcal{M}, \tag{5.6}$$

$$0 \leq \beta_{m,n} \leq 1, \tag{5.7}$$

where $\boldsymbol{\beta}$ denotes the RA matrix of the VLC combined with the RF femtocell system. The effective capacity $\Delta_{m,n}$ of the VLC system and that of the RF femtocell is given by Eq. (4.18) and Eq. (4.19), respectively. Physically, the constraint (5.6) ensures that the total resources allocated in a cell always remain below unity. Whilst, the constraint (5.7) describes the feasible region of the optimization variables.

5.4.2 Decentralized Sub-optimal Resource Allocation Schemes

The problem is a concave one and the associated proof is given in Section 4.4.2. As a result, the problem described by (5.5), (5.6) and (5.7) may also be solved by the distributed algorithm introduced in Section 4.5. Similarly, the Lagrangian function formulated for (5.5), (5.6) and (5.7) may be expressed as:

$$\mathbb{L}\left(\boldsymbol{\beta}, \boldsymbol{\upsilon}\right) = \sum_{m\in\mathcal{M}}\sum_{n\in\mathcal{N}} \left(\log \Delta_{m,n} - \upsilon_m \beta_{m,n}\right) + \sum_{m\in\mathcal{M}} \upsilon_m, \tag{5.8}$$

where we have $\mathbf{0} \leq \boldsymbol{\beta} \leq \mathbf{1}$, while υ_m represents the Lagrange multipliers or prices associated with the mth inequality constraint (5.6). Similarly, the dual objective function $g_{m,n}\left(\upsilon_m\right)$ of MT n supported by network m is written as:

$$g_{m,n}\left(\upsilon_m\right) = \log \Delta_{m,n} - \upsilon_m \beta_{m,n}. \tag{5.9}$$

At the lower level, the optimal resource allocation $\beta_{m,n}$ may be written as:

$$\beta^*_{m,n} = \underset{0\leq\beta_{m,n}\leq 1}{\text{argmax}}\ g_{m,n}\left(\upsilon_m\right). \tag{5.10}$$

It may be readily shown that $g_{m,n}\left(\upsilon_m\right)$ is concave with respect to the variable $\beta_{m,n}$. Hence the maximization of $g_{m,n}\left(\upsilon_m\right)$ may be achieved by finding the partial derivative of $g_{m,n}\left(\upsilon_m\right)$ with respect to the variable $\beta_{m,n}$.

At the higher level, we update the price parameter $\boldsymbol{\upsilon}$ according to:

$$\upsilon_m(t+1) = \left[\upsilon_m(t) - \xi_\upsilon(t)\left(1 - \sum_{n\in\mathcal{N}} \beta^\star_{m,n}\right)\right]^+, \tag{5.11}$$

5.4.2.1 Remarks

The optimal decentralized RA scheme is constituted by an iterative algorithm, which determines the optimal transmission probability in the DL of network m to MT n based on the iterative update

of the price parameters υ_m, over a number of iterations, until the optimal solution is found. Each of the networks m is initialized to a feasible price value υ_m. Then each MT calculates the optimal transmission probability based on the price information $\boldsymbol{\upsilon}$. The optimal RA is derived during this iteration. Each of the networks m updates its price value υ_m based on the newly derived optimal transmission probability $\boldsymbol{\beta}$ and then broadcasts the optimal transmission probability to the MTs. The optimal decentralized RA algorithm is formally described in Table 5.1.

Table 5.1: Decentralized algorithm for Problem 1

Algorithm 1
Input
θ_n: Delay requirement of each MT n $\forall n$,
Initialization
$t \leftarrow 1$;
Price value for each network: $\boldsymbol{\upsilon}(t) = \{\upsilon_1(t), ..., \upsilon_M(t)\} = 0$
step size: positive ξ and ϵ
While t does not reach its maximum
Get optimal $\boldsymbol{\beta}$
For each Network $m \in \mathcal{M}$
For each MT $n \in \mathcal{N}$
Each MT solves the problem presented in Eq. (5.10)
End for
End for
Update price values
For $m \in \mathcal{M}$
Price value υ_m updates according to Eq. (5.11)
End for
$\xi \leftarrow \xi t^{-\frac{1}{2}+\epsilon}$
$t \leftarrow t + 1$
End
Output $\boldsymbol{\beta}^{\star}(t)$

5.5 Results and Discussions

In this section, we present our numerical performance results for characterizing the proposed RA algorithms in the context of the indoor VLC system of Fig. 4.7, where both the ACO-OFDM aided VLC system and a RF femtocell are employed in order to provide indoor coverage. In contrast to Chapter 4, four transmission strategies are considered. We assume that $U = 10$ MTs are uniformly distributed in the room and all experience the same delay exponents. Again, it is assumed that the

transmission power of both the optical VLC system and of the FBS are fixed to their maximum. Firstly, the effects of statistical delay on the overall effective capacity are considered and then the performance of the VLC system and of the RF femtocell is compared. Furthermore, the effects of the LOS blocking probability on the overall effective capacity are considered. Our main system parameters are summarised in Table 4.1.

5.5.1 Effect of The Delay Statistics

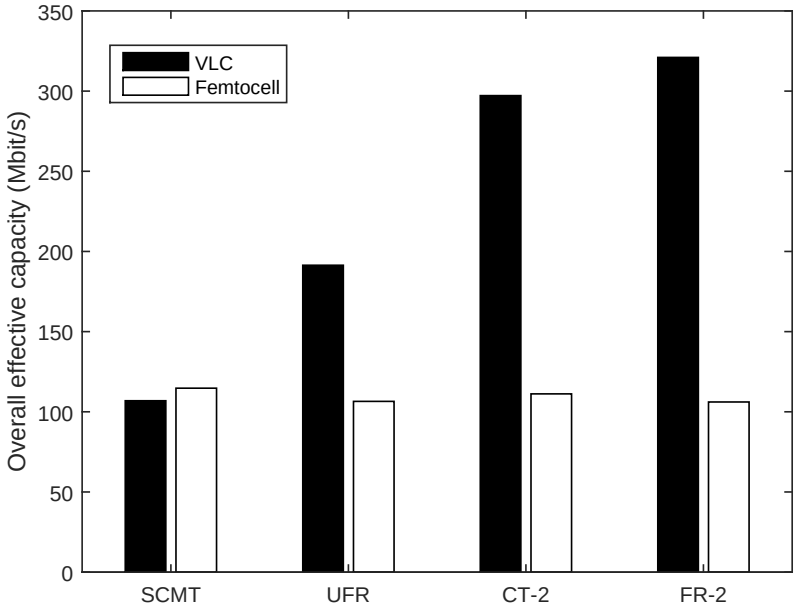

Figure 5.9: The overall effective capacity of the different transmission strategies, with the statistic delay exponent θ set to 0.001 and the LOS blocking probability p to 0.1. All other system parameters are summarized in Table 4.1.

Fig. 5.9, Fig. 5.10 and Fig. 5.11 illustrate the overall effective capacity of indoor MTs supported by both the VLC system and the RF femtocell, when we set the statistical delay $theta$ equals to 0.001, 0.1 and 10, respectively. Here, we assume that the LOS blocking probability of the VLC system equals to 0.1 and the simulation parameters are listed in Table 4.1. Several key observations may be made from these three figures.

1. The specific delay statistics significantly affect the performance of both the VLC system and of the femtocell. Observe from the figures that the overall effective capacity decreases upon increasing the delay exponent, which may be verified from Eq. (4.18) and Eq. (4.19). However, the femtocell and the VLC relying on our different transmission strategies exhibit different system behaviours. The overall effective capacity of the RF femtocell remains

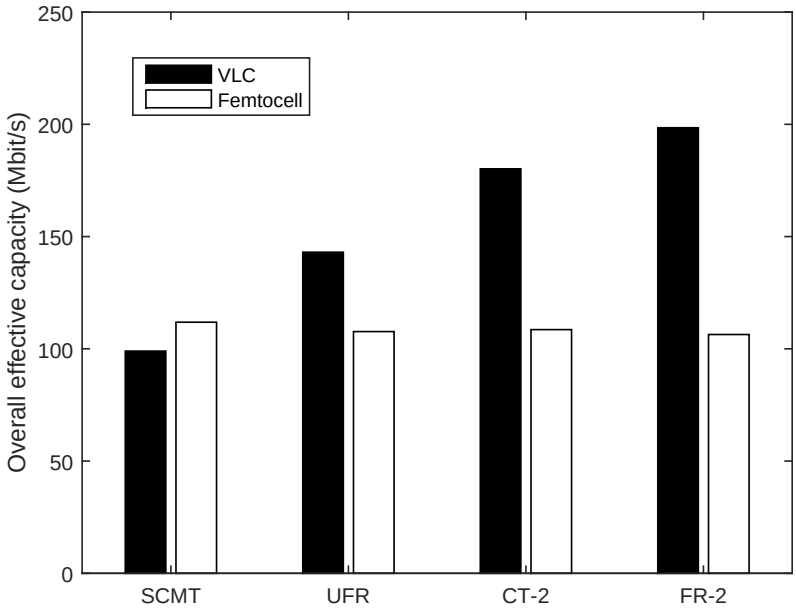

Figure 5.10: The overall effective capacity of the different transmission strategies, with the statistic delay exponent θ set to 0.1 and the LOS blocking probability p to 0.1. All other system parameters are summarized in Table 4.1.

nearly unaffected, when we increase the statistic delay exponent from 0.001 to 0.1, but it is significantly reduced, when the statistic delay exponent is increased from 0.1 to 10. Similar observations are valid for the MTs under the SCMT regime. Explicitly, the effective capacity remains insensitive to the delay exponent, when the exponent is relatively small. By contrast, it is observed that the overall effective capacity of indoor MTs under FR-2 transmission is significantly reduced, even when the statistic delay exponent is low. The reason for this is that the effective capacity of the VLC system may be dominated by the power of received reflected rays. As we have shown in the Fig. 5.5, the FR-2 transmission exhibits the lowest bit rate, when the LOS rays are blocked. As a result, FR-2 transmission are expected to be sensitive to the statistical delay requirement, when there is a non-zero LOS ray blocking probability.

2. Again, observe from Fig. 5.9, Fig. 5.10 and Fig. 5.11 that if the statistic delay requirement is loose, the FR-2 regime outperforms the other three transmission strategies, and the MTs under SCMT exhibit the lowest bit rate. When we tighten the delay requirement and assume $\theta = 10$, the VLC system under the CT-2 regime achieves the highest effective capacity, as decipted in Fig. 5.11. It is also illustrated that the effective capacity of the RF femtocell is lower than that of the VLC system in most of the scenarios considered. However, the effective capacity of the RF femtocell is slightly higher than that of the VLC system under

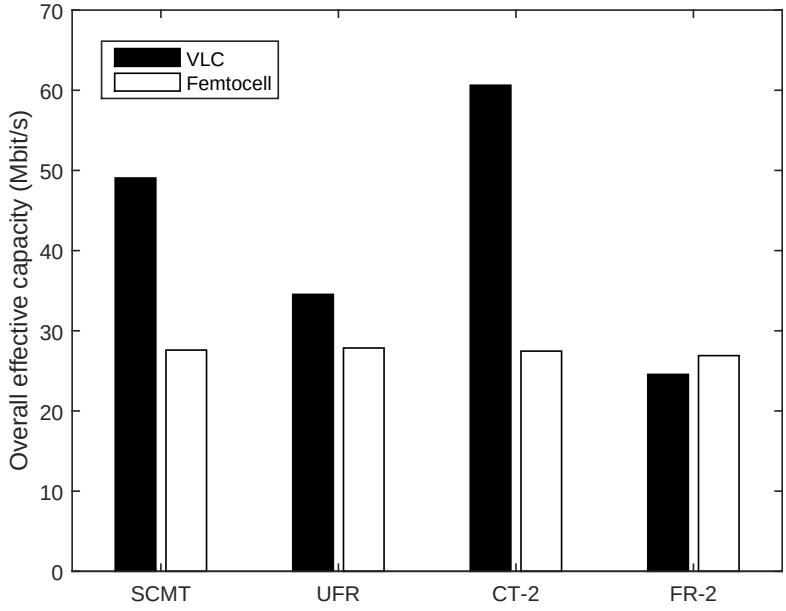

Figure 5.11: The overall effective capacity of the different transmission strategies, with the statistic delay exponent θ set to 10 and the LOS blocking probability p to 0.1. All other system parameters are summarized in Table 4.1.

SCMT, when the statistical delay requirement is loose, i.e. for $\theta = 0.1$. When we tighten the delay requirement, the effective capacity of the RF femtocell becomes higher than that of the VLC under the FR-2 transmission regime.

3. Based on these observations, it becomes plausible that when the delay requirement is loose, the ACO-OFDM aided VLC system has to employ FR-2 transmission, in order to achieve the highest effective capacity. However, the ACO-OFDM aided VLC system operating under the CT-2 regime may become more reliable, when the delay requirements becomes tight.

5.5.2 Effect of The VLC System's LOS Blocking Probability

Let us now quantify the effect of the VLC system's blocking probability. Explicitly, Fig. 5.12 and Fig. 5.13 illustrate the overall effective capacity of indoor MTs supported by both the VLC system and the RF femtocell, when we set the LOS blocking probability p to 0 and 0.2, respectively. Here, we assume that the statistic delay exponent θ of the VLC system is to 0.1 and the simulation parameters are listed in Table 4.1. Several key observations may be made from these two figures.

1. The LOS blocking probability p significantly affects the performance of the VLC system. Observe from Fig. 5.12 and Fig. 5.13 the overall effective capacity decreases upon increasing

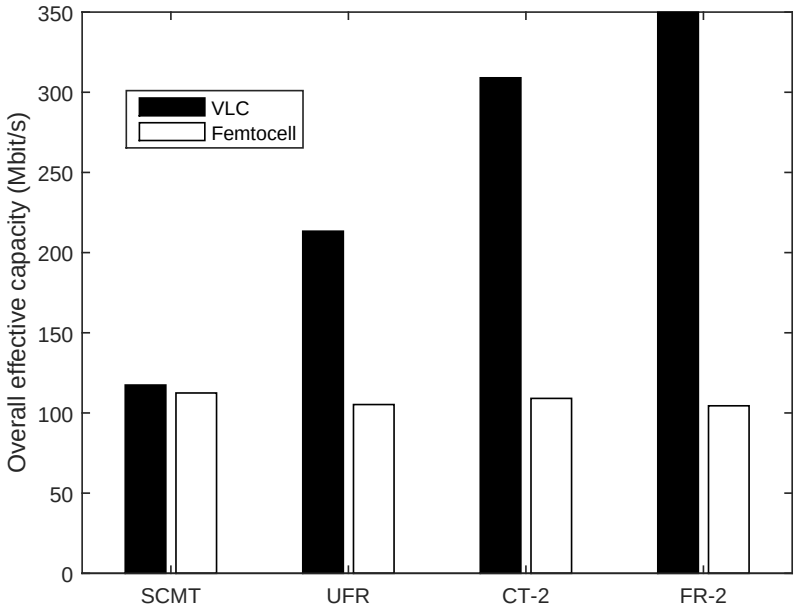

Figure 5.12: The overall effective capacity of the different transmission strategies, with the statistic delay exponent θ set to 0.1 and the LOS blocking probability p to 0. All other system parameters are summarized in Table 4.1.

the delay exponent, which may be verified by observing Eq. (4.18). For the LOS blocking probability considered, the FR-2 transmission regime is capable of achieving the highest effective capacity. We also note from Fig. 5.12 and Fig. 5.13 that CT-2 is capable of obtaining a better performance than the SCMT and UFR transmissions, since CT-2 reduces the intra-cell interference.

2. It is somewhat surprising that the advantage of the FR-2 transmission regime erodes, when we increase the LOS blocking probability. The reason for this is that the performance may be dominated by the cell-edge MTs, which are capable of successfully detecting the reflected rays. As we illustrated in Fig. 5.5, the FR-2 transmission exhibits the lowest bit rate, when the LOS rays are blocked. As a result, the advantage of FR-2 transmission erodes, when the LOS blocking probability increases.

3. In the LOS blocking probability scenario of $p = 0$, the effective capacity of the VLC system is higher than that of the RF femtocell. The increased blocking probability reduces the effective capacity of the VLC system, whilst that of the femtocell remains unchanged. As a result, the RF femtocell constitutes an important complementary network, when there is an non-zero LOS blocking probability.

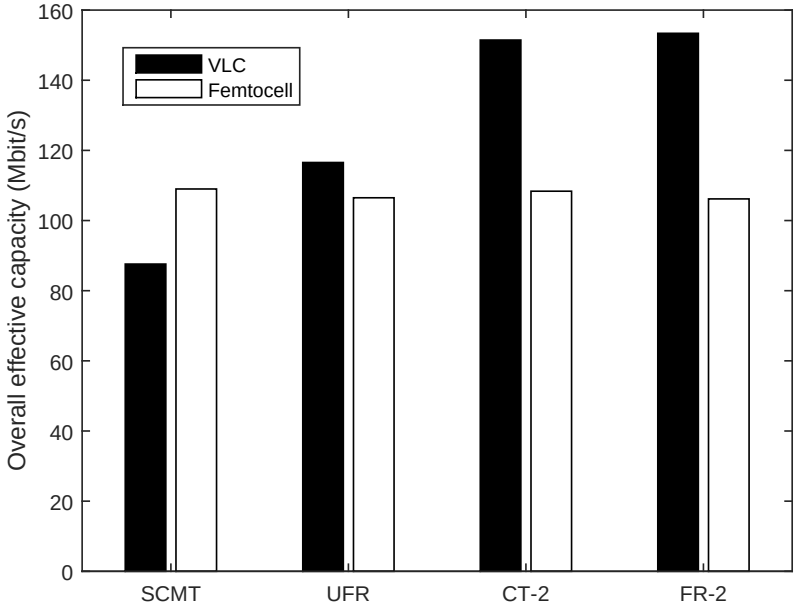

Figure 5.13: The overall effective capacity of the different transmission strategies, with the statistic delay exponent θ set to 0.1 and the LOS blocking probability p to 0.2. All other system parameters are summarized in Table 4.1.

5.6 CONCLUSIONS

In Section 5.2, various ACO-OFDM aided VLC transmission strategies were investigated. In SCMT, all the LED lights jointly forming an attocell and transmit identical signals, as depicted in Fig. 4.2. By contrast, in UFR transmission, a single LED light illuminates an attocell as decipted in Fig. 5.1, which imposes downlink interference on the neighbouring cell. In CT-2, the neighbouring pair of LED lights forms a 'twin-LED' attocell and transmit the signals jointly, as depicted in Fig. 5.2. In the FR-2 transmission regime, each LED light creats its own attocell, and the neighbouring pair of LED lights transmit their information in different frequency band in order to avoid the interference, as depicted in Fig. 5.3. The achievable bit rate and the corresponding BER of indoor MTs supported by the AOC-OFDM aided VLC under different transmission strategies is compared in Fig. 5.4 and Fig. 5.5. It was illustrated that SCMT is able to obtain the highest bit rate. However, since only one MT can be served in one transmission slot, the performance may degrade in a multi-MT scenario. Later, we considered 10 MTs were randomly located, the CDF of the achievable bit rate was illustrated in Fig. 5.6, which shows that FR-2 transmission is capable of achieving the highest bit rate. Furthermore, we investigated the VLC configurations on the achievable bit rate in Fig. 5.7 and in Fig. 5.8. It was illustrated that the bit rate is independent with the value of FOV when the VLC employs SCMT. However, the achievable bit rate of VLC under UFR,

CT-2 and FR-2 degrades when increasing the value of FOV, as shown in Fig. 5.7. It is observed in Fig. 5.8 the achievable bit rate of VLC under all the considered transmission strategies when increasing the value of the semi-angle at half power.

Furthermore, we studied the RA problems of MTs in a VLC system under diverse statistical delay requirements. The objective functions relied upon were shown to be concave. The decentralized algorithms proposed in Chapter 4 were used for solving the associated RA problem. Later, we studied the effects of the statistic delay requirements in Fig. 5.9, Fig. 5.10 and Fig. 5.11, and that of the LOS blocking probability in Fig. 5.12 and Fig. 5.13. It was observed that the FR-2 transmission regimes is capable of achieving the highest effective capacity for a LOS blocking probability of $p = 0$. Compared to the RF femtocell, the VLC system obtains a better performance, since the available bandwidth of VLC is much wider than that of RF femtocell. By contrast, when we consider a non-zero LOS blocking probability, the performance of VLC is significantly affected by the statistic delay requirement. When the delay requirement is loose, FR-2 aided VLC may still obtain the highest effective capacity and the effective capacity of VLC is higher than that of the RF femtocell. However, when we tighten the delay requirements, CT-2 exhibits the highest effective capacity. It is plausible that the FR-2 transmission regime is capable of achieving the highest effective capacity, when the statistical delay requirements are loose. However, CT-2 transmission attains the best performance, when we tighten the delay requirements. Furthermore, the RF femtocell system becomes more reliable, when the VLC LOS blocking probability is high. We have summarized the overall effective capacity of MTs with respect to the statistic delay exponent in Fig. 5.9, Fig. 5.10 and Fig. 5.11 in Table 5.2. Furthermore, we have summarized the overall effective capacity of MTs as a function of the LOS blocking probability in Fig. 5.12, Fig. 5.13 in Table 5.3.

Table 5.2: Performance summary of the indoor HetNet of Fig. 5.9, Fig. 5.10 and Fig. 5.11, parameterized by the statistical delay exponent, for a LOS blocking probability of $p = 0.1$.

	VLC, $\theta = 0.001$	Femtocell, $\theta = 0.001$
SCMT	107 Mbit/s	115 Mbit/s
UFR	191 Mbit/s	106 Mbit/s
CT-2	297 Mbit/s	111 Mbit/s
FR-2	321 Mbit/s	106 Mbit/s
	VLC, $\theta = 0.1$	Femtocell, $\theta = 0.1$
SCMT	99 Mbit/s	112 Mbit/s
UFR	143 Mbit/s	106 Mbit/s
CT-2	180 Mbit/s	108 Mbit/s
FR-2	198 Mbit/s	106 Mbit/s
	VLC, $\theta = 10$	Femtocell, $\theta = 10$
SCMT	49 Mbit/s	28 Mbit/s
UFR	35 Mbit/s	28 Mbit/s
CT-2	61 Mbit/s	27 Mbit/s
FR-2	25 Mbit/s	27 Mbit/s

Table 5.3: Performance summary of the indoor HetNet of Fig. 5.12 and Fig. 5.13, parameterized by the LOS blocking probability, for the statistical delay exponent of $\theta = 0.1$.

	VLC, $p = 0$	Femtocell, $p = 0$
SCMT	117 Mbit/s	112 Mbit/s
UFR	213 Mbit/s	105 Mbit/s
CT-2	309 Mbit/s	109 Mbit/s
FR-2	350 Mbit/s	104 Mbit/s
	VLC, $p = 0.2$	Femtocell, $p = 0.2$
SCMT	88 Mbit/s	109 Mbit/s
UFR	117 Mbit/s	106 Mbit/s
CT-2	151 Mbit/s	108 Mbit/s
FR-2	153 Mbit/s	108 Mbit/s

Chapter 6

Conclusions and Future Work

In this concluding chapter, we will provide the overall summary and conclusions of this treatise in Section 6.1. Then several promising topics will be briefly discussed as future research directions in Section 6.2.

6.1 Conclusions

- **Chapter 2:** In Chapter 2, we focused our attention on some key elements in a HetNet, where the topology modelling of macrocells, femtocells and VLC systems was introduced. In Section 2.1, three types of cellular network modelling techniques were introduced, as depicted in Fig. 2.1. More specifically, the Wyner model was invoked in Section 2.1.1, where the cellular network is characterized as a 1-D linear model. It is assumed having a unit gain from each base station to the tagged user and naturally, a lower gain for the users in the two neighbouring cells, as illustrated in Fig. 2.2. This model has been widely used in analysing the both uplink and downlink capacity of cellular networks. In addition to the 1-D linear model, a modified circular array based Wyner model was also introduced as in Fig. 2.3, assuming that the macrocells are arranged along a circle. A specific drawback of the Wyner model is that this model is quite inaccurate in capturing the randomness of MTs, especially for the downlink transmission. In order to cope with this drawback, the grid-based model may be preferred in practical systems, as illustrated in Fig. 2.4. The history of OCI analysis using the grid-based model was presented in Section 2.1.2. The grid-based cellular network may be capable of accurately capturing the randomness of MTs, but it is not easy to charaterize the OCI in a closed form. Most of the literature calculates the OCI by integrating the interference expression relying on a continuous and uniform user density over a circular region approximating a hexagonal cell. Kelif *et al.* proposed the 'Fluid Model' [20, 62, 63]

concept for characterizing the OCI in the downlink of cellular systems, where the discrete BSs of the cellular networking are assumed to form a continuum. The received SIR of a downlink MT is given by Eq. (2.10). The accuracy of the Fluid Model was verified in Fig. 2.7, indicating that it was accurate in characterizing the downlink received SIR. Another modelling approach assumed that the cellular networks were abstracted to a convenient PPP which captures the network properties, as shown in 2.8. We also derived the DL received SIR of the MTs relying on PPP aided cellular network, as seen in Eq. (2.16).

In order to improve the coverage and enhance the capacity of cellular wireless networks, a popular solution is to reduce the cell size and transmission distance, albeit this increases the number of BSs required and hence the cost. Hence, cellular evolution led to the concept of femtocells, as depicted in Fig. 2.9. The briefly history, modelling and technical challenges of femtocells were discussed in Section 2.2. More specifically, the concept and the brief history of femtocells was presented in Section 2.2.1, while their modelling was detailed in Section 2.2.2, where four modelling approaches were introduced. The first approach considered all the channel gains without specifying the precise spatial model of the MBSs. The second approach considered a single femtocell dropped in a single macrocell. These two approaches share the same topology, which was depicted in Fig. 2.10. In the third approach shown in Fig. 2.11, the femtocells were assumed to be randomly placed within the regular grid model based macrocells. We opted for this approach in Chapter 3 of the thesis. In the fourth approach, both the macrocells and femtocells are randomly placed based on the PPP, which is depicted in Fig. 2.12. Then the state-of-the-art in femtocells was elaborated on in Section 2.2.3, including the access control mode, mobility management, self organisation and interference management. One of the most significant challenges associated with the dense deployment of femtocells is the potentially strong interference as illustrated in Fig. 2.14, when the femtocells rely on the co-channel deployment using the same frequency bands as the macrocells. Various techniques have been proposed for mitigating the interference problems, which may be summarized in Fig. 2.15. The key contributions on interference management techniques were summarized in Table. 2.5, Table. 2.6 and Table. 2.7.

Since the Radio Frequency (RF) bandwidth capable of providing a reasonable spatial coverage is a limiting factor, the visible light band of the electro-magnetic spectrum comes to rescue. As illustrated in Fig. 2.16, the available spectrum of visible light is much wider than that of RF. As a result, there has been an increasing interest in VLC systems as one of the promising technologies complementary to the traditional RF systems. We briefly introduced the history and the state-of-the-art of VLC in Section 2.3. A simple VLC architecture is illustrated in Fig. 2.17, where the transmitter consists of a conventional wireless communication system and an additional of optical driver, where the receiver uses photo-detectors in order to convert the optical signal to current. In practice, the transmitter is an LED array, which is mounted on the ceiling of a room, as depicted in Fig. 2.18. In Section 2.3.1, the

state-of-the-art VLC technologies were briefly presented, including the modulation schemes, multiple-carrier techniques, as well as the VLC networking issues. Furthermore, we investigated the challenges in a combined VLC and RF HetNet scenario. The key contributions of VLC techniques were summarized in Table 2.10, Table 2.11 and Table 2.12. We have summarised the major contributions of Chapter 2 in Table 6.1.

Sections	Contributions
Section 2.1	Reviewed the typical macrocell network modelling approaches, including the Wyner model, grid-based model and the PPP based model.
Section 2.2	Introduced femtocells, where the history, network modelling and the technical challenges of femtocells were investigated.
Section 2.3	Introduced the history of VLC systems and the state-of-the-art of VLC technologies.

Table 6.1: Summary of the contributions of Chapter 2

- **Chapter 3:** Chapter 3 is mainly focused on the downlink of a multi-cell OFDMA network, where the femtocells are overlaid onto the static FFR aided macrocells. The inter-tier interference issues were investigated. Furthermore, we studied the optimal choice of parameters in this HetNet scenario. Before we investigated the two-tier HetNet, the review of classical FFR scheme was presented in Section 3.2. In order to cope with the OCI, the FFR scheme, as depicted in Fig. 3.2, is capable of reducing the OCI, hence improving the performance of macrocells. The corresponding performance investigations were provided in Fig. 3.3 and Fig. 3.4. As expected, the simulation results confirmed that the OP of outdoor MTs is significantly reduced, when the FFR scheme is used, instead of the radical UFR development, especially for the CER MTs. Similar observations are valid for the long-term downlink throughput, i.e. the FFR scheme is capable of achieving a better performance.

  Then, the system model of FFR aided two-tier femtocell networks was investigated in Section 3.3, and the topology of the FFR aided HetNet was depicted in Fig. 3.5. Two different spectrum allocation schemes were considered for the femtocells. In FSA, the femtocells reuse the entire available RF frequency bandwidth, whilst, the femtocells reuse the frequency band that was not assigned to the macrocell in the SSA regime, as shown in Fig. 3.6. Firstly, we considered a HetNet scenario, where the femtocells rely on FSA and the system performance of FFR aided two-tier femtocell networks associated with FSA was investigated in Section 3.4. More specifically, the per-tier OP was derived in Section 3.4.1, where the OP of an outdoor macrocell MT was formulated in Lemma 1, while that of an indoor femtocell MT in Lemma 2. Based on the OP equations derived, the long-term spatially averaged macrocell throughput was derived in Eq. (3.25) and Eq. (3.26). Furthermore, the optimal FFR parameter configurations were studied in Section 3.4.3. We considered two design options, namely

an area-proportional design and a QoS-constrained design. The optimization problem was formulated as Problem 1 of Eq. (3.28) and Eq. (3.29) of the area-proportional design, and that of the QoS-constrained design as Problem 2 of Eq. (3.31) and Eq. (3.32). These two problems were then solved by GA. Then, we considered the scenario, where the femtocells rely on SSA and the corresponding system performance of FFR aided two-tier femtocell networks associated with SSA were investigated in Section 3.5. Similarly, the OP of an outdoor macrocell MT and that of an indoor femtocell MT was derived in Lemma 3 and Lemma 4, respectively. Again, the optimal design problems of the FFR aided two-tier network associated with SSA were solved using a GA.

The performance results of FFR aided two-tier femtocell networks were detailed in Section 3.6, where both the femtocell under FSA and that under SSA were discussed. The OP of an outdoor macrocell MT and that of an indoor macrocell MT were provided in Fig. 3.9 and Fig. 3.10, respectively. As expected, the OP of an outdoor macrocell MT is significantly reduced in both the CCR and CER with the aid of the proposed SSA strategy, whilst the OP of an indoor femtocell MT is reduced for the FBS located in the CCR. As it was confirmed in Fig. 3.9 and Fig. 3.10, our theoretical results were accurate for both the FSA and SSA strategies. The optimal system parameters taking into account the averaged number of femtocells per cell are illustrated in Fig. 3.12, Fig. 3.13, Fig. 3.16 and Fig. 3.15. The simulation results of Fig. 3.14 and Fig. 3.17 demonstrated that the GA based optimization process is capable of increasing the ASE. Furthermore, an increased macrocell throughput was achieved by our SSA using a jointly optimized spectrum allocation and distance threshold policy. However, recall from the long-term spatially averaged femtocell throughput simulation results of Fig. 3.18 that the benefit of SSA scheme accrues at the expense of partitioning the spectrum of femtocells. As a result, the femtocell throughput is degraded for the SSA scheme, as evidenced by Fig. 3.18. It is concluded that the SSA may be treated as a spectrally efficient femtocell solution, which remains fairly unaffected by the FFR aided macrocell at the cost of delivering a limited peak throughput. By contrast, the FSA regime may be treated as a throughput-oriented femtocell design, which may be deemed as being selfish due to disregarding macrocell and its own spectrum efficiency. We have summarised the major contributions of Chapter 3 in Table 6.2.

- **Chapter 4:** We shifted our attention from an outdoor HetNet scenario to an indoor HetNet scenario in Chapter 4, where both femtocell and LED light based VLC are used for providing indoor coverage. Since the optical wireless system uses a different frequency band compared to the RF femtocell, there is no interference between the two networks. An important component of the integrated architecture is its RA scheme. Different types of MTs were considered, namely multi-homing MTs and multi-mode MTs. The related RA scheme is investigated in this chapter, where QoS requirements, such as the achievable data rate, the fairness and the statistic delay requirements are considered.

  In Section 4.2, we firstly introduced the system model of VLC using LED lights, where the

Sections	Contributions
Section 3.2	Reviewed the classical FFR scheme. The DL OP and long-term throughput of the FFR aided cellular macrocell were quantified by simulations.
Section 3.3	Introduced the system model of the FFR aided two-tier femtocell network. Both the channel model as well as the FSA and SSA strategies were considered.
Section 3.4	Derived the OP of both outdoor macrocell MTs and indoor femtocell MTs, when the femtocells use the FSA. Furthermore, the long-term spatially averaged throughput of both outdoor macrocell MTs and indoor femtocell MTs were presented.
Section 3.5	Derived the OP of both outdoor macrocell MTs and indoor femtocell MTs, when the femtocells use SSA. Furthermore, the long-term spatially averaged throughput of both outdoor macrocell MTs and indoor femtocell MTs were presented.
Section 3.6	Provided simulation results and the corresponding analysis.

Table 6.2: Summary of the contributions of Chapter 3

2D model of the room was illustrated in Fig. 4.1. More specifically, the link characteristics of VLC were presented in Section 4.2.1, where the optical VLC channel is modelled as a 'two-rate' transmission channel according to the zero LOS blocking and non-zero LOS blocking scenarios. The SCMT scheme of Section. 4.2.2 was assumed in this chapter, where all LED lights in the room operate as a single transmission cell, as depicted in Fig. 4.2. The received SNR and the achievable bit rate of VLC are given by Eq. (4.10) and Eq. (4.12), respectively. The corresponding received SNR and the ASE were simulated in Section 4.2.3. As confirmed in Fig. 4.3 and Fig. 4.4-4.6, all the MTs are adequately covered by the VLC system, when the density of LED lights is higher than 0.04. It is observed that there are nonetheless SNR fluctuations for the indoor edge MTs owing to the reflected rays. It is also observed in Fig. 4.3 that the SNR becomes near-constant, when the number of LED lights is higher enough in our simulations. We further simplified our indoor model as a 2-D model, and the verification was illustrated in Fig. 4.4-4.6. It was observed that the 2-D model is capable of characterizing the ASE of 3-D model.

The indoor HetNet model was described in Section 4.3, where VLC and RF femtocell network are employed for providing downlink coverage, which is illustrated in Fig. 4.7. Again, the channel characteristics of VLC and femtocell were presented. In order to take the delay requirement into account, the average delay-constraint may be converted into an equivalent average rate-constraint using the effective capacity approach. The effective capacity of both the VLC and of the RF femtocell were formulated in Eq. (4.18) and Eq. (4.19), respectively.

The RA problem formulation was presented for both multi-homing MTs and multi-mode

MTs in the indoor HetNet considered in Section 4.4. More specifically, the fairness of the system was evaluated using a proportional fairness approach in Section 4.4.1, while the RA problems of multi-homing MTs and of multi-mode MTs were formulated in Section 4.4.2 and in Section 4.4.3, respectively. We have demonstrated that these problems are concave with respect to both the transmission probability $\boldsymbol{\beta}$ and to the network selection index $\boldsymbol{x}$. Then, we proposed a decentralized RA algorithm in Section 4.5, where the optimization problems were de-composed into several parallel sub-problems and then the original problems were solved by an iteration approach. The process of the decentralized solutions conceived for multi-homing MTs and multi-mode MTs were presented in Table 4.2 and Table 4.3, respectively.

Our numerical performance results characterizing the proposed RA algorithms in the context of the indoor HetNet considered were presented in Section 4.6. More specifically, the convergence behaviour of the proposed decentralized algorithm was investigated in Fig. 4.8. The results demonstrated that the distributed RA algorithm is capable of finding the optimal RA probability for multi-homing MTs as well as the optimal RA probability and network selection for the multi-mode MTs, respectively. It is observed in Fig. 4.8 that the speed of convergence becomes slower, when we increase the number of MTs. The objective function value converges after 60 iterations in our simulations, when the total number of MTs is set to be 20. We also compared the performance of multi-homing MTs to that of the multi-mode MTs for different fairness factors, as depicted in Fig. 4.9, Fig. 4.10 and Fig.4.11. Observe in these figures that the proposed distributed solution is indeed capable of guaranteeing the associated bit-rate requirements. As expected, the multi-homing MTs are capable of achieving a better performance than multi-mode MTs, since multi-homing MTs are capable of accessing multiple networks. Furthermore, it is observed in Fig. 4.9, Fig. 4.10 and Fig. 4.11 that having a higher α results in a higher grade of fairness. In order to evaluate the effects of the statistical delay parameters θ and that of the LOS blocking probability p, the overall effective capacity was studied both in Fig. 4.12 and in Fig. 4.13. It is observed from Fig. 4.12 that the overall effective capacity is reduced upon increasing the delay exponent. However, the system performance remains fairly insensitive to the delay exponent in the range spanning from 10^{-3} to 10^{-1}. As expected, the performance of a VLC system is significantly affected by the LOS blocking probability. When we have $p = 1$, the LOS ray is blocked, hence the MTs may only receive a reduced optical power due to the first reflected ray. In order to satisfy a particular bit rate requirement, the femtocell has to allocate its resources to the rate MTs having a strict rate guarantee, which is achieved at the price of decreasing the overall effective capacity. Hence it is plausible that when the VLC LOS blocking probability is high, the RF femtocell system becomes more reliable.

We have summarised the major contributions of Chapter 4 in Table 6.3.

- **Chapter 5:** In Chapter 5, we extended the investigations of Chapter 4, by considering different transmission strategies for our VLC system. The topology model and four different

Sections	Contributions
Section 4.2	Introduced the system model of VLC using LED lights. The DL received SNR and achievable rate of the ACO-OFDM aided VLC system were evaluated by simulations.
Section 4.3	Described the system model of heterogeneous VLC and RF femtocells. The effective capacity of both the VLC and femtocell network were derived therein.
Section 4.4	Formulated the RA problems, where the diverse QoS requirements formulated in terms of the data rate, fairness and the statistical delay requirements were considered.
Section 4.5	Proposed decentralized sub-optimal RA schemes for both the multi-homing MTs and the multi-mode MTs, where the RA problems were de-composed into several parallel sub-problems.
Section 4.6	Presented the related simulation results and the corresponding analysis.

Table 6.3: Summary of the contributions of Chapter 4

transmission strategies were introduced in Section 5.2, where the SCMT, UFR transmission, CT-2 and FR-2 transmission were presented. More specifically, SCMT was introduced in Section 5.2.2, where all the indoor LED lights operate by illuminating a single attocell, as depicted in Fig. 4.2. In UFR transmission, each LED light form its own attocell, as depicted in Fig. 5.1. In CT-2, the neighbouring two LED lights are merged into a attocell, as depicited in Fig. 5.2. In FR-2 transmission, the optical frequency band of VLC is divided into two frequency band, forming a VLC system having a frequency reuse factor of 2, as depicted in Fig. 5.3.

In Section 5.3, the performance of ACO-OFDM aided VLC was simulated, where we assumed that 10 MTs are randomly distributed, and the VLC system opts for the round robin scheduling scheme. It was illustrated in Fig. 5.4 that SCMT achieves the highest bit rate. However, since only a single MT can be served in one transmission slot, the performance may degrade in a multi-MT scenario. Furthermore, we assumed that 10 MTs were randomly located, and the CDF of the achievable bit rate was illustrated in Fig. 5.6, which shows that FR-2 transmission is capable of achieving the highest bit rate. By contrast, the FR-2 transmission exhibits the lowest bit rate, when the LOS rays are blocked.

In Section 5.4, we formulated the RA problems of the indoor HetNet considered, where both a femtocell and VLC attocells are used under the consideration of different transmission strategies of VLC. The decentralized algorithm in Section 4.5 was used for solving the RA problems. As a further contribution, the effective capacity of the HetNet was evaluated by

simulations in Section 5.5. The effect of the statistical delay exponent θ on the overall effective capacity was demonstrated in Fig. 5.9, Fig. 5.10 and Fig. 5.11, while that of the LOS blocking probability p was demonstrated in Fig. 5.12 and Fig. 5.13. It was observed that the FR-2 transmission is capable of achieving the highest effective capacity for zero LOS blocking probability. Compared to the femtocell, the VLC system achieves a better performance, since the bandwidth available for VLC is much wider than that of the RF femtocell. By contrast, when we consider a non-zero LOS blocking probability, the performance of VLC may be significantly affected by the statistic delay requirement. When the delay requirement is loose, FR-2 aided VLC may still obtain the highest effective capacity, and the effective capacity of VLC is always higher than that of the femtocell. However, when we tighten the delay requirements, observed in Fig. 5.9, Fig. 5.10 and Fig. 5.11 that CT-2 exhibits the highest performance. It is plausible that the FR-2 transmission is capable of achieving the highest effective capacity, when the statistical delay requirements are loose, because FR-2 is capable of mitigating the interference on neighbouring attocells. However, CT-2 transmission attains the best performance, when we tighten the delay requirements. Furthermore, the RF femtocell system becomes more reliable, when the VLC LOS blocking probability is high, because FR-2 exhibit the lowest achievable bit rate when there is a non-zero LOS blocking probability, as demonstrated in Fig. 5.5. We have summarised the major contributions of Chapter 5 in Table 6.4.

Sections	Contributions
Section 5.2	Introduced the topology model of VLC. Four transmission strategies conceived for VLC were introduced and the corresponding received SNR were presented.
Section 5.3	The simulation results of the achievable bit rate of VLC were provided
Section 5.4	Formulated the RA problems of the indoor HetNet considered, which were solved by the proposed decentralized algorithm.
Section 5.5	Presented our simulation results and the corresponding analysis.

Table 6.4: Summary of the contributions of Chapter 5

6.2 Future Research

In this section, we will briefly discuss a number of future research ideas.

6.2.1 Resource Allocation in Two-Tier Cognitive Femtocells with Imperfect Sensing

In the Chapter 3, we considered a two-tier femtocell network, where the system performance was studied. A SSA scheme was proposed for reducing the inter-tier interference. However, the proposed scheme relies on a static solution, and the co-tier interference may be further reduced using the more sophisticated RA scheme, as discussed in [170–172].

Furthermore, cognitive radio (CR) constitutes a promising paradigm proposed for mitigating the spectrum scarcity problem that has emerged as a result of the increased societal need for anytime anywhere connectivity [252–254]. Briefly, CR is a wireless radio device that can adapt to its operating environment with the aid of spectrum sensing. Femtocells readily support the cognitive capabilities, hence inspiring us to incorporate the CR technology into femtocell networks, where the CR-enabled femtocell users may exploit the spectrum-access opportunities not relied upon the licensed systems such as macrocell networks and TV broadcast systems. RA problems of CR aided two-tier network have already been studied in several contributions, however, researchers only considered the perfect sensing scenario [96, 108]. It is worth considering RA problems with imperfect sensing. The trade-off between the sensing duration and the sensing threshold should be investigated.

6.2.2 Resource Allocation in Vector-Transmission Based VLC and RF Femtocell

In the Chapter 5, we compared four transmission strategies conceived for VLC systems. Recently, a sophisticated transmission strategy was proposed in [255], where the idea of Zero-Forcing (ZF) based vectored DL transmission was employed in order to eliminate the ICI using a beamforming matrix. We propose a transmission strategy, where a pair of neighbouring LED lights constitute an attocell and perform ZF transmission, as depicted in Fig. 6.1. For practical reasons, we should only consider the coordination of a pair of neighbouring LED lights at the first stage, since involving more LED lights would increase the complexity of the system.In the resultant vector transmission (VT) regime, the network set $\mathcal{M}$ is defined as $\mathcal{M} = \{1 \cdots m \cdots, M\}$, where $M = \frac{U}{2}$, assuming that the number of LED lights U is even.

This so called VT-2 transmission regime is capable of simultaneously supporting transmissions in a specific frequency band for a maximum of two MTs. For a given served MT pair $\mathcal{P}_n = \{n_1, n_2\}$, the channel gain matrix $\boldsymbol{H}_{m,\mathcal{P}_n}$ representing the transmissions from network m to the MT pair $\mathcal{P}_n$ is denoted as $\boldsymbol{H}_{m,\mathcal{P}_n} = [H_{m_1,n_1}\ H_{m_2,n_1}; H_{m_1,n_2}\ H_{m_2,n_2}]$, where m_1 and m_2 are the pair of LED lights in network m, respectively. Then the resultant virtual cell is characterized by a weight matrix $\boldsymbol{G}_{m,\mathcal{P}_n}$, which eliminates the interference between the MTs in $\mathcal{P}_n$ so that we have $\boldsymbol{H}_{m,\mathcal{P}_n}\boldsymbol{G}_{m,\mathcal{P}_n} = \boldsymbol{I}^{2\times 2}$, where $\boldsymbol{I}$ is the identity matrix. The matrix $\boldsymbol{G}_{m,\mathcal{P}_n}$ can be readily derived by the pseudo-inverse of $\boldsymbol{H}_{m,\mathcal{P}_n}$, which may be written by: $\boldsymbol{G}_{m,\mathcal{P}_n} = \boldsymbol{H}^T_{m,\mathcal{P}_n}\left(\boldsymbol{H}_{m,\mathcal{P}_n}\boldsymbol{H}^T_{m,\mathcal{P}_n}\right)^{-1}$, where $\boldsymbol{H}^T$ denotes the transpose of $\boldsymbol{H}$. Furthermore, a power-sharing matrix $\boldsymbol{\Omega}_{m,\mathcal{P}_n}$ is also defined

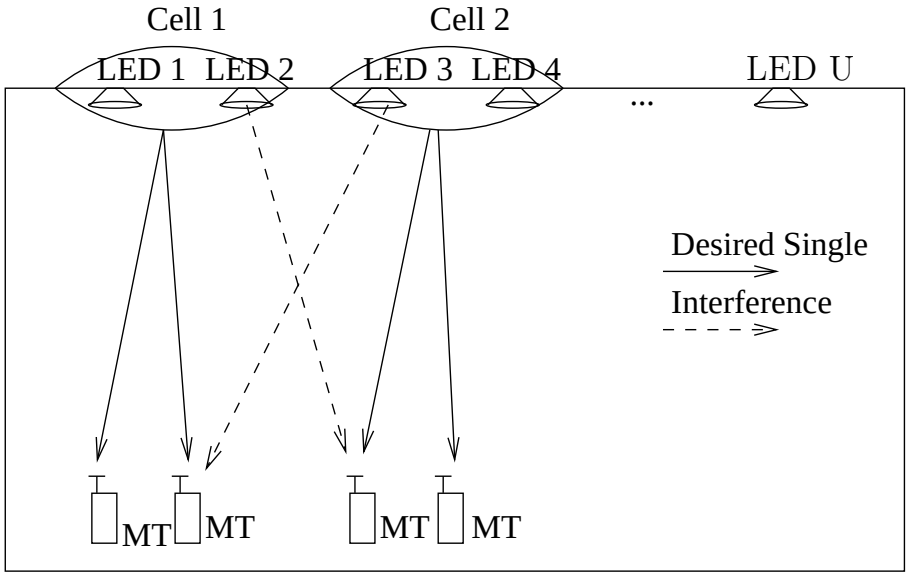

Figure 6.1: The 2D model of the room using the LED light based VLC system, where the VT-2 transmission is assumed.

in order to enforce the per LED power constraint for the sake of maintaining the total original power.

An power allocation solution was proposed in [256], which may be formulated as:

$$\boldsymbol{\Omega}_{m,\mathcal{P}_n} = \omega_{m,\mathcal{P}_n}\boldsymbol{I}, \quad \omega_{m,\mathcal{P}_n} = \min_{\alpha}\left(\frac{1}{\|\boldsymbol{G}_{m,\mathcal{P}_n}(\alpha,:)\|_F}\right), \tag{6.1}$$

where $\boldsymbol{G}_{m,\mathcal{P}_n}(\alpha,:)$ is the αth row of $\boldsymbol{G}_{m,\mathcal{P}_n}$.

If the total number of MTs in the coverage of a virtual cell is higher than two, each cell should carry out a MT pairing process first. In this paper, we propose a two-stage MT pairing algorithm, relying on the *cell association stage* and on an *exhaustive search stage*. In the first stage, each MT measures its the distance to all LED lights and sets up a connection with the LED light at the shortest distance. As a result, this MT is associated with the cell covered by the LED light assigned. After this stage, each cell becomes aware of the identity of the associated MTs. In the second stage, the MTs linked to a specific cell should be sorted into several groups in order to employ VT-2 aided transmission, where each group contains a pair of MTs for transmission. This sorting problem is solved by an exhaustively search in our paper. Assuming that N_m MTs are associated with network m, network m firstly selects two MTs from these N_c MTs as a pair. Then it continues by selecting another two MTs from the remaining (N_c-2) MTs as a pair. Each cell repeats the selection process, until all MTs have been selected and paired. The potential number of MT pairs to be considered by the sorting process $\boldsymbol{\pi}$ equals to $\frac{C_{N_m}^2 C_{N_m-2}^2 \cdots 1}{(\lfloor N_m/2 \rfloor)!}$, where $C_{(\cdot)}^{(\cdot)}$ represents the combination, $\lfloor\cdot\rfloor$ is the floor operation and ! is the factorial operation. After the exhaustive search, each cell chooses the best pairing pattern from all $\boldsymbol{\pi}$ legitimate combinations, namely, the one which provides the highest sum of the achievable bit rates. The corresponding MT pairing algorithm is summarized in Table 6.5.

Table 6.5: MT selection algorithm for VT-2 transmission

Input
The position of MTs and LED lights.
Initialization
Initialize the cell association matrix $\boldsymbol{A} \in \mathbb{R}^{N \times M}$ to be zero matrix
Cell association stage:
For $n \in \mathcal{N}$
MT n find the nearest LED light $u^{\star}$
finds the virtual network $m^{\star}$ containing LED light $u^{\star}$
marks $\boldsymbol{A}(n, m^{\star}) = 1$
End for
Exhaustive search stage:
For $c \in \mathcal{C}$
finds the MTs in its coverage: find $\boldsymbol{A}(:, m) = 1$
determines the number of its serving MTs N_m
lists all possible sorting combination $\boldsymbol{\pi}_m$
For each sorting combination
For each transmission group
derive the sum of the bit rate
End for
records the sum of the bit rate for this sorting combination
End for
finds the best sorting pattern, which achieves the highest rate
End for
Output
The MT groups for all cells

According to the above-mentioned MT selection algorithm, the VLC attocell m may simultaneously serve several groups of MTs. Since the MTs in the same group share the same resources, we may have $\beta_{m,n_1} = \beta_{m,n_2}$, if $\{n_1, n_2\}$ is the MT pair served by the VLC attocell. As a results, the RA problem becomes different from that described by (5.5), (5.6) and (5.7). The resultant RA problem may be formulated as:

$$\textit{Problem 1}: \quad \underset{\boldsymbol{\beta}}{\text{maximize}} \sum_{m\in\mathcal{M}}\sum_{n\in\mathcal{N}} \log\left[\Delta_{m,n}\left(\beta_{m,n}\right)\right] \tag{6.2}$$

$$\text{subject to:} \quad \sum_{n\in\mathcal{N}} \beta_{m,n} \leq 1, \ \forall\, m \in \mathcal{M}, \tag{6.3}$$

$$\beta_{m,n_i} = \beta_{m,n_j}, \ 1 \leq m \leq U/2, \text{if } n_i \text{ and } n_j \text{ are coupled MTs} \tag{6.4}$$

$$0 \leq \beta_{m,n} \leq 1, \tag{6.5}$$

Sophisticated RA schemes should be designed for solving this problem.

6.2.3 Resource Allocation in a Holistic HetNet

In Chapter 3, we considered an outdoor HetNet, where the RF femtocells was overlaid onto macrocells. In Chapter 4 and Chapter 5, an indoor HetNet was considered, where the RA problems were solved for a VLC combined with an RF femtocell scenario. It is interesting to jointly consider both the indoor and outdoor HetNet, forming a holistic HetNet. This topic may involve several technical challenges. For example, the indoor MTs may suffer from the interference imposed by the macrocells, As a result, the RA problem becomes quite different from Chapter 4 and that of Chapter 5. If the femtocells use open access, then it is important to design a resource allocation scheme in order to balance the performance of both the indoor and outdoor MTs, which also constitutes a promising research topic.

Glossary

1-D	One-dimensional
2-D	Two-Dimensinal
3-D	Three-Dimensional
3G	3rd Generation
3GPP	3rd Generation Partnership Project
4G	4th Generation
ACO-OFDM	Asymmetrically Clipped Optical Orthogonal Frequency-Division Multiplexing
ASE	Area Spectrum Efficiency
AWGN	Additive White Gaussian Noise
BER	Bit Error Ratio
BSs	Base Stations
CCR	Cell-Centre Region
CDF	Cumulative Distribution Function
CDMA	Code-Division Multiple-Access
CER	Cell-Edge Region
CIR	Channel Impulse Response
CoMP	Coordinated Multi-Point
CR	cognitive radio
CSG	Closed Subscriber Group
CSK	Colour Shift Keying
CT	Combined Transmission
DCO-OFDM	Direct Current-biased Optical OFDM
DS-CDMA	direct-sequence code-division multiple-access

DSL	Digital Subscriber Line
FBS	Femtocell Base Station
FFR	Fractional Frequency Reuse
FR	Frequency Reuse
FSA	Full Spectrum Access
GA	Genetic Algorithm
HeNBs	Home evolved Node BSs
HetNet	heterogeneous network
ICI	Inter-Cell Interference
ICI	inter-cell interference
IMT-Advanced	International Mobile Telecommunications Advanced
ISI	Inter-Symbol Interference
ITU-R	International Telecommunications Union-Radio
LED	Light Emitting Diodes
LSE	Line Spectrum Efficiency
LTE-A	Long Term Evolution-Advanced
MBSs	Macrocell Base Stations
MCP	Multicell Processing
MCS	Modulation and Coding Schemes
MIMO	Multiple-Input-Multiple-Output
MINLP	mixed-integer non-linear programming
MTs	mobile terminals
NLP	non-linear programming
OCI	Other Cell Interference
OFDMA	Orthogonal Frequency Division Multiple Access
OP	Outage Probability
OWC	Optical Wireless Communications
PAM	Pulse-Amplitude Modulation
PDF	Probability Density Function

PLE	Path Loss Exponent
PPP	Poisson Point Process
QAM	Quadrature Amplitude Modulation
QoS	Quality-of-Service
RA	Resource Allocation
RF	Radio Frequency
RL	Reinforcement Learning
RM	Resource Management
SCMT	Single Cell Multi-point Transmission
SCP	Single-Cell Processing
SIR	Signal to Interference Ratio
SNR	Signal-to-Noise Ratio
SON	Self-Organised Network
SSA	Spectrum Swapping Access
TCSP	Two-Cell-Site Processing
TDMA	Time Division Multiple Access
UFR	Unity Frequency Reuse
UMTS	Universal Mobile Telecommunication System
VLC	Visible Light Communication
WCDMA	Wideband Code Division Multiple Access
Wi-Fi	Wireless Fidelity
WiMAX	Worldwide Interoperability for Microwave Access
WLANs	wireless local area networks

Bibliography

[1] Cisco, "Cisco visual networking index: global mobile data traffic forecast update, 2010-2015," , 2011.

[2] L. Hanzo, H. Haas, S. Imre, D. O'Brien, M. Rupp, and L. Gyongyosi, "Wireless myths, realities, and futures: from 3G/4G to optical and quantum wireless," *Proceedings of the IEEE*, vol. 100, pp. 1853–1888, May 2012.

[3] L. Hanzo, "Bandwidth-efficient wireless multimedia communications," *Proceedings of IEEE*, vol. 86, pp. 1342–1382, July 1998.

[4] C. E. Shannon, "A mathematical theory of communication," *The Bell System Technical Journal*, vol. 27, pp. 623–656, October 1948.

[5] H. S. Dhillon, R. K. Ganti, and J. G. Andrews, "A tractable framework for coverage and outgae in heterogeneous cellular networks," in *Proceedings of 2011 Information Theory and Applications Workshop*, (La Jolla, USA), pp. 1–6, February 2011.

[6] Qualcomm, "LTE advanced: heterogeneous networks," *White Papers*, pp. 1–15, January 2011.

[7] R. Zhang, J. Wang, Z. Wang, Z. Xu, C. Zhao, and L. Hanzo, "Visible light communications in heterogeneous networks: paving the way for user-centric design," *IEEE Wireless Communications*, pp. 1–10, April 2015.

[8] M. Peng, C. Wang, J. Li, H. Xiang, and V. Lau, "Recent advances in underlay heterogeneous networks: interference control, resource allocation, and self-organization," *IEEE Communications Surveys & Tutorials*, vol. pp, pp. 1–31, March 2015.

[9] A. Ahmed, L. M. Boulahia, and D. Gaiti, "Enabling vertical handover decisions in heterogeneous wireless networks: a state-of-the-art and a classification," *IEEE Communications Surveys & Tutorials*, vol. 16, pp. 776–811, Second Quarter 2014.

[10] Y. L. Lee, T. C. Chuah, J. Loo, and A. Vinel, "Recent advances in radio resource management for heterogeneous LTE/LTE-A networks," *IEEE Communications Surveys & Tutorials*, vol. 16, pp. 2142–2180, Fourth Quarter 2014.

[11] L. Wang and G.-S. Kuo, "Mathematical modeling for network selection in heterogeneous wireless networks - a tutorial," *IEEE Communications Surveys & Tutorials*, vol. 15, pp. 271–292, First Quarter 2013.

[12] A. Goldsmith, *Wireless Communications*. Cambridge University Press, 2005.

[13] L. Tassiulasa and A. Ephremides, "Dynamic sever allocation to parallel queues with randomly varying connectivity," *IEEE Transactions on Information Theory*, vol. 39, March 1999.

[14] D. Wu and R. Neigi, "Effective capacity: a wireless link model for support of quality in multiuser OFDM systems," *IEEE Transactions on Wireless Communications*, vol. 2, July 2003.

[15] M. Tao, Y. Liang, and F. Zhang, "Resource allocation for delay differentiated traffic in multiuser OFDM systems," *IEEE Transactions on Wireless Communications*, vol. 7, June 2008.

[16] D. S. W. Hui, V. K. N. Lau, and H. L. Wong, "Cross-layer design for OFDMA wireless systems with heterogeneous delay requirements," *IEEE Transactions on Wireless Communications*, vol. 6, August 2007.

[17] J. Tang and X.Zhang, "Cross-layer resource allocation over wireless relay networks for quality of service provisioning," *IEEE Journal on Selected Areas in Communications*, vol. 25, May 2007.

[18] Y. Cui, V. K. N. Lau, R. Wang, H. Huang, and S. Zhang, "A survey on delay-aware resource control for wireless systems-large deviation theory, stochastic Lyapunov drift and distributed stochastic learning," *IEEE Transactions on Information Theory*, vol. 58, March 2012.

[19] N. McKeown, A. Mekkittikul, V. Anantharam, and J. Walrand, "Achieving 100 percent throughput in an input-queued switch," *IEEE Transactions on Communications*, vol. 47, August 1999.

[20] J. Kelif, M. Coupechoux, and P. Godlewski, "Spatial outage probability for cellular networks," in *IEEE Global Telecommunications Conference (GLOBECOM 07)*, (Washington, USA), pp. 4445–4450, November 2007.

[21] D. Bertsekas and R. Gallager, *Data Networks*. Prentice Hall, 1987.

[22] M. Chiang, S. H. Low, and A. R. Calderbank, "Layering as optimization decomposition: A mathematical theory of network architectures," *Proceedings of the IEEE*, vol. 95, March 2007.

[23] T. K. Sarkar, Z. Ji, K. Kim, A. Medouri, and M. Salazar-Palma, "A survey of various propagation models for mobile communication," *IEEE Transactions on Antennas and Propagation Magazine*, vol. 45, pp. 51–82, June 2003.

[24] C. L. Tsai and Z. Xu, "Line-of-sight visible light communications with InGaN-Based resonant cavity LEDs," *IEEE Photonics Technology Letters*, vol. 25, pp. 1793–1796, September 2013.

[25] M. D. Renzo, A. Guidotti, and G. E. Corazza, "Average rate of downlink heterogeneous cellular networks over generalized fading channels: a stochastic geometry approach," *IEEE Transactions on Communications*, vol. 61, pp. 3050–3071, July 2013.

[26] A. Wyner, "Shannon-theoretic approach to a Gaussian cellular multiple-access channel," *IEEE Transactions on Information Theory*, vol. 6, pp. 1713–1727, November 1994.

[27] J. G. Andrews, F. Baccelli, and R. K. Ganti, "A tractable approach to coverage and rate in cellular networks," *IEEE Transactions on Communications*, vol. 59, pp. 3122–3134, November 2011.

[28] O. Somekh and S. Shamai, "Shannon-theoretic considerations for a Gaussian cellular TDMA multiple-access channel with fading," in *8th IEEE International Symposium on Personal, Indoor and Mobile Radio Communications*, (Helsinki, Finland), pp. 276–280, September 1997.

[29] O. Somekh and S. Shamai, "Shannon-theoretic approach to a Gaussian cellular multiple-access channel with fading," *IEEE Transactions on Information Theory*, vol. 46, pp. 1713–1727, July 2000.

[30] S. Shamai and A. Wyner, "Information-Theoretic considerations for symmetric, cellular, multiple-access fading channels—Part I," *IEEE Transactions on Information Theory*, vol. 43, pp. 1877–1894, November 1997.

[31] S. Shamai and A. Wyner, "Information-Theoretic considerations for symmetric, cellular, multiple-access fading channels—Part II," *IEEE Transactions on Information Theory*, vol. 43, pp. 1895–1911, November 1997.

[32] B. M. Zaidel, S. Shamai, and S. Verdu, "Multicell uplink spectral efficiency of coded DS-CDMA with random signatures," *IEEE Journal on Selected Areas in Communications*, vol. 19, pp. 1556–1569, August 2001.

[33] B. M. Zaidel, S. Shamai, and S. Verdu, "Multicell uplink spectral efficiency of coded DS-CDMA in Rayleigh fading channels," in *6th International Symposium on Communication Techniques and Applications*, (Ambleside, UK), pp. 499–504, July 2001.

[34] D.Aktas, M. N. Bacha, J. S. Evans, and S. V. Hanly, "Scaling results on the sum capacity of cellular networks with MIMO links," *IEEE Transactions on Information Theory*, vol. 52, pp. 1165–1175, July 2006.

[35] D. Kaltakis, M. A. Imran, and C. Tzaras, "Information theoretic capacity of cellular multiple access channel with shadow fading," *IEEE Transactions on Communications*, vol. 58, pp. 1468–1476, May 2010.

[36] S. Shamai and B. M. Zaidel, "Enhancing the cellular downlink capacity via co-processing at the transmitting end," in *Proceedings of IEEE 53rd Vehicular Technology Conference (VTC 2001 Spring)*, (Rhodes, Greece), pp. 1745–1749, May 2001.

[37] O. Somekh, B. M. Zaidel, and S.Shamai, "Sum rate characterization of joint multiple cell-site processing," *IEEE Transactions on Information Theory*, vol. 53, pp. 4473–4497, December 2007.

[38] O. Somekh, O. Simeone, Y. Bar-Ness, and A. M. Haimovich, "Distributed multi-cell Zero-Forcing beamforming in cellular downlink channels," in *IEEE Global Telecommunications Conference*, (San Francisco, USA), pp. 1–6, November 2006.

[39] O. Simeone, O. Somekh, Y. Bar-Ness, and U. Spagnolini, "Throughput of low-power cellular systems with collaborative base stations and relaying," *IEEE Transactions on Information Theory*, vol. 54, pp. 459–467, January 2008.

[40] O. Simeone, O. Somekh, H. V. Poor, and S.Shamai, "Local base station cooperation via finite-capacity links for the uplink of linear cellular networks," *IEEE Transactions on Information Theory*, vol. 55, pp. 190–204, January 2008.

[41] N. Levy and S.Shamai, "Clustered local decoding for Wyner-Type cellular models," *IEEE Transactions on Information Theory*, vol. 55, pp. 4967–4985, November 2009.

[42] J. Xu, J. Zhang, and J. G. Andrews, "On the accuracy of the Wyner model in cellular networks," *IEEE Transactions on Wireless Communications*, vol. 10, pp. 3098–3109, Sepetmber 2011.

[43] M. Hata, "Empirical formula for propagation loss in land mobile radio services," *IEEE Transactions on Vehicular Technology*, vol. 29, pp. 317–325, August 1980.

[44] J. B. Andersen, T. S. Rappaport, and S. Yoshida, "Propagation measurements and models for wireless communications channels," *IEEE Transactions on Communications Magazine*, vol. 33, pp. 42–49, January 1995.

[45] J. S. Evans and D. Everitt, "On the teletraffic capacity of CDMA cellular networks," *IEEE Transactions on Vehicular Technology*, vol. 48, pp. 153–165, January 1999.

[46] G. Jeney, "Practical limits of femtocells in a realistic environment," in *Proceedings of IEEE 73rd Vehicular Technology Conference (VTC Spring)*, (Yokohama, Japan), pp. 1–5, May 2011.

[47] Cost Action 231, "Digital mobile radio towards future generation systems: final report," in *European commission*, (Brussels, Belgium), 1999.

[48] G. R. Cooper and R. W. Nettleton, "A spread-spectrum technique for high-capacity mobile communications," *IEEE Transactions on Vehicular Technology*, vol. 27, pp. 264–275, November 1978.

[49] C. C. Chan and S. V. Hanly, "The capacity improvement of an integrated successive decoding and power control scheme," in *Proceedings of International Conference on Universal Personal Communications*, (San Diego, USA), pp. 800–804, October 1997.

[50] K. S. Gilhousen, I. M. Jacobs, R. Padovani, A. J. Viterbi, L. A. Weaver, and C. E. Wheatley, "On the capacity of a cellular CDMA system," *IEEE Transactions on Vehicular Technology*, vol. 40, pp. 303–312, May 1991.

[51] S. Elayoubi, T. Chahed, and G. Hébuterne, "On the capacity of multi-cell UMTS," in *IEEE Global Telecommunications Conference (GLOBECOM 03)*, (San Francisco, USA), pp. 487–491, December 2003.

[52] D. Staehle, K. Leibnitz, K. Heck, B. Schroder, A. Weller, and P. Tran-Gia, "Approximating the othercell interference distribution in inhomogeneous UMTS networks," in *Proceedings of IEEE Vehicular Technology Conference (VTC 2002-Spring)*, (Birmingham, USA), pp. 1640–1644, May 2002.

[53] T. Liu and D. Everitt, "Other-cell interference characterization in the UMTS systems with shadowing effect," in *Proceedings of 12th European Wireless Conference (European Wireless 2006)*, (Athens, Greece), pp. 1–6, April 2006.

[54] T. Liu and D. Everitt, "Analytical approximation of other-cell interference in the uplink of CDMA cellular systems," in *Proceedings of IEEE Vehicular Technology Conference (VTC 2006-Spring)*, (Melbourne, Australia), pp. 693–697, May 2006.

[55] C. Ho, J. A. Copeland, C. Lea, and G. L. Stüber, "On call admission control in DS/CDMA cellular networks," *IEEE Transactions on Vehicular Technology*, vol. 50, pp. 1328–1343, November 2001.

[56] A. J. Viterbi, A. M. Viterbi, and E. Zehavi, "Other cell interference in cellular power controlled CDMA," *IEEE Transactions on Communications*, vol. 42, pp. 1501–1504, February/March/April 1994.

[57] S. S. Kolahi, A. G. Williamson, and K. W. Sowerby, "Other-cell interference in CDMA systems," *IET Electronics Letters*, vol. 40, pp. 1134–1135, October 2004.

[58] Y. H. Chew, J. Tham, and B. S. Yeo, "Cell capacity of CDMA networks taking the effect of mobile locations into consideration," in *Proceedings of IEEE Vehicular Technology Conference (VTC 2006-Spring)*, (Melbourne, Australia), pp. 976–980, May 2006.

[59] Y. Tokgoz and B. D. Rao, "Performance analysis of maximum ratio transmission based multi-cellular MIMO systems," *IEEE Transactions on Wireless Communications*, vol. 5, pp. 83–89, January 2006.

[60] S. H. Kim, B. C. Jung, and D. K. Sung, "Effect of other-cell interference on multiuser diversity in cellular networks," in *Proceedings of International Symposium on Communications and Information Technologies (ISCIT '07)*, (Sydney, Australia), pp. 521–525, October 2007.

[61] S. Moon, S. Lee, and I. Lee, "Sum-rate capacity of random beamforming for multi-anenna broadcast channels with other cell interference," *IEEE Transactions on Wireless Communications*, vol. 10, pp. 2440–2444, August 2011.

[62] J. Kelif, M. Coupechoux, and P. Godlewski, "A fluid model for performance analysis in cellular networks," *EURASIP Journal on Wireless Communications and Networking*, vol. 2010, pp. 1–11, August 2010.

[63] J. Kelif, M. Coupechoux, and P. Godlewski, "Spatial outage probability formula for CDMA networks," in *Proceedings of IEEE Vehicular Technology Conference (VTC 07 Fall)*, (Baltimore, USA), pp. 101–105, September 2007.

[64] J. Kelif, M. Coupechoux, and P. Godlewski, "Fluid model of the outage probability in sectored wireless networks," in *Proceedings of IEEE Wireless Communications and Networking Conference (WCNC 08)*, (Las Vegas, USA), pp. 2933–2938, March-April 2008.

[65] J. Kelif, M. Coupechoux, and P. Godlewski, "Effect of shadowing on outage probability in fluid cellular radio networks," in *Proceedings of International Symposium on Modeling and Optimization in Mobile, Ad Hoc, and Wireless Networks and Workshops (WiOPT 2008)*, (Berlin, Germany), pp. 141–150, April 2008.

[66] J. Kelif and M. Coupechoux, "Impact of topology and shadowing on the outage probability of cellular networks," in *Proceedings of IEEE International Conference on Communications (ICC 2009)*, (Dresden, Germany), pp. 1–6, June 2009.

[67] H. ElSawy, E. Hossain, and M. Haenggi, "Stochastic geometry for modeling, analysis, and design of multi-tier and cognitive cellular wireless networks: a survey," *IEEE Communications Surveys & Tutorials*, vol. 15, pp. 996–1019, Third Quarter 2013.

[68] F. Baccelli, M. Klein, M. Lebourges, and S. Zuyev, "Stochastic geometry and architecture of communication networks," *Journal on Telecommunication Systems*, vol. 7, pp. 209–227, January 1997.

[69] T. X. Brown, "Cellular performance bounds via shotgun cellular systems," *IEEE Journal on Selected Areas Communications*, vol. 18, pp. 2443–2455, November 2000.

[70] A. Guo and M. Haenggi, "Spatial stochastic models and metrics for the structure of base stations in cellular networks," *IEEE Transactions on Wireless Communications*, vol. 12, pp. 5800–5812, November 2013.

[71] C.-H. Lee, C.-Y. Shih, and Y.-S. Chen, "Stochastic geometry based models for modeling cellular networks in urban areas," *Springer Wireless Networks*, vol. 19, pp. 1063–1072, October 2012.

[72] T. T. Vu, L. Decreusefond, and P. Martins, "An analytical model for evaluating outage and handover probability of cellular wireless networks," in *International Symposium on Wireless Personal Multimedia Communications (WPMC 2012)*, (Taipei, China), pp. 643–647, September 2012.

[73] S. Lee and K. Huang, "Coverage and economy of cellular networks with many base stations," *IEEE Communication Letters*, vol. 16, pp. 1038–1040, July 2012.

[74] S. M. Yu and S.-L. Kim, "Downlink capacity and base station density in cellular networks," in *International Symposium on Modeling, Optimization in Mobile, Ad Hoc & Wireless Networks (WiOpt 2013)*, (Tsukuba, Japan), pp. 119–124, May 2013.

[75] S. Akoum and R. W. Heath, "Multi-cell coordination: A stochastic geometry approach," in *IEEE International Workshop on Signal Processing Advances in Wireless Communications (SPAWC 2012)*, (Cesme, Turkey), pp. 16–20, Jun 2012.

[76] S. Akoum and R. W. Heath, "Interference coordination: random clustering and adaptive limited feedback," *IEEE Transactions on Signal Processing*, vol. 61, pp. 1822–1834, April 2013.

[77] M. D. Renzo and P. Guan, "A mathematical framework to the computation of the error probability of downlink MIMO cellular networks by using stochastic geometry," *IEEE Transactions on Communications*, vol. 62, pp. 2860–2879, August 2013.

[78] T. D. Novlan, H. S. Dhillon, and J. G. Andrews, "Analytical modeling of uplink cellular networks," *IEEE Transactions on Wireless Communications*, vol. 12, pp. 2669–2679, May 2013.

[79] D. Stoyan, W. Kendall, and J. Mecke, *Stochastic Geometry and Its Applications, 2nd Edition*. John Wiley and Sons, 1996.

[80] J. G. Andrews, H. Claussen, M. Dohler, S. Rangan, and M. C. Reed, "Femtocell: Past, Present, and Future," *IEEE Journal on Selected Areas in Communications*, vol. 30, pp. 497–508, April 2012.

[81] V. Chandrasekhar, J. G. Andrews, and A. Gatherer, "Femtocell networks: a survey," *IEEE Communications Magazine*, vol. 46, pp. 59–67, September 2008.

[82] H. Claussen, L. T. W. Ho, and L. G. Samuel, "An overview of the femtocell concept," *Bell Labs Technical Journal*, vol. 13, pp. 221–245, May 2008.

[83] T. Zahir, K. Arshad, A. Nakata, and K. Moessner, "Interference management in femtocells," *IEEE Communications surveys & Tutorials*, vol. 15, pp. 293–311, First Quarter 2013.

[84] R. Zhang and L. Hanzo, "Wireless Cellular Networks," *IEEE Vehicular Technology Magazine*, vol. 5, pp. 31–39, December 2010.

[85] R. Brickhouse and T. Rappaport, "Urban in-building cellular frequency reuse," in *IEEE Global Telecommunications Conference*, (London, UK), pp. 1192–1196, November 1996.

[86] D. Chambers, "Femtocell history."

[87] L. Wang, Y. Zhang, and Z. Wei, "Mobility management schemes at radio network layer for LTE femtocells," in *IEEE 69th Vehicular Technology Conference (VTC Spring 2009)*, (Barcelona, Spain), pp. 1–5, April 2009.

[88] N. Saquib, E. Hossain, L. B. Le, and D. I. Kim, "Interference management in OFDMA femtocell networks: issue and approaches," *IEEE Wireless Communications*, vol. 19, pp. 86–95, July 2012.

[89] "Small cell forum," *www.smallcellforum.org*.

[90] Y. Jeong, H. Shin, and M. Win, "Superanalysis of optimum combining with application to femtocell networks," *IEEE Journal on Selected Areas in Communications*, vol. 30, pp. 509–524, April 2012.

[91] S.-Y. Yun, Y. Yi, D.-H. Cho, and J. Mo, "The economic effects of sharing of femtocells," *IEEE Journal on Selected Areas in Communications*, vol. 30, pp. 595–606, April 2012.

[92] Q. Zhang, X. Zhu, L. Wu, and K. Sandrasegaran, "A coloring-based resource allocation for OFDMA femtocell networks," in *IEEE Wirelss Communications and Networking Conference (WCNC 2013)*, (Shanghai, China), pp. 673–678, April 2013.

[93] D. Lopez-Perez, X. Chu, A. V. Vasilakos, and H. Claussen, "Power minimization based resource allocation for interference mitigation in OFDMA femtocell networks," *IEEE Journal on Selected Areas in Communications*, vol. 32, pp. 333–344, February. 2014.

[94] P. Xia, V. Chandrasekhar, and J. G. Andrews, "Open vs. closed access femtocells in the uplink," *IEEE Transactions on Wireless Communications*, vol. 9, pp. 3798–3809, December 2010.

[95] X. Kang, R. Zhang, and M. Motani, "Price-based resource allocation for spectrum-sharing femtocell networks: A stackelberg game approach," *IEEE Journal on Selected Areas in Communications*, vol. 30, pp. 538–549, April 2012.

[96] R. Urgaonkar and M. J. Neely, "Opportunistic cooperation in cognitive femtocell networks," *IEEE Journal on Selected Areas in Communications*, vol. 30, pp. 607–616, April 2012.

[97] J. Zhang and J. G. Andrews, "Distributed antenna systems with randomness," *IEEE Transactions on Wireless Communications*, vol. 7, pp. 36–46, September 2008.

[98] V. Chandrasekhar and J. G. Andrews, "Uplink capacity and interference avoidance for two-tier femtocell networks," *IEEE Transactions on Wireless Communications*, vol. 8, pp. 3498–3509, July 2009.

[99] F. Pantisano, M. Bennis, W. Saad, and M. Debbah, "Spectrum leasing as an incentive towards uplink macrocell and femtocell cooperation," *IEEE Journal on Selected Areas in Communications*, vol. 30, pp. 617–630, April 2012.

[100] L. Saker, S. E. Elayoubi, R. Combes, and T. Chahed, "Optimal control of wake up mechanisms of femtocells in heterogeneous networks," *IEEE Journal on Selected Areas in Communications*, vol. 30, pp. 664–672, April 2012.

[101] F. Jin, R. Zhang, and L. Hanzo, "Frequency-swapping aided femtocells in twin-layer cellular networks relying on fractional frequency reuse," in *Proc. IEEE Wirless Communications and Networking Conference*, (Paris, France), pp. 3097–3101, April 2012.

[102] F. Jin, R. Zhang, and L. Hanzo, "Fractional frequency reuse aided twin-layer femtocell networks: analysis, design and optimization," *IEEE Transactions on Wireless Communications*, vol. 61, pp. 2074–2085, May 2013.

[103] J. Zhang, F. Jin, R. Zhang, G. Li, and L. Hanzo, "Analysis and design of distributed antenna-aided twin-layer femto- and macrocell networks relying on fractional frequency reuse," *IEEE Transactions on Vehicular Technology*, vol. 63, pp. 763–774, February 2014.

[104] H. S. Dhillon, R. K. Ganti, F. Baccelli, and J. G. Andrews, "Modeling and Analysis of K-Tier downlink heterogeneous cellular networks," *IEEE Journal on Selected Areas in Communications*, vol. 30, pp. 550–560, April 2012.

[105] S. Mukherjee, "Distribution of downlink SINR in heterogeneous cellular networks," *IEEE Journal on Selected Areas in Communications*, vol. 30, pp. 575–585, April 2012.

[106] W. C. Cheung, T. Q. S. Quek, and M. Kountouris, "Throughput optimization, spectrum allocation, and access control in two-tier femtocell networks," *IEEE Journal on Selected Areas in Communications*, vol. 30, pp. 561–574, April 2012.

[107] Y. Zhong and W. Zhang, "Multi-channel hybrid access femtocells: a stochastic geometric analysis," *IEEE Transactions on Communications*, vol. 61, pp. 3016–3026, July 2013.

[108] C.-H. Lee and C.-Y. Shih, "Coverage analysis of cognitive femtocell networks," *IEEE Wireless Communications Letters*, vol. 3, pp. 177–180, April 2014.

[109] D. Lopez-Perez, A. Valcarce, G. de la Roche, E. Liu, and J. Zhang, "Access methods to WiMAX femtocells: a downlink system-level case study," in *IEEE Singapore International Conference on Communication Systems (ICCS 2008)*, (Guangzhou, China), pp. 1657–1662, April 2008.

[110] D. Choi, P. Monajemi, S. Kang, and J. Villasenor, "Dealing with loud neighbors: the benefits and tradoffs of adaptive femtocell access," in *IEEE Global Telecommunications Conference (GLOBECOM 2008)*, (New Orleans, USA), pp. 1–5, December 2008.

[111] A. Valcarce, D. Lopez-Perez, G. de la Roche, and J. Zhang, "Limited access to OFDMA femtocells," in *IEEE International Symposium on Personal, Indoor and Mobile Radio Communications*, (Tokyo, Japan), pp. 1–5, September 2009.

[112] H.-S. Jo, P. Xia, and J. G. Andrews, "Open, closed, and shared access femtocells in the downlink," *EURASIP Journal on Wireless Communications and Networking*, vol. 2012, pp. 1–16, December 2012.

[113] A. Golaup, M. Mustapha, and L. B. Patanapongipibul, "Femtocell access control strategy in UMTS and LTE," *IEEE Communications Magazine*, vol. 2009, pp. 117–123, September 2009.

[114] G. de la Roche, A. Valcarce, and D. Lopez-Perez, "Access control mechanisms for femtocells," *IEEE Communications Magazine*, vol. 2010, pp. 33–39, January 2010.

[115] J. Moon and D. Cho, "Novel handoff decision algorithm in hierarchical macro/femto-cell networks," *IEEE Communications Magazine Letter*, vol. 13, pp. 755–757, October 2009.

[116] D. Lopez-Perez, A. Ladanyi, A. Juttner, and J. Zhang, "OFDMA femtocells: intracell handover for interference and handover mitigation in two-tier networks," in *IEEE Wireless Communications and Networking Conference (WCNC 2010)*, (Sydney, Australia), pp. 1–6, April 2010.

[117] Z. Becvar and P. Mach, "Adaptive hysteresis margin for handover in femtocell networks," in *IEEE 6th International Conference on Wireless and Mobile Communications (ICWMC 2010)*, (Valencia, Spain), pp. 256–261, September 2010.

[118] A. Ulvan, R. Bestak, and M. Ulvan, "The study of handover procedure in LTE-based femtocell networks," in *IEEE Third Joint IFIP Wireless and Mobile Networking Conference (WMNC 2010)*, (Budapest, Hungary), pp. 1–6, October 2010.

[119] S. Wu and S. Lo, "Handover scheme in LTE-based networks with hybrid access mode femtocells," *Journal of Convergence Information Technology*, vol. 6, pp. 68–78, July 2011.

[120] B. Jeong, S. Shin, I. Jang, N. W. Sung, and H. Yoon, "A smart handover decision algorithm using location prediction for hierarchical macro/femto-cell networks," in *IEEE Vehicular Technology Conference (VTC Fall 2011)*, (San Francisco, USA), pp. 1–5, September 2011.

[121] H. Zhang, W. Ma, W. Li, Z. W, X. Wen, and C. Jiang, "Signalling cost evaluation of handover management schemes in LTE-Advanced femtocell," in *IEEE Vehicular Technology Conference (VTC Spring 2011)*, (Yokohama, Japan), pp. 1–5, May 2011.

[122] S. Wu, R. Zheng, Z. Yin, Y. Fang, and D. Yang, "Handover study concerning mobility in the two-hierarchy network," in *IEEE Vehicular Technology Conference (VTC Spring 2009)*, (Barcelona, Spain), pp. 1–5, April 2009.

[123] H. Zhang, X. Wen, B. Wang, W. Zheng, and Y. Sun, "A novel handover mechanism between femtocell and macrocell for LTE based networks," in *IEEE 2nd International Conference on Commnucation Software and Networks (ICCSN 2010)*, (Singapore), pp. 228–231, February 2010.

[124] D. Xenakis, N. Passas, L. Merakos, and C. Verikoukis, "Mobility management for femtocells in LTE-Advanced: key aspects and survey of handover decision algorithms," *IEEE Communications Surveys & Tutorials*, vol. 16, pp. 64–91, First Quarter 2014.

[125] H. Claussen, L. T. W. Ho, and L. G. Samuel, "Self-optimization of coverage for femtocell deployments," in *Wireless Telecommunications Symposium (WTS 2008)*, (Pomona, USA), pp. 278–285, April 2008.

[126] D. Lopez-Perez, A. Ladanyi, A. Juttner, and J. Zhang, "OFDMA femtocells: a self-organizing approach for frequency assignment," in *IEEE 20th International Symposium on Personal, Indoor and Mobile Radio Communications*, (Tokyo, Japan), pp. 2202–2207, September 2009.

[127] Y. J. Sang, H. G. Hwang, and K. S. Kim, "A self-organized femtocell for IEEE 802.16e system," in *IEEE Global Telecommunications Conference (GLOBECOM 2009)*, (Honolulu, USA), pp. 1–5, December 2009.

[128] F. Bernardo, R. Agusti, J. Cordero, and C. Crespo, "Self-optimization of spectrum assignment and transmission power in OFDMA femtocells," in *Sixth Advanced International Conference on Telecommunications (AICT 2010)*, (Barcelona, Spain), pp. 404–409, May 2010.

[129] L. G. U. Garcia, I. Z. Kovacs, K. Pedersen, G. W. O. Costa, and P. Mogensen, "Autonomous component carrier selection for 4G femtocells- a fresh look at an old problem," *IEEE Journal on Selected Areas in Communications*, vol. 30, pp. 525–537, April 2012.

[130] J. Liu, T. Kou, H. Sherali, and Q. Chen, "Femtocell base station deployment in commercial buildings: a global optimization approach," *IEEE Journal on Selected Areas in Communications*, vol. 30, pp. 652–663, April 2012.

[131] Y.-Y. Li, M. Macuha, E. Sousa, T. Sato, and M. Nanri, "Cognitive interference management in 3G femtocells," in *IEEE 20th International Symposium on Personal, Indoor and Mobile Radio Communications (PIMRC 2009)*, (Tokyo, Japan), pp. 1118–1122, September 2009.

[132] A. Adhikary, V. Ntranos, and G. Caire, "Cognitive femtocells: Breaking the spatial reuse barrier of cellular systems," in *Information Theory and Applications Workshop (ITA 2011)*, (La Jolla, USA), pp. 1–10, February 2011.

[133] J. Zhang and G. de la Roche, *Femtocell: Technologies and deployment*. John Wiley-IEEE Press, 2010.

[134] V. Chandrasekhar, M. Kountouris, and J. G. Andrews, "Coverage in multi-antenna two-tier networks," *IEEE Transactions on Wireless Communications*, vol. 8, pp. 5314–5327, October 2009.

[135] T. Alade, H. Zhu, and J. Wang, "Uplink co-channel interference analysis and cancellation in femtocell based distributed antenna system," in *IEEE International Conference on Communications (ICC 2010)*, (Cape Town, South Africa), pp. 1–5, May 2010.

[136] D. Hu and S. Mao, "Multicast in femtocell networks: a successive interference cancellation approach," in *IEEE Global Telecommunications Conference (GLOBALCOM 2011)*, (Houston, USA), pp. 1–6, December 2011.

[137] B. Kaufman, E. Erkip, J. Lilleberg, and B. Aazhang, "Femtocells in cellular radio networks with successive interference cancellation," in *IEEE International Conference on Communications Workshop (ICC 2011)*, (Kyoto, Japan), pp. 1–5, June 2011.

[138] M. Ndong and T. Fujii, "Interference cancellation for spectrum shared femtocell networks with macrocell information feedback," in *IEEE Third International Conference on Ubiquitous and Future Networks (ICUFN 2011)*, (Dalian, China), pp. 224–229, June 2011.

[139] T. Villa, R. Merz, and R. Knopp, "Interference management in femtocell networks with hybrid-ARQ and interference cancellation," in *Conference Record of the Forty Fifth Asilomar Conference on Signals Systems and Computers (ACSSC 2011)*, (Pacific Grove, USA), pp. 1358–1362, November 2011.

[140] C. Xu and J. Wang, "Uplink receiver algorithm of femtocell against interference," in *8th International Conference on Wireless Communications, Networking and Mobile Computing (WiCOM 2012)*, (Shanghai, China), pp. 1–5, September 2012.

[141] Y. Li, S. Chen, J. Li, and M. Peng, "Multiuser MISO beamforming and interference cancellation in two-tier femtocell networks," in *IEEE Global Telecommunications Conference (GLOBALCOM 2013)*, (Atlanta, USA), pp. 736–741, December 2013.

[142] B. Branco, F. Ganhao, L. Irio, L. Bernardo, R. Dinis, R. Oliveira, P. Amaral, and P. Pinto, "SC-FDE femtocell energy saving using IB-DFE interference cancellation techniques," in *21st International Conference on Telecommunications (ICT 2014)*, (Lisbon, Portugal), pp. 328–332, May 2014.

[143] H. A. Ghani, M. K. Gurcan, and Z. He, "Two-group resource allocation with channel ordering and interference cancellation," in *IEEE Wirelss Communications and Networking Conference (WCNC 2010)*, (Sydney, Australia), pp. 1–6, April 2010.

[144] H. Claussen, "Performance of macro- and co-channel femtocells in a hierarchical cell structure," in *IEEE International Symposium on Personal, Indoor and Mobile Radio Communications (PIMR 2007)*, (Athens, UK), pp. 1–5, September 2007.

[145] M. Morita, Y. Matsunaga, and K. Hamabe, "Adaptive power level setting of femtocell base stations for mitigating interference with macrocells," in *IEEE 72nd Vehicular Technology Conference (VTC 2010 Fall)*, (Ottawa, Canada), pp. 1–5, September 2010.

[146] N. Arulselvan, V. Ramachandran, S. Kalyanasundaram, and G. Han, "Distributed power control mechanisms for HSDPA femtocells," in *IEEE 69th Vehicular Technology Conference (VTC 2009 Spring)*, (Barcelona, Spain), pp. 1–5, April 2009.

[147] X. Li, L. Qian, and D. Kataria, "Downlink power control in co-channel macrocell femtocell overlay," in *43rd Annual Conference on Information Sciences and Systems (CISS 2009)*, (Baltimore, USA), pp. 383–388, March 2009.

[148] X. Chu, Y. Wu, D. Lopez-Perez, and X. Tao, "On providing downlink services in collocated spectrum-sharing macro and femto networks," *IEEE Transactions on Wireless Communications*, vol. 10, pp. 4306–4315, December 2011.

[149] M. Bennis and S. M. Perlaza, "Decentralized cross-tier interference mitigation in cognitive femtocell networks," in *IEEE International Conference on Communications (ICC 2011)*, (Kyoto, Japan), pp. 1–5, June 2011.

[150] S. Guruacharya, D. Niyato, D. I. Kim, and E. Hissain, "Hierarchical competition for downlink power allocation in OFDMA femtocell networks," *IEEE Transactions on Wireless Communications*, vol. 12, pp. 1543–1553, April 2013.

[151] M. Bennis and M. Debbah, "On spectrum sharing with underlaid femtocell networks," in *IEEE International Symposium on Personal, Indoor and Mobile Radio Communications (PIMR 2010)*, (Instanbul, Turkey), pp. 185–190, September 2010.

[152] D. T. Ngo, L. B. Le, T. Le-Ngoc, E. Hossain, and D. I. Kim, "Distributed interference management in two-tier CDMA femtocell networks," *IEEE Transactions on Wireless Communications*, vol. 11, pp. 979–989, March 2012.

[153] H. Wang and Z. Ding, "Macrocell-queue-stabilization-based power control of femtocell networks," *IEEE Transactions on Wireless Communications*, vol. 13, pp. 5223–5236, September 2014.

[154] A. Galindo-Serrano and L. Giupponi, "Distributed Q-learning for interference control in OFDMA-based femtocell networks," in *IEEE 71st Vehicular Technology Conference (VTC 2010 Spring)*, (Taipei, China), pp. 1–5, May 2010.

[155] H.-S. Jo, C. Mun, J. Moon, and J.-G. Yook, "Interference mitigation using uplink power control for two-tier femtocell networks," *IEEE Transactions on Wireless Communications*, vol. 8, pp. 4906–4910, October 2009.

[156] V. Chandrasekhar, J. G. Andrews, T. Muharemovic, Z. Shen, and A. Gatherer, "Power control in two-tier femtocell networks," *IEEE Transactions on Wireless Communications*, vol. 8, pp. 4316–4328, August 2009.

[157] Q. Han, B. Yang, X. Wang, K. Ma, C. Chen, and X. Guan, "Hierarchical-game-based uplink power control in femtocell networks," *IEEE Transactions on Vehicular Technology*, vol. 63, pp. 2819–2835, July 2014.

[158] I. Guvenc, M.-R. Jeong, F. Watanabe, and H. Inamura, "A hybrid frequency assignment for femtocells and coverage area analysis for co-channel operation," *IEEE Communications Letters*, vol. 12, pp. 880–882, December 2008.

[159] Y. Bai, J. Zhou, and L. Chen, "Hybrid spectrum usage for overlaying LTE macrocell and femtocell," in *IEEE Global Telecommunications Conference (GLOBECOM 2009)*, (Honolulu, USA), pp. 1–6, December 2009.

[160] Y. Sun, R. P. Jover, and X. Wang, "Uplink interference mitigation for OFDMA femtocell networks," *IEEE Transactions on Wireless Communications*, vol. 11, pp. 614–625, February 2012.

[161] L. G. U. Garcia, K. I. Pedersen, and P. E. Mogensen, "Autonomous component carrier selection: interference management in local area environments for LTE-Advanced," *IEEE Communications Magazine*, vol. 47, pp. 110–116, September 2009.

[162] D. Lopez-Perez, G. de la Roche, A. Valcarce, A. Juttner, and J. Zhang, "Interference avoidance and dynamic frequency planning for WiMAX femtocells networks," in *IEEE Singapore International Conference on Communications Systems (SICCS 2008)*, (Guangzhou, China), pp. 1579–1584, November 2008.

[163] M. E. Sahin, I. Guvenc, M.-R. Jeong, and H. Arslan, "Handling CCI and ICI in OFDMA femtocell networks through frequency scheduling," *IEEE Transactions on Consumer Electronics*, vol. 55, pp. 1936–1944, November 2009.

[164] A. Hatoum, N. Aitsaadi, R. Langar, R. Boutaba, and G. Pujolle, "Fcra: femtocell cluster-based resource allocation scheme for OFDMA networks," in *IEEE International Conference on Communications (ICC 2011)*, (Kyoto, Japan), pp. 1–6, June 2011.

[165] A. Hatoum, N. Aitsaadi, R. Langar, R. Boutaba, and G. Pujolle, "Cluster-based resource management in OFDMA femtocell networks with QoS Guarantees," *IEEE Transactions on Vehicular Technology*, vol. 63, pp. 2378–2391, June 2014.

[166] S. Uygungelen, G. Auer, and Z. Bharucha, "Graph-based dynamic frequency reuse in femtocell networks," in *IEEE Vehicular Technology Conference (VTC 2011 Spring)*, (Yokohama, Japan), pp. 1–6, May 2011.

[167] Y.-S. Liang, W.-H. Chung, G.-K. Ni, I.-Y. Chen, H. Zhang, and S.-Y. Kuo, "Resource allocation with interference avoidance in OFDMA femtocell networks," *IEEE Transactions on Vehicular Technology*, vol. 61, pp. 2243–2255, June 2012.

[168] T.-H. Kim and T.-J. Lee, "Throughput enhancement of macro and femto networks by frequency reuse and pilot sensing," in *IEEE International Performance, Computing and Communications Conference (IPCCC 2008)*, (Austin, USA), pp. 390–394, December 2008.

[169] D. T. Ngo, S. Khakurel, and T. Le-Ngoc, "Joint subchannel assignment and power allocation for OFDMA femtocell networks," *IEEE Transactions on Wireless Communications*, vol. 13, pp. 342–355, January 2014.

[170] H.-C. Lee, D.-C. Oh, and Y.-H. Lee, "Mitigation of inter-femtocell interference with adaptive fractional frequency reuse," in *IEEE International Conference on Communications (ICC 2010)*, (Cape Town, South Africa), pp. 1–5, May 2010.

[171] A. Abdelnasser, E. Hossain, and D. I. Kim, "Clustering and resource allocation for dense femtocells in a two-tier cellular OFDMA network," *IEEE Transactions on Wireless Communications*, vol. 13, pp. 1628–1641, March 2014.

[172] J. Chen, C.-C. Yang, and S.-T. Sheu, "Downlink femtocell interference mitigation and achievable data rate maximization: using FBS association and transmit power-control schemes," *IEEE Transactions on Vehicular Technology*, vol. 63, pp. 2807–2818, July 2014.

[173] S.-Y. Lien, C.-C. Tseng, K.-C. Chen, and C.-W. Su, "Cognitive radio resource management for QoS guarantees in autonomous femtocell networks," in *IEEE International Conference on Communications (ICC 2010)*, (Cape Town, South Africa), pp. 1–5, May 2010.

[174] S. Park, W. Seo, Y. Kim, S. Lim, and D. Hong, "Beam subset selection strategy for interference reduction in two-tier femtocell networks," *IEEE Transactions on Wireless Communications*, vol. 13, pp. 342–355, January 2014.

[175] T. M. Nguyen, Y. Jeong, T. Q. S. Quek, W. P. Tay, and H. Shin, "Interference alignment in a poisson field of MIMO femtocells," *IEEE Transactions on Wireless Communications*, vol. 12, pp. 2633–2645, June 2013.

[176] B. Guler and A. Yener, "Selective interference alignment for MIMO cognitive femtocell networks," *IEEE Journal on Selected Area in Communications*, vol. 32, pp. 439–450, March 2014.

[177] A. R. Elsherif, Z. Ding, and X. Liu, "Dynamic MIMO precoding for femtocell Interference Mitigation," *IEEE Transactions on Communications*, vol. 62, pp. 648–666, February 2014.

[178] P. Jacob, A. S. Madhukumar, and A. Alphones, "Interference mitigation through cross polarized transmission in femto-macro network," *IEEE Communications Letters*, vol. 17, pp. 1940–1943, October 2013.

[179] M. D. Renzo, H. Haas, A. Ghrayeb, S. Sugiura, and L. Hanzo, "Spatial modulation for generalized MIMO: challenges, opportunities, and implementation," *Proceedings of the IEEE*, vol. 102, pp. 56–103, January 2014.

[180] A. G. Bell, "Apparatus for signalling and communicating, called photophone," *US Patent 235199*, 1880.

[181] K. C. Kao and G. A. Hockham, "Dielectric-fibre surface waveguides for optical frequencies," *Proceedings of the institution of Electrical Engineers*, vol. 113, pp. 1151–1158, July 1966.

[182] F. R. Gfeller and U. Bapst, "Wireless in-house data communication via diffuse infrared radiation," *Proceedings of the IEEE*, vol. 67, pp. 1474–1486, November 1979.

[183] A. Sevincer, A. Bhattarai, M. Bilgi, M. Yuksel, and N. Pala, "LIGHTENTs: smart LIGHTing and mobile optical wireless networks - a survey," *IEEE Communications survey & Tutorials*, vol. 15, pp. 1620–1641, Fourth Quarter 2013.

[184] J. M. Kahn and J. R. Barry, "Wireless infrared communications," *Proceedings of the IEEE*, vol. 85, pp. 265–298, February 1997.

[185] T. Komine and M. Nakagawa, "Fundamental analysis for visible-light communication system using LED lights," *IEEE Transactions on Consumer Electronics*, vol. 50, pp. 100–107, February 2004.

[186] J. Grubor, S. Randel, K.-D. Langer, and J. W. Walewski, "Broadband information broadcasting using LED-based interior lighting," *Journal of Lightwave Technology*, vol. 26, pp. 3883–3892, December 2008.

[187] H. Elgala, R. Mesleh, H. Haas, and B. Pricope, "OFDM visible light wireless communication based on white LEDs," in *IEEE 65th Vehicular Technology Conference (VTC 2007 Spring)*, (Dublin, Ireland), pp. 2185–2189, April 2007.

[188] T. Kominet and M. Nakagawa, "Performance evaluation of visible-light wireless communication system using white LED lightings," in *The 9th International Symposium on Computers and Communications (ISCC 2004)*, (New York, USA), pp. 258–263, June 2004.

[189] H. Burchardt, N. Serafimovski, D. Tsonev, S. Videv, and H. Haas, "Visible light communications VLC: beyond point-to-point communication," *IEEE Communications Magazine*, vol. 52, pp. 98–105, July 2014.

[190] Y. Tanakat, T. Kominet, S. Haruyama, and M. Nakagawa, "Indoor visible communication utilizing plural white LEDs as lighting," in *IEEE 12th International Symposium on Personal, Indoor and Mobile Radio Communications (PIMRC 2001)*, (San Diego, USA), pp. 81–85, September 2001.

[191] "IEEE standard for local and metropolitan area networks-part 15.7: short-range wireless optical communication using visible light," *IEEE Std 802.15.7-2011*, September 2011.

[192] R. Singh, T. O'Farrell, and J. P. R. David, "Performance evaluation of ieee 802.15.7 csk physical layer," in *Proc. IEEE GLOBECOM Workshops*, (Atlanta, USA), pp. 1064–1069, December 2013.

[193] J. Jiang, R. Zhang, and L. Hanzo, "Analysis and design of colour shift keying aided visible light communications," *IEEE Transactions on Vehicular Technology (Accept)*, 2015.

[194] M. Noshad and M. Brandt-Pearce, "Application of expurgated PPM to indoor visible," *Journal of Lightwave Technology*, vol. 32, pp. 875–882, March 2014.

[195] J. Vucic, C. Kottke, S. Nerreter, K.-D. Langer, and J. W. Walewski, "513 Mbit / s visible light communications link based on DMT-modulation of a white LED," *Journal of Lightwave Technology*, vol. 28, pp. 3512–3518, December 2010.

[196] J. B. Carruthers and J. M. Kahn, "Multiple-subcarrier modulation for nodirected wireless infrared communication," *IEEE Journal on Selected Areas in Communications*, vol. 14, March 1996.

[197] B. K. C. Liang and J. Evans, "Diversity combining for asymmetrically clipped optical OFDM in im/dd channels," in *Proc. IEEE GLOBECOM Workshops*, (Honolulu, USA), pp. 1–6, December 2009.

[198] R. Mesleh, H. Elgala, and H. Haas, "On the performance of different OFDM based optical wireless communication systems," *Journal of Optical Communications and Networking*, vol. 3, pp. 620–628, October 2011.

[199] R. Zhang and L. Hanzo, "Multi-layer modulation for intensity modulated direct detection optical OFDM," *Journal of Optical Communications and Networking*, vol. 5, pp. 1402–1412, December 2013.

[200] D. Tsonev, S. Videv, and H. Haas, "Light fidelity (Li-Fi): Towards all-optical networking," *SPIE Proceedings*, pp. 1–10, February 2013.

[201] C. Chen, N. Serafimovski, and H. Hass, "Fractional frequency reuse in optical wireless cellular networks," in *Proc. IEEE 24th International Symosium on PIMRC*, (London, UK), pp. 3594–3598, September 2012.

[202] C. Chen, D. Tsonev, and H. Hass, "Joint transmission in indoor visible light communication downlink cellular networks," in *Proc. IEEE GLOBECOM Workshops*, (Atlanta, USA), pp. 1127–1132, December 2013.

[203] X. Li, R. Zhang, and L. Hanzo, "Cooperative load balancing in hybrid visible light communications and WiFi," *IEEE Transactions on Communications (Accept)*, vol. IEEEXplore, Early Access, 2015.

[204] D. Bykhovsky and S. Arnon, "Multiple access resource allocation in visible light communication systems," *Journal of Lightwave Technology*, vol. 32, pp. 1594–1600, March 2014.

[205] D. J. T. Heatley, D. R. Wisely, I. Neild, and P. Cochrane, "Optical wireless: the story so far," *IEEE Communications Magazine*, vol. 36, October 1998.

[206] J. D. Hou and D. C. O'Brien, "Vertical handover decision-making algorithm using fuzzy logic for the integrated radio-and-OW system," *IEEE Transactions on Wireless Communications*, vol. 5, January 2006.

[207] K. Wang, A. Nirmalathas, C. Lin, and E. Skafidas, "High-speed duplex optical wireless communication system for indoor personal area networks," *Optical Express*, vol. 18, November 2010.

[208] M. Rahaim, A. Vegni, and T. D. C. Little, "A hybrid radio frequency and broadcast visible light communication system," in *Proc. IEEE GLOBECOM Workshops*, (Huston, USA), pp. 792–796, December 2011.

[209] H. Chowdhury and M. Katz, "Data download on move in indoor hybrid (radio-optical) WLAN-VLC hotspot coverages," in *IEEE 77th Vehicular Technology Conference (VTC 2013 Spring)*, (Dresden, Germany), pp. 1–5, June 2013.

[210] F. Jin, R. Zhang, and L. Hanzo, "Resource allocation under delay-guarantee constraints for heterogeneous visible-light and RF femtocell," *IEEE Transactions on Wireless Communications*, vol. 14, February 2015.

[211] X. Bao, X. Zhu, T. Song, and Y. Ou, "Protocol design and capacity analysis in hybrid network of visible light communication and OFDMA systems," *IEEE Transactions on Vehicular Technology*, vol. 63, May 2014.

[212] H. Ekstrom, A. Furuskar, M. M. J. Karlsson, S. Parkvall, J. Torsner, and M. Wahlqvist, "Technical solutions for the 3G long-term evolution," *IEEE Communications Magazine*, vol. 44, pp. 38–45, March 2006.

[213] A. Ghosh, D. Wolter, J. Andrews, and R. Chen, "Broadband wireless access with WiMAX/802.16: current performance benchmarks and future potential," *IEEE Communications Magazine*, vol. 43, pp. 129–136, February 2005.

[214] V. Chandrasekhar and J. G. Andrews, "Spectrum allocation in tiered cellular networks," *IEEE Transactions on Information Theory*, vol. 57, pp. 3059–3068, October 2009.

[215] K. Yeung and S. Nanda, "Channel management in microcell/macrocell cellular radio systems," *IEEE Transactions on Vehicular Technology*, vol. 45, pp. 601–612, November 1996.

[216] J. Lee, S. Bae, Y. Kwon, and M. Chung, "Interference analysis for femtocell deployment in OFDMA systems based on fractional frequency reuse," *IEEE Communication Letter*, vol. 15, pp. 425–427, April 2011.

[217] T. D. Novlan, R. K. Ganti, and J. G. Andrews, "Coverage in two-tier cellular networks with fractional frequency reuse," in *IEEE Global Telecommunications Conference*, (Houston, USA), pp. 1–5, December 2011.

[218] Z. Xu, G. Y. Li, and C. Yang, "Optimal threshold design for FFR schemes in multi-cell OFDMA networks," in *IEEE International Conference on Communications (ICC 2011)*, (Kyoto, Japan), pp. 1–5, June 2011.

[219] Z. Xu, G. Y. Li, C. Yang, and X. Zhu, "Throughput and optimal threshold for FFR schemes in OFDMA cellular networks," *IEEE Transactions on Wireless Communications*, vol. 11, pp. 2776–2785, August 2012.

[220] M. Amer, "Optimal configuration of fractional frequency reuse system for LTE cellular networks," in *IEEE Vehicular Technology Conference (VTC 2012 Fall)*, (Quebec City, Canada), pp. 1–5, September 2012.

[221] D. Bilios, C. Bouras, V. Kokkinos, A. Papazois, and G. Tseliou, "Optimization of fractional freqency reuse in long term evolution networks," in *IEEE Wireless Communications and Networking Conference (WCNC 2012)*, (Shanghai, China), pp. 1853–1857, April 2012.

[222] N. Saquib, E. Hossain, and D. I. Kim, "Fractional frequency reuse for interference management in LTE-Advance HetNet," *IEEE Wireless Communications*, vol. 20, pp. 113–122, April 2013.

[223] X. Qiu and K. Chawla, "On the performance of adaptive modulation in cellular systems," *IEEE Transactions on Communications*, vol. 47, pp. 884–895, August 1999.

[224] M. Haenggi, J. G. Andrews, F. Baccelli, O. Dousse, and M. Franceschetti, "Stochastic geometry and random graghs for the analysis and design of wireless networks," *IEEE Journal on Selected Areas in Communications*, vol. 27, pp. 1029–1046, September 2009.

[225] I. S. Gradshteyn and I. M. Ryzhik, *Table of Integrals, Series, and Products*. Elsevier Inc., 2007.

[226] J. Holland, *Adaptation in Naturaland Artificial Systems*. University of Michigan Press, 1975.

[227] D. Larose, *Data Mining Methods and Models*. Wiley-IEEE Press, 2006.

[228] M. Mitchell, *An Introduction to Genetic Algorithms*. MIT Press, 1996.

[229] I. Stefan, H. Burchardt, and H. Haas, "Area spectral efficiency performance comparision between vlc and rf femtocell networks," in *IEEE International Conference on Communications (ICC 2013)*, (Budapest, Hungary), pp. 3825–3829, June 2013.

[230] C. Luo, H. Ji, and Y. Li, "Utility based multi-service bandwidth allocation in the 4G heterogeneous wireless access networks," in *Proceedings of IEEE Wireless Communications and Networking Conference (WCNC 2009)*, (Budapest, Hungary), pp. 1–5, April 2009.

[231] M. Ismail and W. Zhuang, "A distributed multi-service resource allocation algorithm in heterogeneous wireless access medium," *IEEE Journal on Selected Areas in Communications*, vol. 30, February 2012.

[232] M. Ismail and W. Zhuang, "Decentralized radio resource allocation for single-network and multi-homing services in cooperative heterogeneous wireless access medium," *IEEE Transactions on Wireless Communications*, vol. 11, November 2012.

[233] M. Ismail, A. Abdrabou, and W. Zhuang, "Cooperative decentralized resource allocation in heterogeneous wireless access medium," *IEEE Transactions on Wireless Communications*, vol. 12, February 2013.

[234] M. Uchida and K. J, "An information-theoretic characterization of weigthed α-proportional fairness," in *Proceedings of IEEE INFOCOM 2009*, (Rio de Janeiro, Brazil), pp. 1053–1061, April 2009.

[235] J. Mo and J. Walrand, "Fair end-to-end window-based congestion control," *IEEE Transactions on Networking*, vol. 8, October 2000.

[236] Y. Yi and M. Chiang, "Stochastic network utility maximization: a tribute to Kelly's paper published in this journal a decade ago," *European Transactions on Telecommunications* , vol. 00, January 2007.

[237] A. Sang, X. Wang, M. Madihian, and R. D. Gitlin, "A flexible downlink scheduling scheme in cellular packet data systems," *IEEE Transactions on Wireless Communications*, vol. 5, March 2006.

[238] S. Boyd and L. Vandenberghe, *Convex Optimization*. Cambridge University Press, 2004.

[239] S. Dimitrov, S. Sinanovic, and H. Haas, "Clipping noise in OFDM-based optical wireless communication system," *IEEE Transactions on Communications*, vol. 60, pp. 1072–1081, April 2012.

[240] X. Li, R. Mardling, and J. Armstrong, "Channel capacity of IM/DD optical communication systems and of ACO-OFDM," in *Proceedings of IEEE International Conference on Communications (ICC 2007)*, (Glasgow, UK), pp. 2128–2133, June 2007.

[241] J. Armstrong, "OFDM for optical communications," *Journal of Lightwave Technology*, vol. 27, pp. 189–204, February 2009.

[242] C.-S. Chang, "Stability, queue length, and delay of deterministic and stochastic queueing networks," *IEEE Transactions on Automatic Control*, vol. 39, May 1994.

[243] C.-S. Chang and J. A. Thomas, "Effective bandwidth in high-speed digital networks," *IEEE Journal on Selected Areas in Communications*, vol. 13, August 1995.

[244] J. G. Kim and M. Krunz, "Bandwidth allocation in wireless networks with guaranteed packet-loss performance," *IEEE/ACM Transactions on Networking*, vol. 8, June 2000.

[245] J. Tang and X. Zhang, "Quality-of-service driven power and rate adaptation for multichannel communications over wireless links," *IEEE Transactions on Wireless Communications*, vol. 6, June 2007.

[246] F. P. Kelly, "Charging and rate control for elastoc traffic," *European Transactions on Telecommunications*, vol. 8, January 1997.

[247] J. M. Steele, *The Cauchy-Schwarz Master Class*. The Mathematical Association of America, 2004.

[248] P. Bonami, L. T. Biegler, A. R. Conn, G. Cornuejols, I. E. Grossmann, C. D. Laird, J. Lee, A. Lodi, F. Margot, and A. Waechter, "An algorithmic framework for convex mixed integer nonliner programs," *Discret Optimization*, vol. 24, August 2008.

[249] D. P. Palomar and M. Chiang, "A tutorial on decomposition methods for network utilit maximization," *IEEE Journal on Selected Areas in Communications*, vol. 54, July 2006.

[250] W. Yu and R. Lui, "Dual methods for nonconvex spectrum optimization of multicarrier systems," *IEEE Transactions on Communications*, vol. 54, July 2006.

[251] T. Yoo and A. Goldsmith, "On the optimality of multiantenna broadcasr scheduling using zero-forcing beamforming," *IEEE Journal on Selected Areas in Communications*, vol. 24, March 2006.

[252] S. Haykin, "Cognitive radio: brain-empowered wireless communications," *IEEE Journal on Selected Areas in Communications*, vol. 23, February 2005.

[253] Y.-C. Liang, Y. Zeng, E. C. Y. Peh, and A. T. Hoang, "Sensing-throughput tradeoff for cognitive radio networks," *IEEE Transactions on Wireless Communications*, vol. 7, April 2008.

[254] T. Yucek and H. Arslan, "A survey of spectrum sensing algorithms for cognitive radio applications," *IEEE Communications Surveys and Tutorials*, vol. 11, First Quarter 2009.

[255] F. Jin, X. Li, R. Zhang, C. Dong, and L. Hanzo, "Resource allocation under delay-guarantee constraints for visible-light communication," *submitted to IEEE Transactions on Vehicular Technology*, 2015.

[256] H. Zhang and H. Dai, "Cochannel interference mitigation and cooperative processing in downlink multicell multiuser MIMO networks," *Journal on Wirelss Communications and Networking*, pp. 222–235, December 2004.

Index

Author Index

C

D

E

F

G

H

I

J

K

L

M

N

O

T

U

V

Z